

Arrhythmia mechanisms in acute ischaemia and chronic infarction in rabbit heart

A thesis submitted in fulfilment of the degree of

Doctor of Philosophy

To

University of Glasgow

Faculty of Biomedical and Life Sciences

By

Soontaree Petchdee

DVM (Hons), MSc (Physiology)

Department of Integrative and Systems biology

Faculty of Biomedical and Life Sciences

2009

Table of Contents

1. Introduction	3
1.1 Acute myocardial ischaemia (AMI) and infarction	4
1.1.1 Definition	4
1.1.2 Classification	4
1.2 Clinical consequences of myocardial ischaemia and infarction	5
1.2.1 Electrophysiological marker of myocardial ischaemia and infarction ..	5
1.2.2 Surrogate marker of damaged cardiac myocardium	7
1.2.3 Metabolic changes in myocardial ischaemia and infarction	8
1.3 Cardiac electrophysiology	10
1.3.1 The cardiac action potential	10
1.3.2 Variations in action potential morphology	12
1.3.3 Refractoriness	13
1.3.4 Cardiac electrical conduction system	16
1.4 Electrophysiology of myocardial ischaemia and infarction	17
1.4.1 Action potential and electrical conduction system	17
1.4.2 Cellular electrophysiology	17
1.4.2.1 Cardiac action potential	17
1.4.2.2 Excitation-contraction coupling during ischaemia	19
1.4.2.3 Myocardial tissue properties	20
1.4.2.4 Changes in conduction velocity during ischaemia	21
1.5 AMI and Chronic myocardial infarction	21
1.5.1 Role of Gap junction on myocardial ischaemia and infarction	21
1.5.2 Border zone as an arrhythmogenic site during myocardial ischaemia and infarction	23
1.5.3 Myocardial ischaemia and reperfusion injury	26
1.5.4 Cardioprotection: preconditioning and postconditioning	28
1.6 Cardiac arrhythmias	30
1.6.1 Basic mechanisms	30
1.6.2 Ventricular arrhythmias in myocardial ischaemia and infarction	34
1.6.3 Cardiac mechano-electric feedback and the relationship to arrhythmias	35
1.6.4 Assessment of arrhythmogenic status of the myocardium	36
1.7 Model of AMI in the isolated whole heart	37
1.7.1 Global myocardial ischaemia	37
1.7.2 Local myocardial ischaemia	39
1.8 Aims and hypotheses	40
2 Methods	42
2.1 Optical mapping	43
2.1.1 General Principles	43
2.1.2 Voltage sensitive dyes	45
2.1.3 Optical mapping set up	47
2.2 Preparation for coronary artery occlusion during Langendorff perfusion .	50
2.2.1 Initial attempt to produce reproducible occlusion of rabbit coronary artery using loop technique	50
2.2.2 Coronary artery occlusion by using ligation technique	53
2.3 Pacing protocols	56
2.3.1 Atrial pacing (APACE)	56
2.3.2 Ventricular pacing (VPACE)	56
2.4 Electrophysiological analysis	58
2.4.1 Optical action potentials	58

2.4.2	Isochronal maps of activation	61
2.4.3	Conduction velocity	61
2.5	Statistical analysis	63
3	Acute regional myocardial ischaemia model in the rabbit	64
3.1	Introduction	65
3.1.1	Experimental models of myocardial ischaemia and infarction	65
3.1.2	Rat model of myocardial ischaemia and infarction	66
3.1.3	Rabbit model of myocardial ischaemia and infarction	67
3.2	Methods	67
3.2.1	Langendorff perfusion and left coronary artery occlusion	67
3.2.2	Fluorescent tracers of the rabbit coronary artery perfusion	68
3.2.3	Experimental protocols	68
3.3	Results	70
3.3.1	Rabbit coronary artery anatomy	70
3.3.2	Effects of regional acute myocardial ischaemia on APD	71
3.4	Discussion	73
3.4.1	Coronary artery anatomy of New Zealand White rabbits	73
4	Use of motion artefact blockers	75
4.1	Introduction	76
4.1.1	BDM	77
4.1.2	Blebbistatin	77
4.2	Methods	78
4.2.1	Experimental protocols	78
4.2.1.1	Acute local ischaemia	78
4.2.1.2	Acute global ischaemia	79
4.2.2	Optical action potential recordings	79
4.2.3	Statistical analysis	80
4.3	Results	80
4.3.1	Use of BDM to inhibit movement artefact	80
4.3.1.1	Regional ischaemia	80
4.3.1.2	Global ischaemia using lowered flow	83
4.3.2	Use of Blebbistatin to inhibit movement artefact	86
4.3.2.1	Regional ischaemia	86
4.3.2.2	Global ischaemia induced by low flow	89
4.3.3	Effect of Blebbistatin on ECGs characteristic	92
4.4	Discussion and conclusion	94
4.4.1	Effects of BDM	94
4.4.2	Effects of Blebbistatin	95
5	Use of RH237 to study regional myocardial flow	96
5.1	Introduction	97
5.2	Methods (A)	98
5.2.1	Cell isolation	98
5.2.1.1	Isolation of ventricular cardiomyocytes from the rabbit	98
5.2.2	Quantifying the binding of RH237 in rabbit ventricular myocytes	98
5.2.3	Measurement of kinetics and relative affinity of RH237 for cardiac cell membranes	100
5.2.3.1	Protocol A	100
5.3	Results A	101
5.3.1	Measurement of the capacity and relative affinity of cardiomyocytes for RH237	101
5.3.2	Sigmoidal fitting curve of RH237 binding with rabbit ventricular myocytes	102
5.3.3	B_{max} and $K_{1/2}$ of saturating [RH237] binding to rabbit ventricular myocytes	104

5.3.3.1	B _{max} of the saturating [RH237] fluorescence.....	104
5.3.3.2	K _{1/2} of the saturating [RH237] fluorescence.....	105
5.3.4	Correlation between amount of saturating [RH237] binding to rabbit heart tissue.....	106
5.4	Methods B.....	107
5.4.1	Measurement of the relative flow.....	107
5.4.1.1	Protocol B.....	110
5.5	Results B.....	110
5.5.1	Relative perfusion rate during acute global low-flow ischaemia.....	110
5.5.2	Relative perfusion rate during acute regional myocardial ischaemia.....	112
5.6	Discussion and conclusion.....	113
6	Arrhythmias, APD alternans and conduction in acute regional and global myocardial ischaemia.....	115
6.1	Introduction.....	116
6.2	Methods.....	118
6.2.1	Chronic Infarct induction.....	118
6.2.2	Measurement of APD and repolarization alternans.....	118
6.2.2.1	Experimental protocol.....	119
6.2.3	Measurement of CV.....	120
6.3	Results.....	121
6.3.1	Incidence of repolarization alternans during myocardial ischaemia and reperfusion.....	121
6.3.2	APD and repolarization alternans during regional myocardial ischaemia.....	124
6.3.3	Alternans magnitude during acute regional myocardial ischaemia.....	125
6.3.3.1	Alternans magnitude during acute regional ischaemia in heart <i>with arrhythmia</i>	125
6.3.3.2	Alternans magnitude during acute regional ischaemia in heart <i>without arrhythmia</i>	127
6.3.4	APD and repolarization alternans during global low-flow and no-flow ischaemia.....	128
6.3.5	Epicardial conduction during acute regional ischaemia.....	130
6.3.6	Epicardial activation during low flow ischaemia.....	131
6.3.7	Epicardial activation during global ischaemia.....	133
6.3.8	Summary of CV during regional ischaemia.....	134
6.3.9	Alternate beat analysis of local APDs at the sites of conduction block during local ischaemia.....	136
6.3.9.1	CV vectors in alternate beats in hearts <i>without arrhythmia</i>	136
6.3.9.2	CV in heart <i>with arrhythmia</i>	139
6.3.10 Ischaemia superimposed on LV with myocardial infarction.....	141
6.4	Discussion.....	145
6.4.1	The effects of mechanical uncouplers on ischaemia induced arrhythmias.....	145
6.4.2	Correlation between T-wave and APD alternans.....	146
6.4.3	Mechanisms for AP and conduction changes during ischaemia.....	148
6.4.4	Epicardial electrophysiology that precede arrhythmias.....	149
6.4.5	The effects of local ischaemia on hearts with an existing infarct.....	150
7	Spatial and temporal heterogeneity of electrophysiological response to acute and global myocardial ischaemia.....	152
7.1	Introduction.....	153
7.2	Methods.....	154
7.2.1	Acute regional myocardial ischaemia induction.....	154
7.2.2	Experimental protocol.....	154

7.2.3	Data analysis	155
7.2.3.1	Frequency analysis.....	155
7.2.3.2	Sequence analysis.....	156
7.2.4	Statistical analysis.....	157
7.3	Results.....	157
7.3.1	Time of onset of ventricular arrhythmias during acute ischaemia and reperfusion	157
7.3.2	Electrophysiology associated with re-entrant arrhythmias.....	159
7.3.2.1	Hearts <i>without arrhythmia</i> during acute regional ischaemia	159
7.3.2.2	Heart <i>with arrhythmias</i> during acute regional ischaemia....	160
7.3.2.3	Gradients of APD ₅₀ and T _{Rise} in acute myocardial ischaemia	162
7.3.2.4	Frequency analysis of VF in acute regional ischaemia.....	164
7.3.2.5	Frequency analysis of VF in acute global no-flow ischaemia	167
7.3.3	Non uniform changes in APD ₅₀ and T _{Rise} during acute myocardial ischaemia	169
7.3.3.1	Spatial variability of electrophysiology in acute regional and global ischaemia.....	169
7.3.3.2	Temporal variability of electrophysiology in acute regional and global ischaemia.....	170
7.3.4	VF following local ischaemia in infarcted hearts.....	174
7.4	Discussion and conclusion	176
7.4.1	Onset of VF	176
7.4.2	Temporal variability of electrophysiological parameters	177
7.4.3	Frequency analysis of VF	178
8	Optical mapping of prolonged ischaemia	180
8.1	Introduction	181
8.2	Methods	182
8.3	Results.....	182
8.3.1	Prolonged ischaemia	182
8.4	Discussion	187
9	Discussion	189
9.1	Technical aspects in acute regional ischaemia model using optical mapping	190
9.2	Electrical activity in the ischaemic area	191
9.3	Future work.....	192
9.4	Clinical relevance	193
9.5	Conclusion	193
10	Appendix	194
	Preliminary data on electrophysiological effects of coronary vasodilation in acute ischaemic myocardium	194
10.1	Introduction	194
10.2	Methods	195
10.3	Results.....	196
10.4	Discussion and conclusion	201
	References	203

List of Tables

Table 1.1 Classification of transmural and non transmural MI	5
Table 1.2 The time course of main metabolic changes after myocardial ischaemia.	9
Table 1.3 Techniques for measurement of repolarization time and refractory period.....	16
Table 2.1 Characteristic of commonly used voltage-sensitive dyes in cardiac mapping	47
Table 6.1 Incidence of alternans and arrhythmias in the normal hearts (stock)	122
Table 6.2 Comparison of numbers of alternans and arrhythmias in the chronic infarcted hearts.....	123
Table 6.3 Values are mean and standard error (SEM) of the CV in the rabbit heart during acute regional ischaemia.	135
Table 6.4 Mean and standard error (SE) of the CV during global low flow ischaemia	136
Table 8.1 Comparison of APD ₅₀ and T _{Rise} between prolonged and short ischaemia	186
Table 8.2 Comparison of velocity magnitudes	187

List of Figures

Figure 1.1 An example of the typical ST changes in acute myocardial infarction	6
Figure 1.2 Ion currents determine the 5 phases of cardiac action potential	12
Figure 1.3 Regional variation in morphology of action potential varies between regions	13
Figure 1.4 Refractory periods	14
Figure 1.5 The transportation of Ca^{2+} in the ventricular myocyte	20
Figure 1.6 Cx43 immunofluorescence micrographs	23
Figure 1.7 Structure of infarct depend on species in human, rabbit and dog	25
Figure 1.8 Values of $[\text{K}^+]_o$, pH, $[\text{ATP}]_i$ and $[\text{ADP}]_i$ along the 1-dimensional strand	26
Figure 1.9 The figure summarises evidence of myocardial ischaemia-reperfusion injury	27
Figure 1.10 Summary of IPC and IPost mechanisms	29
Figure 1.11 Initiation of re-entrant circuit of the atrio-ventricular junction	31
Figure 1.12 Functional re-entry	33
Figure 1.13 Diagram of the timing of EAD and DAD	34
Figure 1.14 Rabbit coronary artery	40
Figure 2.1 Electrochromic mechanism for dye response to membrane potential	44
Figure 2.2 Chemical structure of RH237 and the principle of voltage-sensitive fluorescence	46
Figure 2.3 Photographs of the optical mapping chamber	49
Figure 2.4 Diagram of the optical mapping set-up	50
Figure 2.5 A novel model of rabbit coronary artery occlusion	51
Figure 2.6 Photographs of the optical mapping chamber	52
Figure 2.7 Initial surgery to attach snare	54
Figure 2.8 Langendorff perfusion apparatus	55
Figure 2.9 Photographs of atrial pacing electrodes	57
Figure 2.10 Map of 256 optical action potentials recorded from the ventricular epicardial surface of a rabbit heart	57
Figure 2.11 The space constant equation	58
Figure 2.12 Example of OAPS from rabbit heart	59
Figure 2.13 Illustrations of OAPs recorded from contracting sites (A) compared with the minimized motion artefact sites (B)	60
Figure 2.14 APD and activation time calculation	60
Figure 2.15 Example of activation maps of left ventricular epicardial surface	61
Figure 2.16 CV calculation from epicardial pacing and radial approach to CV assessment	63
Figure 3.1 The pattern of rabbit coronary artery	71
Figure 3.2 Effects of acute myocardial ischaemia on APD	72
Figure 4.1 Isochronal maps of APD_{50} and rise time represent before, during and after coronary artery occlusion	81
Figure 4.2 The changes in APD_{50} and Rise time over the period of occlusion in selected sites	82
Figure 4.3 Mean of APD_{50} and Rise Time	83
Figure 4.4 Isochronal maps of APD_{50} and Rise time	84
Figure 4.5 Changes in APD_{50} and Rise time over the period of low flow perfusion in selected sites	85
Figure 4.6 Mean APD_{50} and Rise Time	86
Figure 4.7 Isochronal maps of APD_{50} and Rise time	87

Figure 4.8 The changes in APD ₅₀ and T _{Rise} over the period of occlusion in selected sites	88
Figure 4.9 Mean of APD ₅₀ and Rise Time	89
Figure 4.10 Isochronal maps of APD ₅₀ and Rise time	90
Figure 4.11 The changes in APD ₅₀ and Rise time over the period of low flow perfusion in selected sites	91
Figure 4.12 Mean of APD ₅₀ and T _{Rise}	92
Figure 4.13 Effects of blebbistatin on psECG	94
Figure 5.1 Kinetics of binding between RH237 and ventricular myocytes.....	102
Figure 5.2 Relationship between fluorescence and RH237 concentration as measured on spectrophotometer.....	103
Figure 5.3 Correlation between the number of myocytes per millilitre and B _{max}	104
Figure 5.4 Correlation between the number of myocytes per millilitre and K _{1/2}	105
Figure 5.5 Relationship between total cells in gram wet weight, fluorescence at saturation and amount of RH237 required for 50% binding	107
Figure 5.6 The optical signals from left ventricular epicardial of the rabbit heart	109
Figure 5.7 Experimental protocol	110
Figure 5.8 Relative flow and APD ₅₀ during multiple flow rate.....	111
Figure 5.9 Relative flow vs. APD ₅₀	112
Figure 6.1 Experimental protocol	119
Figure 6.2 Example of CV analysis from optical mapping recordings.....	121
Figure 6.3 APD and T-wave alternans during acute myocardial ischaemia.....	125
Figure 6.4 APD and repolarization alternans in heart with arrhythmia	126
Figure 6.5 APD and repolarization alternans in heart without arrhythmia	128
Figure 6.6 AP and repolarization alternans in low-flow and no-flow ischaemia	129
Figure 6.7 Epicardial activation during coronary artery ligation.....	131
Figure 6.8 Epicardial activation during global low-flow ischaemia.....	132
Figure 6.9 Epicardial activation during global no-flow ischaemia	134
Figure 6.10 Comparison of APD ₅₀ and regional myocardial flow	137
Figure 6.11 Alternating conduction velocities (non-arrhythmic heart)	139
Figure 6.12 Alternating conduction velocities (leading to arrhythmia)	141
Figure 6.13 The effects of local ischaemia on hearts with an existing infarction scar.....	144
Figure 7.1 Experimental protocol	155
Figure 7.2 Power spectrum analysis	156
Figure 7.3 ECG traces and OAPs from the ischaemic region.....	158
Figure 7.4 Time before onset of arrhythmias after start of acute regional ischaemia	159
Figure 7.5 Time course of changes in APD ₅₀ and T _{Rise} in heart without arrhythmia	160
Figure 7.6 Time course of changes in APD ₅₀ and T _{Rise} in heart with arrhythmia	161
Figure 7.7 T _{Rise P95%} in hearts with and without arrhythmia.....	162
Figure 7.8 Rise time vs. APD ₅₀ during acute regional and global no-flow ischaemia	164
Figure 7.9 Non-uniform changes in electrophysiology during acute regional ischaemia	165
Figure 7.10 Mean values of VF parameters after regional ischaemia	166
Figure 7.11 Non-uniform changes during acute global no-flow ischaemia	167
Figure 7.12 Mean values of VF parameters after global no-flow ischaemia	168
Figure 7.13 Time course of changes in parameter variability during acute regional ischaemia, global no-flow and low flow ischaemia.....	170
Figure 7.14 Colour maps of variability of APD ₅₀ (i) and T _{Rise} distribution (ii) ...	171

Figure 7.15 Normalized variability of APD ₅₀ and T _{Rise} gradient during acute regional and global ischaemia	172
Figure 7.16 SD variability, range variability and difference variability of APD ₅₀ and T _{Rise}	173
Figure 7.17 Electrophysiological changes in ischaemic region of chronic infarcted heart	174
Figure 7.18 Comparison of VF frequency parameters in normal vs infarcted hearts	175
Figure 8.1 Optical mapping of prolonged ischaemia	184
Figure 8.2 Isochronal maps of activation during prolonged ischaemia	185
Figure 10.1 The balance of vascular tone	194
Figure 10.2 Experimental protocol.....	196
Figure 10.3 ECG traces from PDA during acute ischaemia	197
Figure 10.4 Optical imaging of APD ₅₀ during acute regional and global low-flow ischaemia	198
Figure 10.5 Optical mapping of flow and APD during local and low flow ischaemia	199
Figure 10.6 Correlation between APD ₅₀ and percentage of the number of sites	200
Figure 10.7 Colour map of variability of APD ₅₀ gradient (i) and T _{Rise} gradient (ii)	201

Acknowledgement

Throughout this work, I have been supported and guided by Prof Godfrey Smith and Dr Francis Burton. I would like to thank them for their intelligence, technical skills and their friendship. The Thai government has been generous in their funding of my research. Moreover, to everybody in the lab, thank you for making it a pleasurable time in Glasgow. Thank you also to my family in Thailand, who encouraged and supported me throughout.

Author's declaration

The permanent coronary artery ligation on rabbit was carried out by the technical staffs (Mrs Diane Smillie, Mr Michael Dunne and Mr Graham Deuchar) at the Department of Medical Cardiology Glasgow Royal Infirmary under the supervision of Dr. Martin Hicks. The isolated myocytes was carried out by Mrs June Irvine and Mrs Aileen Rankin at Department of Integrative and System Biology, IBLS. All the experimental work contained in this thesis was undertaken by me. The material has not been submitted previously for any other degree. Some of the results obtained were published and are detailed below.

- Optical mapping reveals gradients of action potential duration during coronary artery occlusion in isolated rabbit hearts. S Petchdee, FL Burton, GL Smith *Biophysical Society*, Long Beach, USA.
- Local ischaemia causes arrhythmias unrelated to T-wave alternans. S Petchdee, FL Burton, GL Smith *Physiological Society*, Cambridge, UK.
- T-wave alternans in a model of acute local ischaemia. S Petchdee, FL Burton, GL Smith *2nd International Cardiovascular Symposium*, Glasgow, UK.

Abbreviations

AF	Atrial fibrillation
AP	Action potential
APD	Action potential duration
APD ₅₀	Action potential duration at 50% repolarization
ARP	Absolute refractory period
ATP	Adenosine triphosphate
AV	Atrio-ventricular
AVN	Atrio-ventricular node
BDM	2,3-Butane-Dione Monoxime
BZ	Border zone
CAD	Coronary artery disease
CCD	Charged-coupled device
CD	Conduction delay
CL	Cycle length
CV	Conduction velocity
Cx	Connexin
DAD	Delayed after-depolarisation
DF	Dominant frequency

DFD	Dispersion of dominant frequencies
dV/dt_{\max}	Maximum rate of depolarisation/upstroke velocity
EAD	Early after depolarisation
ECG	Electrocardiogram
ERP	Effective refractory period
FFT	Fast fourier transform
I_{Ca-L}	L-type calcium current
I_K	Delayed rectifier current, (potassium current)
I_{K1}	Inward rectifier current
I_{Kto}	Transient outward potassium current
I_{Na}	Fast sodium current
IP	Ischaemic preconditioning
IZ	Infarcted zone
KCl	Potassium chloride
$[K^+]_o$	Extracellular potassium concentration
LAD	Left anterior descending artery
LV	Left ventricle
MAP	Monophasic action potential
MEF	Mechano-electrical feedback
MF	Median frequency

MI	Myocardial infarction
NA	Numerical aperture
NAD ⁺	Nicotinamide adenine dinucleotide
NADH	Reduced form of NAD ⁺
NZ	Non-infarcted zone
OAP	Optical action potential
PCL	Pacing cycle length
PDA	Photodiode array
psECG	pseudoECG
pO ₂	Amount of dissolved oxygen in the blood
RA	Right atrium
RMP	Resting membrane potential
RRP	Relative refractory period
RV	Right ventricle
RyR ₂	Ryanodine receptor
SAN	Sinoatrial node
SCD	Sudden cardiac death
SEM	Standard error of the mean
SERCA	Sarcoplasmic Ca-ATPase
SR	Sarcoplasmic reticulum

T_{Act}	Time to activation (from stimulus to the midpoint of the upstroke of the action potential)
T_{Rise}	Action potential rise time from 10-90% depolarisation
TAP	Transmembrane action potential
VE	Virtual electrode
VF	Ventricular fibrillation
V_{max}	Maximum rate of depolarisation
VT	Ventricular tachycardia

ABSTRACT

In this thesis, a method for studying the electrophysiological consequences of acute regional ischaemia in rabbit heart was established using a combination of a novel snare technique and optical mapping. The purpose of this approach was to discover the mechanistic link between acute coronary infarction and the occurrence of arrhythmias. The electrophysiology of the epicardial surface of isolated hearts was examined using the voltage sensitive dye RH237 and optical action potentials were recorded from a 13x13mm area of left ventricular epicardium using a 16x16 element Hamamatsu photodiode array. Contraction motion artefacts were practically eliminated with blebbistatin (5 μ M). An alternative mechanical uncoupler, BDM, was found to be not suitable for the study of arrhythmic behaviour associated with ischaemia.

After occlusion of the left coronary artery, a progressive reduction in action potential duration (APD), and slowing of upstroke was observed in an area of the left ventricle anterior surface, accompanied by ECG S-T segment elevation. These effects were reversed when the coronary artery occlusion was released. Ligation (duration 12-15mins) caused a decrease in APD₅₀ (APD at 50% repolarisation), in the zone of reduced perfusion, from 141 \pm 5.2ms to 53.3 \pm 9.3ms (mean \pm SEM, n=10 hearts, P<0.001). After ligation was reversed and full perfusion restored, APD₅₀ returned to normal values (149 \pm 7.0ms, n.s.). T_{rise} (action potential rise time from 10-90% depolarisation) increased from 7.2 \pm 1.0ms to 15.8 \pm 2.8ms (P<0.01). In the non-infarcted area of myocardium, no significant changes in APD₅₀ (147 \pm 7.0ms vs. 147 \pm 8.1ms) or T_{rise} (6.4 \pm 0.4ms vs 8.8 \pm 1.4ms) were observed during occlusion. T-wave alternans behaviour was observed frequently during local ischaemia and associated with alternans of optical action potentials (OAPs) in the ischaemic border zone (BZ) and in ischaemic zone (IZ). T-wave alternans amplitude was not maintained during local ischaemia but OAPs continued to show alternating behaviour. Arrhythmias (VT and VF) were common when conduction block occurred at the interface between the normal and ischaemic zone, but arrhythmias were absent when conduction into the IZ was retained. This observation suggests that the conduction block was the crucial precipitating event for the generation of arrhythmias.

Acute local ischaemia was also imposed in a heart with an existing infarct scar to examine the effects of pre-existing ischaemic damage. The incidence of arrhythmias was similar to that observed in the absence of an infarct scar indicating that pre-existing damage did not predispose the heart to arrhythmias. Global ischaemic challenges, both low flow and zero flow produced similar reductions in APD and rise time and were followed by arrhythmias, but the associated changes in the ECG were complex and could not be easily interpreted. Significant temporal variability in electrophysiology was observed in global ischaemia, but absent in the local ischaemic challenge. The underlying mechanisms of these temporal fluctuations in cardiac electrophysiology may be dictated by either cellular metabolism or fluctuations in coronary flow.

Long-term local ischaemia (~60mins) did not reveal a second phase of arrhythmias after 40-45mins as observed in other animal models, and nor were there signs of significant further electrophysiological changes as a consequence of the additional period of local ischaemia.

1. Introduction

The aim of this introduction is to provide an overview of the phenomena of acute myocardial ischaemia and chronic myocardial infarction, and to examine the electrophysiological processes of isolated rabbit heart that are thought to be affected by them.

1.1 Acute myocardial ischaemia (AMI) and infarction

1.1.1 Definition

Acute myocardial ischaemia is generally defined as an abrupt decrease in blood flow to the heart muscle commonly caused by an obstruction of one or more coronary arteries.

Coronary arteries have their origin at the aorta and distribute on the epicardial surface of the heart as intramural branches that supply blood to the cardiac muscle (Day & Johnson, 1958). Myocardial ischaemia can be defined from seven points of view: pathological, biochemical, electrocardiography, imaging, clinical trials, epidemiological and public policy. In terms of pathology, myocardial infarction is defined by myocardial cell death and necrosis leading to the infiltration of the myocardium with polymorphonuclear leukocytes and fibroblasts (Thygesen & Alpert, 2007). Myocardial ischemia is normally more extensive in the sub-endocardial region because in most species these deeper myocardial layers are the furthest from the blood supply (Wilensky *et al.*, 1986; Homans *et al.*, 1994; Li *et al.*, 1998).

1.1.2 Classification

Myocardial ischaemia and myocardial infarction (MI) can be divided into two types on the basis of morphology and anatomical classification as shown in Table 1.1: transmural and non-transmural. A transmural MI is characterized by ischaemic necrosis across the full thickness of the affected heart muscle, extending from the endocardium through myocardium to the epicardium. In the case of a non-transmural MI, the area of ischaemic necrosis does not extend through the full thickness of myocardial wall (Engblom *et al.*, 2005; Branyas *et al.*, 1990; Engels *et al.*, 1995; Widimsky *et al.*, 1984). Under these circumstances,

the least perfused regions and those most vulnerable to ischaemia are in the endocardial and subendocardial zones of the myocardial wall (Ryan *et al.*, 1996).

One other method of classification of MI is based on clinical diagnostic criteria, for example, by the presence or absence of Q waves on an electrocardiogram (ECG). However, this indicator cannot distinguish a transmural from a non-transmural MI (Ryan *et al.*, 1996; Sievers *et al.*, 2004). Myocardial infarction is usually classified by size, location and pathological appearance such as developing (less than 6 hours), acute (6 hours to 7 days), healing (7-28 days), and healed or beyond 29 days (Thygesen & Alpert, 2007).

Characteristic	Transmural MI	Non transmural MI
Area of necrosis	Entire ventricular wall from endocardium to epicardium	Interior 2/3 of ventricular wall
Distribution	Single coronary artery	Extends beyond perfusion territory of single coronary artery
Association	Coronary atherosclerosis, plaque rupture, thrombosis	Diffuse stenosis coronary atherosclerosis

Table 1.1 Classification of transmural and non transmural MI

1.2 Clinical consequences of myocardial ischaemia and infarction

1.2.1 Electrophysiological marker of myocardial ischaemia and infarction

The clinical diagnosis of acute MI is based on ECG findings which can be divided into two types: a ST-elevation MI and a non-ST-elevation MI. The presence of Q waves or ST segment elevation is associated with higher mortality and morbidity rates (Fozzard & DasGupta, 1976; Kleber, 2000). However, the other pathological

conditions such as left ventricular hypertrophy, left bundle branch block, pericarditis, hyperkalaemia and early repolarization can alter the ECG in similar ways to MI (Kolipaka *et al.*, 2005;Fozzard & DasGupta, 1976).

Commonly, ECG changes in myocardial ischaemia and infarction can be diagnosed from typical T-wave and ST segment changes. For example, symmetrical T-waves in at least two adjacent leads, progressively increasing R-wave amplitude and width, tall T-waves are all recognised indicators of ischaemic myocardium (Martin *et al.*, 2007;Sievers *et al.*, 2004;Jastrzebski *et al.*, 2008)). Figure 1.1 illustrates a typical ST segment elevation in acute myocardial ischaemia.



Figure 1.1 An example of the typical ST changes in acute myocardial infarction

This tracing shows sinus rhythm. The rate is 80 beats/minute. Beat #11 and #14 (as indicated by circle) are premature ventricular beats as suggested by the wide QRS complex, the compensatory pause (first beat) and the absence of a preceding P wave.

An acute infarction is suggested by the presence of slight ST segment elevation and Q-waves in leads II, III and aVF. (Adapted from <http://sprojects.mmi.mcgill.ca/dir/heart.html>)

In addition, several biochemical markers are released into the bloodstream when myocardial cells are damaged, and may be used in combination with ECG evidence to aid in diagnosis.

1.2.2 Surrogate marker of damaged cardiac myocardium

Biochemical markers are proteins or peptides released from the heart tissue when heart cells are damaged that enter the blood stream. The presence in the serum of the enzymes, Serum glutamic oxaloacetic transaminase (SGOT) and Lactate dehydrogenase (LDH) were used to clinically diagnose cardiac tissue damage until the 1980s (Henderson *et al.*, 1998). Currently the metabolic enzyme creatine kinase (CK) and the myofilament protein cardiac troponin (cTn) are now the preferred markers. The cardiac troponin sub unit I (cTnI) and T (cTnT) are used as a specific biochemical marker of injured myocardial cells, these proteins are immediately released after cell injury. Cardiac-TnT stays in the bloodstream for the next few days and levels return to normal in the following 1-2 weeks. Cardiac-TnT can be found in the blood when the heart tissue is continuously damaged. However, cTnT may not rise during reversible myocardial ischaemia (Hake *et al.*, 1993). Ischemia Modified Albumin (IMA) has recently shown to be a sensitive and early biochemical marker of myocardial ischaemia. The sensitivity and selectivity of this indicator is such that it alone is sufficient evidence to indicate an ischaemic event without requiring confirmatory ECG evidence (Sinha *et al.*, 2003;Sinha *et al.*, 2002a;Sinha *et al.*, 2002b).

One other clinical approach for detecting AMI is via hypoxia markers (Giordano, 1999). Angiogenic peptides such as hypoxia inducible factor1 (HIF-1) and vascular endothelial growth factor (VEGF) may be used as markers for acute myocardial infarction. However, this approach is not sensitive enough, to detect AMI under a myocardial stunning condition, so this technique may be more suited to chronically ischaemic tissue (Chung *et al.*, 2002;Giordano, 1999;Michiels *et al.*, 2000;Sinusas, 2004).

Commonly used non-invasive imaging techniques in myocardial ischaemia and infarction are echocardiography, radionuclide imaging and magnetic resonance imaging. Radionuclide imaging is a technique which can be directly used for detecting the viable myocytes. Hypoxic tissue is detected by using radiopharmaceuticals imaging, such as Thallium-201, Tetrofosmin, Nitroimidazoles and Technetium-99m (Cook *et al.*, 1998;Baer *et al.*,

1994;Kolipaka *et al.*, 2005;Miller *et al.*, 2003). However, this method is less well suited to detecting small areas of infarction. In addition, nitroimidazoles and Technetium-99m have been used to detect transient ischaemia in a research setting, but remain to be clinically proven in detecting myocardial ischaemia.

1.2.3 Metabolic changes in myocardial ischaemia and infarction

Insufficient blood supply to the myocardium leads rapidly to disturbances in myocardial metabolism (Cascio *et al.*, 1995). Due to the rapid fall in pO_2 , oxidative phosphorylation and mitochondrial ATP production cease within a few seconds after myocardial ischaemia, and is replaced by anaerobic metabolism which sustains ATP production, but with a net production of lactic acid. During this phase, creatine phosphate concentration decreases and breakdown products such as adenosine and inorganic phosphate accumulate. Free fatty acids are generated, followed by accumulation of lactate, protons, and reduced nicotinamide adenine dinucleotide (NADH) due to anaerobic glycolysis and glycogenolysis (Braasch & Bing, 1968). Intracellular potassium (K^+) and magnesium (Mg^{2+}) are lost from the myocardial cells due to the loss of energy-dependent transmembrane control. Similarly, extracellular sodium (Na^+) and extracellular calcium (Ca^{2+}) accumulate in the cells due to insufficient metabolism to drive their extrusion processes. This redistribution of electrolytes leads to osmotic changes and cellular oedema (Berkich *et al.*, 2003).

Prolonged ischaemia of more than twenty minutes induces changes in ultrastructure such as disappearance of glycogen granules and oedema of mitochondria and sarcoplasmic reticulum. These organelles are severely disrupted and their plasma membranes deteriorate within an hour after myocardial ischaemia. Myocardial cell death and necrosis occur in the acute phase followed by inflammation and fibrosis in the healing stage. The time course of main metabolic changes is shown in Table1.2.

Myocardial ischaemia	Cell death and Tissue necrosis or Myocardial infarction	
	→	
Seconds	Minutes	Hours (irreversible damage)
Reduced oxygen availability	Leakage of lactate	Increasing cellular oedema
Disturbances of transmembrane ionic balance	Leakage of adenosine, inosine and other metabolites	Loss of mitochondrial respiratory control
Reduction of mitochondrial activity and oxidative phosphorylation	Vasodilation	Non-specific electrocardiographic changes
Reduced ATP production	Increasing cellular acidosis	Complete depletion of energy reserves
Reduction of amplitude and duration of Action potential	Increasing depletion of energy stores	Metabolic disruption
Leakage of K ⁺ , accumulation of Na ⁺ and Cl ⁻	Cell swelling	Loss mitochondrial components
Catecholamine release	Development of mitochondrial damage	Severe ultrastructure damage and membrane deterioration
Cyclic AMP mediated activation of phosphorylase	Inhibition of glycolysis	Cellular, mitochondrial and cell membrane disruption
Stimulation of glycogenolysis	Severe reduction of ATP	Extensive enzyme leakage
Accumulation of H ⁺ , CO ₂ , PO ₄ ³⁻	Minor ultrastructure changes such as mitochondrial swelling	Cellular autolysis
Development of intracellular acidosis		
Reduction or blockage of mitochondrial electron transport		
Accumulation of NADH		

Table 1.2 The time course of main metabolic changes after myocardial ischaemia.

(Berkich *et al.*, 2003), (Giordano, 2008; Hausenloy & Yellon, 2006; Cascio *et al.*, 1995; Michiels *et al.*, 2000; Yellon *et al.*, 1992; Yellon & Opie, 2006; Michiels, 2004; Heusch & Schulz, 1996; Kleber & Wilde, 1986; Braasch & Bing, 1968).

1.3 Cardiac electrophysiology

The electrophysiology of cardiac cells can be characterized as periodic changes in the potential differences between cytoplasm and extracellular region. The changing pattern of cardiac electrical activity and amplitude are determined by differences in ion concentration across the cell membrane and the presence of ion-permeable channels in the membrane.

The passive transport mechanisms through specific channels are important for short term electrical behaviour of the cardiac cells. In the case of cardiac myocytes, the principle ionic currents are: a fast inward sodium current (I_{Na}), the inward L-type Ca^{2+} current ($I_{Ca,L}$), the transient outward potassium current (I_{to}), and an inwardly rectifying background potassium current (I_{K1}).

On the other hand, active transport mechanisms are important for the long term electrical behaviour. For example, Na^+K^+ ATPase, transports $2K^+$ into the cell while extruding $3Na^+$ for each molecule of ATP hydrolysis. Coupled transport, such as Na^+-Ca^{2+} exchanger (NCX), helps to regulate the resting intracellular calcium concentration, by transporting $3Na^+$ inwardly for each Ca^{2+} outward.

1.3.1 The cardiac action potential

The cardiac action potential (AP) can be divided into 5 phases as shown in Figure1.2.

Phase 0 is shown by the steep action potential upstroke, the rapid depolarisation caused by opening of the fast Na^+ channels and entry of Na^+ ions. The membrane potential rapidly moves toward the Na^+ equilibrium potential (E_{Na}) at approximately +52 mV. The driving force for Na^+ ion movement declines as the membrane potential approaches the equilibrium for Na^+ .

Phase 1 at the peak of the upstroke, the membrane potential reaches between +20 and +40mV and undergoes rapid repolarization by the transient outward current (I_{to}) which carries mostly K^+ ions with some contribution by a Cl^- influx (via a Ca^{2+} -dependent Cl^- channel). The I_{to} current is composed of I_{to1} which is a Ca^{2+} - independent, K^+ current and I_{to2} which is a Ca^{2+} dependent K^+ current.

Phase 2 is the plateau of cardiac action potential. During this phase of maintained depolarisation (and prolonged refractoriness) the cardiac muscle relaxes before the subsequent action potential. The plateau arises from the near balance of positive inward and outward currents. The inward L-type Ca^{2+} current ($I_{\text{Ca,L}}$) and outward slow activating K^+ current or delayed rectifier (I_{K}) predominate initially. The electrogenic NCX transiently operates in reverse mode to bring Ca^{2+} into the cell and extract Na^+ contributing to the net outward current during this phase due to the 3 Na^+ :1 Ca^{2+} stoichiometry. However, the major depolarizing influence is from $I_{\text{Ca,L}}$, which induces further calcium release from the sarcoplasmic reticulum and activates contractile proteins.

Phase 3 of the AP occurs as the plateau is terminated and the onset of late rapid repolarization starts. This phase is caused by decay of $I_{\text{Ca,L}}$ as the L-type Ca^{2+} current inactivates, a process that depends on time, voltage and intracellular Ca^{2+} . Repolarization occurs very rapidly because the dominant repolarising current (I_{K}) is increased and the NCX returns to the Ca^{2+} efflux (forward) mode. Eventually, the membrane potential approaches its resting value dictated mainly by the inward rectifying background potassium conductance (I_{K1}).

Phase 4 in ventricular myocytes, the resting membrane potential is stable at 90 mV. The major outward currents are (i) $I_{\text{Na-K}}$ from Na^+ - K^+ pump and (ii) I_{K1} current, a K^+ current that flows through inward rectifying K1 channel. The major inward currents are (i) Na^+ and (ii) Ca^{2+} leakage currents, both are relatively small in magnitude during this phase.

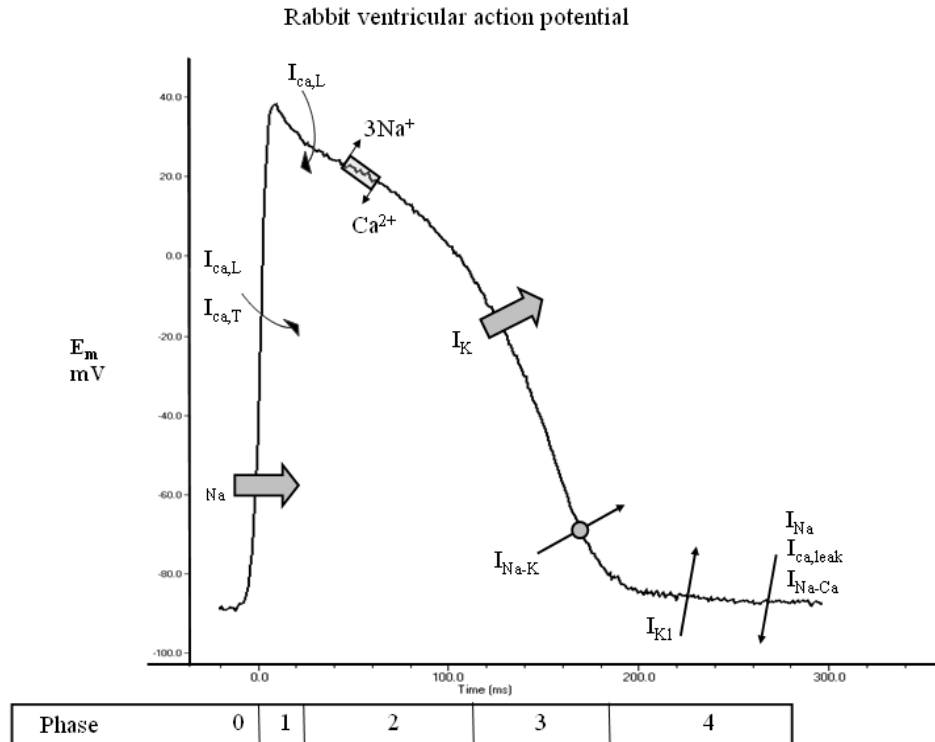


Figure 1.2 Ion currents determine the 5 phases of cardiac action potential

The arrows that are pointed into the area under the trace represent currents that enter the cell, pointing outward arrows represent currents that leave the cell. E_m is the membrane potential. Key currents are represented in thick arrow (Lewick, 2003).

1.3.2 Variations in action potential morphology

Differences in action potential morphology occur between cardiac regions such as sinoatrial node (SAN), atrio-ventricular node (AVN) and Purkinje cell. Pacemaker cells have unstable membrane potential in diastole. The potentials gradually approach threshold and then depolarise rapidly when the threshold is reached. Under normal conditions, cardiac activation starts at SAN and cardiac cells in this area or pacemaker cells have a faster intrinsic rate than other cells in the heart.

The maximum diastolic potential of the SAN is less negative than ventricular cells and these nodal cells also have a lower permeability to potassium. Therefore the resting potential is less negative than in ventricular cells. The threshold of these nodal cells is also different, at approximately -35 mV because

I_{Na} is absent. The action potential upstroke in these cells results exclusively from I_{Ca} current flow.

How AP morphology varies among regions and between ventricular tissues is shown in Figure 1.3 A, B and C.

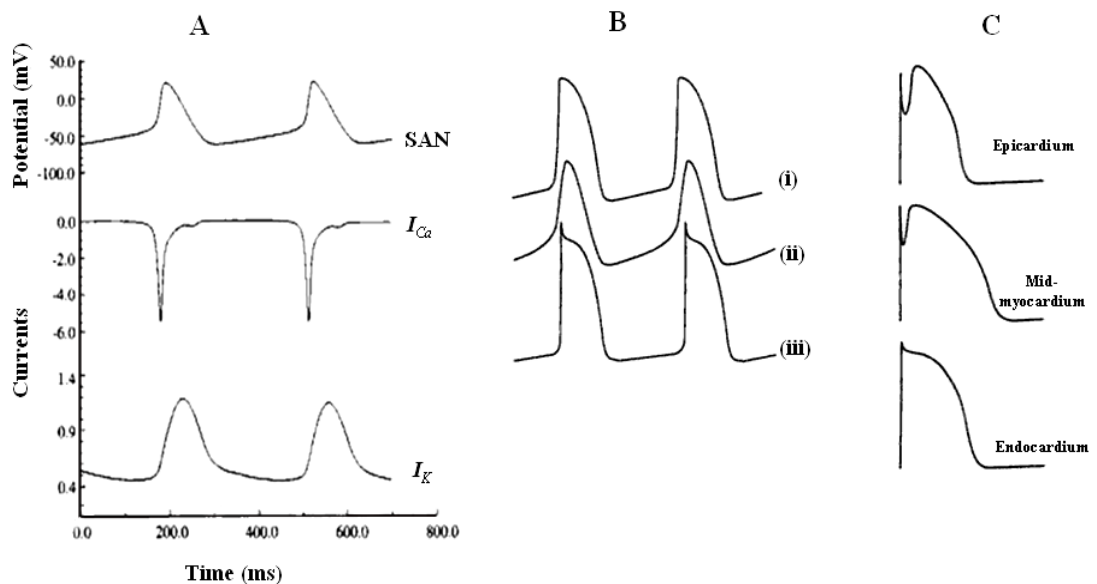


Figure 1.3 Regional variation in morphology of action potential varies between regions

A: Action potential from SAN and major ionic currents. The upstroke is mediated by I_{Ca} and I_K dominates the repolarisation phase.

B: AP morphology from AVN which varies between regions, (i) atrio-nodal, (ii) nodal and (iii) transitional region between the node and the bundle of His.

C: Diversity of AP morphology in ventricular tissues (in dog). The shape of the AP varies across the myocardium wall. Spike and dome AP morphology is evident in the epicardium and mid-myocardium, absent in the endocardium.

1.3.3 Refractoriness

The term refractory period refers to the interval during which cardiac muscle cells cannot be re-excited by way of conduction or stimulation. Functionally it gives time for the heart to fill between the contractions. Absolute refractory period (ARP) is used to describe the period of inexcitability, during this phase Na^+ current are inactivated. ARP extends from phase 1 through phase 2 and

includes approximately half of phase 3 of repolarisation. In terms of the ECG, this is the duration between the Q wave and the peak of the T-wave.

Excitability in the subsequent relative refractory period (RRP) is gradually recovered and during this time a new action potential can be elicited with a supranormal stimulus. When action potentials are generated very early in RRP, the upstroke is not as steep as the normal action potential. Effective refractory period (ERP) is defined as the period of time that action potentials can be generated but fail to propagate through the tissue. The duration of this period depends on the time required for Na^+ and Ca^{2+} channels to be able to become activated again. ERP extends from phase 0 of the action potential through the middle of phase 3. Relationship among membrane potential, ECG and refractory period is shown in Figure 1.4 (Wit & Janse, 1993).

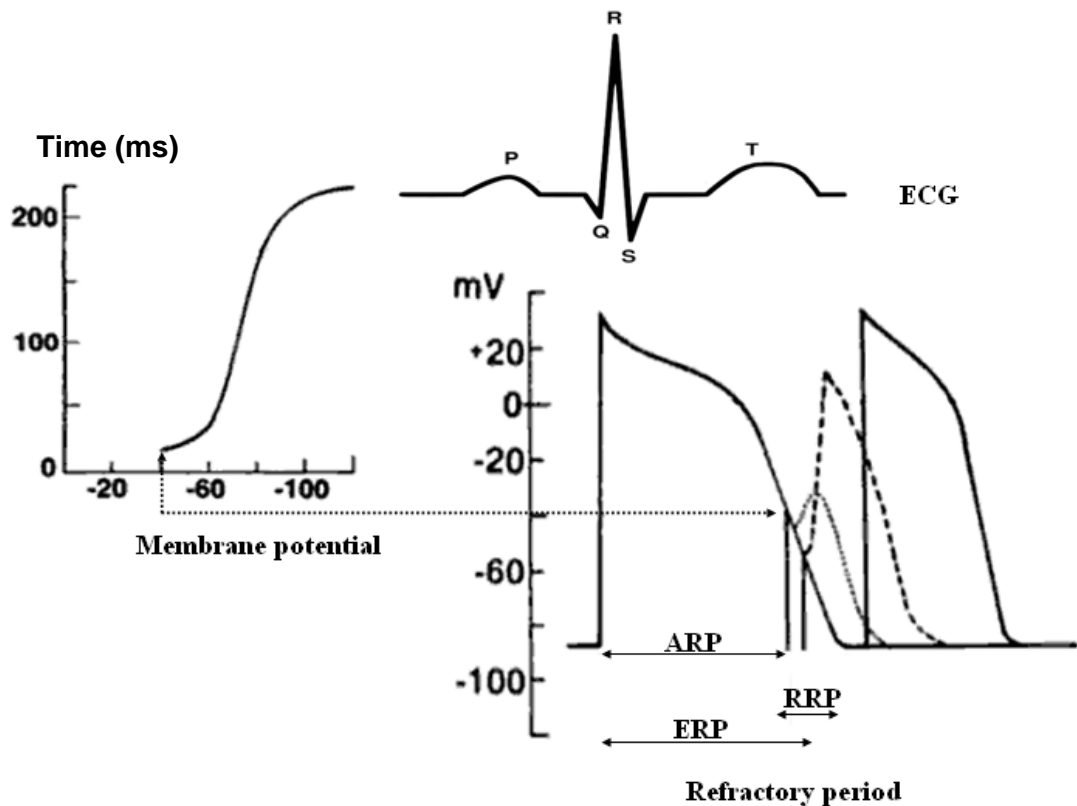


Figure 1.4 Refractory periods

Refractory period is important in arrhythmogenesis because it influences re-entrant circuit wavelength. The wavelength of cardiac impulse is defined as the distance between the depolarisation wave front and the newly repolarized tissue at the tail of the wave. It depends on both refractory period and conduction velocity, being the product of these two quantities: $\text{wavelength} = \text{RP} \times \text{CV}$ (Smeets *et al.*, 1986). The first study correlating repolarisation pattern with initiation of arrhythmias was performed using infarcted dog myocardium in 1985 (Gough *et al.*, 1985).

Repolarization time is measured directly from the AP which can be recorded in several ways. (i) Glass microelectrode (floating), (ii) suction electrodes, and (iii) optical mapping. Advantages and disadvantages of each method are:

(i) Voltage signals from a glass floating microelectrode impaled into a single cell on surface of the myocardium is one of the most accurate ways of recording transmembrane potential. But it is difficult to record for prolonged periods of time in a contracting muscle. Furthermore, simultaneous recording from more than one impalement site is technically difficult.

(ii) A suction electrode measures a potential difference between a small depolarised (damaged) region of the myocardium and the area of normal myocardium. This "injury potential" provides an accurate measurement of APD but cannot be used to measure absolute membrane potentials. The technique can be used to a limited extent to measure the dispersion of repolarization in the whole tissue with the use of multiple suction electrode units but the spatial resolution is limited to 1-2mm (Avitall *et al.*, 1988; Burton & Cobbe, 2001).

(iii) Signals from voltage sensitive dyes introduced into the myocardium have enabled optical techniques to be used to measure the APD across the surface of the myocardium (Efimov *et al.*, 1994; Efimov *et al.*, 2004; Burton & Cobbe, 2001). Optical techniques have been proposed to measure beat to beat changes in the dispersion of repolarization by use of optical mapping. Optical mapping makes it possible to obtain maps of activation, repolarization and refractory periods with high temporal and spatial resolution in intact beating heart. However, currently the recording of optical action potentials is limited to fixed locations therefore the movement of the tissue has to be reduced by using uncoupler agents such as

2,3- butanedione monoxime (BDM) and cytochalasin-D (cyto-D) (de Tombe *et al.*, 1992; Stapleton *et al.*, 1998). Moreover, recording the repolarization of OAPs is more likely to become distorted than the activation due to the delay between activation and muscle shortening (Burton & Cobbe, 2001).

Table 1.3 summarises the variety of ways to measurement of repolarization time and refractory period (Burton & Cobbe, 2001).

Method	Location	Can be used in vivo?	Maximum simultaneous recordings	Spatial resolution	Temporal resolution
Repolarization time					
Single cell microelectrode	Transmural ^a	No	1	Cell	High
Floating microelectrode	Surface, transmural in perfused wedge	No	~3	Cell	High
Optical mapping	Superficial	No	Hundreds–thousands	μm–cm	High
Monophasic action potentials	Surface	Yes	~12	cm	High
Activation–recovery intervals	Transmural	Yes	Hundreds	mm	High
ECG QT interval dispersion	–	Yes	1	??	High
Refractory period					
Extrastimulus technique	Transmural	Yes	1	mm	Low
VF intervals	Transmural	Yes	Hundreds	mm	Low

^a After dissociation.

Table 1.3 Techniques for measurement of repolarization time and refractory period

1.3.4 Cardiac electrical conduction system

The electrical conducting pathway in the heart comprised 5 elements: SAN, AVN, the bundle of His, left and right bundle branches and the Purkinje fibre network. This specialized conducting system produces a specific sequence of depolarisation coordinating contraction of atria and ventricles. The temporal change in magnitude and direction of the electrical fields accompanying depolarisation and repolarization can be detected as the difference in voltage between points on the body surface and represented in the ECG. Abnormalities in wave direction and corresponding changes in ECG configuration can be used as a tool for diagnosis in many cardiac pathologies including myocardial ischaemia and infarction.

1.4 Electrophysiology of myocardial ischaemia and infarction

1.4.1 Action potential and electrical conduction system

There are several publications which indicate that ST segment elevation is a marker of AMI (reviewed in (Kleber, 2000)). The two basic processes which determine the ECG changes in myocardial ischaemia are the changes in transmembrane AP and in cell-to-cell electrical coupling (Li *et al.*, 1998). Transmembrane AP is changed by a loss of membrane polarization during the diastole phase. This causes a decrease in amplitude and duration of AP, and a slowing of upstroke velocity (Fozzard, 1980; Nygren *et al.*, 2006). These changes occur within the first 10-15 minutes of perfusion being blocked and are thought to arise from: (i) changes in the metabolic state of the myocardium associated with the rapid onset of hypoxia and (ii) accumulation of K⁺ and extracellular and intra/extracellular acidosis associated with the restricted perfusion of the extracellular space (Fozzard, 1980; Fozzard & Makielski, 1985; Yan & Kleber, 1992; Rodriguez *et al.*, 2002). These changes are not uniform across the IZ since any remaining vascular flow pattern will influence the relative metabolic state of the tissue (Ehlert & Goldberger, 1997; Rodriguez *et al.*, 2002).

1.4.2 Cellular electrophysiology

1.4.2.1 Cardiac action potential

An enhanced diastolic relaxation is an early change in cardiac function observed after a few seconds of myocardial ischaemia and is followed by a decline in contractile function (Fozzard, 1980; Fozzard, 1985). These mechanical changes are the result of an accompanying decrease in APD.

There are two major mechanisms underlying the decrease in cardiac APD during ischaemia:

- (i) The accumulation of extracellular potassium (K_o) in the ischaemic tissue is the main factor determining resting membrane potential and contributes to the shortening of the cardiac APD (Elena *et al.*, 2008;Rodriguez *et al.*, 2002). Cardiac membrane potentials decrease from the normal baseline -80 and -95mV to between -50 and -60mV within minutes of myocardial ischaemia. This is accompanied by a decrease in duration and amplitude of the AP (Kleber, 1984;Janse *et al.*, 1977;Janse & Kleber, 1981;Kleber & Wilde, 1986;Yan *et al.*, 1989).

- (ii) APD is initially maintained during hypoxia/anoxia challenges suggesting that the raised K^+ is responsible for the initial APD changes. However, longer periods of hypoxia results in a dramatic decrease in APD which cannot be due to the accumulation of K_o^+ . The opening of ATP sensitive K^+ channels (K_{ATP}) triggered by lowered ATP concentration is thought to be the underlying mechanism, but it is unclear whether the small ATP depletion observed co-incidently with the shortening of the APD is sufficient to activate (Elliott *et al.*, 1989;Janse *et al.*, 1977;Janse & Wit, 1989;Kleber & Janse, 1982;Kleber & Wilde, 1986).

Other aspects of the action potential and the underlying ionic currents are altered during acute ischaemia:

- (i) On activation by depolarisation, the Na^+ channel kinetically moves from a closed to an open state and subsequently to an inactive state. Before the channel can be activated again, the channel has to recover from the inactive state to the closed state. The rate and extent of recovery depends on membrane potential, if as is the case in ischaemia, the membrane potential is depolarised compared to normal, proportionately more Na^+ channels will exist in the inactive state during the diastolic period and there less Na^+ channels will be available for the subsequent action potential (Scamp & Vassort, 1994). Therefore, membrane excitability is reduced during ischaemia, leading to reduction in maximum rate of depolarisation or V_{max} , an effect that reduces the conduction velocity of the action potential.

(ii) The inward (L-type) Ca^{2+} current is not much affected during early ischaemia and is not thought to contribute to the changes in APD (Allen & Orchard C.H., 1983).

The effects of ischaemia are not necessarily uniform across the ventricular myocardium. Studies of isolated myocardial cells report that APDs and upstroke velocities are reduced more in sub-epicardial cells than in sub-endocardial cells isolated from the same heart and experiencing the same ischaemic conditions. The major difference in cardiac electrophysiology across the transmural surface is the amplitude of I_{to} component which is significantly larger in cells isolated from the epicardium than in endocardium.

1.4.2.2 Excitation-contraction coupling during ischaemia

The processes linking electrical excitation to contraction is summarised in Figure 1.5 (Bers, 2002). Briefly, the L-type Ca^{2+} current triggers the release of larger amount of Ca^{2+} from the sarcoplasmic reticulum (SR) by acting of the SR Ca^{2+} release channels (ryanodine receptors - RyR2). This Ca^{2+} binds to and activates the contractile proteins to cause the subsequent contraction. Ca^{2+} is resequestered back into the SR via the sarcoplasmic/endoplasmic Ca^{2+} -ATPase (SERCA) and a small amount of Ca^{2+} equivalent to the L-type mediated influx is removed from the cell on every beat mainly via the NCX.

During ischaemia, the level of intracellular Ca^{2+} increases because of the rise of intracellular H^+ reduces the ability of NCX to extrude intracellular Ca^{2+} to the extracellular space. Furthermore, protons are thought to compete for Ca^{2+} on the Ca^{2+} binding sites (predominately the contractile proteins) within the heart. The displacement of Ca^{2+} with protons contributes to the rise of free Ca^{2+} concentration when the intracellular conditions become acidic. Finally, acidic conditions reduce the rate of SR uptake via the SERCA (Chou & Chen, 2007;Corretti *et al.*, 1991;Xia *et al.*, 1998b;Samie *et al.*, 2000). The sum of these effects result in contractile failure and may contribute to the occurrence of early after-depolarisation (EAD) and delayed after-depolarisation (DAD) (Burashnikov & Antzelevitch, 1998;Cha *et al.*, 1994;Coronel *et al.*, 2002;Efimov *et al.*, 1994;Ehlert & Goldberger, 1997;Gough *et al.*, 1985).

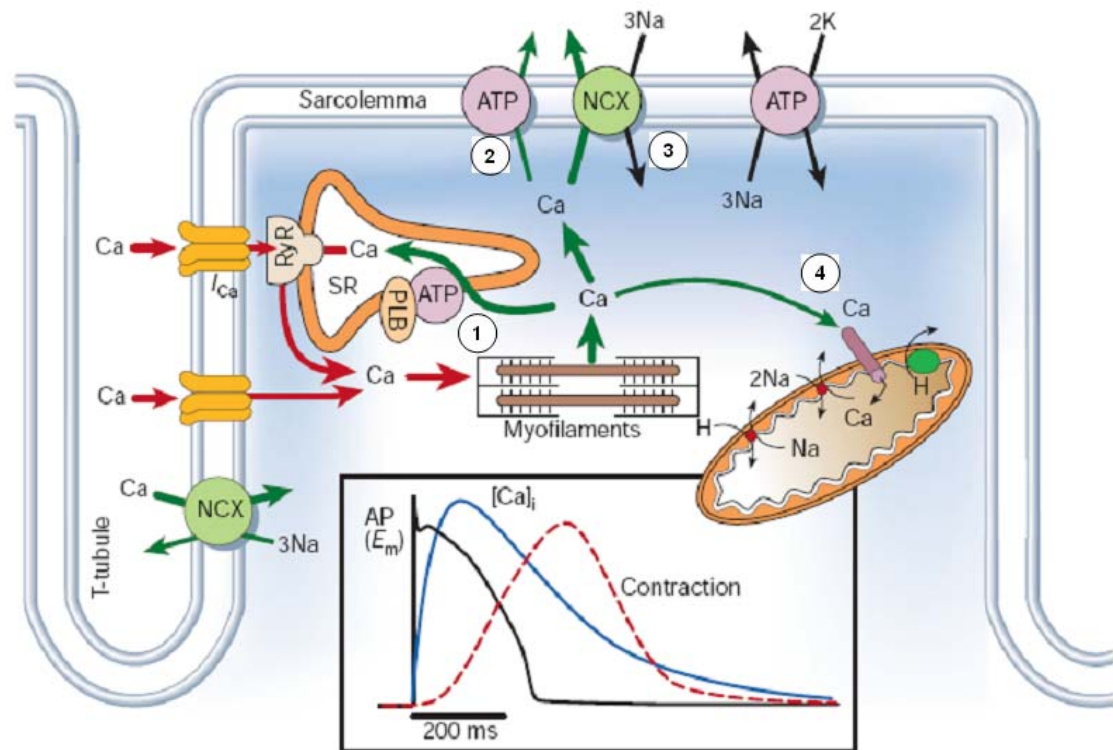


Figure 1.5 The transportation of Ca^{2+} in the ventricular myocyte

The inserted small picture shows the time course of an AP, Ca^{2+} transient and contraction in a rabbit ventricular myocyte. Ca^{2+} enters to the cell by depolarisation-activated Ca^{2+} channels (I_{Ca}) that contributes to the phase 2 of action potential (plateau). Ca^{2+} entry induces Ca^{2+} release from SR and this increases free intracellular $[\text{Ca}^{2+}]$ which is followed by muscle contraction from the binding between Ca^{2+} and myofilament troponin C. In the relaxation processes, $[\text{Ca}^{2+}]$ decreases, Ca^{2+} leave the cytosol through the 4 pathways as represent by (1), (2), (3) and (4) (Adapted from Bers, 2002).

During myocardial ischaemia, oxidative phosphorylation and mitochondrial ATP production are disturbed; Mg^{2+} -ATPase and Na^+ - Mg^{2+} exchanger channels may lose the ability to remove Mg^{2+} subsequent to an increase in cytoplasmic Mg^{2+} (Dubey & Solomon, 1989; Hix, 1993). These Mg^{2+} changes may influence the behaviour of other channels and their carrier abilities such as blocking NCX and causing inward rectification of the K^+ channels (Pinto & Boyden, 1999).

1.4.2.3 Myocardial tissue properties

As described above there are several changes in the cellular electrophysiology of myocardial cells during ischaemic zone that will increase tissue heterogeneity of

APD may be a substrate for arrhythmias (Cascio *et al.*, 2005; Cabo & Wit, 1997; Cascio *et al.*, 1995). Another aspect of the electrophysiology of the heart cells is post-repolarization refractoriness, raised extracellular K^+ in the ischaemic zone results in a longer refractory period in the ischaemic area compare to the normal area contributing to inhomogeneity of electrophysiology between two zones. (Janse *et al.*, 1979; Janse *et al.*, 1977; Janse & Wilms-Schopman, 1982).

1.4.2.4 Changes in conduction velocity during ischaemia

The changes in the cellular action potential during ischaemia can also have a considerable impact on propagation conduction velocity (Kleber & Janse, 1982; Kleber & Wilde, 1986). These effects can be summarised below:

- (i) Accumulation of extracellular K^+ may raise the conduction velocity by bringing membrane potential closer to the threshold.
- (ii) The fall of action potential upstroke velocity and amplitude decreases conduction velocity.

The net effect of all these two opposing influences will depend on the extent of the rise of extracellular K^+ . Previous studies have shown that 2-3mM increases in K_o^+ will cause minor increases in conduction velocity while larger changes (5-8mM) decrease conduction velocity (Spach *et al.*, 1988; Mizumaki *et al.*, 1993)

1.5 AMI and Chronic myocardial infarction

1.5.1 Role of Gap junction on myocardial ischaemia and infarction

The main component of the gap junction associated with electrically active tissue is protein connexin (Cx). The ventricular cardiomyocyte expresses multiple Cx isotypes, for example, Cx43, Cx45 and Cx40. The most abundant in the heart tissue is the 43 kDa isoform connexin or Cx43 (Alex *et al.*, 2005). Conduction velocity is normally anisotropic, i.e. faster (~60cm/s) along the main myocardial fibre axis and slower (~30 cm/s) along an angle transverse to the

main fibre direction. Intracellular acidosis and an increase in intracellular Ca^{2+} during myocardial ischaemia induces longitudinal movement of connexins from the intercalated disc region to lateral surfaces of the cardiomyocyte (Duffy *et al.*, 2002) resulting in a reduced longitudinal conduction velocity and altered anisotropy of conduction velocity. This is due to the preferential orientation of gap junctions at the intercalated discs of the heart cells over a period of 1-2 hours (de Groot & Coronel, 2004; Owens *et al.*, 1996).

Further ischaemia results in cellular uncoupling due to increases of intracellular Ca^{2+} causing the uncoupling of gap junctions and the electrical isolation of the IZ (4-8 hours) (Cascio *et al.*, 2005; Boengler *et al.*, 2005; Lindsey *et al.*, 2006; Lerner *et al.*, 2001; de Groot & Coronel, 2004). Rat ventricular myocytes that are subjected to 5 hours hypoxia showed marked reduction in the number of Cx43 compared with normoxic myocytes (Lerner *et al.*, 2001). In addition, gap junctions are implicated in the genesis of ischaemic preconditioning (IP) during myocardial ischaemia-reperfusion (Boengler *et al.*, 2005). IP initiates a redistribution of Cx43 from the natural position in the gap junction toward the free plasma membrane (Vetterlein *et al.*, 2006; Severs *et al.*, 2004) (Figure 1.6).

Although the detrimental effects of connexin changes have been implicated in the generation of arrhythmias, these changes may have an important protective role by reducing the transfer of cytotoxic metabolites from the ischaemic to normoxic zones (Cascio *et al.*, 2005; de Groot & Coronel, 2004; Lerner *et al.*, 2001).

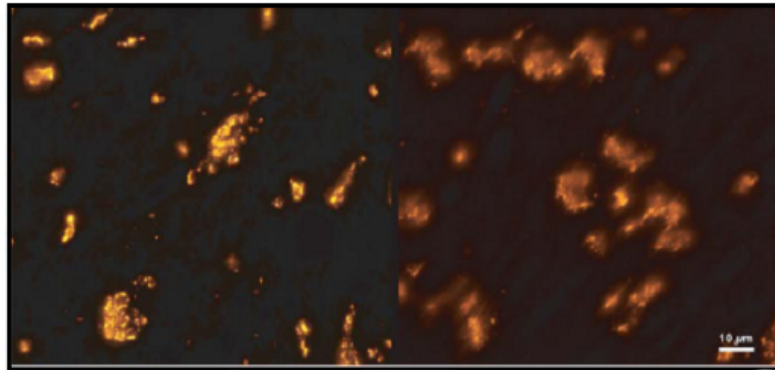
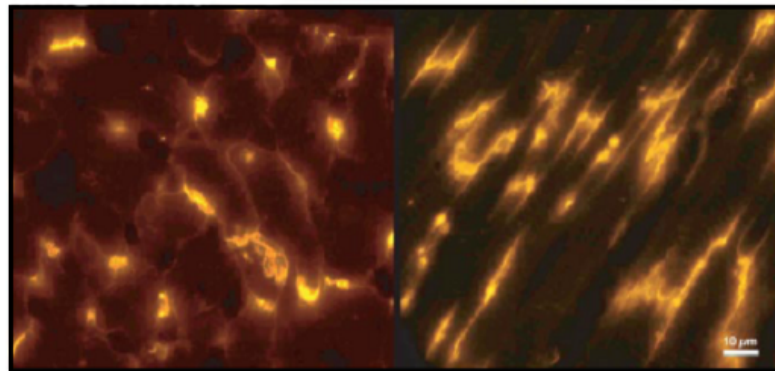
A: Non ischaemic**B: 15 min ischaemia**

Figure 1.6 Cx43 immunofluorescence micrographs

Adapted from (Vetterlein *et al.*, 2006). Tetramethylrhodamine isothiocyanate labelled cross sections (*left*) and longitudinal sections (*right*) of rat myocardium exposed to control conditions, i.e., no ischemia (*A*), Ischaemia 15 min (*B*). The immunostaining resulted from labelling of plasma membrane outside gap junctions. Panel B shows the effects of 15 minutes of ischaemia on Cx43 distribution. At the end of a continuous 15 minutes period of ischaemia, the immunofluorescence appeared to have spread out of the gap junction without having reached the entire circumference of the cell when compared with non ischaemic cell.

1.5.2 Border zone as an arrhythmogenic site during myocardial ischaemia and infarction

The border zone (BZ) of myocardial infarct (permanently occluded coronary artery) is defined as boundary between infarcted and normal myocardium. BZ is the area of reversibly damaged myocardium next to an evolving infarct and within the area supplied by the occluded artery. In the dog coronary artery ligation model of MI, the BZ has been shown to extend up to 4 mm outside the

sub-epicardial edge of infarcts less than 5 hours old. In this preparation, BZ is predominantly sub-epicardial and varies with the degree of pre-existing collateral circulation (Gottlieb *et al.*, 1981).

The characteristics of the BZ are not yet well understood. The number and pattern of surviving myocytes in the sub-epicardium and sub-endocardium is species dependent:

(i) Canine hearts have a well-developed epicardial collateral circulation that maintains perfusion after coronary occlusion. Coronary artery occlusion for ~30 mins causes the development of necrotic tissue within the sub-endocardium of the left ventricle as shown in Figure 1.7. Over 3-4 hrs, this area of necrosis spreads to the epicardial surface but leaves a distinct rim of epicardial myocytes (~300µm thick). Within 12 hrs, the wavefront of necrosis has extended to the endocardium, only the strands of Purkinje fibres survive on the endocardium surface (Fenoglio J.J.Jr *et al.*, 1979). The connective tissue and fibroblasts replace necrotic tissue over the subsequent 6-8 weeks, but the Purkinje fibres and epicardium rim remain (Fenoglio J.J.Jr *et al.*, 1979;Friedman *et al.*, 1975). The availability of epicardial rim (frequently referred as epicardial BZ) has been used in many electrophysiological studies (Fenoglio J.J.Jr *et al.*, 1979;Bolick *et al.*, 1986;Luke & Saffitz, 1991;Ursell *et al.*, 1985).

(ii) Human hearts have a less prominent epicardial rim than canine hearts (Bolick *et al.*, 1986), and a larger surviving sub-endocardial rim with several layers of cardiac myocytes including Purkinje fibres (Bolick *et al.*, 1986). Correlation of infarct structure with cardiac electrophysiology in humans is still unclear because of ethical and technical reason.

(iii) Rabbit hearts have a prominent sub-endocardial rim of myocytes and a thin scattered rim of epicardial myocytes similar to that reported in humans (Burton *et al.*, 2000). The infarct contained numerous fibroblasts suggesting that active connective tissue deposition was still in process. This will be correlated with the underlying structure and offer possibility of understanding the electrophysiological consequences of various infarcted structures.

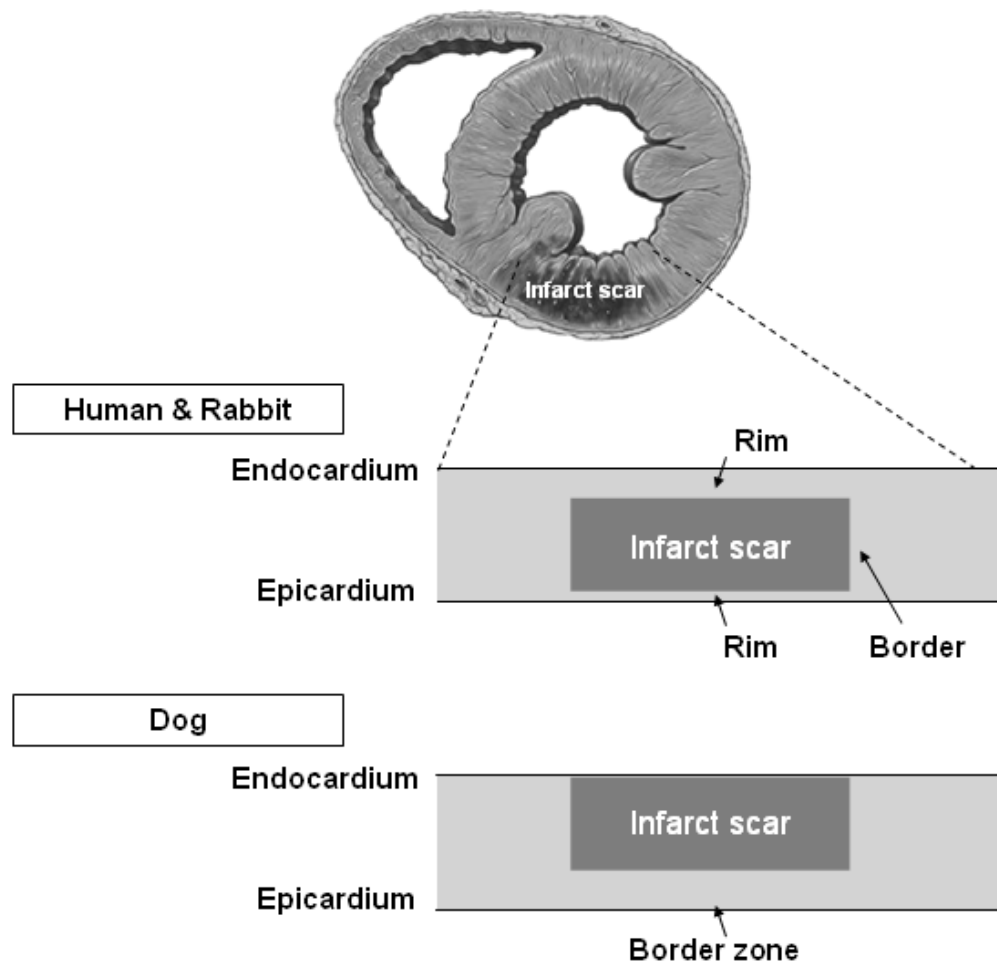


Figure 1.7 Structure of infarct depend on species in human, rabbit and dog

After 150 minutes of myocardial ischaemia produced by occluding the coronary artery, the BZ contained injured viable myocardial cells. Perfusion was partially retained inside the BZ, and could be reversed by reperfusion (Sladek *et al.*, 1984). There is evidence to suggest that the conduction delay during AMI is greater in the subepicardium BZ than in subendocardium region. Thus, the border zone may be the source of triggered activity and may also be involved in promoting re-entrant arrhythmia (Cha *et al.*, 1994; Kleber & Fast, 1997; Bernus *et al.*, 2005; Abe *et al.*, 1989).

The BZ presents a variety of electrophysiological properties and metabolic changes (Cox *et al.*, 1973). Differences in extracellular K^+ and pH between ischaemic and normoxic sites may allow the diffusion of these ion currents between two sites leading to a gradient of ion and electrical properties between normoxic and ischaemic zones as shown in Figure 1.8

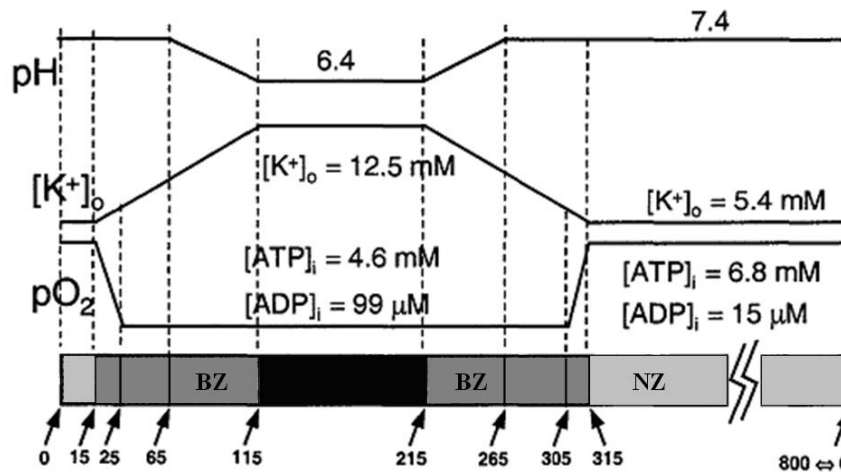


Figure 1.8 Values of $[K^+]_o$, pH, $[ATP]_i$ and $[ADP]_i$ along the 1-dimensional strand

Numbers of the bottom indicate cell number. Black area represents IZ, BZ stand for the border zone, and NZ is a normal zone (Ferrero *et al.*, 2000).

1.5.3 Myocardial ischaemia and reperfusion injury

Myocardial ischaemia can be reversed by reperfusion and early reperfusion can allow the recovery of ischaemic tissue. Myocardial ischaemia-reperfusion is associated with a rapid restoration of perfusion and re-energizing of the myocardium. However, reperfusion may also cause myocardial tissue damage (Zhao & Vinten-Johansen, 2006). Prolonged occlusion more than 20 minutes can cause persistent tissue damage and cellular remodelling including: (i) disruption of sarcolemma and myofibril, (ii) cellular oedema, (iii) ultrastructural damage, and (iv) Ca^{2+} phosphate deposition in intra-mitochondria space. These changes in myocardial tissue properties lead to irreversible tissue injury after reperfusion (Lalu *et al.*, 2005; Yellon *et al.*, 1992; Neumann *et al.*, 1997; Gunduz *et al.*, 2006).

Two important cellular mechanisms that mediate myocardial reperfusion injury are cellular Ca^{2+} loading and free radical formation (Peuhkurinen, 2000; Corretti *et al.*, 1991; Yellon & Baxter, 2000; Giordano, 2008). Myocardial ischaemia followed by reperfusion promotes free radical formation which appears primarily to be the phenomenon causing myocardial injury in many investigations (Asimakis & Lick, 2002; Yoshida *et al.*, 2000).

There are several oxidant and free radical mediators which may play a role in reperfusion injury. Obvious candidates are reactive oxygen species (ROS), nitric oxide synthase (NOS) and enzyme xanthine oxidase, all of which are greatly increased in the ischaemic heart. Free radicals such as ROS are very reactive; they can initiate peroxidation of unsaturated fatty acids and phospholipids, and can disrupt the activities of mitochondria and cellular membrane via inactivation of membrane enzymes. The main mechanisms that produce ROS are shown in Figure 1.9 (Seshiah, 2002; Xia *et al.*, 1998b; Xia *et al.*, 1998a; Griending *et al.*, 2008; Sawyer, 2002). Understanding the major roles of these free radicals in ischaemia reperfusion injury may provide pointer to clinical treatment of acute coronary syndrome.

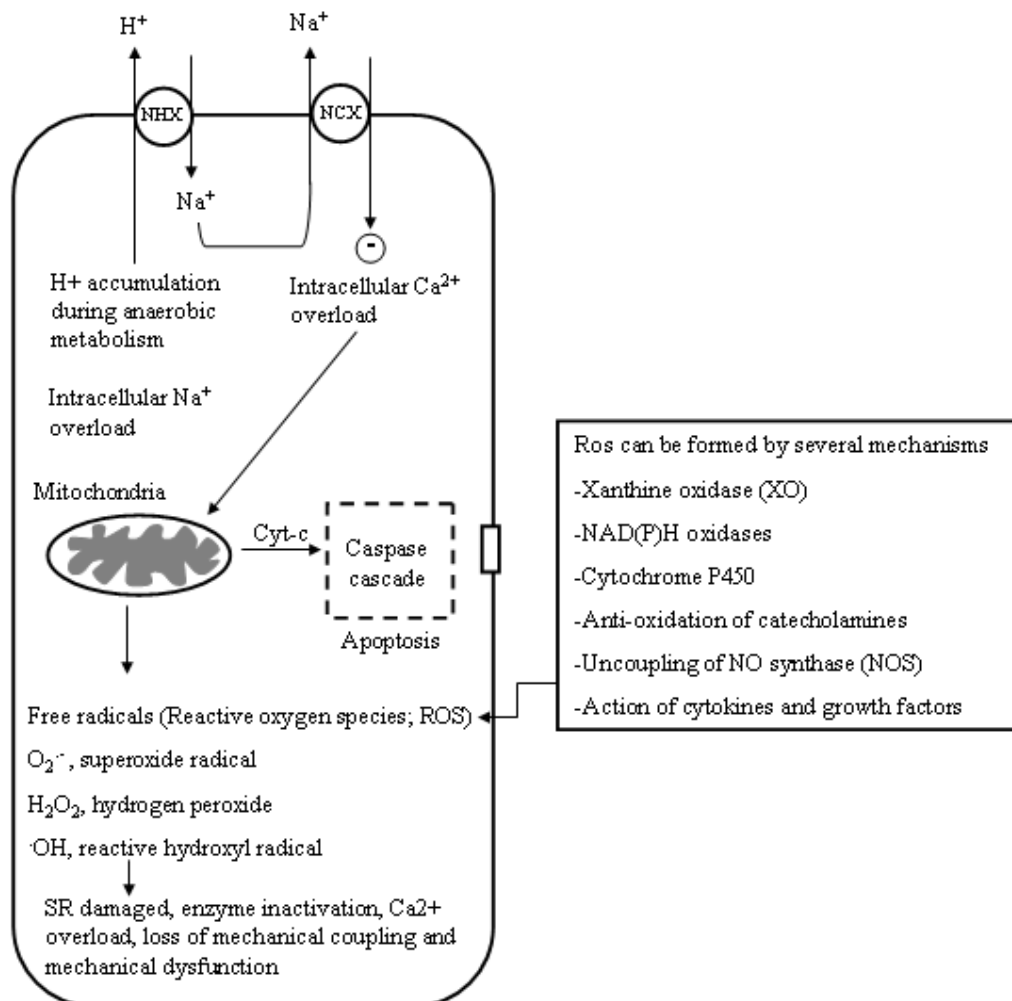


Figure 1.9 The figure summarises evidence of myocardial ischaemia-reperfusion injury

Intracellular accumulation of protons during ischaemia induces the activation of sarcolemma sodium-hydrogen exchanger (NHX) and consequent to intracellular Na⁺ overload. Na⁺ overload

causes the activation of sarcolemma Na^+ - Ca^{2+} exchanger (NCX) and intracellular Ca^{2+} overload. Ca^{2+} overload and oxidative stress after ischaemia and reperfusion act as stimulators of apoptosis. These changes open mega channels in mitochondrial membranes and cause efflux of mitochondrial constituents such as, cytochrome c (Cyt-c). Cyt-c can act as the messenger for caspase activation and cell death through apoptosis. Myocardial ischaemia-reperfusion makes the alteration in myocardial oxygen consumption and leads to generation of reactive oxygen species products or ROS. These products have a significant effect on cardiac function, including hypertrophy, ion flux and Ca^{2+} handling, EC coupling, extracellular matrix configuration, metabolism, gene expression and downstream signalling of several growth factors and cytokines.

1.5.4 Cardioprotection: preconditioning and postconditioning

Protection of the heart from reperfusion injury is afforded by ischaemic preconditioning (IPC) and ischaemic postconditioning (IPost). IPC was first discovered in 1986 as the potent intervention for reducing myocardial infarct size, it is defined as one or more cycles of 5-10 minutes of myocardial ischaemia followed by short period of reperfusion (Yellon *et al.*, 1992; Yellon & Opie, 2006; Vinten-Johansen *et al.*, 2005; Schulz, 2000; Gross & Gross, 2006; Murray *et al.*, 1986). There are many mediators of IPC protection for example, adenosine, bradykinin, catecholamines and acetylcholine. These bind to specific receptors, activation of which leads to activation of protein kinase C which in turn has a downstream signalling cascade. One of these is the Reperfusion Injury Salvage Kinase pathway (RISK) which leads to phosphorylation of ATP sensitive K^+ channel in sarcolemma or mitochondrial membranes (Mt-K_{ATP}). Opening of the Mt-K_{ATP} channel enhances myocyte viability during ischaemia by preserving mitochondria integrity and ATP generating capacity thus reducing myocyte death and the subsequent myocardial infarct size. Many studies report that intracellular acidosis and ischaemic injury are less severe in IPC than in non-preconditioned myocardium. Moreover, reperfusion induced arrhythmias are also less common in this condition.

IPost is defined as brief periods of reperfusion alternated with myocardial ischaemia during the early stages of reperfusion (Zhao & Vinten-Johansen, 2006). The duration of reperfusion and ischaemic periods are measured in seconds shorter periods are appropriate in small species (10-15 seconds in rats and mice), while longer periods are effective in larger animals (30 seconds in dogs and rabbits) and approximately 60 seconds is appropriate for humans (Staat

et al., 2005). IPost also demonstrates cardioprotective effects whose mechanisms are mediated by ligands such as adenosine and opioids as similar as IPC. The concept of using IPost therapeutically was introduced in 2003; it offers a treatment that can be applied at the time of myocardial reperfusion and gives a new strategy for cardioprotection (Zhao *et al.*, 2003). IPC and IPost are shown in Figure 1.10.

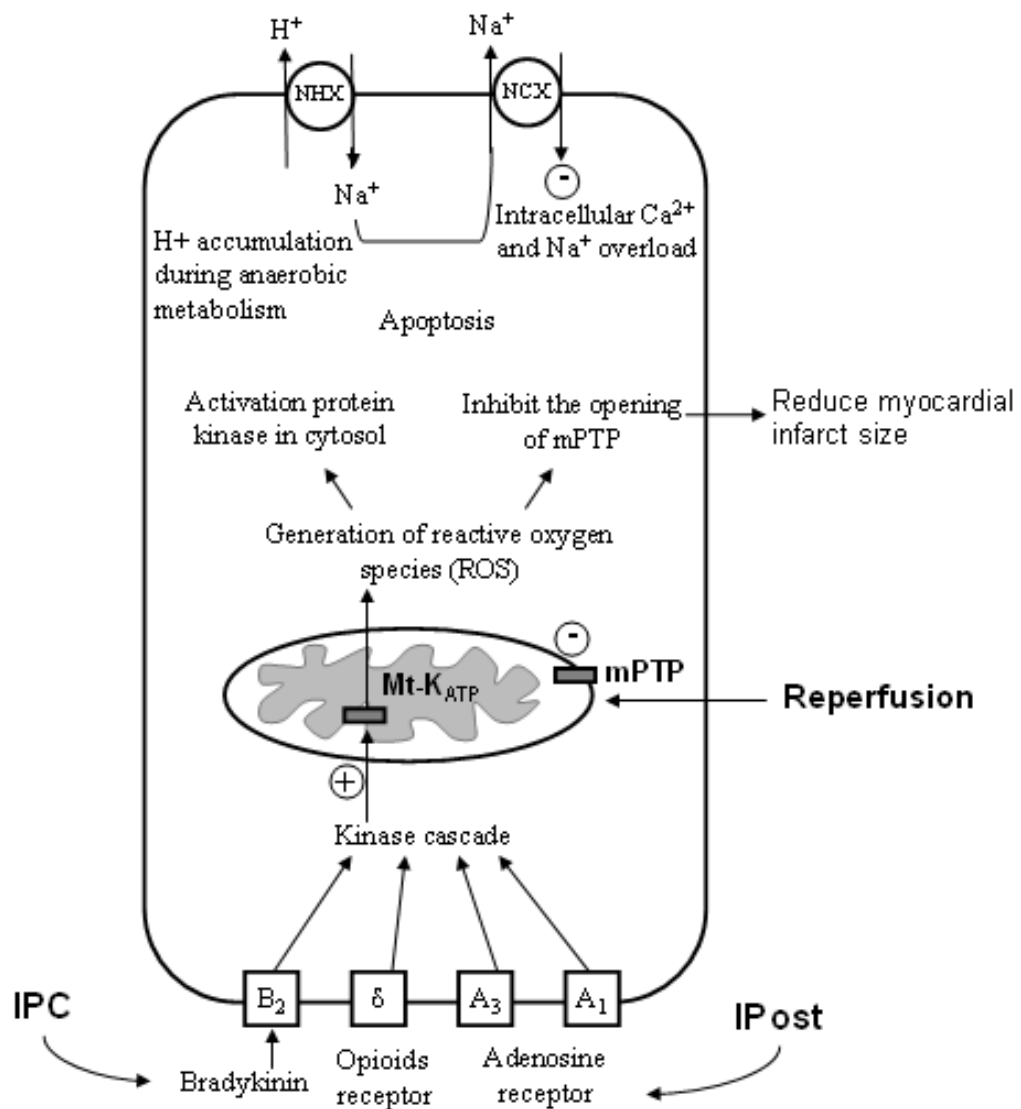


Figure 1.10 Summary of IPC and IPost mechanisms

1.6 Cardiac arrhythmias

1.6.1 Basic mechanisms

Cardiac arrhythmias are caused by abnormal impulse initiation or abnormal impulse conduction, or both. Abnormal formation of electrical impulse is the result of abnormal automaticity or triggered activity. For instance, increases in the automaticity of the SAN results in rapid heart rate by increasing the rate of impulse generation. The term triggered activity describes impulse initiation which is dependent on after-depolarisation (Wit & Janse, 1993).

An abnormal spontaneous impulse from a site other than SAN, such as AVN, Purkinje fibres, or ventricular muscle fibres, arises at a higher rate than impulse from the normal sinus and causes a premature depolarisation. Increases in automaticity of the SAN or other cardiac fibres by enhancing activity of sympathetic nervous system or inhibiting parasympathetic activity can also cause arrhythmias. Many factors including anti-arrhythmic drugs may lead to abnormal increases in automaticity and triggered activity for example, hypoxia, digitalis toxicity, hypokalaemia and hypomagnesaemia (Nuss *et al.*, 1999).

Abnormal impulse conduction is the other major class of arrhythmias. This can be further subdivided into block of impulse conduction and re-entrant conduction. Re-entry is defined as an impulse that re-excites the same volume of tissue repeatedly after the end of refractory period.

Re-entry initiation requires the existence of three conditions, (i) two pathways for impulse propagation, (ii) decrease in conduction velocity, and (iii) unidirectional conduction block. The block can consist of either a physical barrier for example a non-conducting section of an infarct or a functional block that can result from heterogeneous prolongation of refractoriness. The process of re-entrant circuit formation is illustrated in Figure 1.11 (Wit & Janse, 1993).

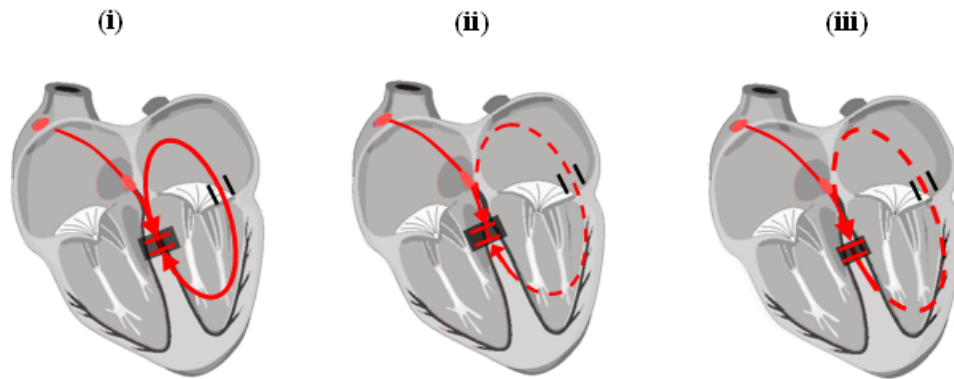


Figure 1.11 Initiation of re-entrant circuit of the atrio-ventricular junction

Slow impulse conduction represented by dashed line (---) (i) Bidirectional conduction block does not result in a re-entrant loop. (ii) Slow impulse conduction in one downstream direction with normal refractoriness in other direction, the retrograde impulse may re-enter the area of unidirectional block. (iii) Prolongation of refractory period in one downstream direction with normal downstream conduction in other direction which results in unidirectional conduction block, the retrograde impulse may re-enter the area of block and can be initiated tachyarrhythmia.

Several mechanisms can give rise to the unidirectional conduction block involving active and passive electrical properties of the cardiac cells. For instance, regional differences in refractoriness that determine the differences in ERP between two adjacent tissue regions. Here AP conduction may be blocked in the region with the longest ERP but can continue through the region with shorter ERP.

Unidirectional conduction block is also associated with depolarized transmembrane potentials and reduced excitability of cardiac fibres. For example, impulses can propagate across a poorly perfused region of myocardium (e.g. IZ) to emerge and activate a normally perfused region, but because depolarising currents from the poorly perfused region may be insufficient to depolarize the healthy myocardium, conduction may be blocked.

Another property that influences block is tissue architecture, such as the sudden changes in cell diameter or membrane area. A block can occur when the impulse travels from a small diameter of fibre to a larger diameter fibre with an abrupt transition in diameter at the junction. Here the conduction velocity transiently slows because the current sink created by the larger tissue may be of sufficient

size as to be prevent the larger membrane area reaching threshold for AP generation i.e. there is a source-sink mismatch (Wit & Janse, 1993).

The parameter called safety factor (SF) is another consideration for initiating block and has been defined as a quantitative parameter related to propagation. SF has given interesting insights to action potential propagation processes and conduction block. Romero. et al (Romero *et al.*, 2007) reported an analysis of re-entry taking into account SF during regional acute ischemia. This study suggested that a low safety factor is thought to be the cause of conduction block.

Anatomical re-entry can describe as an anatomic block. The wave front is fixed in location because of the block. In contrast, functional re-entry does not require a fixed anatomical substrate. Instead, the re-entrant circuit is formed in one of several possible ways (El-Sherif *et al.*, 1981):

- (i) In leading circle re-entry, the circuit propagates around a refractory core.
- (ii) In figure of eight re-entry, the two rotating waves circulate simultaneously clockwise and anticlockwise around the block.
- (iii) In spiral wave re-entry, a single wave is the interaction between wavefront and tail during rotation and results in variable of the waves (Allessie *et al.*, 1990).

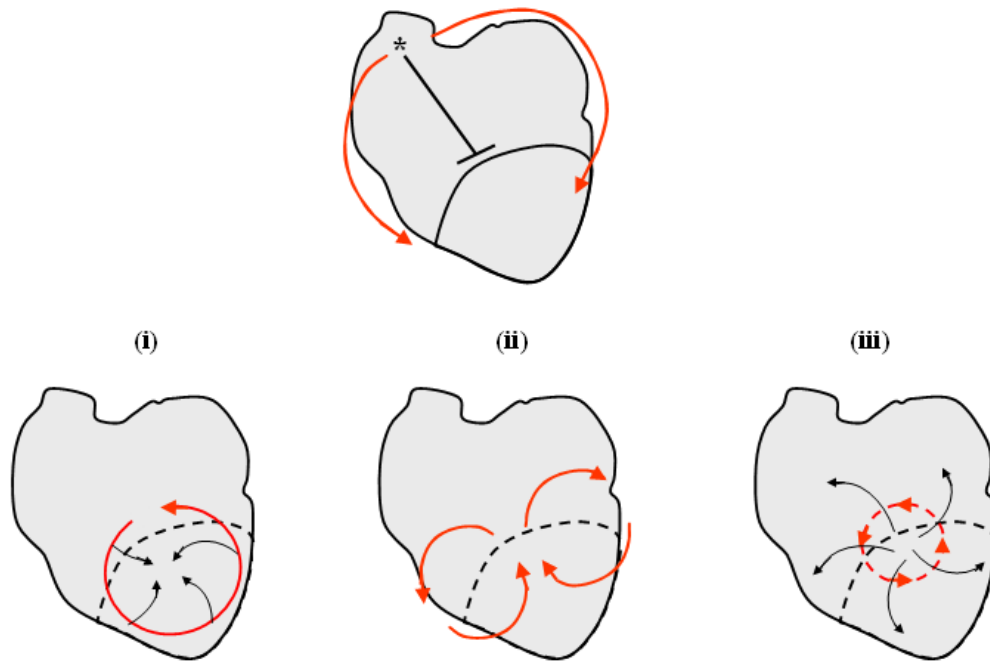


Figure 1.12 Functional re-entry

The impulse arising at (*) and spread through the myocardium. The conduction block represents by (—). (i) Re-entry impulse propagates centripetally (Leading circle). (ii) Continuous circulation wave reenters round from the other sides of heart (Figure of eight). (iii) Core excitable generates a spiral wave.

Spatial electrophysiological inhomogeneities during myocardial ischaemia are thought to contribute to development of life threatening arrhythmia including ventricular fibrillation. VF is defined as a large amount of irregularity in the electrical waves during ventricular excitation (Cha *et al.*, 1994). VF is initiated by rapid and asynchronous excitation of ventricle which changes in several aspects of ECG such as frequency, contour and amplitude (Hongo *et al.*, 1997). However, the mechanisms underlying the onset and maintenance of VF remain poorly understood.

Several factors are likely to be involved in facilitating VF for example, EADs and DADs believed to be a trigger for re-entry (Gelzer *et al.*, 2008; Bers, 2001). The two types of trigger activity, EADs and DADs are illustrated in Figure 1.13, EAD is an abnormal depolarisation which occurs during phase 2 and 3 of the membrane potential and results in lengthening of T-wave in ECG.

On the other hand, abnormal depolarisation which begins during phase 4 after complete repolarization is DAD. EADs can be induced by increasing the stimulation rate when in a Ca^{2+} overloaded state. Some evidences suggested that in the heart failure model, EADs is independent of the concentration of intracellular Ca^{2+} . In contrast, DADs can be triggered by an overload of Ca^{2+} and are associated with upregulating NCX (Burashnikov & Antzelevitch, 1998; Nuss *et al.*, 1999; Rosen MR *et al.*, 1973; Pogwizd *et al.*, 1999).

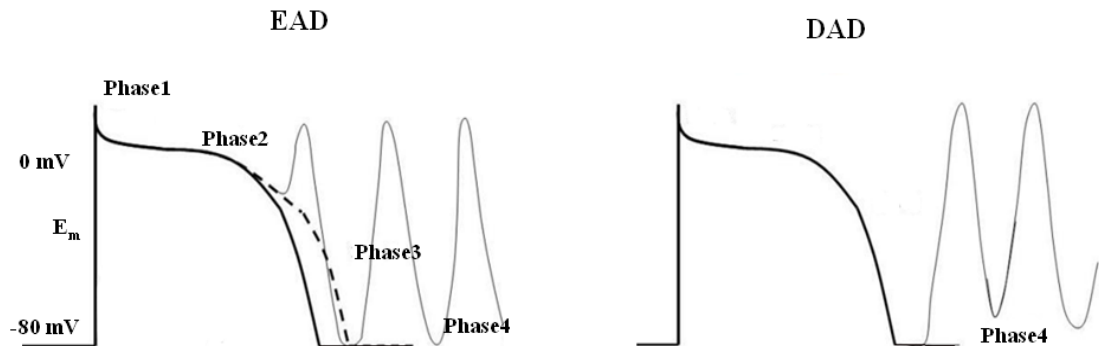


Figure 1.13 Diagram of the timing of EAD and DAD

In addition, the wave break may provide a fragmentation of spiral waves that causes the increasing of rapid and irregular spiral wave. This can lead to sustained VF. VF can be terminated in the early stage of its initiation and is more difficult after more than 2 minutes of the onset (Cha *et al.*, 1994; Gray *et al.*, 1995; Indik *et al.*, 2006; Gelzer *et al.*, 2008). The understanding of the underlying mechanisms associated with ischaemia induced VF will help design optimal procedures to terminate ischaemia-induced VF.

1.6.2 Ventricular arrhythmias in myocardial ischaemia and infarction

Research over the last 100 years has revealed two phases of vulnerability to ventricular arrhythmias in experimental animal models of coronary artery occlusion: (i) early and (ii) late arrhythmias (Lewis, 1909). A similar two phases of ventricular arrhythmias was reported by Harris in the 1950s termed "Harris phase I" appearing after 10-30 minutes of coronary artery occlusion, and "Harris phase 2" appearing after 6-8 hours (Harris & Rojas, 1943; Harris, 1950).

Currently, ventricular arrhythmia during the first hour of myocardial ischaemia is divided into 2 phases: immediate ventricular arrhythmia or phase 1A occurs from 2-15 minutes of ischaemia, and delayed phase or phase 1B occurs from 15-30 minutes of ischaemia (Coronel *et al.*, 2002;de Groot *et al.*, 2001).

The phase 1B arrhythmia is believed to be related to gap junction uncoupling (Cascio *et al.*, 2005). However, the exact time and mechanisms of arrhythmogenesis during AMI, whether the arrhythmias rise during phase 1A or 1B, whether they are re-entrant or non-re-entrant in origin and whether the mechanisms linking electrical and metabolite changes are still unclear (Cascio *et al.*, 1995;Kleber & Fast, 1997;Rosenbaum & Jalife, 2001;Wit & Janse, 1993).

1.6.3 Cardiac mechano-electric feedback and the relationship to arrhythmias

Mechano-electric feedback (MEF) is defined as the intracardiac pathway that leads from changes in the cardiac mechanical environment to alter electrical activity. Clinical observations of mechanically induced heart rhythm disturbances have been reported by Meola, F in 1879 (Meola, 1879). The first report of cloning of mechano-sensitive ion channels was in 1994, followed by identifying the first stretch-activated channels (SAC) and then confirmation of the involvement of SACs in atrial arrhythmogenesis in 2001 (Bold *et al.*, 2001).

Mechanical events e.g. stretch can modulate the electrophysiology of the heart cell via a variety of mechano-sensitive ion channels that have been identified over the years. Chloride, potassium, nonselective cation ion channels and also some ion transporters (Na^+/H^+ exchanger) have all been implicated. Through this route, mechanical factors can be the arrhythmogenic, e.g. acute stretch initiates atrial fibrillation (AF) and applying of stretch-activated channel blocker terminates the AF (Bold *et al.*, 2001). Similarly the acute and chronic mechanical stimulation of ventricle can be the arrhythmogenic via the same set of these mechanisms (Janse *et al.*, 2003). However, the clinical importance of mechano-electric feedback in the development of arrhythmias still needs the further investigation.

MEF is important in the context of this study because contraction is routinely inhibited using uncoupling agents (see Methods). This means it is not possible to directly address the arrhythmic mechanisms that depend on MEF-related phenomena in this study.

1.6.4 Assessment of arrhythmogenic status of the myocardium

In the study of arrhythmias, direct electrical recording from the *in situ* heart is impractical. Often, an indirect approach is used to study arrhythmogenic potential of the myocardium in particular electrical stimulation is commonly used to determine the ease which tachycardia and ventricular fibrillation can be induced. The two main types of stimulation protocol used are (i) overdrive stimulation and (ii) programmed premature stimulation.

(i) Overdrive stimulation involves stimulating the ventricle at a faster rate than sinus rhythm. The number of stimuli in the overdrive train and the cycle length may be varied. Interestingly, a number of studies suggest that arrhythmias caused by automaticity are tolerant to overdrive stimulation (Gelzer *et al.*, 2008). The tachycardic pacing is maintained for a significant period of time before stopping stimulation and examining whether the heart returns to the normal previous sinus rate or maintains a ventricular tachycardia.

(ii) Programmed stimulation of the ventricle involves delivering single or multiple premature stimuli to the ventricle during the cycle length of the dominant rhythm. The programmed extra-stimulus is applied earlier than the next expected rhythm. (Burashnikov & Antzelevitch, 1998). The timing and number of extra-stimuli can be varied, but the arrhythmogenic potential is assessed from the amplitude of stimuli required to induce ventricular tachycardia.

These approaches have been used by numerous studies to assess the threshold for arrhythmias but they do not necessarily represent the common pathophysiological situation.

The purpose of this study was to investigate the ability of the common trigger for ventricular arrhythmias, i.e. occlusion of the coronary artery to alter the activation pattern of the ventricle.

1.7 Model of AMI in the isolated whole heart

1.7.1 Global myocardial ischaemia

Myocardial ischaemia is defined as a sudden interruption of the coronary flow leading to insufficient blood supply to the myocardium. Coronary artery occlusion in humans most often happens from the result of arteriosclerosis (Neumann *et al.*, 1997). In experimental study of myocardial ischaemia, the isolated heart model developed by Oscar Langendorff became common place. This technique allows the examination of physiological effects of the heart without some of the complications of the intact animal model such as the complication that the cardiac output determines the extent of coronary flow and complication that associated with anaesthetic and surgery (Nygren *et al.*, 2006).

In normal circulation, blood is supplied under pressure to the coronary arteries. Langendorff perfusion maintains the isolated heart using physiological saline delivered to the heart under pressure (this technique is described in detail later in the methods section). However, solution is supplied via coronary arteries as a retrograde flow that flows directly from the aorta in contrast to the normal situation in which blood enters the aorta from the left ventricle.

The choice of species used in the animal heart model is guided by the response of the heart to physiological stimuli or metabolic and biochemical effects. The most common animal heart models are rat, rabbit, pig and dog (de Groot *et al.*, 2001;Owens *et al.*, 1996). The extent of any collateral circulation is an important factor in choosing an appropriate animal model that can mimic the natural events of coronary artery occlusion in the human heart because collateral flow provides an alternative source of blood supply to myocardial area affected by ischaemia.

Collateral coronary artery is not critical to the survival of the heart during vascular occlusion of short duration. Occurrence of the innate collateral

coronary artery varies with species (White *et al.*, 1992). Collateral flow in dog is abundance in epicardial layers but lacking in the deeper layer of the myocardium. This epicardial collateral model in dog responds with increased blood flow after treating with vasodilator drug such as Ca²⁺ channel blocker (Heusch *et al.*, 1987). In contrast, the response of human collateral vessels to vasodilator is variable (Higuchi *et al.*, 2007).

In contrast to the dog, a comparative study of collateral circulation between humans and swine showed a similar response to an ischaemic stimulus (White *et al.*, 1992). In contrast, the pig collateral vessels are endomural and have subendocardial plexuses of anastomoses and are not present in the epicardial layer similar to human collateral vessels. Therefore, the porcine model of collateral artery is considered to be a good model for human coronary collateral development in coronary artery disease.

In rabbit hearts, there is minimal vessel collateralization and they therefore lack a transmural gradient of collateral blood flow (Miura *et al.*, 1989). In addition, arrhythmias and sudden cardiac death due to coronary artery occlusion are minimal in rabbit including less variable in distribution and size when compare with other species. Thus, the rabbit model serves as a good model for generating MI by occlusion the coronary artery (Lee *et al.*, 2002).

Ischaemia can be produced by either reducing the flow rate or completely stopping the flow (Wilensky *et al.*, 1986). The latter intervention does not correlate well with human pathology because, in the clinical situation, complete cessation of flow occurs only during cardiac arrest or hypovolaemic shock. However, local myocardial ischaemia from occlusion of the coronary artery is more common. In addition, studying the conduction system and arrhythmias in global myocardial ischaemia must be interpreted with caution because low perfusion flow results in progressively lengthening of the PR interval over time unless the ventricles can be stimulated artificially through the conducting system at normal rates.

1.7.2 Local myocardial ischaemia

The choices of animal models of local myocardial ischaemia are similar to those for global ischaemia. Local ischaemia can be performed by intraluminal or extraluminal manipulation of the coronary artery. Intraluminal occlusion of the coronary artery can be achieved by inflation of a balloon within the artery lumen. Extraluminal occlusion can be performed by ligating the coronary artery. The technique of tying off the coronary artery via a snare was developed in 1980 in order to produce myocardial infarction and to study the electrophysiological consequences of MI and reperfusion on reversal of ligation (Clark *et al.*, 1980).

Many studies use a rat model for acute local ischaemia because the rat coronary artery structure is well defined. However, using the rat heart is limiting because of the differences in the shape of the cardiac action potential compared to human heart (Nygren *et al.*, 2006).

The coronary arteries of the rabbit heart originate from the anterior part of the circumference of the aorta, located above the free margin of the semilunar valves and the main stem of the left coronary artery divides into several branches. In virtually all rabbit hearts, there are two anatomical branching patterns of left coronary artery (LCA): bifurcation or trifurcation. In the bifurcation pattern, the coronary artery divides into 2 main divisions: anterior division (AD) and postero-lateral division (PLD). Occlusion of the coronary artery with this bifurcation pattern can be performed by ligation at 75% in distance from the apex along the course of PLD level. In the trifurcation pattern, the coronary artery divides to 3 main divisions: AD, lateral division (LD) and posterior division (PD) as illustrated in Figure 1.14 (Podesser *et al.*, 1997; Lee *et al.*, 2002).

In this study a technique to occlude the rabbit coronary artery using a snare was developed and was used in conjunction with the optical mapping to investigate the electrophysiological properties during the acute phase of myocardial ischaemia.

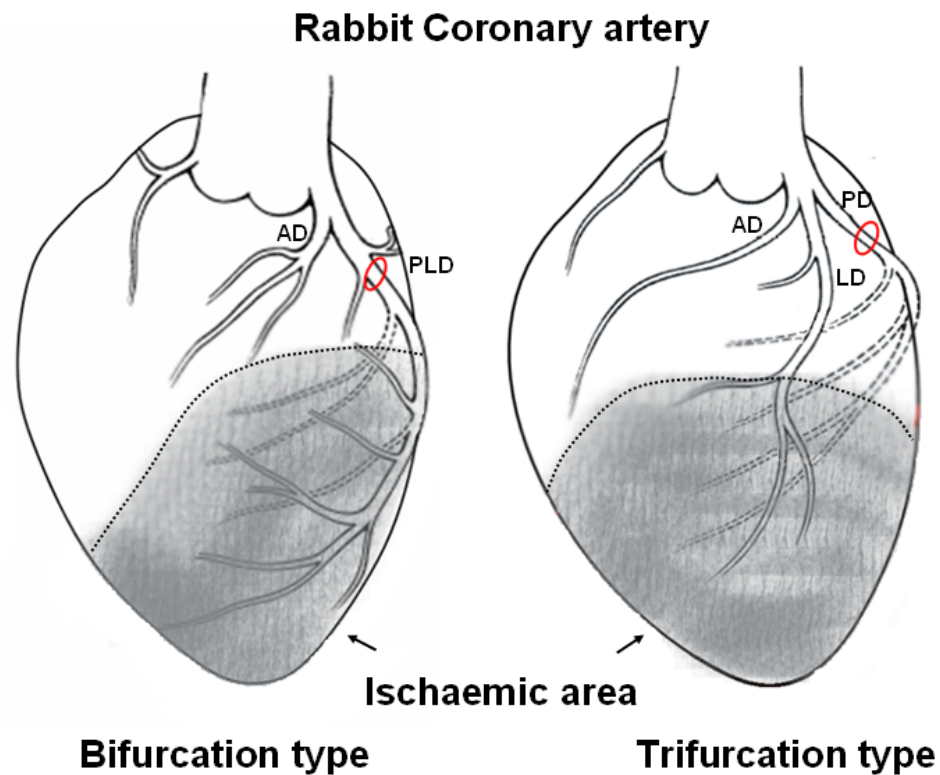


Figure 1.14 Rabbit coronary artery

Picture illustrates the branching pattern of rabbit coronary artery. Circle indicates the site where the left coronary artery was ligated. Bifurcation pattern of the coronary artery divides into 2 main divisions: anterior division (AD) and postero-lateral division (PLD). Trifurcation pattern of the coronary artery divides to 3 main divisions: anterior division (AD), lateral division (LD) and posterior division (PD).

1.8 Aims and hypotheses

The aims of this thesis were to: -

- (i) Develop a method of reliably producing acute regional ischaemia and reperfusion in the rabbit heart that can be used in conjunction with optical voltage recording.
- (ii) Monitor the electrical effects of acute regional ischaemia and reperfusion.

- (iii) Examine the characteristics of voltage-sensitive fluorescence dye loading under a series of flow rates in order to quantify relative myocardial perfusion in local and global ischaemia.

The hypotheses of this thesis were:-

- (i) Steep gradients in APD in the border zone between ischaemic and non ischaemic regions cause conduction block leading to re-entrant arrhythmia.
- (ii) Slowed conduction in ischaemic and border zone regions provides a substrate for arrhythmogenesis.

2 Methods

2.1 Optical mapping

2.1.1 General Principles

Optical mapping allows a simultaneous recording of the electrical properties from a number of sites on the myocardial surface. Optical mapping consists of three main components (Salama & Choi, 2001; Rosenbaum & Jalife, 2001):

- (i) Tissue stained with voltage sensitive fluorescence dye such as RH237, Di-4-ANNEPS or Di-8-ANNEPS.
- (ii) A system of optics to illuminate the tissue, filter the emitted light and focus the image onto the photodetector, and
- (iii) Acquisition system to collect, display and store signals from the photo detection system.

This technique is based on recording fluorescence that resulted from the membrane binding with the dye. Membrane bound dye is excited by short wavelength light and emitted at the longer wavelengths. The characteristic of the fluorescence varies with membrane potentials. One general mechanism that can explain the dye response to membrane potential is electrochromism as shown in Figure 2.1.

The intramembrane electrical field can change the spectrum of the dye without involvement of any molecular motion. In a polarized membrane, the electrical field coupling with the chromophore-charge decreases the energy difference between the ground and the excited states of the delocalised electrons in the aromatic groups. This results in a shift of both excitation and emission spectra. Membrane depolarisation results in a relative decrease of the fluorescence at the longer wavelengths. When the membrane repolarizes, the spectrum returns to what it was previously, resulting in increase of fluorescence to the previous level.

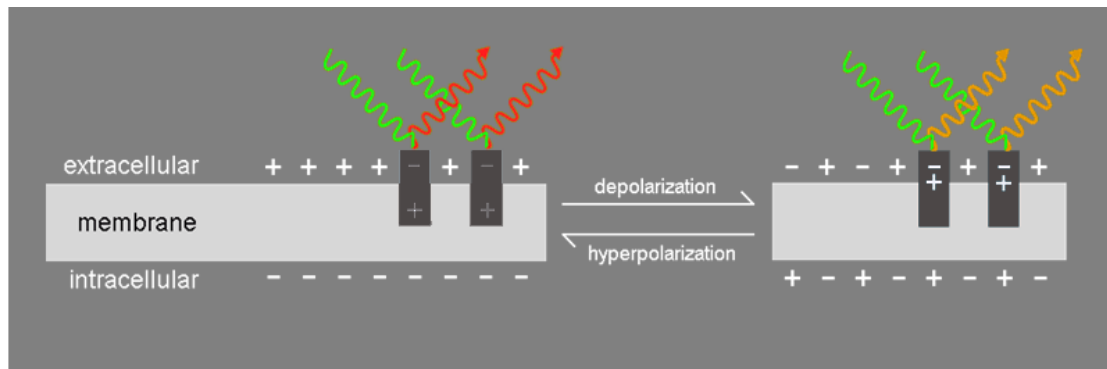


Figure 2.1 Electrochromic mechanism for dye response to membrane potential

A major problem of the optical mapping technique is the movement artefact that results from muscle contraction. Two methods are used in order to eliminate the artefacts. Mechanically stabilizing the heart by compressing or restricting movement inside the chamber is one method that can limit movement while maintaining normal physiological conditions such as the level of extracellular Ca^{2+} . However, this method has the disadvantage that compressing the surface of the heart, may result in ischaemia.

The other method is to use electro-mechanical uncoupling agents that reduce the movement artefact during the recording. These include BDM which is the myofibrillar ATPase inhibitor (Blanchard *et al.*, 1990), and Cyto-D which impairs actin filament polymerization (Krucker *et al.*, 2000). Blebbistatin is the most recently discovered uncoupling agent that is considered to have minimal effects on the level of extracellular Ca^{2+} , ion channel kinetics and action potential characteristics. Blebbistatin works by inhibiting myosin-II ATPase activity (Farman *et al.*, 2007; Fedorov *et al.*, 2007). However, their use necessarily disrupts the normal physiological processes that sense tension or muscle length and alter electrophysiology via mechano-electric feedback.

Optical methods of cardiac electrophysiology have been developed over a couple of decades by many groups (Efimov *et al.*, 1994; Cheng *et al.*, 2004; Knisley & Neuman, 2003; Mills *et al.*, 2006; Nygren *et al.*, 2006; Salama & Choi, 2001; Takahashi & Lopshire, 2004). Originally, optical signals were thought to be limited to the epicardial surface, but work comparing the signals from solid-state and optical signals reveals that a significant component of the optical

signal is derived from tissue below the epicardial surface (Knisley & Neuman, 2003). The depth of focus is calculated from the equation below that is based on the optics used in this thesis (see section 2.1.3 for details).

$$\text{Depth of focus} = 1000\mu\text{m}/[(7 \times \text{NA} \times \text{magnification}) + \lambda_{\text{ex}}/2(\text{NA})^2]$$

$$= 1000/[(7 \times 1.4 \times 1.2) + 0.535/2 \times 1.4^2]$$

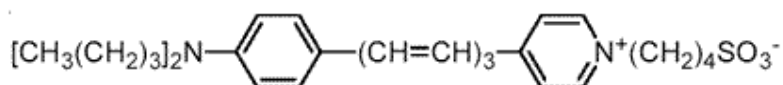
$$= 90 \mu\text{m} \quad (\text{NA} = \text{Numerical Aperture})$$

The proportion of excitation and emission light that penetrates the myocardial preparation was estimated in a theoretical study (Ding *et al.*, 2001). In the system used in this study, this work suggests that 80% of the optical signal originates from the tissue within 90 μm of the surface.

2.1.2 Voltage sensitive dyes

Ideally, the dye should be non-toxic, have high sensitivity, minimal photo bleaching and no additional pharmacological and photodynamic effects on the heart.

As mentioned above, voltage sensitive dye transduces changes in membrane potential into spectral shifts. How this is sensed is further illustrated in Figure 2.2 (Rosenbaum & Jalife, 2001). Depolarisation of transmembrane potential shifts the fluorescence emission spectrum to the right. From their resting potential of $V_m = -90 \text{ mV}$, cells depolarize to less negative membrane potentials represented as $V_m = -45$ and 0 mV . The shaded area under each spectrum corresponds to the amount of light that is transmitted through the emission filter and measured by the light detector.



Chemical structure of RH237

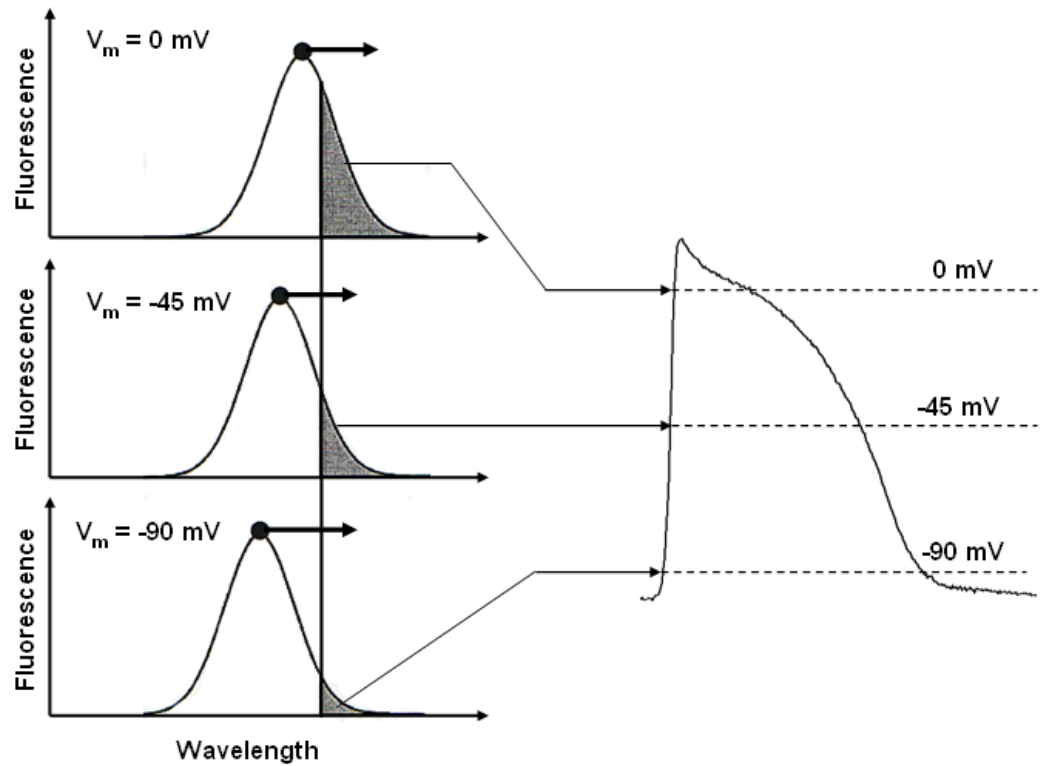


Figure 2.2 Chemical structure of RH237 and the principle of voltage-sensitive fluorescence

Adapted from (Rosenbaum & Jalife, 2001).

When choosing the dye its excitation and emission wavelength should be considered mainly in relation to illumination. There are three main dyes that are commonly used in optical mapping systems of AP: RH237, Di-4-ANNEPS and Di-8-ANNEPS (Rosenbaum & Jalife, 2001). The characteristic of these dyes is shown in the Table 2.1.

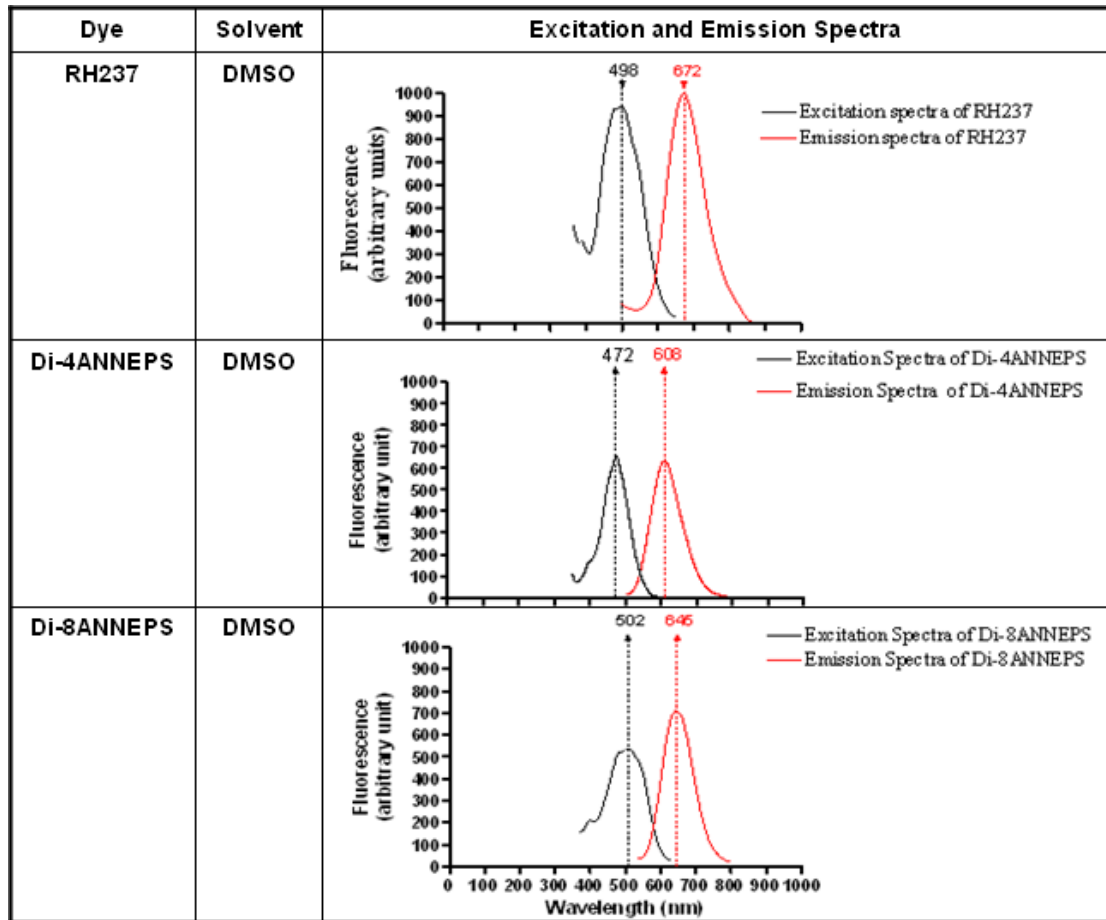


Table 2.1 Characteristic of commonly used voltage-sensitive dyes in cardiac mapping

2.1.3 Optical mapping set up

Fluorescence signals were recorded from the anterior surface of the heart. The heart was placed into the custom-made Perspex chamber (Figure 2.3). The exterior surface of heart was maintained at 37°C by filling the chamber with 37°C perfusate solution. Motion artefact was further reduced during optical recordings by gentle compression against the front-plate by sliding forward the back piston. (Figure 2.3B)

The heart was loaded with a 100µl bolus of RH237 (Molecular Probes), RH237 (1mM) was dissolved in DMSO. The bolus of dye was delivered to the coronary circulation by slow injection through the port of a bubble trap (Figure 2.8). RH237 was taken up by all the membrane structures accessed by the coronary arterial circulation, including endothelial cell layers of both arteries and the

capillary bed of the coronary vasculature as well as the cardiomyocytes. The membrane-bound dye was excited by light at 505 and 535 nm. The emitted fluorescence light passed through a 645nm long-pass filter (Comar Instruments) (Figure 2.4). The emitted light was collected by a 256 (16 × 16) photodiode array (PDA) (C4675-102, Hamamatsu Photonics). The fractional fluorescence decrease caused by an action potential was in the range 2 to 6%.

Four pixels, one in each corner, were reserved for ECG and pacing signals; optical signals were acquired from the remaining 252 pixels. Each pixel had a sensing area of 0.95mm × 0.95 mm. The distance between the centres of adjacent recording pixels (pitch) was 1.1 mm. An optical magnification was ×1.2, so each pixel detected light from an epicardial area of 0.8mm × 0.8mm. Signal-to-noise ratio was defined as the signal amplitude divided by the standard deviation of the noise. The current from each pixel was converted to a voltage and amplified in parallel. Signals were fed to a multiplexor, converted by an analogue-to-digital converter at 1 kHz, saved onto disk, and analysed offline.

The lens system magnified and focused the image of the left ventricular epicardial surface onto either a charged-coupled device video camera (CCD) or PDA, depending on whether a 45° mirror was present or not. The CCD and PDA were exactly aligned using a square test pattern.

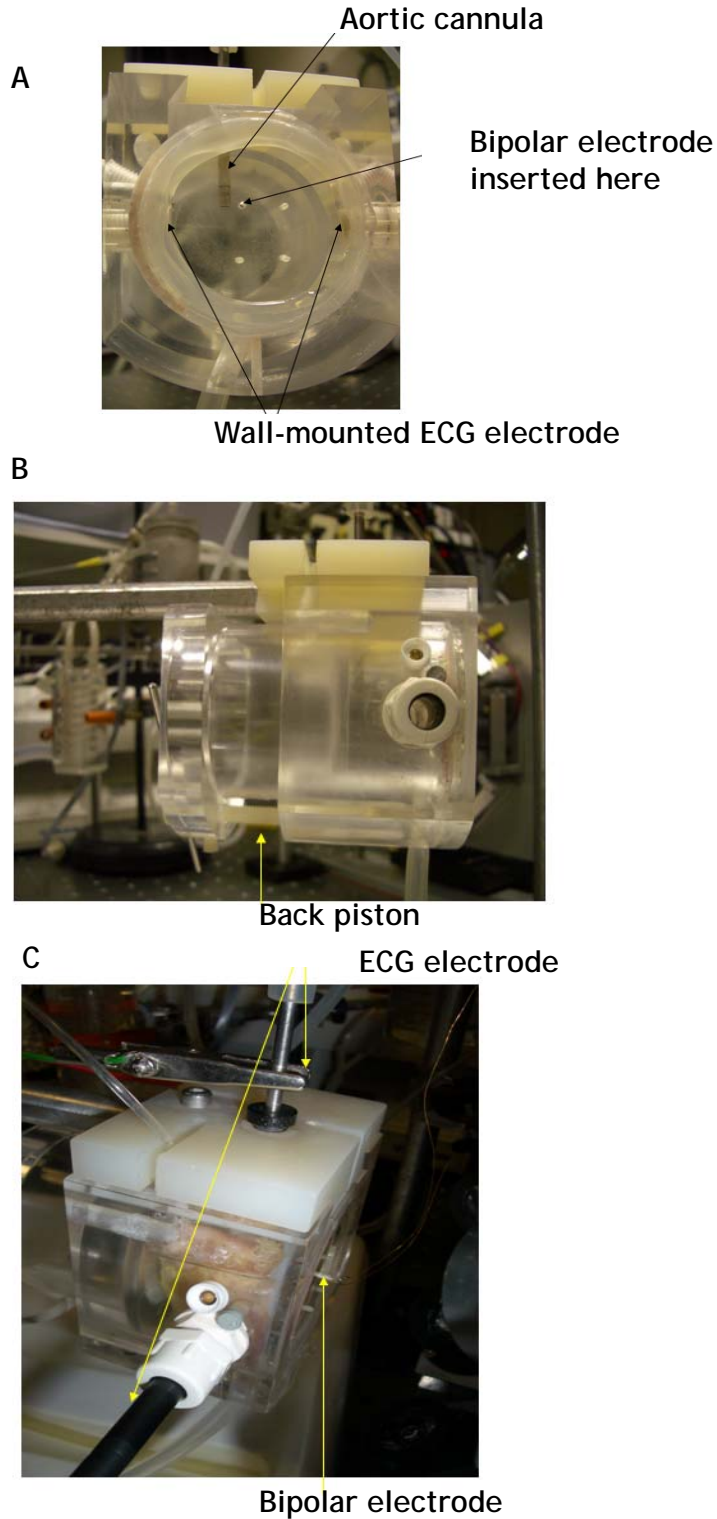


Figure 2.3 Photographs of the optical mapping chamber

A: Aortic cannula, 1mm-hole at the Perspex chamber frontal-plate use to insert a bipolar electrode and wall-mounted ECG electrode. B: The back piston, when sliding forward allowing gentle compression of the heart against the front plate. C: Bipolar electrode, and the ECG electrodes.

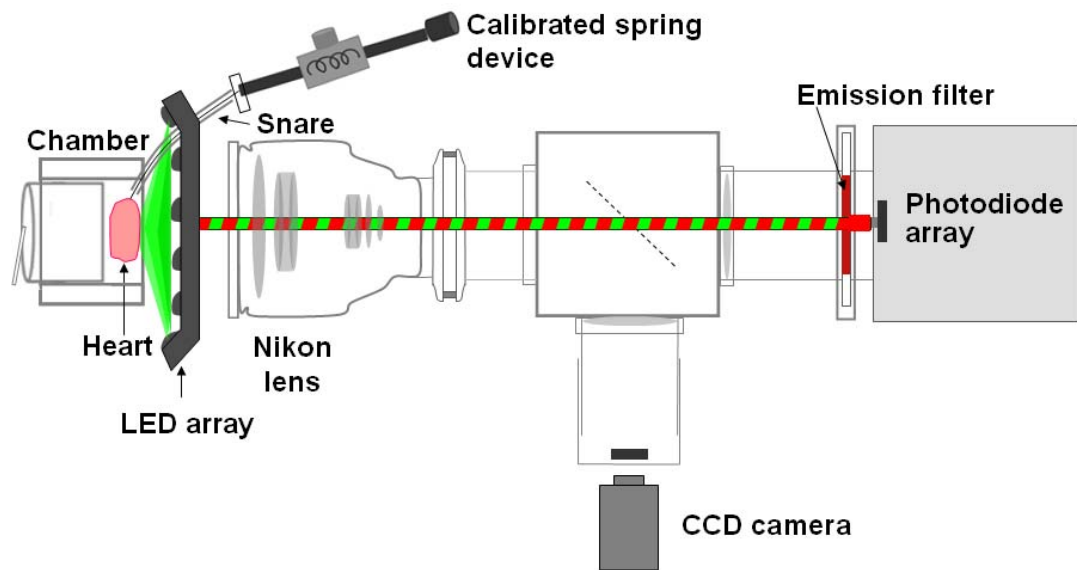


Figure 2.4 Diagram of the optical mapping set-up

2.2 Preparation for coronary artery occlusion during Langendorff perfusion

2.2.1 Initial attempt to produce reproducible occlusion of rabbit coronary artery using loop technique

Adult male New Zealand White rabbits (2.5 - 3.5 kg) were sacrificed by intravenous injection of sodium pentobarbitone 100 mg/kg (Rhône Mérieux) and 1000 IU of heparin into the left marginal ear vein. The hearts were rapidly removed and placed in chilled Tyrode's solution (in mM: Na^+ 134.5, K^+ 5.0, Ca^{2+} 1.9, Mg^{2+} 1.0, Cl^- 101.8, SO_4^{2-} 1.0, HPO_4^- 0.7, HCO_3^- 20, acetate (CH_3COO^-) 25 and glucose 25) to stop the heart contracting. The heart was then perfused retrogradely with chilled Tyrode's solution at a rate of 20 ml min^{-1} (Gilson Minipuls 3 peristaltic pump) to allow the coronary artery to be differentiated from the superficial coronary vein under a dissecting microscope.

The pattern of coronary artery branching was noted and the left posterior division of the coronary artery was cannulated with a silicone Foley catheter of 1mm diameter to form a loop as shown in Figure 2.5. Subsequently, the heart

was transferred to the optical rig and perfused with standard Tyrode's solution at 37°C and maintained pH at 7.4 by bubbling with a 95%O₂/5%CO₂ gas mixture. Perfusion rate was controlled at 30 or 35ml/min depending on the heart size. Perfusion pressure was monitored with a transducer inline with the aortic cannula. The loop was inserted through the frontal plate of the chamber, and could be occluded by clamping. Reperfusion was possible by releasing the clamp as shown in Figure 2.6A and B.

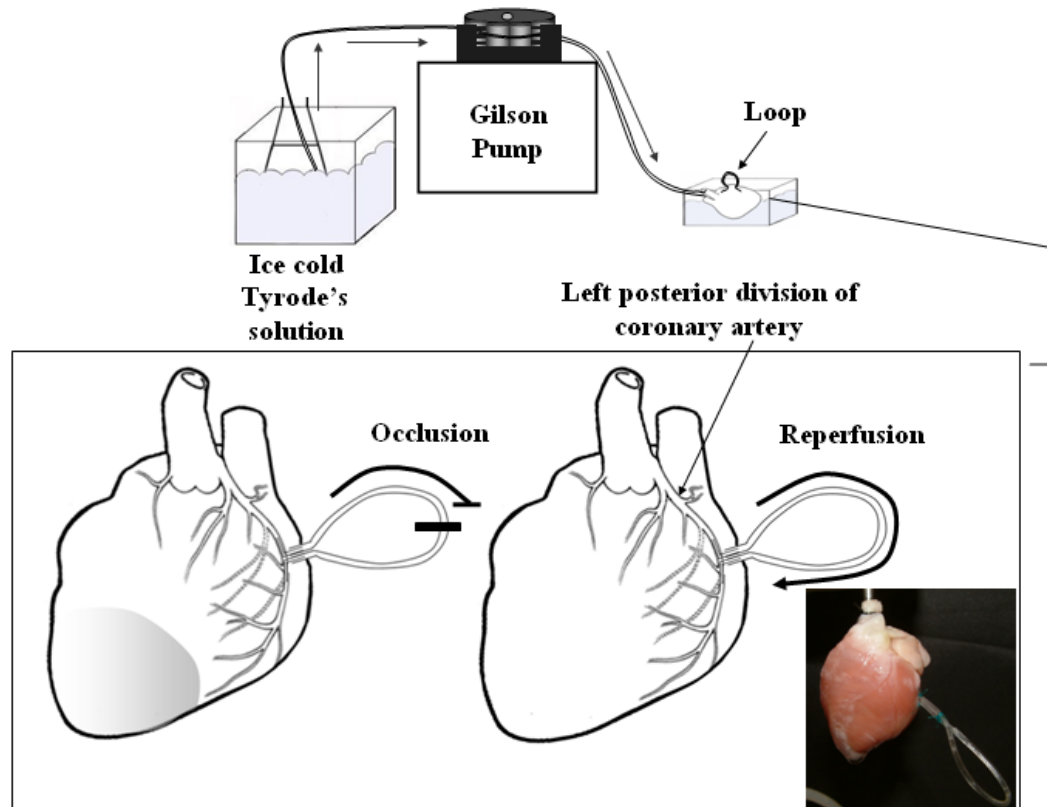
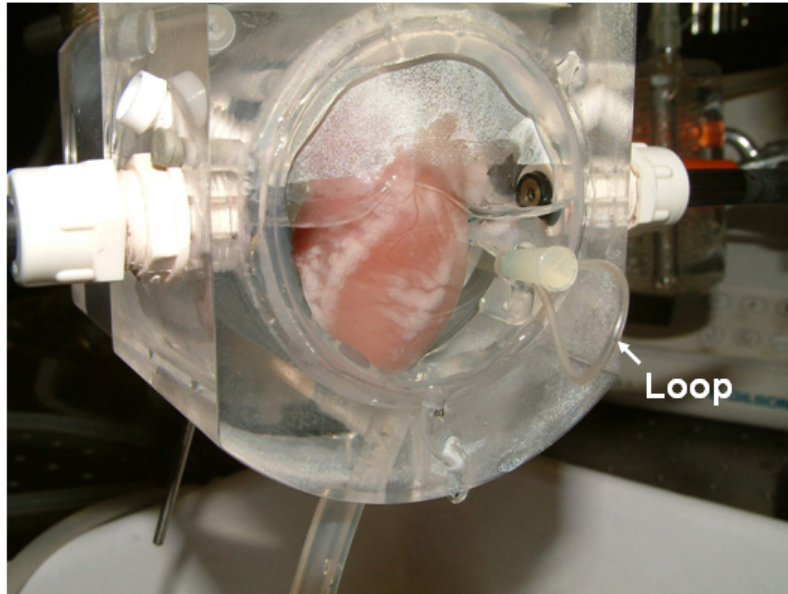


Figure 2.5 A novel model of rabbit coronary artery occlusion

A



B

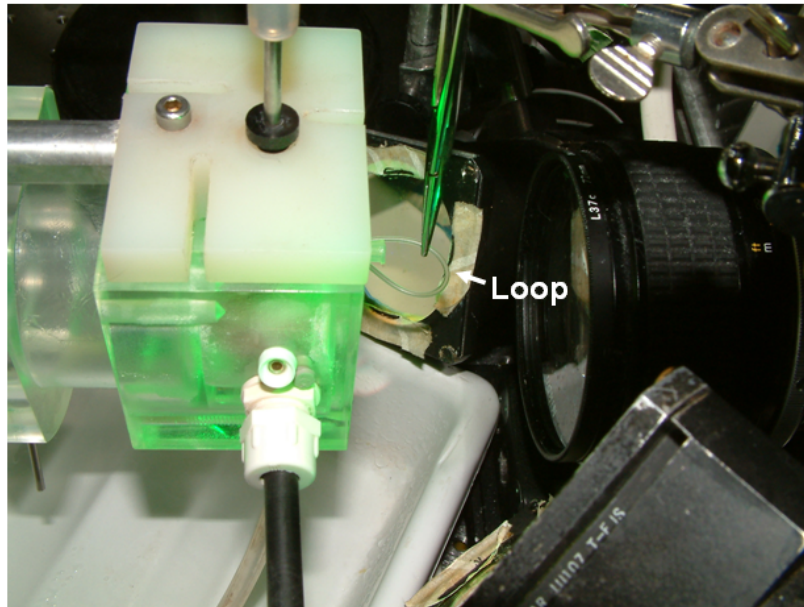


Figure 2.6 Photographs of the optical mapping chamber

A: Heart in the chamber with the loop inserted through 1mm-hole in frontal plate.

B: Occlusion of the left coronary artery by clamping the loop with the artery forceps.

2.2.2 Coronary artery occlusion by using ligation technique

Adult male New Zealand White rabbits were sacrificed as described previously. Hearts were rapidly removed and placed in chilled Tyrode's solution to stop contractions temporarily. To visualize the vessel of interest, a Gilson Minipuls 3 peristaltic pump was used to perfuse the Tyrode's solution to the heart ($20 \text{ cm}^3 \text{ min}^{-1}$). The left posterior division of the coronary artery (Podesser *et al.*, 1997; Day & Johnson, 1958) was occluded with a suture (4-0 polyester, Ethibond™) using a short piece of polyethylene tubing of 2 mm diameter to form a snare (Figure 2.7). This process took about 5 min.

The snared heart was then mounted onto an aortic cannula and retrogradely perfused (Figure 2.8). The heart was placed in a Perspex chamber to limit gross movement and further motion artefact was reduced by perfusing the heart with $5 \mu\text{M}$ Blebbistatin (BioMol) (Fedorov *et al.*, 2007) in Tyrode's solution (in mM: Na^+ 134.5, K^+ 5.0, Ca^{2+} 1.9, Mg^{2+} 1.0, Cl^- 101.8, SO_4^{2-} 1.0, HPO_4^- 0.7, HCO_3^- 20, acetate (CH_3COO^-) and glucose 25). The solution was filtered through a $5 \mu\text{m}$ filter (Whatman) before use. The solution pH was maintained at 7.4 by bubbling with a 95% O_2 /5% CO_2 gas mixture (BOC, UK). The perfusion solution was maintained at 37°C by a glass-column heat exchanger connected to a thermostat-controlled water bath (Figure 2.8). The Langendorff perfusion was set at a constant rate of 30-35ml/min.

Perfusion rates of 1, 2, 5, 10 and 15ml/min were used in flow analysis experiments (described in section 5.4) and global ischaemia experiments. A transducer connected to the aortic cannula was used to monitor perfusion pressure. The typical initial pressures were approximately 20-30mmHg. Pressures would typically rise over the course of the experiment (2-3 hours) by 10-20 mmHg. Sometimes perfusion pressure increased more rapidly, probably due to air embolus. Stopping the flow momentarily and withdrawing solution with a 5 ml syringe through the side-arm used to inject dye boluses occasionally resulted in removing an air bubble and restoring a lower perfusion pressure. The heart could not always be rescued this way, and pressure would continue to rise. If the pressure rose above 80 mmHg, the experiment was terminated. Nevertheless,

perfusion pressure was followed closely throughout the experiment as a check for continued viability of the preparation.

To produce a local ischaemia, the snare was tightened for 15 minutes. At the end of this period the snare was loosened again to reperfuse the heart. Tension was adjusted by connecting the ligature to a calibrated spring device (Figure 2.4). This device provided a way of producing a calibrated force on the snare and therefore allowed the minimum force required to produce occlusion to be used repeatedly. Previous attempts in this laboratory using a snare to occlude the coronary artery were not successful because excessive forces were used that irreversibly damaged the tissue (including coronary vessels).

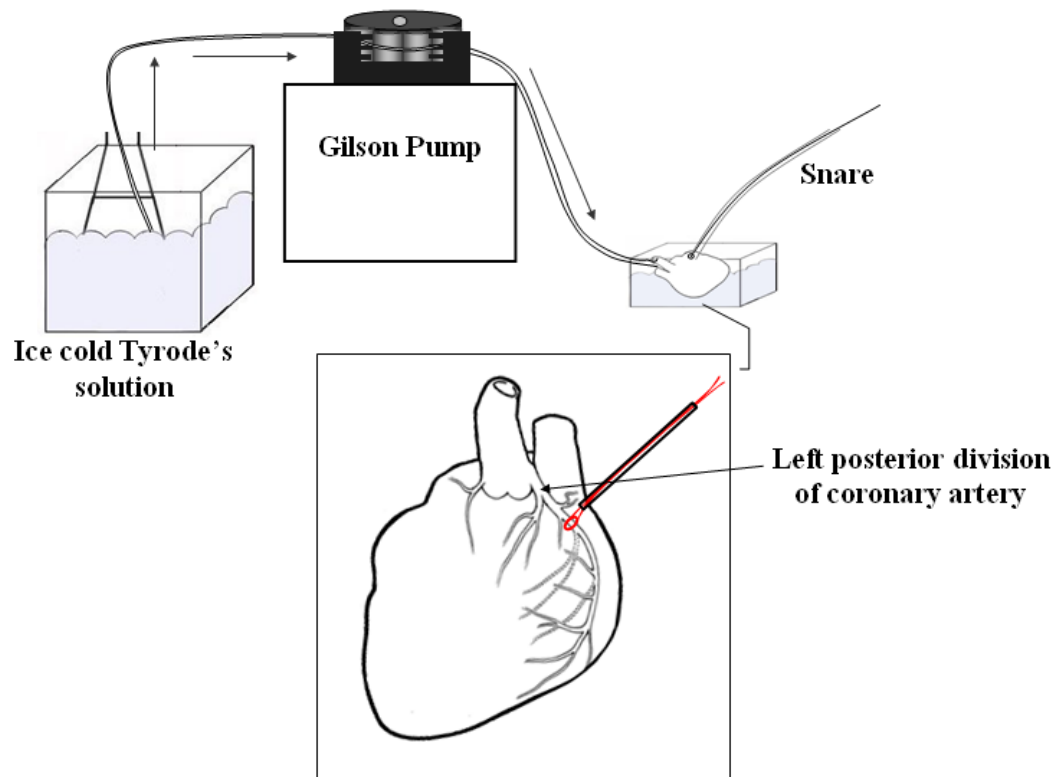


Figure 2.7 Initial surgery to attach snare

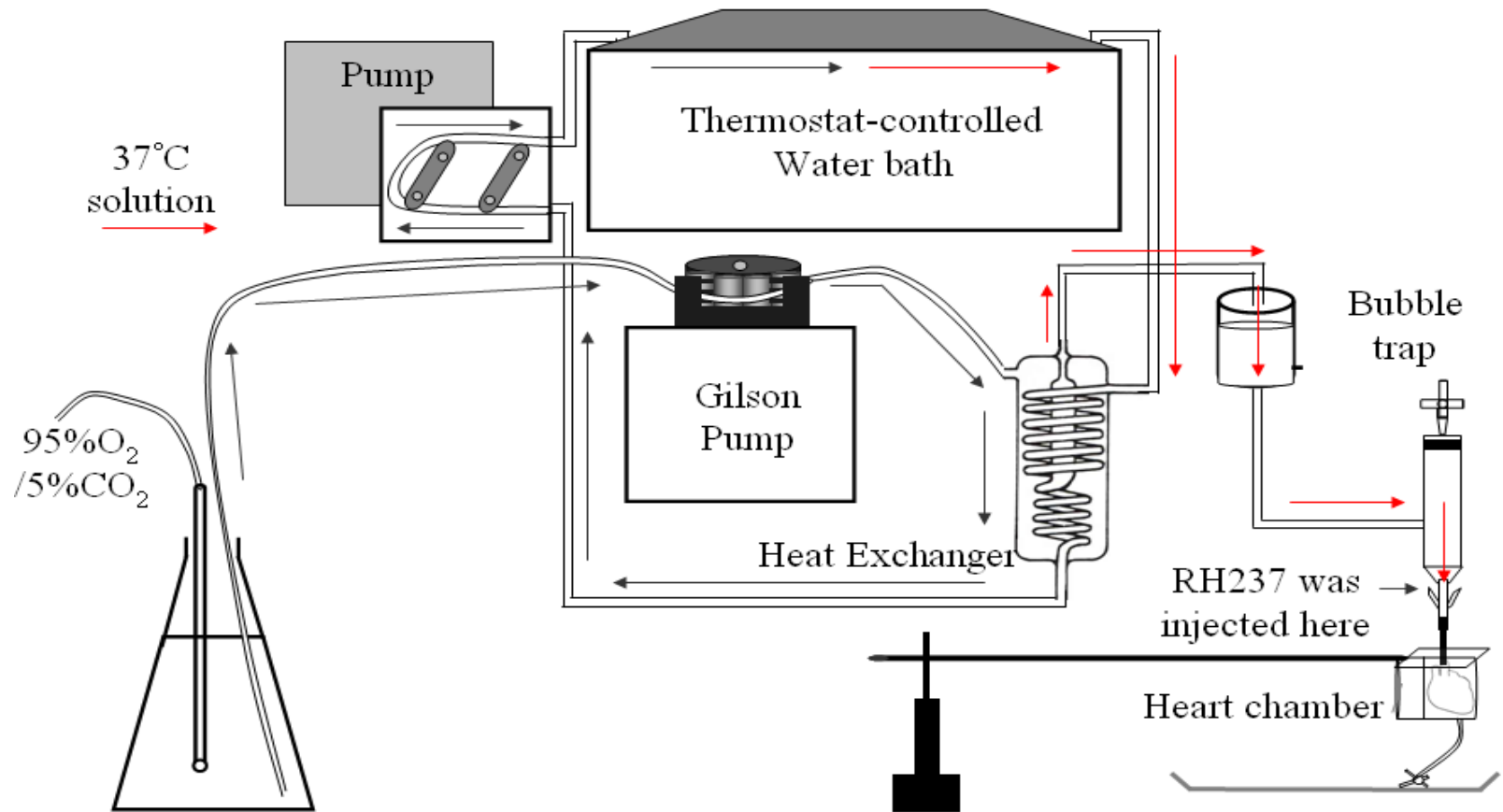


Figure 2.8 Langendorff perfusion apparatus

2.3 Pacing protocols

2.3.1 Atrial pacing (APACE)

Atrial pacing was performed via a pair of platinum hook electrodes located in the right atrial appendage using a Digitimer DS2A-MK.II constant voltage stimulator. The threshold stimulus was measured and the voltage set at 2 times threshold for the duration of the experiment. The heart was paced at a range of pacing cycle lengths: 300ms, 250ms, 200ms and 150ms. The atrial pacing electrode is shown in Figure 2.9

2.3.2 Ventricular pacing (VPACE)

Ventricular pacing was the main pacing method used in this study to assess epicardial conduction velocity. The bipolar platinum electrode was inserted into 1 mm hole in a front plate of the Perspex chamber as shown in Figure 2.9. For conduction velocity analysis, the heart was paced at 250 ms cycle length. Pacing was achieved by connecting the electrodes to a stimulator which provided a constant square voltage pulse of 2ms width, at twice diastolic threshold. Pulse timing was computer controlled using a locally developed program (Dr FL Burton, University of Glasgow). A pseudo-ECG was also recorded. Recordings from ECG electrodes were connected to a MAP amplifier (custom built by Medical Electronics, University of Glasgow) that was connected to an oscilloscope (Nicolet Instrument Corporation, Wisconsin, USA.) to allow real-time viewing of the ECG, in addition to recording in one of the corner channels. The pacing stimulus was recorded in another channel (Figure 2.10).

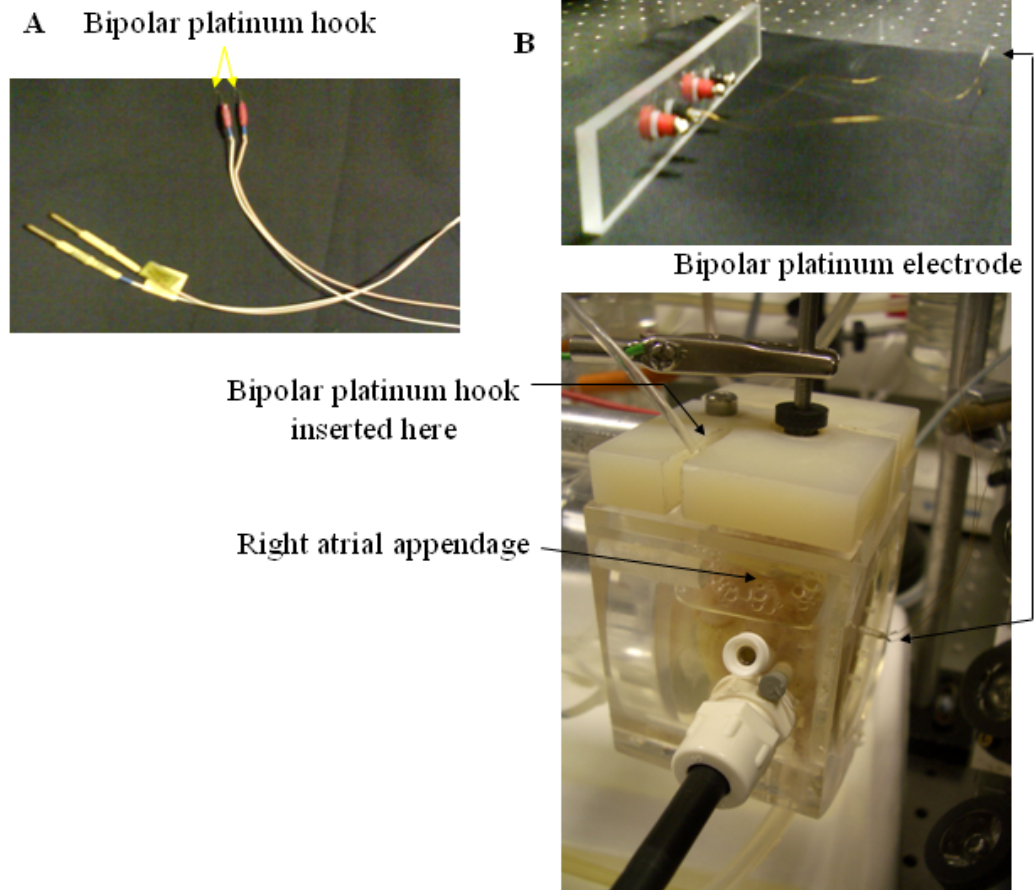


Figure 2.9 Photographs of atrial pacing electrodes

A: Atrial-pacing electrode, B: ventricular pacing electrodes.

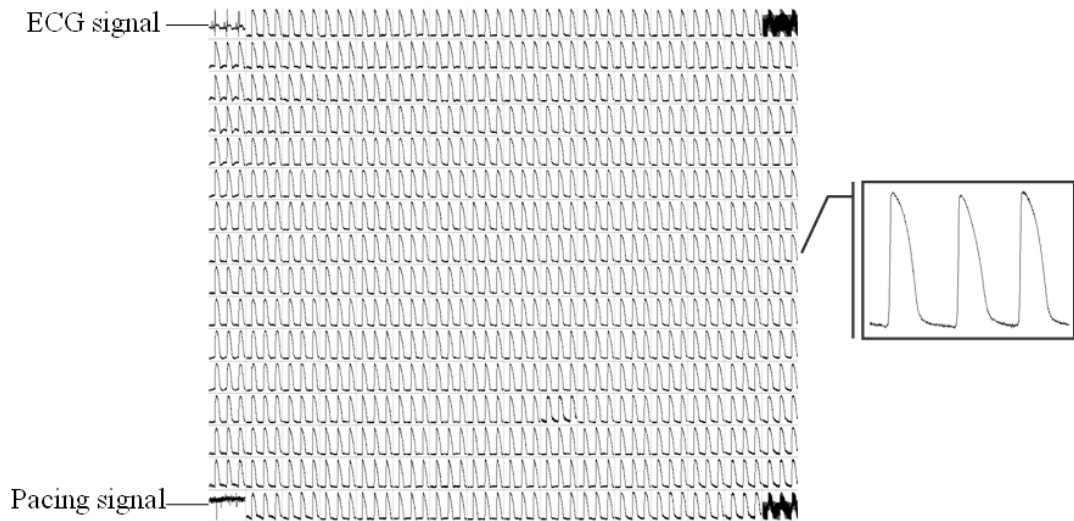


Figure 2.10 Map of 256 optical action potentials recorded from the ventricular epicardial surface of a rabbit heart

The 256 action potentials were recorded simultaneously at a rate of 1000 frames per second. Top left corner shows a bipolar electrocardiogram (ECG) that simultaneously recorded along with the 252 optical signals and left-bottom corner shows a pacing signal. (Unused corner channels were left open-circuit). Right panel shows optical action potentials (OAPs) from a single element.

2.4 Electrophysiological analysis

2.4.1 Optical action potentials

The shape of recorded optical action potentials (OAPs) depends not only on the cellular AP shape but also on how these APs are coordinated amongst all the cells within a pixel. The OAP represents the activation of a group of cells, whose number depends on the pixel size and depth of field. In this thesis the volume of optical pixel on the epicardial surface is 0.056mm^2 ($0.8 \times 0.8 \times 0.09\text{mm}$). Although this represents only ~1000 cardiomyocytes, the volume of myocardium contributing to the voltage signal will depend on the electrical space constant for the tissue. Estimates of the space constant of rabbit myocardium during diastole suggest values ranging from ~1.5mm (longitudinal) to 0.8mm (transverse) (Akar *et al.*, 2001). But as is indicated in Equation 2.1, this value will decrease as the membrane resistance decreases during an AP. Spatial resolution is limited by optical magnification. However, signal quality (signal to noise ratio) is reduced at higher magnification, because fewer cells contribute to the total signal in the pixel.

$$\lambda = \sqrt{\frac{R_m}{(R_i + R_o)\beta}}$$

Equation 2.1

Figure 2.11 The space constant equation

Where λ is a space constant, R_m is a membrane resistance, R_i is an intracellular resistance and R_o is extracellular resistance.

Signal to noise ratio depends on other factors too. Depolarisation results in a transient reduction of fluorescence intensity by approximately 5% of the total fluorescence recorded. Therefore, OAPs illustrated in this thesis represent background-subtracted and inverted signals. Signal amplitude, and therefore signal to noise ratio, also depends on dye loading and illumination intensity.

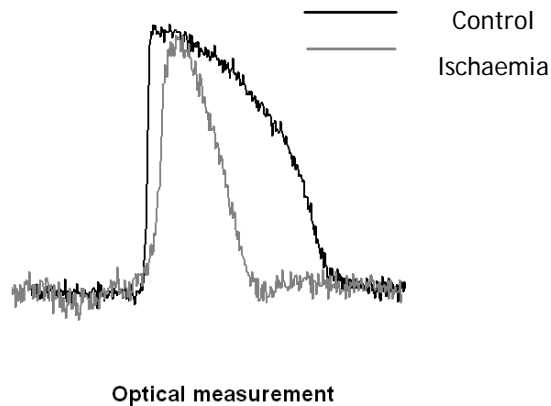


Figure 2.12 Example of OAPS from rabbit heart

For the repolarization phase of the OAP to be measured accurately, the motion artefact must be minimised. The motion artefact distorts the plateau and repolarization phase of the action potential predominantly (Figure 2.13). In this study, 5-10 μ M Blebbistatin was used to reduce the motion artefact by inhibiting myosin-II ATPase activity. Blebbistatin suppressed heart contraction without the significant side effects on the electrophysiology of the myocardium as shown in Figure 4.7 to 4.13 (see Results section for control experiments).

An analysis programme OPTIQ (locally developed by Dr FL Burton, University of Glasgow) was used to analyse all 252 channels and determine the activation and repolarization times as shown in Figure 2.11. OPTIQ could also generate a visual display of the spread of activation across the ventricular epicardial surface. Other parameters, such as APD, were derived.

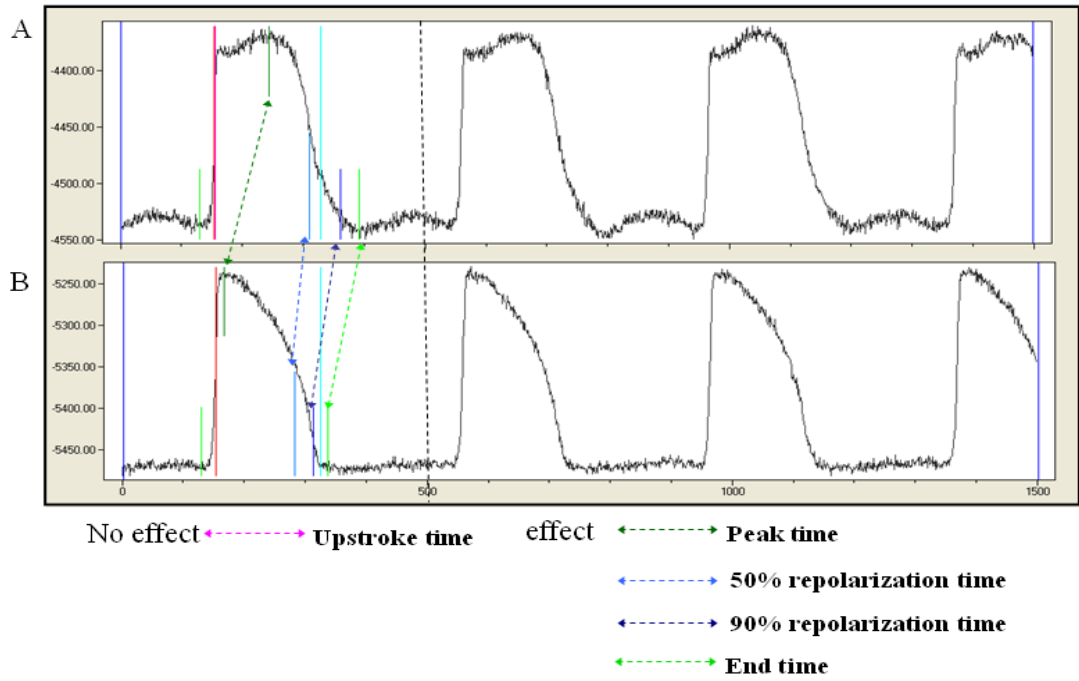


Figure 2.13 Illustrations of OAPs recorded from contracting sites (A) compared with the minimized motion artefact sites (B)

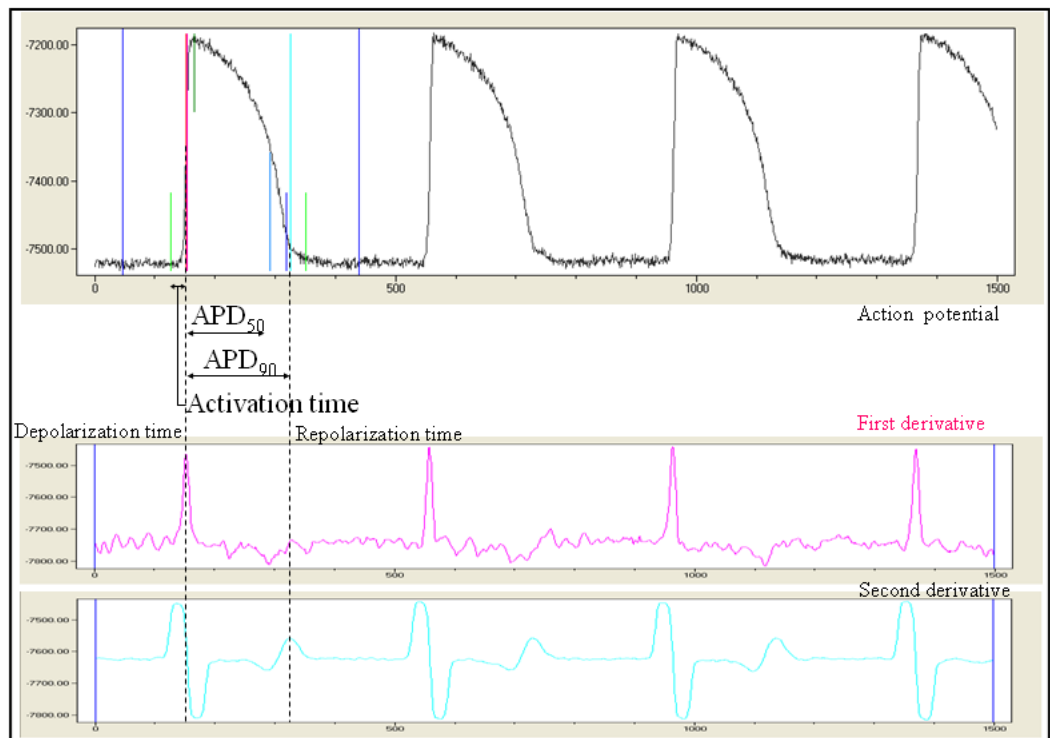


Figure 2.14 APD and activation time calculation

APD₅₀ and APD₉₀ were determined from the difference between 50% and 90% (respectively) of repolarization time and activation time.

2.4.2 Isochronal maps of activation

The activation time in each channel was defined as the time of fastest upstroke (maximum 1st derivative) of the optical signal (Figure 2.15). The map of contour lines can then be constructed by using the resultant matrix of activation times. Data were exported to Contour Tool, MATLAB 7.0 (The MathWorks Inc, Natick, MA., developed by Dr FL Burton, University of Glasgow). An isochronal map of activation was shown in Figure 2.16. Different colours were used to mark the timing of the activation process, each shade marking the left ventricular epicardium area activated in each 1 ms time frame from sinus rhythm and 5 ms time frame from ventricular pacing. White to black colour scale represented the earliest to the latest depolarised sites in the map.

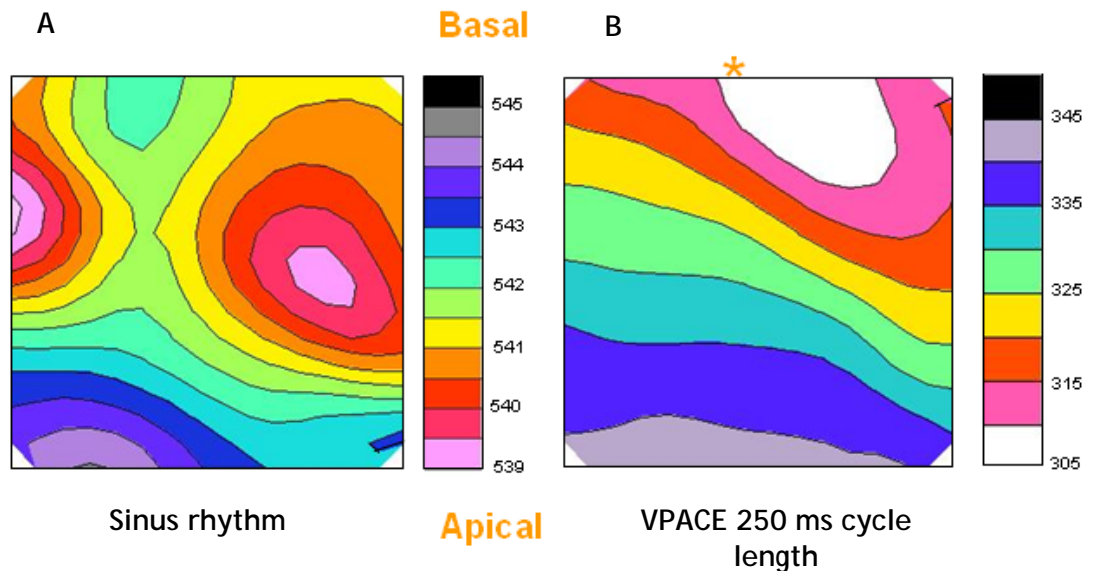


Figure 2.15 Example of activation maps of left ventricular epicardial surface

A: Sinus rhythm, isochrones are spaced at 1 ms intervals and activation initiated from two basal areas and spreading to the apex.

B: Ventricular pacing at 250 ms cycle length produced map spreading basal to apical. Isochrones from Panel B were drawn with 5 ms apart.

2.4.3 Conduction velocity

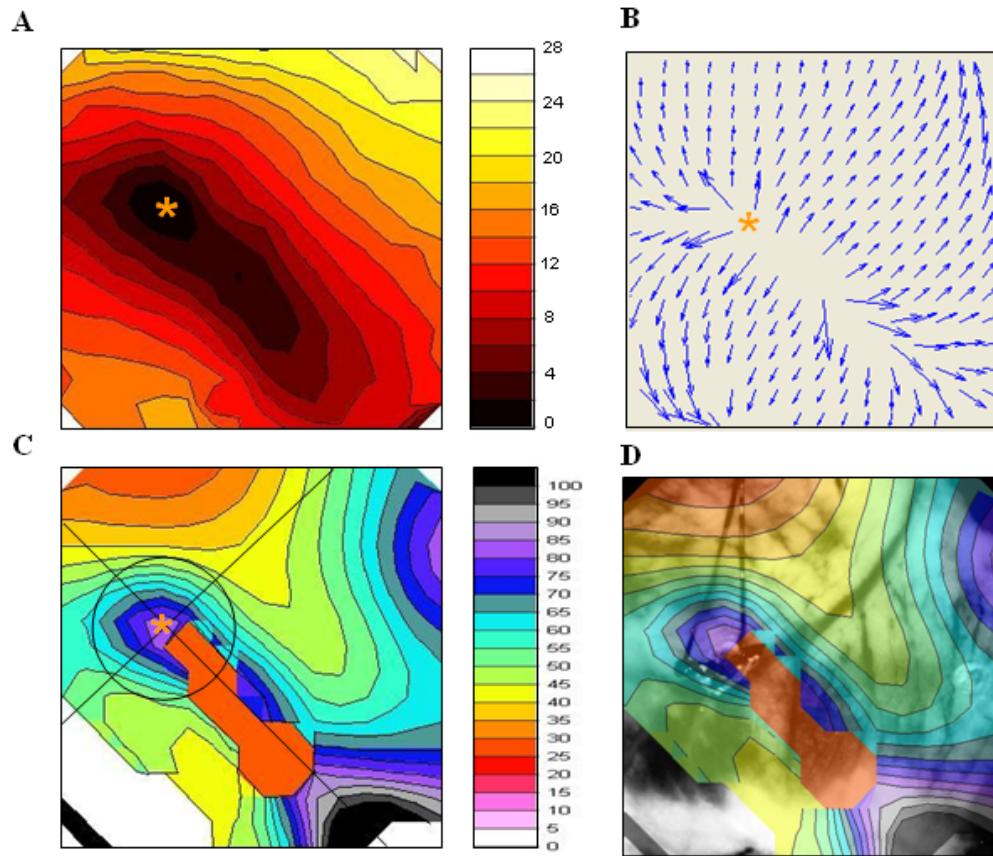
CV was determined during epicardial pacing rather than atrial pacing or spontaneous activity because of the potential artefact from transmural

conduction. Epicardial ventricular pacing was performed via bipolar electrodes touching the epicardial surface towards the base, as shown in figure 2.9.

The method of analysing conduction velocity in this thesis is based on work by Bayly (Bayly *et al.*, 1998). This method fitted a polynomial surface to the epicardial activation times and used this curve to generate two-dimensional velocity vectors (2 axes) over the recordings area (x- and y- axes) (Figure 2.16C). This was implemented by Velocity Tool (software developed by Dr Francis Burton in MATLAB 7.0).

In estimating epicardial conduction velocity, unrealistic values, such as due to the contamination by intramural breakthrough to the epicardial surface must be ignored. In general, the measurements indicate a faster conduction along the longitudinal axis and slower conduction along the transverse axis.

Figure 2.16 shows a typical isochronal map, resulting from epicardial pacing of the left ventricle. The stimulation point was identified as the central point of activation (* in Figure 2.16A), and can be confirmed by the bipolar electrode location from the CCD image recorded during the experiment (Figure 2.16D). The conduction velocity was assessed around a 5mm radius circle from the stimulation point, the peak axis of activation was indicated by a line in longitudinal and transverse axis as shown in Figure 2.16C. The velocity values from the entire array (252 pixels) were exported to OPTIQ to analyse the statistical velocity and angle of maximum velocity.



16/09/08

Figure 2.16 CV calculation from epicardial pacing and radial approach to CV assessment

Ventricular epicardial surface of 8-week infarcted heart

A: Isochronal activation map.

B: Illustration of 2D velocity vectors derived from the activation times of Panel C.

C: Velocity with stimulation point (*) and circle of 5mm radius for radial CV assessment.

D: Image background from CCD camera to confirm the location of bipolar electrode.

2.5 Statistical analysis

All data in this thesis are expressed as mean \pm standard error of the mean (SEM). Paired t-test was used to compare between groups of data. Data were imported into InStat3 (GraphPad Software Inc., USA) in order to test the significance between two groups, p-value of less than 0.05 was considered significant. Linear and non-linear regression testing were performed using GraphPad Prism4 Software Inc., USA.

3 Acute regional myocardial ischaemia model in the rabbit

3.1 Introduction

Coronary artery disease (CAD) is a common precursor of sudden cardiac death in UK and third world countries. Most of CAD begins when the coronary artery is occluded by a thrombus and results in profound reduction of coronary blood flow (Li *et al.*, 2008). Prolonged coronary artery occlusion leads to myocardial cell damage and cell death as a result of myocardial ischaemia. AMI is a common cause of life threatening arrhythmia e.g. VF which is the responsible for a large proportion of sudden cardiac deaths (National center for health statistics, 1992; American heart association statistics committee and stroke statistics subcommittee, 2007).

Animal heart models have been used for many years to gain insights into the disturbance of normal mechanical, physiological and biochemical function in the human heart (Podesser *et al.*, 1997; Lancaster, 1882). Each animal model has advantages and disadvantages, and several factors relating to ethics, economics, accessibility and reproducibility are considered in choosing an appropriate model for the each study (Muders & Elsner, 2000; Hasenfuss, 1998; Vanoli *et al.*, 2004). In the case of myocardial ischaemia, coronary artery ligation and microembolization have been used to produce myocardial ischaemia and infarction in various species from small animal such as rat and rabbit up to large animals such as dog and pig (Vanoli *et al.*, 2004). Because large animal models are more expensive and tend to be limited for the ethical reasons, small animal models are used preferentially for studying myocardial ischaemia and infarction.

3.1.1 Experimental models of myocardial ischaemia and infarction

Myocardial ischaemia and infarction are consequences of occlusion of the coronary artery. Experimentally induced myocardial ischaemia models such as coronary ligation, coronary embolism and electrocution have been used to create infarcted myocardium. Schwartz *et al* (Schwartz *et al.*, 1984) applied the micro-embolization technique in a canine model to induce chronic myocardial

infarction. Although this technique has informed several lines of research and generated a stable model for studying heart failure, it has failed to provide a full explanation of ischaemia-induced arrhythmias mechanisms (Vanoli *et al.*, 2004). Among the alternative approaches, coronary ligation technique has been one of the most commonly used (Clark *et al.*, 1980; Liu *et al.*, 1997).

3.1.2 Rat model of myocardial ischaemia and infarction

Advantages of using rats include short gestation period and inexpensive housing and care. However, the use of rat heart is limited by the differences in myocardial function from humans. For example, (i) α -myosin heavy chain isoform predominates rather than β -myosin heavy chain isoform (ii) the action potential of the rat myocardium is shorter and lacks a plateau phase, and (iii) the resting heart rate is considerably faster than human (Bers, 2001). At the cellular level, calcium is removed predominantly via sarcoplasmic reticulum (SR) in rat relative to NCX. In humans NCX has a more predominant role.

Despite these functional differences, Sprague-Dawley rats are widely used in medical research including myocardial infarction study because this rat model is well characterised across many cardiovascular functions. Ligation of the left anterior descending (LAD) of a coronary artery results in variable sizes of the infarcted area (Pfeffer *et al.*, 1979). After long-term ligation of the coronary artery, the surviving myocardium exhibits decreased in SERCA mRNA and protein level and there is an increased in severity of congestive heart failure.

The shortcoming of the *in vivo* MI model in Sprague-Dawley rats is a high peri-operative mortality rate and variability of infarct size (Pfeffer *et al.*, 1979; Johns & Olson, 1954; de Tombe *et al.*, 1996; Yang *et al.*, 1993). However, Liu *et al.* (Liu *et al.*, 1997) reported a uniformly large infarct and low mortality rate using the Lewis rat. A number of experimental models have been generated and developed in various other species to produce stable animal models of myocardial ischaemia and infarction (Ye *et al.*, 1997).

3.1.3 Rabbit model of myocardial ischaemia and infarction

Rabbits are commonly used to produce experimental models of human heart failure and myocardial infarction in human. Rabbits are less expensive than dogs, have less variability in distribution, size, and length of the coronary arteries compared to dogs. Rabbit myocardium also shows important similarities of function to the human heart, such as the predominant β -myosin heavy chain isoform and excitation-contraction coupling processes. As in human myocardium, the force-frequency relation is positive, and Ca^{2+} removal from the cytosol is 70% by the activity of the sarcoplasmic reticulum and 30% by NCX activity (Hasenfuss, 1998; Bers, 2001; Hasenfuss *et al.*, 1991). Rabbit models have been modified for use in other experimental studies e.g. systemic hypertension, pressure and volume overload, cardiomyopathy, myocarditis, and pacing-induced heart failure including myocardial ischaemia (Currie & Smith, 1999; Pennock *et al.*, 1997; Chen *et al.*, 1997; Alexander *et al.*, 1993).

On the other hand, some studies reported variable pattern of coronary artery anatomy between rabbits, and it is still unclear in many studies exactly the pattern or level of the coronary artery ligated (Miura *et al.*, 1989; Ytrehus *et al.*, 1994; Lee *et al.*, 2002). One of these studies (Lee *et al.*, 2002) described a pattern and the level of ligation of the left coronary artery (LCA) required to produce a reliable chronic heart failure model in a rabbit. However, investigations of the electrophysiological effects during acute stage of ischaemia using the isolated-perfused rabbit heart are still few in number.

The aim of this study was to develop a method of acute regional ischaemia reperfusion in the rabbit heart that can be used in conjunction with optical voltage recordings.

3.2 Methods

3.2.1 Langendorff perfusion and left coronary artery occlusion

Adult male New Zealand White rabbits (2.5 - 3.5 kg) were sacrificed by the procedure that was described earlier, and then the hearts was transferred from

chilled saline to the surgical rig and perfused with ice cold Tyrode's solution at perfusion rate of 20 ml/min. The pattern of coronary artery branching was recorded. The left posterior division of the coronary artery was ligated with a suture (4-0 polyester, Ethibond™) threaded into a 2mm piece of polyethylene tubing to form a snare. Heart plus snare were rapidly transferred to the optical rig and perfused at 30-35ml/min standard Tyrode's solution at 37°C, maintained at pH 7.4 by bubbling with a 95%O₂/5%CO₂ gas mixture. Perfusion pressure was monitored with the transducer in line with the aortic cannula. The snare tubing was passed through a hole in the wall of the chamber and the ends of the ligature were connected to the calibrated spring device as described previously. Initially, the ligature was tightened only by as much as was needed to take the slack out of the threads.

3.2.2 Fluorescent tracers of the rabbit coronary artery perfusion

Fluorescent tracers were used to map the route of the vessels through the tissue (Page, 2004). Dextran-conjugated fluorescein (Molecular Probes) is an effective water-soluble marker for such tracing. Dextran labelled fluorescein 50mg/ml (20,000 daltons) was prepared in standard Tyrode's solution. At this molecular weight, diffusion of tracer into the extracellular space is very slow and produced negligible residual tissue fluorescence in these experiments.

The heart was perfused with standard Tyrode's solution containing 15 mM of uncoupler (BDM) at the rate of 30 ml/min. After the motion artefact was suppressed, injection of a bolus of dextran-fluorescein through the circulation via a port in the bubble trap was used to highlight the coronary arteries. The dextran-fluorescein excitation wavelength is 494 nm and peak emission wavelength is 521 nm. The fluorescent indicator was observed by illuminating the heart in the chamber with blue-visible light.

3.2.3 Experimental protocols

The acute local ischaemia protocol consisted of 4 steps:

- (i) Infusion of mechanical uncoupler and stabilization,
- (ii) Control measurements,
- (iii) measurements during ligation and
- (iv) on

reperfusion/recovery. Steps (ii)-(iv) were repeated one or more times in some experiments.

(i) Uncoupler and stabilization

The heart was initially perfused with standard Tyrode's solution for 5 minutes and then changed to solution with uncoupler (15 mM BDM). The heart was perfused with BDM solution until movement was largely inhibited (5-10 mins). Injection of the tracer bound fluorescent dye was performed by rapidly injecting the dextran-fluorescein (Molecular Probes) dissolved in standard Tyrode's solution through the circulation via a port of the bubble trap and illuminated with the blue light. A sequence of snapshot images of the heart were collected over 20 seconds or so. After this time, the vessels were largely flushed of dye and overall fluorescence returned towards pre-injection values. The chamber was then opened and drained of remaining dye-containing solution in order to ready the heart for the next step.

(ii) Control

The heart was loaded with a 100 μ l bolus of RH237. This RH237 was delivered to the coronary circulation by slow injection through the port of a bubble trap as described in Chapter 2.

(iii) Ligation

Local ischaemia was established by tightening the snare to a set tension using the spring device. There then followed a period of 15 minutes at the end which dextran-fluorescein was injected through the port of the bubble trap. The images of the heart were recorded under illumination with blue visible light.

(iv) Reperfusion

Normal perfusion was restored by loosening the snare (zero spring tension). After 20 mins recovery time, a further bolus of dextran-fluorescein was injected through the circulation in order to view the coronary vessels. Images of the heart were recorded as before and the chamber drained of perfusate.

3.3 Results

3.3.1 Rabbit coronary artery anatomy

In the current study, two anatomical branching patterns of the left coronary artery were observed: a bifurcation and a trifurcation pattern (Figure 1.14). Similar patterns have been reported previously for rabbit coronary artery (Lee *et al.*, 2002; Podesser *et al.*, 1997).

Figure 3.1 represents the anterior surface of the LV imaged by the CCD camera. Bolus injection of dye has revealed the network of coronary vessels.

Figure 3.1 A (i) and (ii) show the perfusion distribution seen in the bifurcated pattern after the heart was perfused with standard Tyrode's solution for 10 minutes and after occlusion of the left posterior division of the coronary artery for 20 minutes. In Panel A (i), the light background of fluorescence extending over all of the visible epicardial surface indicates that coronary artery perfusion of tissue is widespread. After the coronary artery is occluded, as shown in panel A (ii), a darkened patch becomes apparent in the left 60% or so of the image indicating reduced perfusion in this area. Figure 3.1 B (i) and (ii) show the perfusion distribution seen in the trifurcated pattern under the same conditions as A. Here a reduction in tissue perfusion is much less evident compared to the bifurcated case.

Out of 36 hearts, 72.2% displayed the bifurcated pattern and 27.8% of trifurcated pattern.

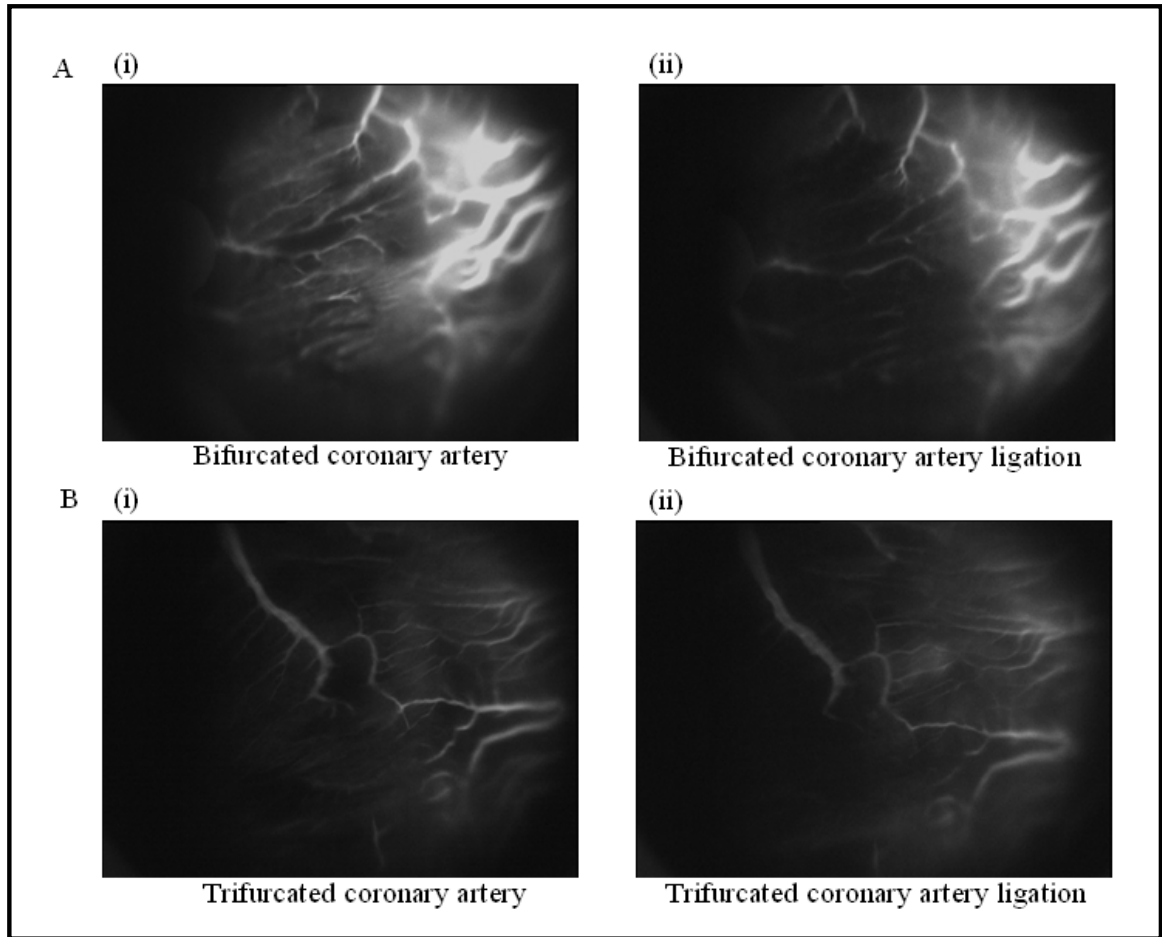


Figure 3.1 The pattern of rabbit coronary artery

3.3.2 Effects of regional acute myocardial ischaemia on APD

In these experiments, OAPs were also recorded. Figure 3.2A shows contour maps of APD_{50} with example OAPs in panel B, during and after performing coronary artery occlusion. The data illustrated below were obtained using the loop-clamp method. Following occlusion, a progressive decrease in APD occurred over 5-10 minutes (panel C). The effects were reversed when the coronary artery occlusion was released, and APD_{50} values at most sites were in fact slightly longer comparing to pre-occlusion values.

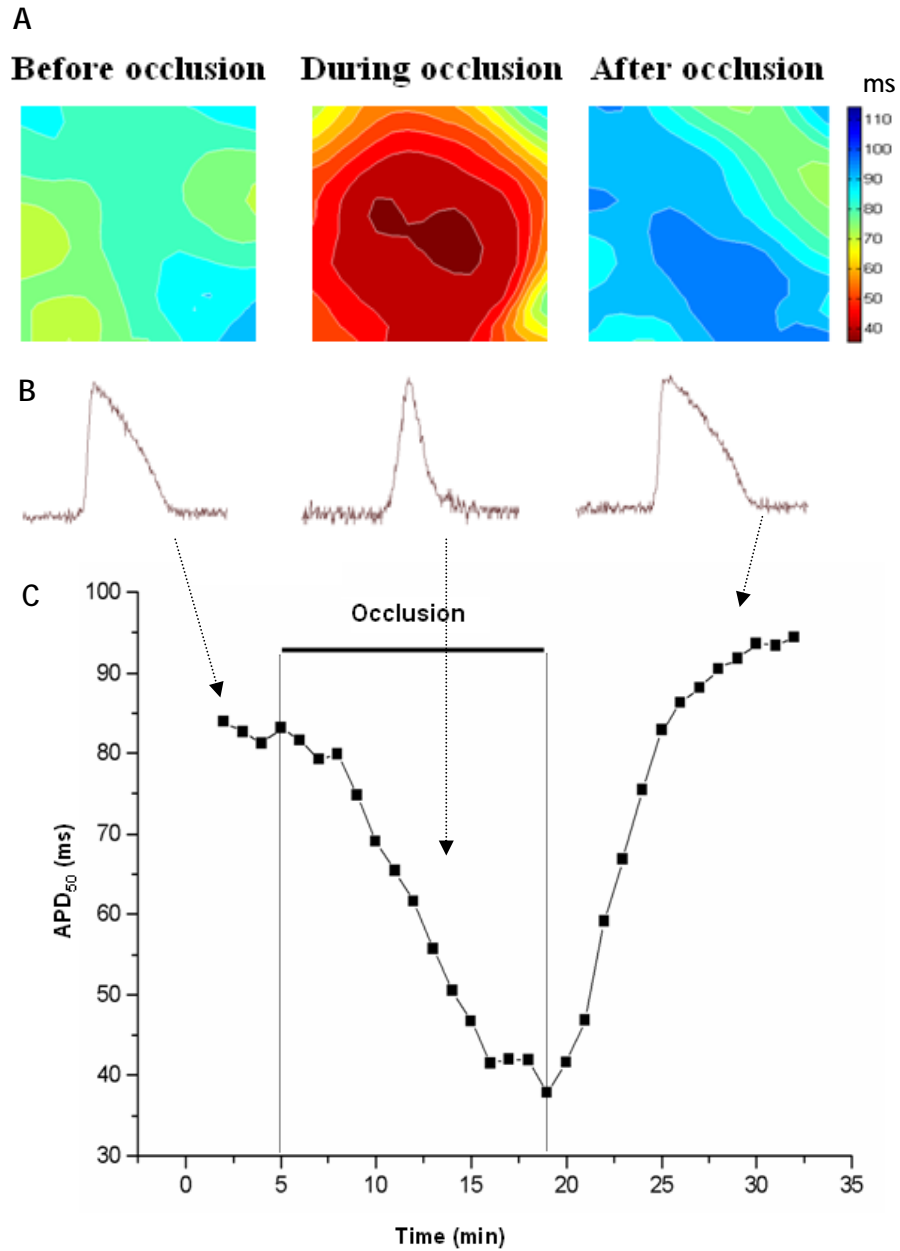


Figure 3.2 Effects of acute myocardial ischaemia on APD

Panel A: Contour maps of APD₅₀ before, during and after coronary artery are blocked.

Panel B: Example of optical action potentials represent from the different stages.

Panel C: Change in average of APD₅₀ from 3x3sites over time. The duration of coronary artery occlusion is shown by the solid bar.

3.4 Discussion

The rabbit model of experimental chronic myocardial infarction has been used for several years and has been shown to model closely ischaemic heart disease in humans (Lee *et al.*, 2002; Miura *et al.*, 1989). Previous studies have described a reliable chronic heart failure model and investigated the possible mechanisms of arrhythmogenesis in the rabbit. However, so far no study has looked specifically at the acute stage.

Previous findings on bifurcation/trifurcation of rabbit coronary branching pattern, it has been inconsistency in either which branch has been chosen or which part of the branch has been ligated (Lee *et al.*, 2002). In an attempt to develop the acute ischaemia model for use in conjunction with the optical mapping, catheterization of the rabbit coronary artery was the first experimental approach. Unfortunately this model gave a low success rate (only 2 out of 10 worked). Even so, catheterization model provides much useful information and preliminary data.

The second experimental trial is a snare technique gave a much higher success rate. However, to produce acute myocardial ischaemia, it was important to characterize the branching pattern of the coronary artery because occlusion of the same artery in the trifurcated pattern produced no clear ischaemic region on the anterior surface of the heart, the most convenient surface for the purposes of recording the electrical properties by using optical mapping techniques.

3.4.1 Coronary artery anatomy of New Zealand White rabbits

Consistent with previous findings, both bifurcation and trifurcation of coronary branching pattern were observed. The more common bifurcated pattern gave the larger and clearer response to block on the anterior surface of the heart. When trifurcated anatomy was present, the ischaemic area which developed as a result of ligation of the left posterior division of the coronary artery was much less evident on the anterior surface. This suggests that, when this pattern is present, the remaining branches can supply the anterior surface adequately. The option to ligate other coronary arteries was not available because a) they were

located in regions inaccessible with the fixed chamber, and b) they did not produce an apically located infarction suitable for optical mapping. Fortunately, the incidence of the trifurcated anatomy was sufficiently low that an acceptable number of ligation procedures produced useable infarcts.

Initial studies with the looped catheter indicated that this procedure had an unacceptably low success rate, due to damage to the surrounding myocardium, including the overlying vein, caused when the surface was cut open for insertion of the catheter.

On the other hand, the snare technique gave a much higher success rate and in conjunction with the bifurcated coronary anatomy reliably produced a number of periods of acute apical ischaemia. Therefore, this procedure was adopted for subsequent experiments described in this thesis.

4 Use of motion artefact blockers

4.1 Introduction

The concept of imaging action potential propagation in the heart was first described in 1913 when Mines investigated the pathway of re-entry in an “auricle-ventricle” tissue preparation from the electric ray, using an electrocardiogram recorded on a smoked drum (Mines, 1913). For the subsequent 9-10 decades, further work has documented the mapping of irregular rhythm in the human heart using the latest available technology (Barker *et al.*, 1930). Mapping of the human heart was developed for use during surgeries and it was developed for use in isolated hearts in Langendorff mode (Durrer *et al.*, 1970). Subsequently, optical mapping techniques based on voltage sensitive dyes became a major tool for studying electrophysiological properties of isolated animal heart models.

Optical mapping techniques have many advantages for imaging electrical or other functional parameters in hearts when compared to other non-invasive imaging techniques such as positron emission tomography, magnetic resonance and ultrasound imaging (Efimov *et al.*, 2004). However, currently the technique is severely limited by the presence of motion artefacts. These can be suppressed using mechanical restraint or pharmacological agents such as BDM or cyto-D. But these blockers have side effects on myocardial electrophysiology in many experimental animals (Nygren *et al.*, 2006). Recently the agent blebbistatin has been suggested as the agent of choice for optical measurements on rabbit hearts due to an absence of effects on the underlying electrophysiology of the heart (Fedorov *et al.*, 2007; Farman *et al.*, 2007). But studies examining the efficacy of blebbistatin have not examined the behaviour of the heart under conditions of metabolic compromise such as hypoxia and ischaemia, conditions that might affect the effectiveness of the drug.

4.1.1 BDM

BDM is a myofibril ATPase inhibitor agent that is commonly used to reduce contraction amplitude by inhibiting myofilament force. However, BDM is known to inhibit many ion currents in a dose dependent manner (Blanchard *et al.*, 1990; Cheng *et al.*, 2004; Artigas *et al.*, 2006; de Tombe *et al.*, 1992). For instance, BDM at 15 mM in mouse heart showed a reduction in conduction velocity but a lengthening of the APD (Baker *et al.*, 2000). However, in other animal models such as swine, sheep and guinea pig, BDM has been reported to decrease APD₉₀ at 5-20 mM (Liu *et al.*, 1993; Lee *et al.*, 2001) and also shown to affect intracellular Ca²⁺ signalling and inhibit ATP transport across mitochondrial membranes in isolated heart cells (Stapleton *et al.*, 1998). In addition, the presence of BDM altered the nature of shock induced arrhythmias and reduced the effectiveness of cardioplegic solutions (Cheng *et al.*, 2004; Boban *et al.*, 1993). But few studies appear to have examined the effectiveness of BDM under conditions of metabolic compromise.

4.1.2 Blebbistatin

Blebbistatin is a more recently reported contraction blocker which acts by inhibiting myosin II ATPase in the actin detached state (Stapleton *et al.*, 1998; Straight *et al.*, 2003; Allingham *et al.*, 2005). Blebbistatin specifically inhibits non-muscle and skeletal muscle myosin isoforms without interfering with smooth muscle isoforms or other members of myosin family. Blebbistatin at 10 µM has been reported to uncouple cardiac myofilament activation from the activating Ca²⁺ without affecting the intracellular Ca²⁺ signal or the electrophysiology of rabbit heart tissue (Fedorov *et al.*, 2007). Therefore, the specificity of blebbistatin is potentially advantageous in the study of many fields that involve immobilization of tissue or organ including optical imaging of the heart.

However, the inhibitory effect of Blebbistatin on the contractile proteins has been reported to reverse when exposed to the short wavelength light such as UV (365 nm) and visible blue (450-490 nm) (Sakamoto *et al.*, 2005; Fedorov *et al.*, 2007; Kolega, 2004). According to recent studies (Fedorov *et al.*, 2007) using

similar optical techniques to those employed in this thesis the signals from voltage sensitive dye such as RH237 and Di-4-ANNEPS, indicated that the effect of Blebbistatin was unaffected by illumination at the the longer wavelengths light (525 ± 30 nm) used with RH237 and Di-4-ANNEPS. Blebbistatin itself also has the intrinsic fluorescence with peak excitation and emission wavelengths at 330 and 500 nm, respectively (personal communication, Iffath A. Ghouri, University of Glasgow).

In summary, despite the known side effects, BDM has been used extensively as a mechanical uncoupler in many studies including those involving optical dyes because of its relatively low cost and apparently readily reversible effects. Blebbistatin is a recently reported uncoupler with apparently fewer effects under normoxic conditions but no studies have examined the effects of this drug under ischaemic conditions. The purpose of this study was to investigate the comparative electrophysiological effects of BDM and Blebbistatin in the rabbit heart in order to establish a reliable methodology for optical recording of action potentials from the epicardial surface of the heart under acute regional and global ischaemic conditions.

4.2 Methods

4.2.1 Experimental protocols

4.2.1.1 Acute local ischaemia

The heart was perfused with standard Tyrode's solution for 5 minutes at a constant rate of 30-35 ml/min by using Gilson Minipuls 3 peristaltic pump. Then the solution was changed to one containing uncoupler: either 15 mM BDM or 5 μ M blebbistatin. The heart was perfused until movement artefacts were reduced, the transition taking approximately 10 minutes. Local ischaemia was produced using the calibrated snare device as described in Methods. The coronary artery was occluded for 15 minutes after which the snare was loosened to reperfuse the heart. Recordings were made every minute for at least 20 minutes of reperfusion.

4.2.1.2 Acute global ischaemia

The heart was initially perfused with standard Tyrode's solution for 5 minutes and then changed to solution with uncoupler (15mM BDM or 5 μ M of blebbistatin). A series of low flow perfusion periods were imposed at 0, 1, 5 and 10 ml/min. The heart was perfused for 15 minutes at each of these low flow rates and reperfused by returning to 30-35 ml/min for 20-30 minutes. During low flow perfusion, the exterior temperature of the heart was maintained at 37°C by extra filling the chamber with standard Tyrode's solution.

4.2.2 Optical action potential recordings

The bipolar platinum electrode was inserted into 1 mm hole in a frontal platter of the Perspex chamber and the heart was paced at a 250 ms cycle length. The ECG electrodes were connected to the MAP amplifier and signals monitored on an oscilloscope (Nicolet Instrument Corporation, Wisconsin, USA.). Both stimulus and ECG-wave recorded to disk along with the optical signals. The ECG traces were interpreted in a standard fashion as interpreted in the human limb lead recording (Garibyan & Lily, 2007):

- (i) PR interval is measured from the onset of P-wave to the onset of QRS
- (ii) QRS width is measured from the beginning to the end of the QRS complex
- (iii) QT interval is measured from the beginning of the QRS to the end of the T wave
- (iv) RR interval is measured from the peak of R wave to the peak of the next R wave

For the analysis, epicardial membrane potentials were averaged from several pixels as described in methods section.

4.2.3 Statistical analysis

All data are expressed as mean \pm SEM. Paired t-test was used to compare between groups of data. Data were imported to InStat3 (GraphPad Software Inc., USA) in order to test the significance between two groups, p-value of less than 0.05 was considered significant.

4.3 Results

4.3.1 Use of BDM to inhibit movement artefact

4.3.1.1 Regional ischaemia

Figure 4.1 shows an isochronal map of APD₅₀ and rise time with OAPS from the selected site before, during and after performing the coronary artery occlusion in the presence of BDM. Following occlusion, a progressive decrease in APD and a slight slowing in upstroke slope occurred over the subsequent 5-10 minutes. The effects were reversed when the coronary artery occlusion was released, with a return to normal values for APD and rise time, although the recovery of rise time was not uniform across the epicardial surface with the left hand side showing pronounce prolongation.

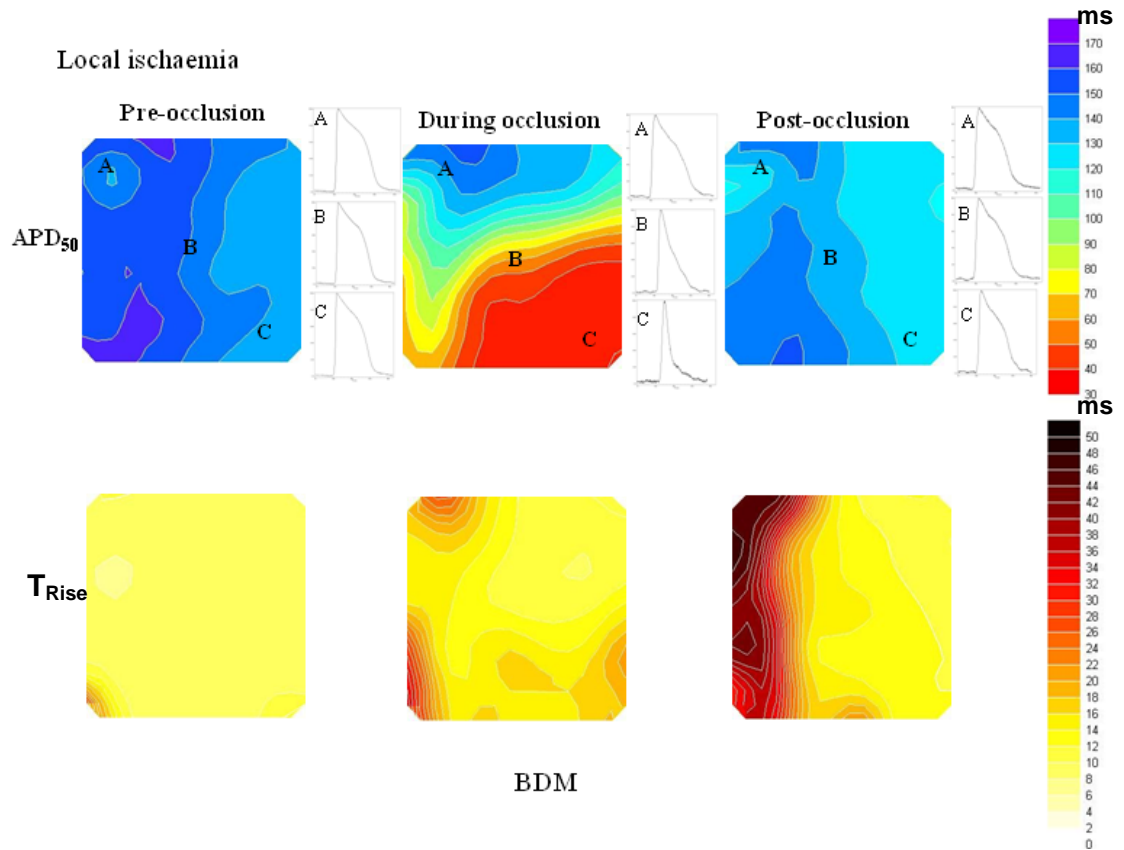


Figure 4.1 Isochronal maps of APD₅₀ and rise time represent before, during and after coronary artery occlusion

The upper panel shows maps of APD₅₀ and lower panel shows maps of T_{Rise}. The optical action potentials show from three selected sites, A: Normal zone, B: Border zone and C: Ischaemic zone.

Figure 4.2 shows the time course of the changes in APD₅₀ and T_{Rise} over the time of occlusion and recovery. The APD₅₀ was dramatically decreased in the border zone and ischaemic area but there were no significant changes in non-ischaemia area. However, the time of upstroke was marked slower during occlusion only in the ischaemic zone. After releasing the snare, both APD₅₀ and the rise time completely returned to the normal values.

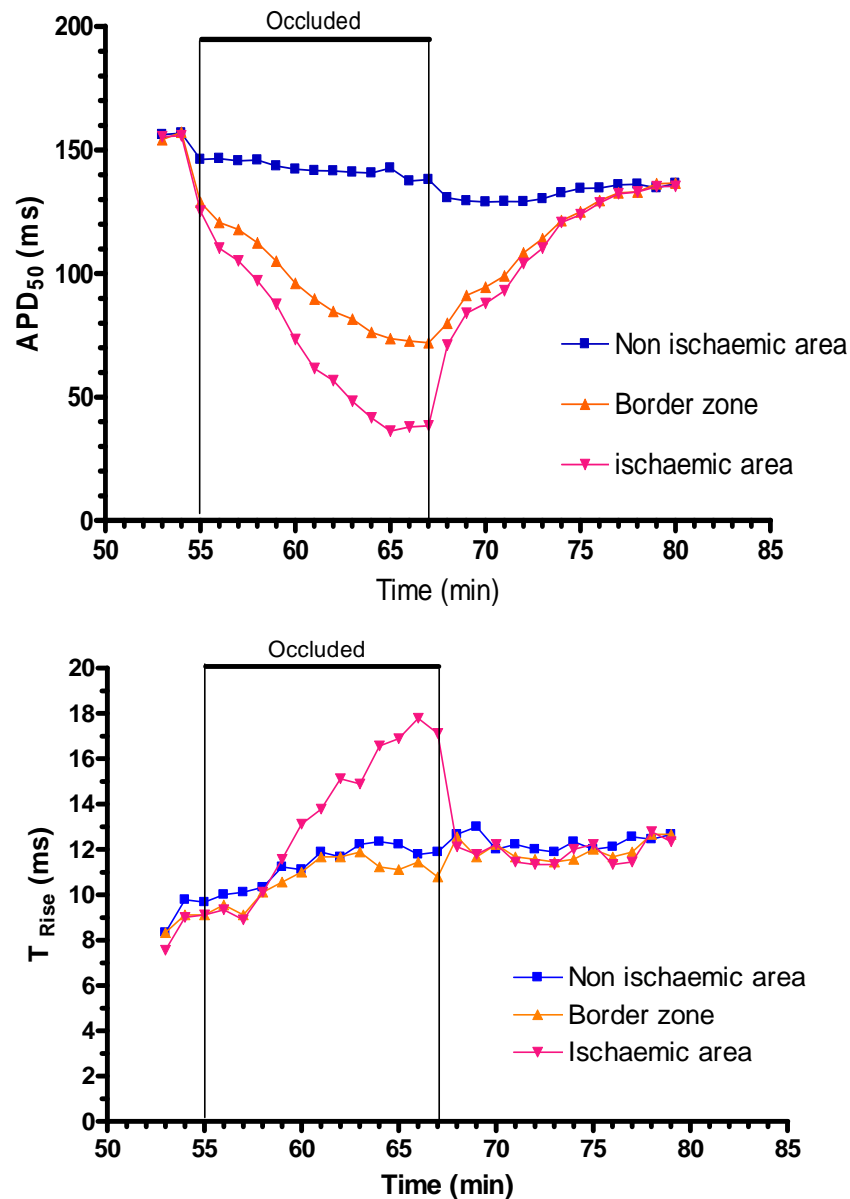


Figure 4.2 The changes in APD₅₀ and Rise time over the period of occlusion in selected sites

Figure 4.3 displays bar graphs showing the average of APD₅₀ and rise time from normal zone (NZ) and ischaemic zone (IZ) before, during and after coronary artery occlusion. Data are expressed as mean \pm SEM from 10 hearts. By 12-15 minutes, ligation had caused a significant decrease in APD₅₀ in the zone of reduced perfusion from 130.9 ± 4.7 ms to 74.8 ± 4.2 ms (mean \pm SE, $n=10$, $P < 0.0001$). After restoring full perfusion, APD₅₀ returned to a value not significantly different from normal (121.1 ± 3.1 ms). In addition to the marked changes in APD, the rise time of the action potential (T_{Rise}) showed increases from 8.1 ± 0.5 ms to

16.8±1.8ms (P<0.005). In the non-infarcted area of myocardium, no significant changes in APD₅₀ (134.9±5.6ms vs. 127.6±4.3ms) were observed during occlusion.

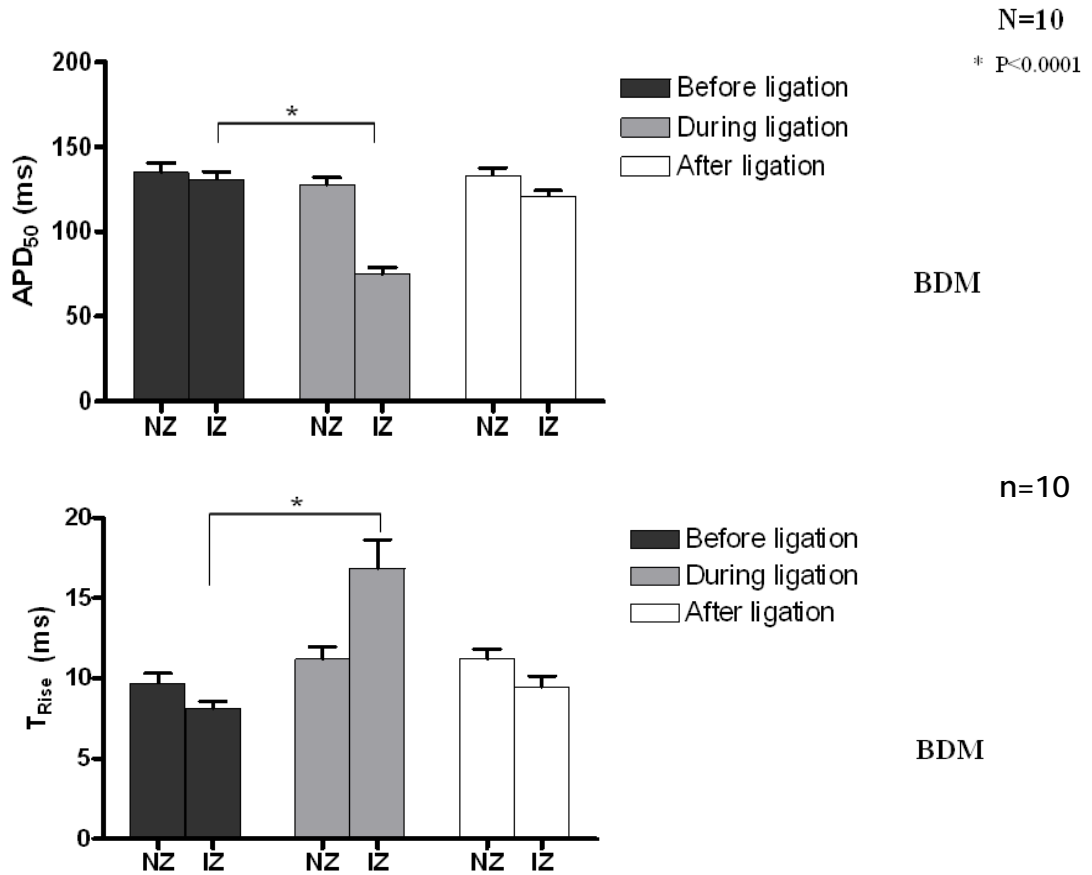


Figure 4.3 Mean of APD₅₀ and Rise Time

The APD₅₀ and Rise Time are recorded at two epicardial sites (NZ and IZ) on heart from sham animal that perfused by standard Tyrode's solution and BDM. Asterisks (*) represent statistically significant differences between groups.

4.3.1.2 Global ischaemia using lowered flow

Figure 4.4 illustrates isochronal map of APD₅₀ and Rise time with OAPS from the selected site before, during and after decreasing the flow rate to 5ml/min. Following low flow perfusion, a spatially widespread decrease in APD and progressive decrease in T_{Rise} occurred over the subsequent 2-5 minutes. The effects were incompletely reversed when returned the perfusion rate to 30ml/min. APD₅₀ was shorter and the rise time was longer compared to the normal perfusion condition.

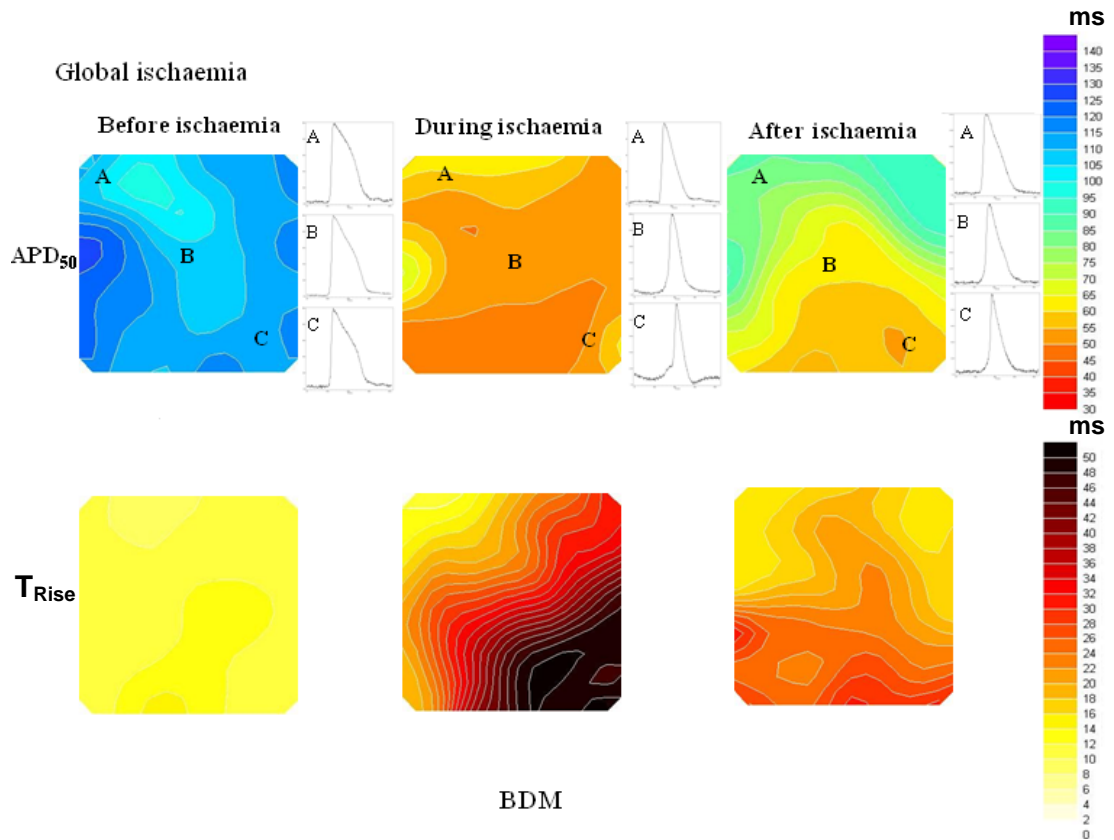


Figure 4.4 Isochronal maps of APD_{50} and Rise time

Isochronal maps represent before, during and after reduced the flow rate to 5ml/min. The optical action potentials show from three selected sites: A, B and C.

Figure 4.5 shows the time course of the changes in APD_{50} and Rise Time over the time of perfusion at 5ml/min. The APD_{50} is dramatically decreased in all of the selected zones albeit it did not reach statistical significance (see Figure 4.6). However, the time of upstroke is slightly slower during low flow ischaemia in zone C but markedly slower in A and B. After reperfusion at 30ml/min, neither APD_{50} nor the rise time completely returned to the normal values.

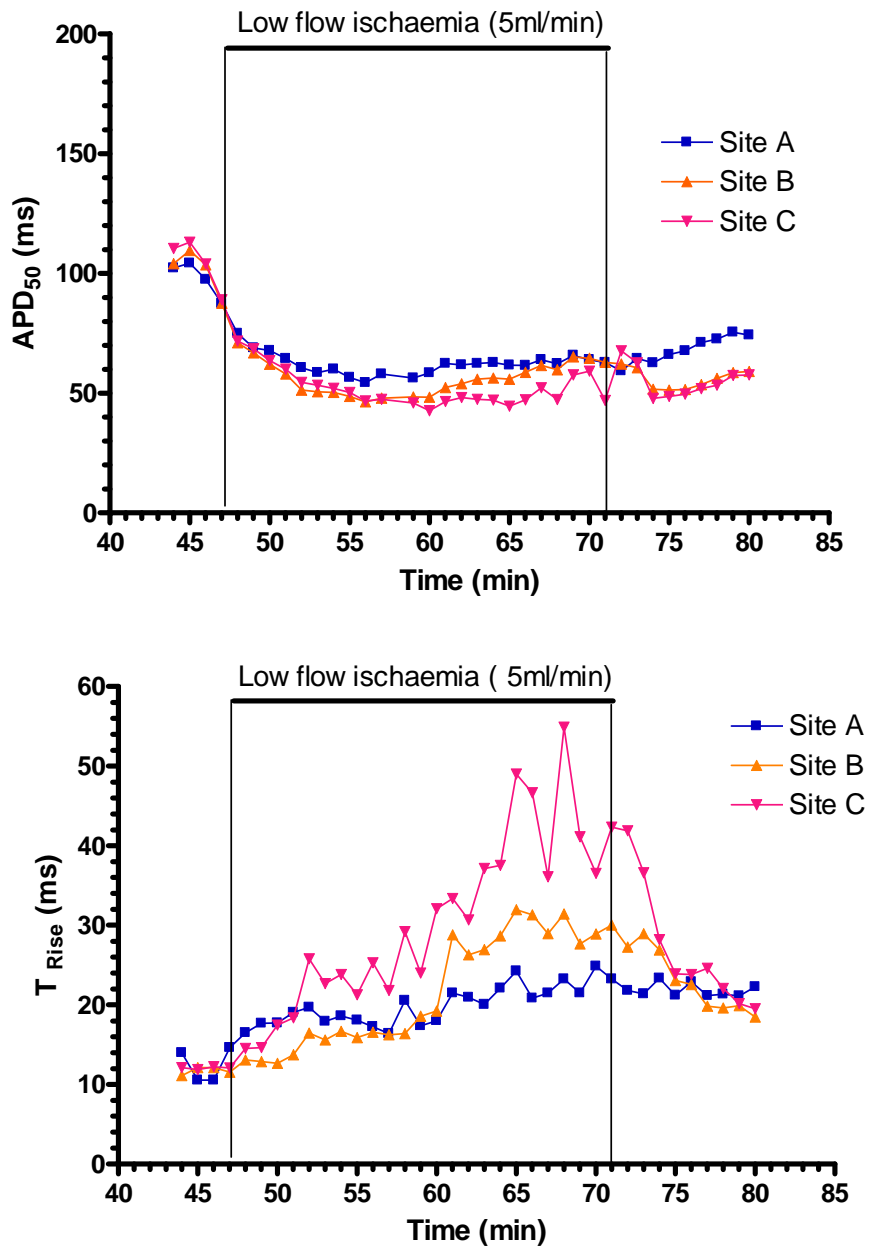


Figure 4.5 Changes in APD₅₀ and Rise time over the period of low flow perfusion in selected sites

Figure 4.6 shows average APD₅₀ and rise time from zone A and B before, during and after the perfusion rate was reduced to 5ml/min. Low flow perfusion for 15-20 minutes caused a non-significant decrease in APD₅₀ between two zones from 101.7 ± 9.3 ms to 66.1 ± 10.4 ms (mean \pm SEM, $n=7$, $P>0.05$). After restoring full perfusion, APD₅₀ returned to a value not significantly different from normal (103.6 ± 9.6 ms). The changes in time of upstroke (T_{Rise}) showed increases from

10.3±1.1ms to 16.8±3.6ms ($P<0.05$). No significant changes in APD_{50} were observed between zone A and B.

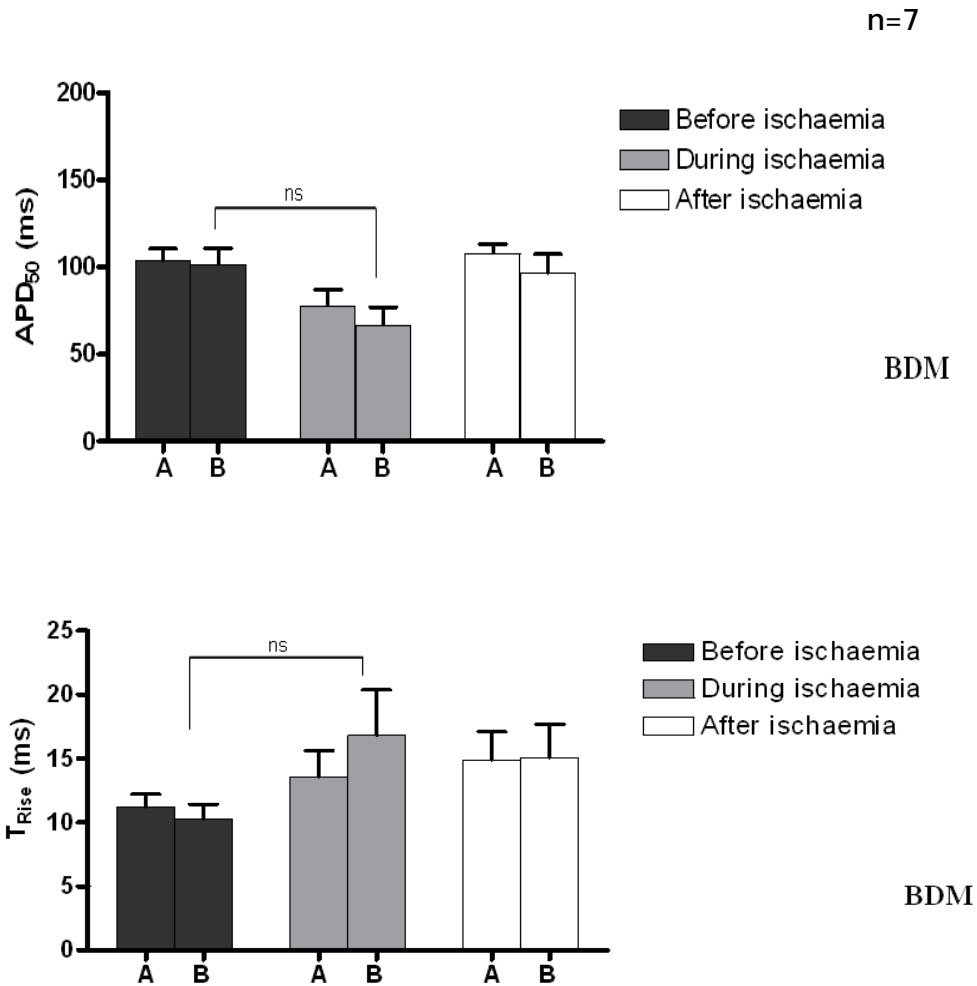


Figure 4.6 Mean APD_{50} and Rise Time

The APD_{50} and Rise Time are recorded at two epicardial sites (A and B) on heart from sham animal that perfused by standard Tyrode's solution and BDM. ns indicates no statistically significant difference.

4.3.2 Use of Blebbistatin to inhibit movement artefact

4.3.2.1 Regional ischaemia

Figure 4.7 illustrates isochronal map of APD_{50} and Rise time with OAPs from the selected site before, during and after performing the coronary artery occlusion during perfusion with blebbistatin. Following occlusion, a progressive decrease in APD and slight decrease in upstroke slope occurred over the subsequent 5-10

minutes. The effects were completely reversed when the coronary artery occlusion was released.

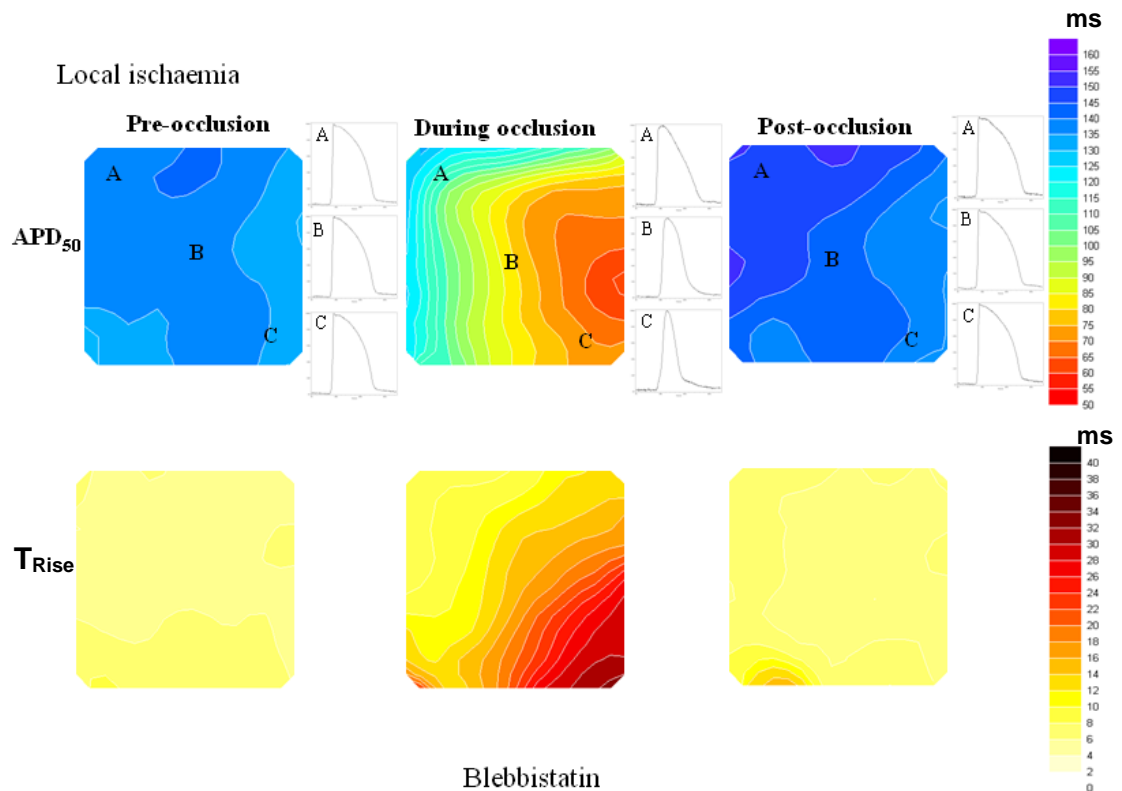


Figure 4.7 Isochronal maps of APD_{50} and Rise time

Isochronal maps represent before, during and after coronary artery occlusion. The optical action potentials show from three selected sites, A: Normal zone, B: Border zone and C: Ischaemic zone.

Figure 4.8 shows the time course of changes in APD_{50} and T_{Rise} over the time of occlusion. The APD_{50} was dramatically decreased in the border zone and ischaemic area but no significant changes were visible in non-ischaemia area. However, the time of upstroke was markedly slower during occlusion in the zone of ischaemia and slightly slower in the border zone. After releasing the snare, both APD_{50} and the rise time completely returned to the pre-occlusion value.

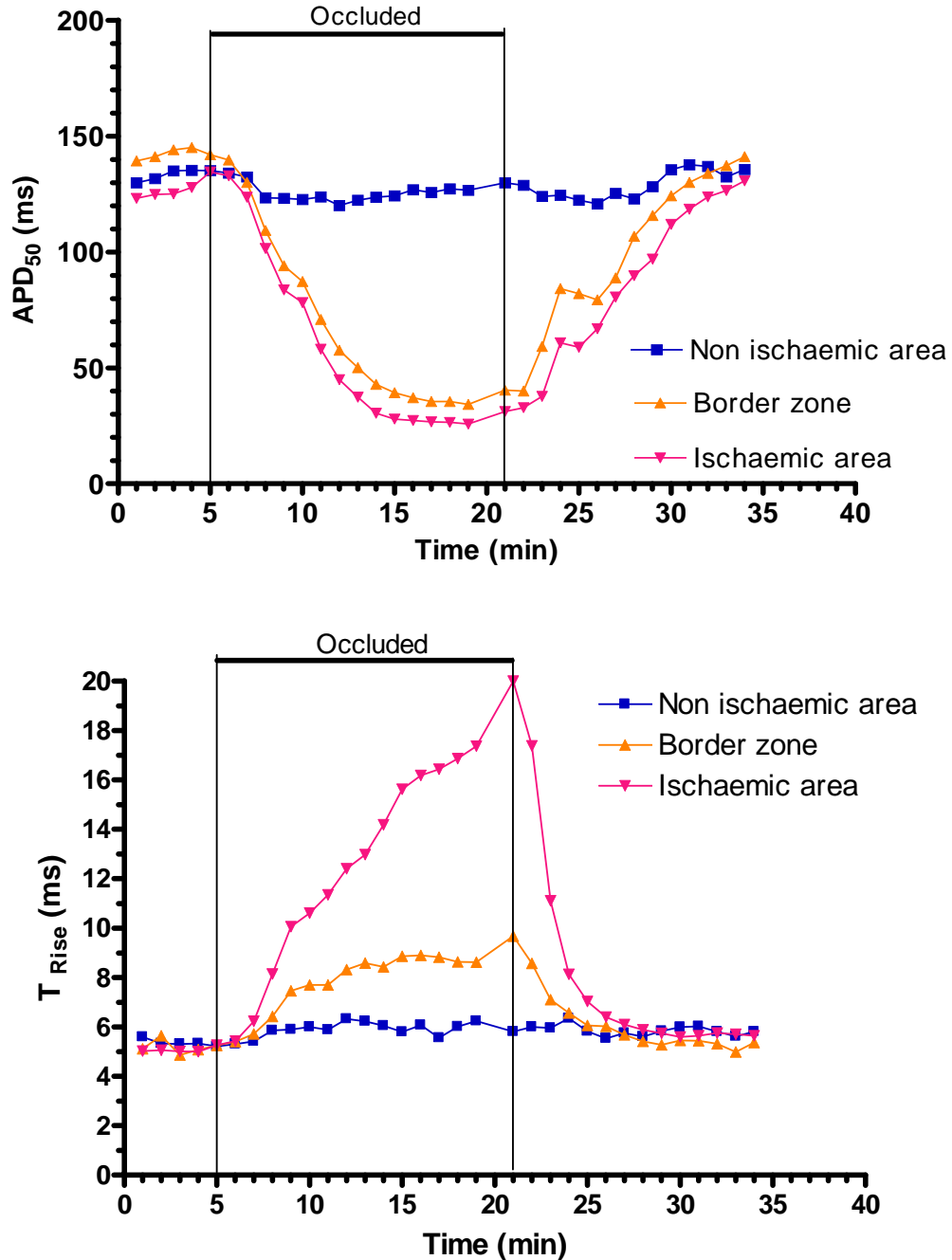


Figure 4.8 The changes in APD₅₀ and T_{Rise} over the period of occlusion in selected sites

Figure 4.9 shows APD₅₀ and rise time from normal zone and ischaemic zone before, during and after coronary artery occlusion. Ligation 12-15 minutes caused a significantly decrease in APD₅₀ in the zone of reduced perfusion from 141.4±5.2ms to 55.4±9.4ms (mean±SE, n=10, P<0.0001). After restoring full perfusion, APD₅₀ returned to a value not significantly different from normal (148.9±6.9ms). T_{Rise} showed increases from 7.3±1.0ms to 17.5±2.9ms (P<0.005).

In the non-infarcted area of myocardium, no significant changes in APD_{50} (146.6 ± 7.0 ms vs. 147.8 ± 8.0 ms) were observed during occlusion.

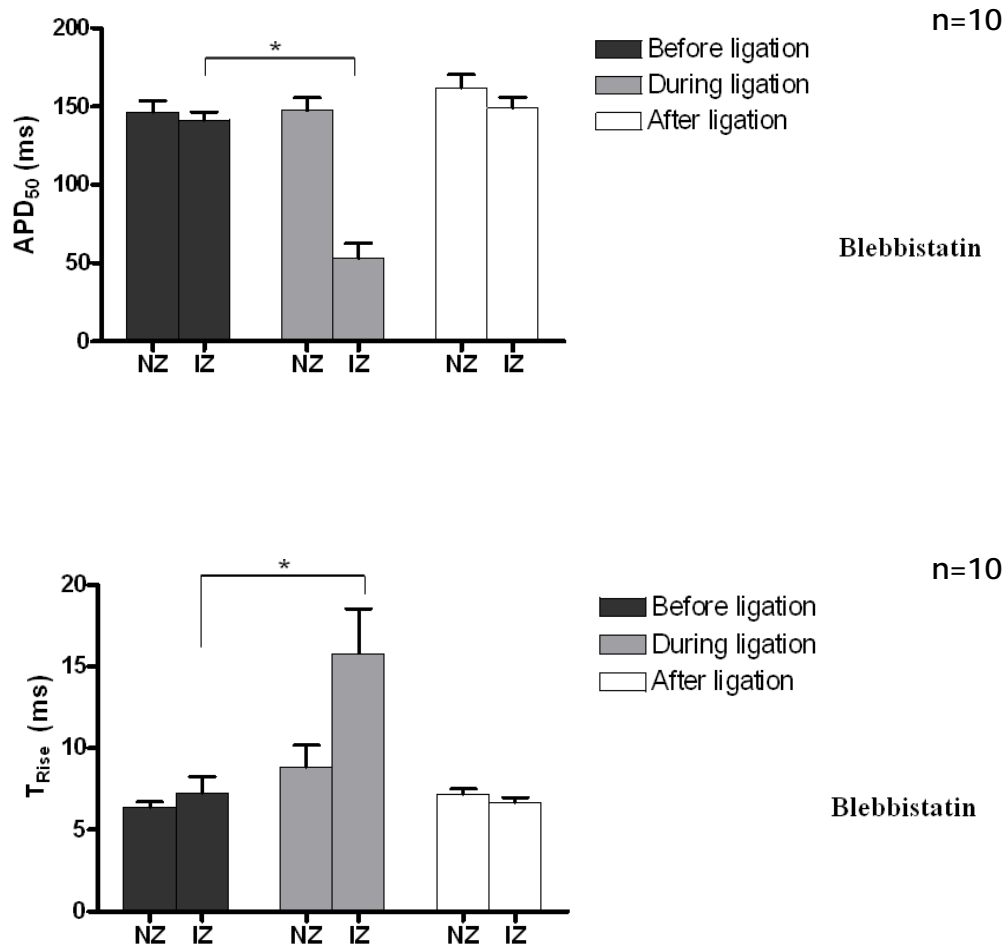


Figure 4.9 Mean of APD_{50} and Rise Time

The APD_{50} and Rise Time are recorded at two epicardial sites on heart from sham animal that perfused by standard Tyrode's solution and blebbistatin. Asterisks (*) represent statistically significant different between groups.

4.3.2.2 Global ischaemia induced by low flow

Figure 4.10 shows isochronal maps of APD_{50} and Rise times from the selected sites A, B and C before, during and after decreasing the flow rate to 5ml/min. Following low flow perfusion, a progressive decrease in APD and a slight decrease in upstroke slope occurred over the subsequent 5-10 minutes. The

effects were incompletely reversed when fully reperfused. APD_{50} is slightly longer than the normal perfusing condition.

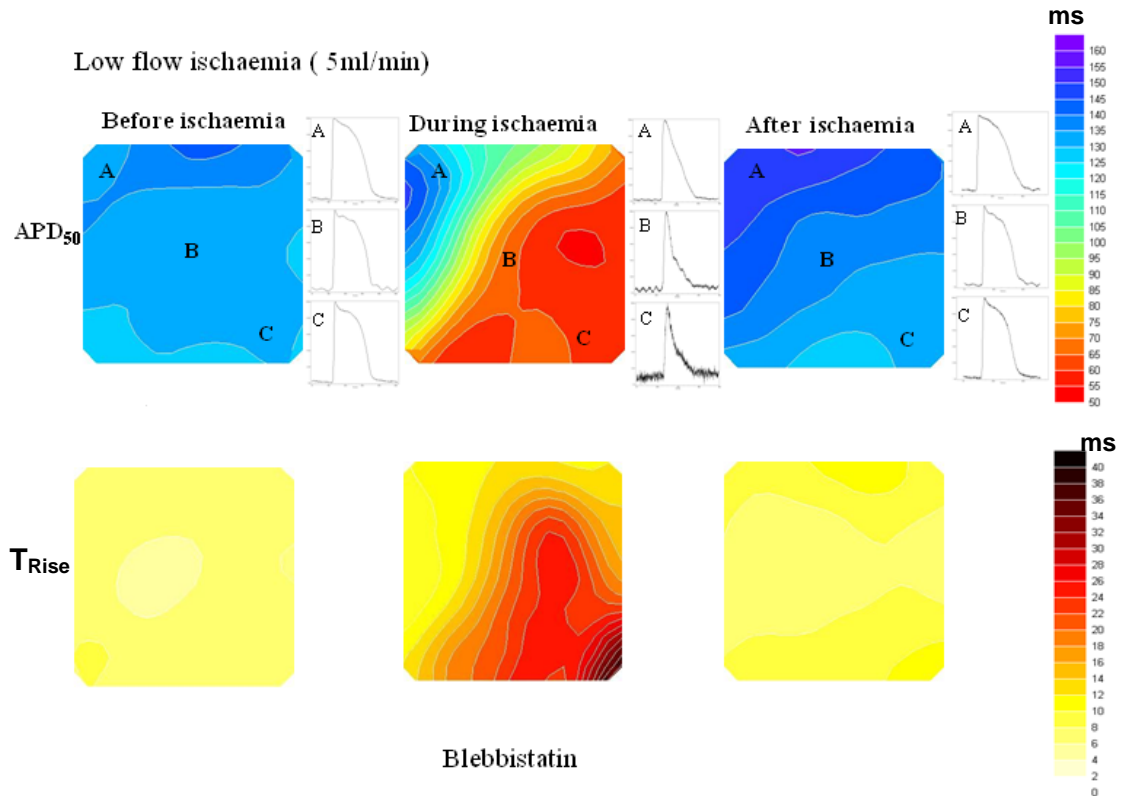


Figure 4.10 Isochronal maps of APD_{50} and Rise time

Isochronal maps represent before, during and after reduced the flow rate to 5ml/min. The optical action potentials show from three selected sites, A, B and C.

Figure 4.11 shows the time course of changes in APD_{50} and Rise Time over the time of low flow ischaemia. The APD_{50} was uniformly decreased and the time of upstroke was also slower during occlusion in all three zones. After releasing the snare, both APD_{50} and T_{Rise} returned completely to their normal values.

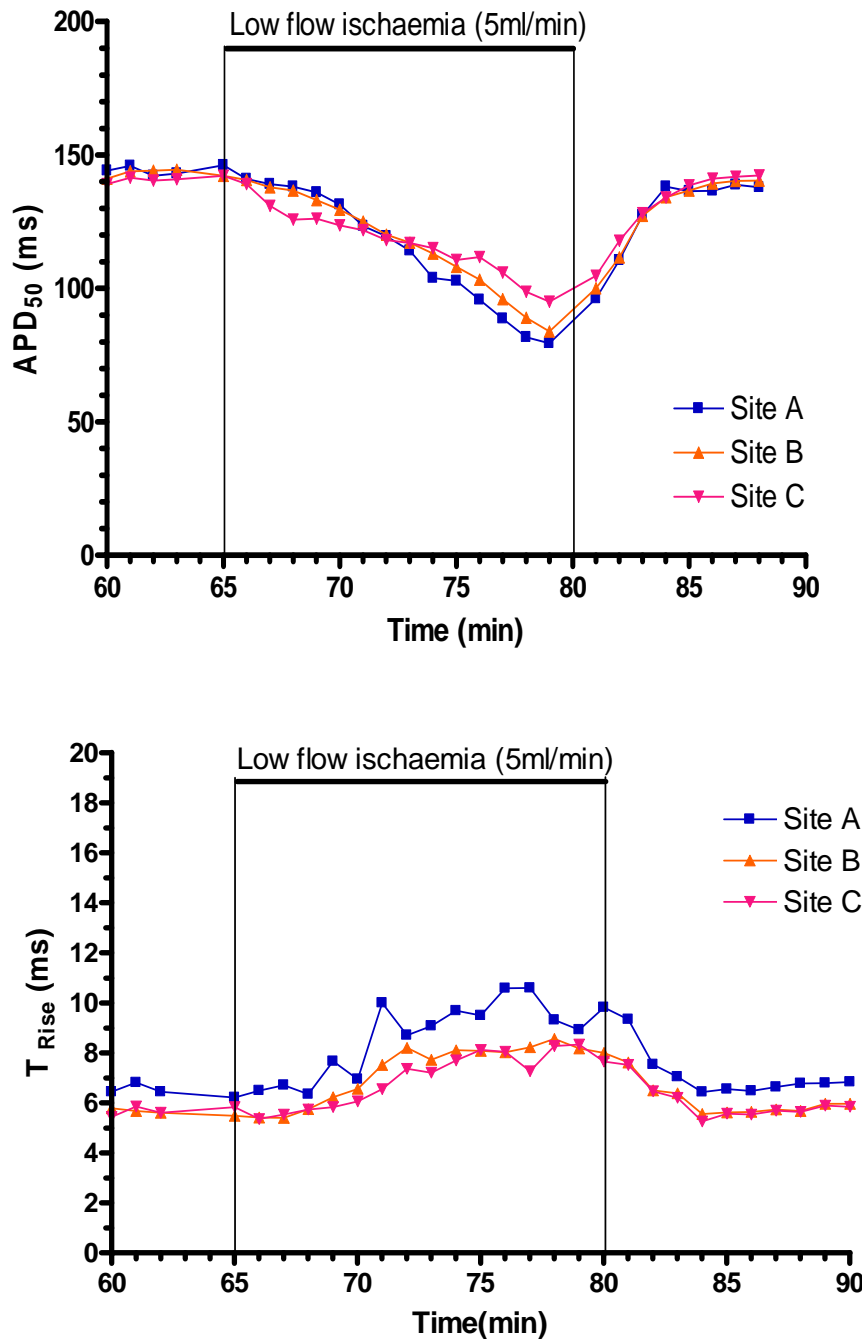


Figure 4.11 The changes in APD₅₀ and Rise time over the period of low flow perfusion in selected sites

Figure 4.12 shows APD₅₀ and rise time from 2 selected zones before, during and after the perfusion rate was reduced to 5ml/min. Low flow perfusion of 15-20 minutes caused a significant decrease in APD₅₀ in the zone B from 146.5 ± 7.7 ms to 65.3 ± 7.4 ms (mean \pm SEM, n=7, P<0.001). After returning to a perfusion rate of

30ml/min, APD₅₀ returned to a value not significantly different from normal (136.7±10.9ms). The rise time of the action potential showed increases from 6.5±0.4ms to 13.3±2.6ms (P<0.05). The changes in APD₅₀ seen during low flow ischaemia were not significantly different between zone A and B.

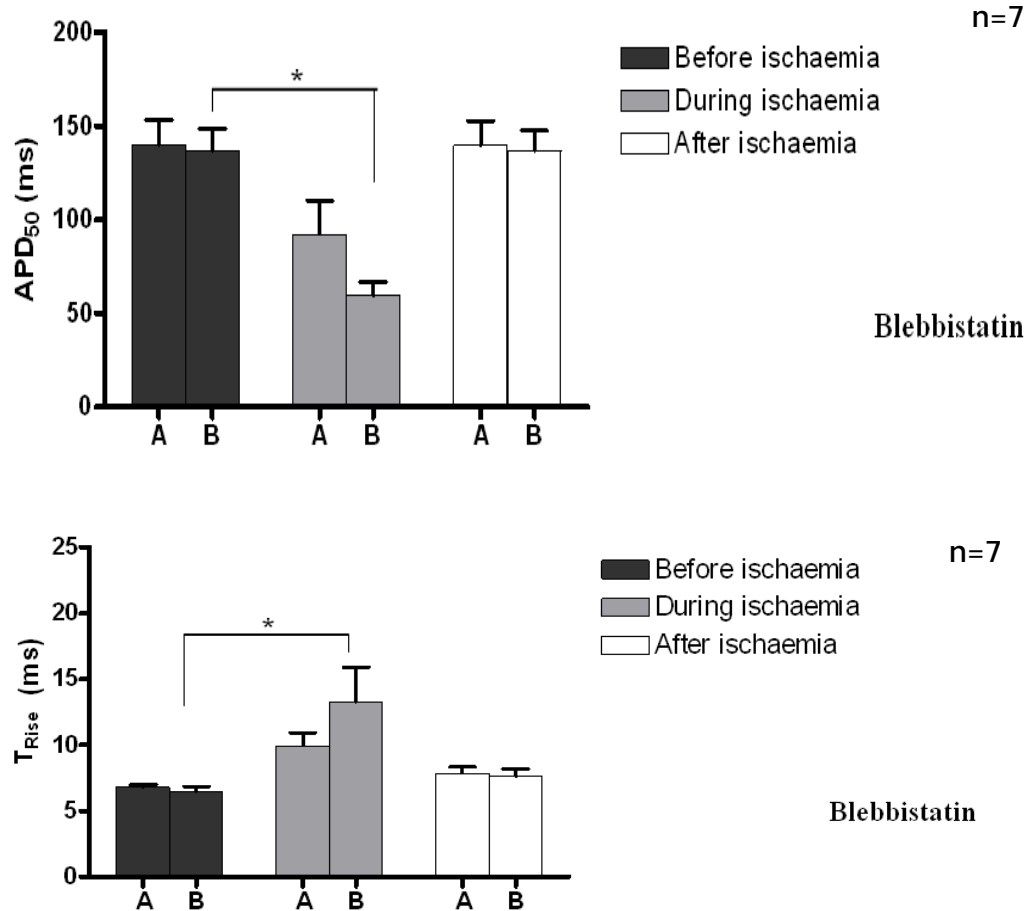


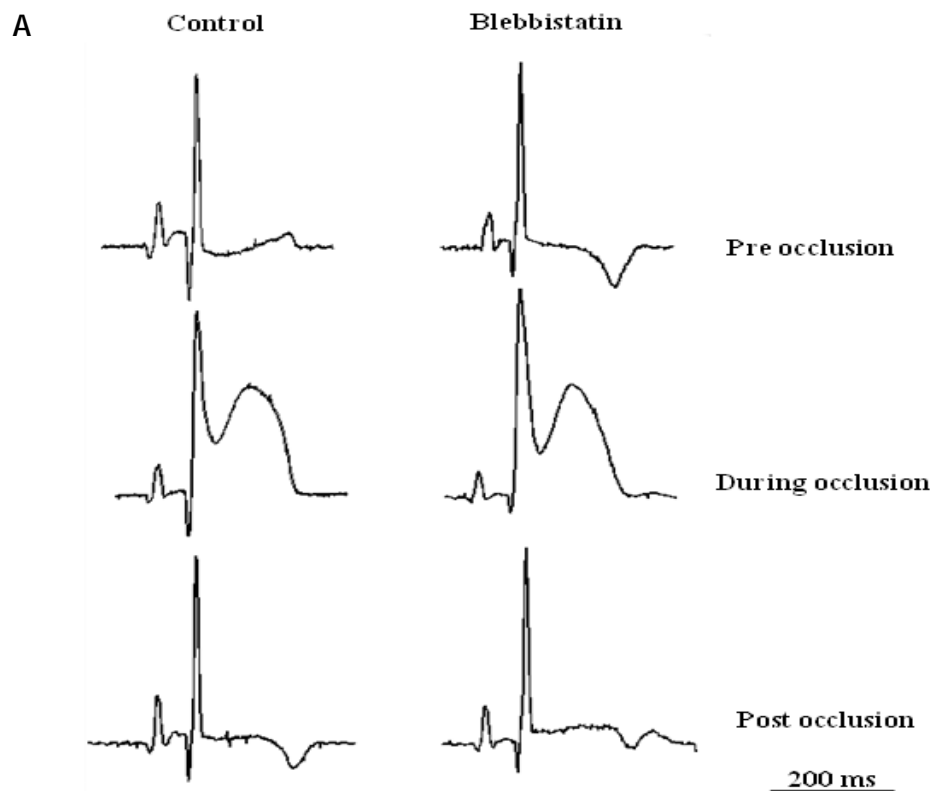
Figure 4.12 Mean of APD₅₀ and T_{Rise}

The APD₅₀ and Rise Time are recorded at two epicardial sites on heart from sham animal that perfused by standard Tyrode's solution and blebbistatin. Asterisks (*) represent statistically significant different between groups.

4.3.3 Effect of Blebbistatin on ECGs characteristic

While clearly blebbistatin appeared to not have long term effects on cardiac electrophysiology, it was not clear whether the electrophysiology of the heart was normal in the presence of the uncoupler. To study this in detail, measurements were made to compare the ECG signal from hearts without

uncouplers with those treated with blebbistatin. Figure 4.13 shows the effects of blebbistatin (5 μ M) on the electrocardiogram of the Langendorff-perfused rabbit heart recorded before, during and after occlusion. Control represents the recordings during perfusion with standard Tyrode's solution before adding uncoupler. Panel A shows the ECG recordings between control group and blebbistatin group, the QT interval was not significantly altered after occlusion, due to the QT interval reflecting the whole heart, which may mask regional changes. Panel B summarizes PR interval, QRS width and, QT and RR intervals in standard Tyrode's solution and Tyrode's solution with blebbistatin before occlusion and during occlusion. Blebbistatin had no consistent effect on ECG shape beyond the variation between hearts observed normally. The results indicates that the over all electrophysiology of the heart was unaffected by the uncoupler.



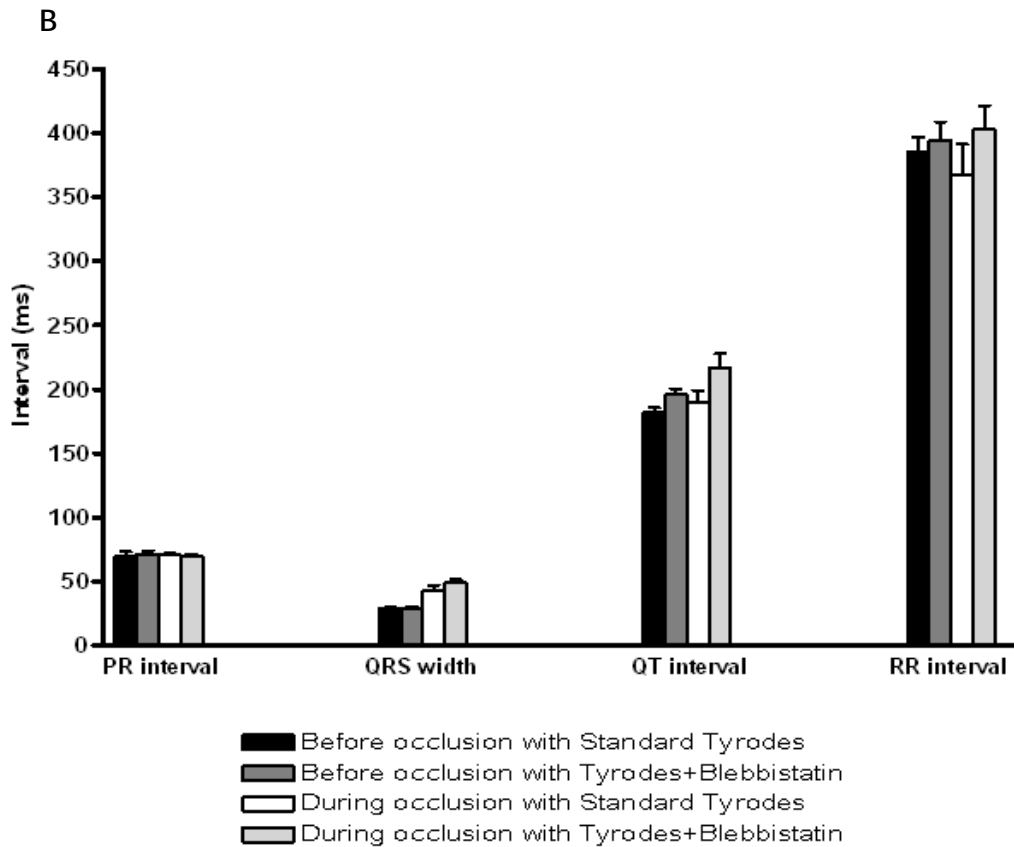


Figure 4.13 Effects of blebbistatin on psECG

Panel A: Pseudo-electrocardiogram (ECG) recorded during the period of coronary artery occlusion

Panel B: Averaged PR, QRS width, QT and RR interval (N=6), with error bars.

4.4 Discussion and conclusion

The purpose of this chapter was to investigate the electrophysiological effects of BDM or Blebbistatin under normal and ischaemic conditions.

4.4.1 Effects of BDM

In this study, similar effects of BDM on APD were observed as previously reported in canine myocardium (Riccio *et al.*, 1999). At 15 mM BDM slightly shortened APD₅₀ and lengthened the time to upstroke in both regional ischaemia and low flow ischaemia (5ml/min). As shown in Figure 4.1 and 4.2 for regional ischaemia,

Figure 4.4 and 4.5 for global ischaemia induced by a low flow rate, there are clear implications for the use of BDM as a motion artefact blocker. Because the APD₅₀ and rise time do not recover fully on reperfusion, this agent is not suitable for investigation of APD in the rabbit. However, no statistical change of APD₅₀ and rise time between ischaemic and normoxic area were observed using the BDM.

4.4.2 Effects of Blebbistatin

Blebbistatin substantially depressed the motion artefact at concentration of 5µM which is half the concentration previously reported. However, the duration of action at the lower concentration was the same as usual concentration at 10 µM. The transition is taking approximately 40 minutes after applying blebbistatin (Fedorov *et al.*, 2007). In the current study, blebbistatin had no effect on electrophysiological properties comparable to previous results reported in rat and rabbit (Fedorov *et al.*, 2007; Sakamoto *et al.*, 2005). However, there were small effects of blebbistatin on APD with lower flow rate of 5ml/min as shown in Figure 4.10. Therefore, studies of global myocardial ischaemia by using lower flow rates or stopped the flow in the presence of blebbistatin must be interpreted with caution.

From this investigation of BDM (15 mM) and blebbistatin (5 µM) are the effective agents for suppressing the movement artefact in whole rabbit heart. However, the effects of BDM on electrical properties were substantial whereas those of blebbistatin were minimal.

While clearly blebbistatin appeared to not have long term effects on cardiac electrophysiology, it was not clear whether the electrophysiology of the heart was normal in the presence of the uncoupler. To study this in detail, measurements were comparing the ECG signal from hearts without uncouplers with those treated with blebbistatin.

5 Use of RH237 to study regional myocardial flow

5.1 Introduction

CAD is the leading cause of sudden cardiac death in UK and third world countries. Detecting regional myocardial perfusion abnormalities is a cornerstone in the diagnosis of coronary artery disease and determination of myocardial viability. Many approaches have been used in an attempt to provide precise measurements of regional myocardial blood flow.

To date, myocardial blood flow in humans can be assessed by several techniques for example: the inert gas wash out technique, positron emission tomography (PET) or injection of radio-labelled microspheres or ultrasound contrast agents.

PET is a technique that allows non-invasive quantification of regional myocardial flow in humans, *in vivo* but the technique requires special equipment that is costly and therefore is not widely available. Myocardial contrast echocardiography (MCE) is an emerging technique that is able to rapidly assess myocardial perfusion at the capillary level in many different clinical settings (Kamiya *et al.*, 2002; Kaufmann & Camici, 2005; Lichten & Engel, 1979). The thermal diffusion method allows real-time continuous tissue blood flow measurement based on relationship between blood flow and changes in temperature gradient using a thermal probe. This technique can be used in beating hearts and in other organs (i.e. liver and brain) during surgery (Kamiya *et al.*, 2002)).

Although several methods are available to measure regional flow, there has been no study to date that has specifically looked at the correlation between the regional myocardial flow and electrophysiological properties during reductions in coronary perfusion. Experimental measurement of relative flow in acute myocardial ischaemia could provide a novel procedure for the measurement of regional myocardial flow but not applicable *in vivo* due to the (unknown) toxicity of dyes.

The purpose of this study was to validate a new method to assess relative myocardial blood flow using the dye RH237. Preliminary experiments measuring

the kinetics of RH237 binding to rabbit ventricular myocytes were performed. Subsequently the methods were used to estimate relative myocardial blood flow in the Langendorff perfused rabbit heart with the optical mapping method.

5.2 Methods (A)

5.2.1 Cell isolation

5.2.1.1 Isolation of ventricular cardiomyocytes from the rabbit

Adult male New Zealand White rabbits weighing between 2.5 - 3.5 kg were euthanized as previously described and the heart was quickly removed and placed into a sterile beaker containing sterile, cold Krebs' solution. The aorta of the heart was then quickly mounted and tied onto the cannula of Langendorff retrograde perfusion system. Calcium-free solution maintained at 37°C was perfused through the heart at 25ml/min to wash out the remaining blood and Ca²⁺, and followed by perfusion with collagenase/protease solution (3 mg protease and 50mg collagenase in 75ml sterile Ca²⁺ free Krebs' solution).

The perfusate enzyme solution was collected from the heart and re-circulated to continue the digestion for 5-6 minutes. The enzyme solution was then washed out of the heart by perfusion with 100ml of sterile Krebs' solution containing 1% (w/v) Bovine serum albumin (BSA).

Right ventricular tissue was removed and immersed in Krebs' solution containing 1mM EGTA in order to reduce Ca²⁺ contamination and the tissue was subsequently finely chopped in this solution. Cardiac myocytes were dissociated by triturating the solution. Dissociated cardiac myocytes were then filtered through gauze mesh to remove undigested tissue and other debris. Maintaining low extracellular Ca²⁺ ensured a high yield of rod shaped myocytes.

5.2.2 Quantifying the binding of RH237 in rabbit ventricular myocytes

RH237 is highly lipophilic and is thought to partition preferentially within the outer layer of the lipid bilayer of biological membranes. For quantification

purposes, its reaction with biological membranes can be described as the absorption of chemical compounds onto the membrane. Because RH237 in free solution is essentially non-fluorescent, dye fluorescence is a measure of the concentration of RH237 bound to membrane.

Langmuir isotherms are widely used to quantify absorption of substance onto surfaces. An equation was developed by Irving Langmuir in 1916 to describe the absorption of a substrate onto a monolayer (Langmuir, 1916), as follows:

$$\theta = \frac{\alpha * P}{1 + \alpha * P}$$

Equation 5.1

where θ is the percentage coverage of the surface, P is the concentration of the measured component, and α is a constant (Han *et al.*, 2008).

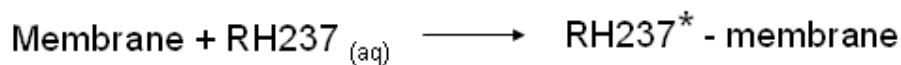
In the case of the adsorption of RH237 molecules at the membrane surface of ventricular myocytes, the equation can be expressed as;

$$F = \frac{K_{1/2} * [Dye]}{1 + K_{1/2} * [Dye]}$$

Equation 5.2

where F is the fluorescence signal, $[Dye]$ is concentration of RH237, and K is a constant reflecting the relative affinity of the dye for the membrane.

The process is summarized by the following kinetic scheme:



$\text{RH237}^* = \text{fluorescent form}$

We assume that the reaction occurs uniformly across the membrane of heart cells (including non-myocytes). This analysis was used to assess the behaviour of the interaction of the dye with cardiac myocytes to confirm that the adsorption of the dye with membrane is both rapid and to quantify the relative affinity of the dye for the cardiomyocyte membrane.

5.2.3 Measurement of kinetics and relative affinity of RH237 for cardiac cell membranes

Myocytes were loaded with RH237 by addition of 0.3 μ l - 30 μ l of 1mM stock to 1.5ml cell suspension. The time course and concentration dependence of RH237 binding was measured using a Perkin-Elmer fluorescence spectrophotometer (model LS55). The software (Timedrive) application was used to measure the change in fluorescence at 1 sample/second. An excitation wavelength of 475nm and an emission wavelength of 675 nm were used with excitation and emission slit width set at 20nm. These values were based on the spectra shown in Methods (section 2.1.2).

5.2.3.1 Protocol A

(i) Time course of RH237 binding

Cell concentration ranged from 1.25×10^3 to 4×10^4 . The following concentrations of RH237 were used: 0.3 μ M, 1 μ M, 3 μ M, 10 μ M and 30 μ M.

1. The different concentrations of cells (2×10^3 cells/ml and 4×10^3 cells/ml) were prepared.
2. Krebs' solution with cells was placed into the cuvette and the acquisition software was initiated.
3. RH237 was first added at concentration of 0.3 μ M, and immediately mixed into the suspension with a pipette while the application was still running.
4. RH237 at a series of concentrations was added, at concentrations of 1 μ M, 3 μ M, 10 μ M and 30 μ M, and immediately stirred using the pipette.

5. The protocol 1-4 was repeated with next concentration of cells.

(ii) Concentration dependence of RH237 binding

RH237 concentrations from 0.3 μM to 30 μM were used with a range of cell concentration: 1.25×10^3 , 2.5×10^3 , 5×10^3 , 1×10^4 , 2×10^4 , 3×10^4 and 4×10^4 cells/ml.

1. The different concentrations of RH237 (0.3 μM , 1 μM , 3 μM , 10 μM and 30 μM) were prepared in order to determine the time course of the RH237/membrane interaction.

2. Krebs' solution without cells was placed into the cuvette and the acquisition software was initiated.

3. 0.3 μl of RH237 was added and immediately stirred with a pipette while the application was still running.

4. A series of cell concentrations were then added, at concentrations of 1.25×10^3 , 2.5×10^3 , 5×10^3 , 1×10^4 , 2×10^4 , 3×10^4 and 4×10^4 cells/ml, and immediately stirred using the pipette.

5. The protocol 1-4 was repeated with next concentration of RH237.

5.3 Results A

5.3.1 Measurement of the capacity and relative affinity of cardiomyocytes for RH237

Figure 5.1 illustrates the rapid time-course of the fluorescence increase on addition of RH237 to a cell suspension (1×10^5 cells /ml). The rise of fluorescence had a time-course that was comparable to that achieved by simply adding cells previously loaded with fluorescent dye. These data suggest that RH237 binds as fast as the mixing of solution (< 2sec)

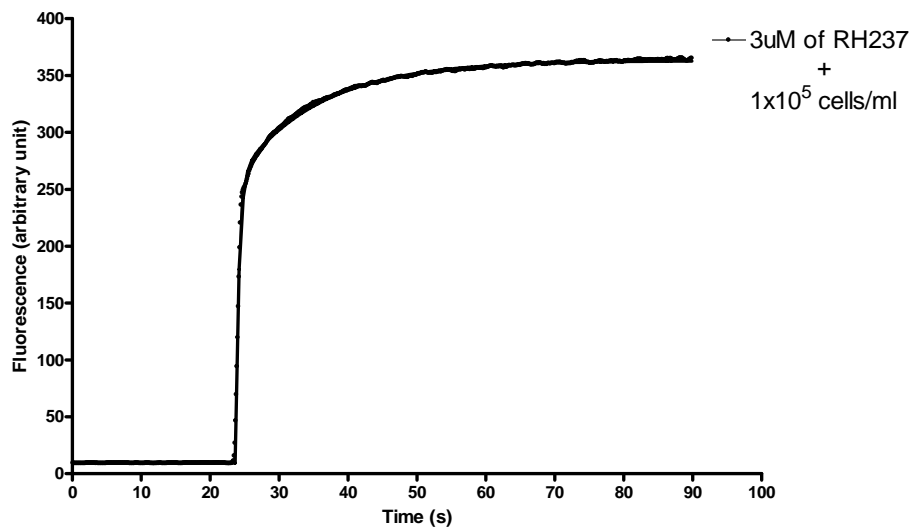


Figure 5.1 Kinetics of binding between RH237 and ventricular myocytes

5.3.2 Sigmoidal fitting curve of RH237 binding with rabbit ventricular myocytes

Figure 5.2 shows the relationship between RH237 concentration and fluorescence for 3 sample cardiomyocyte cell concentrations (Panel A-C). At each cell concentration the relationship was fitted with a sigmoidal relationship described in Equation 5.2 (see Figure legend). The values of predicted maximum fluorescence (B_{max}) and relative affinity ($K_{1/2}$) are given on each graph. This relationship was measured for 7 separate cell concentrations ranging from 1.25×10^3 to 4×10^4 .

Three typical graphs are shown below (Figure 5.2).

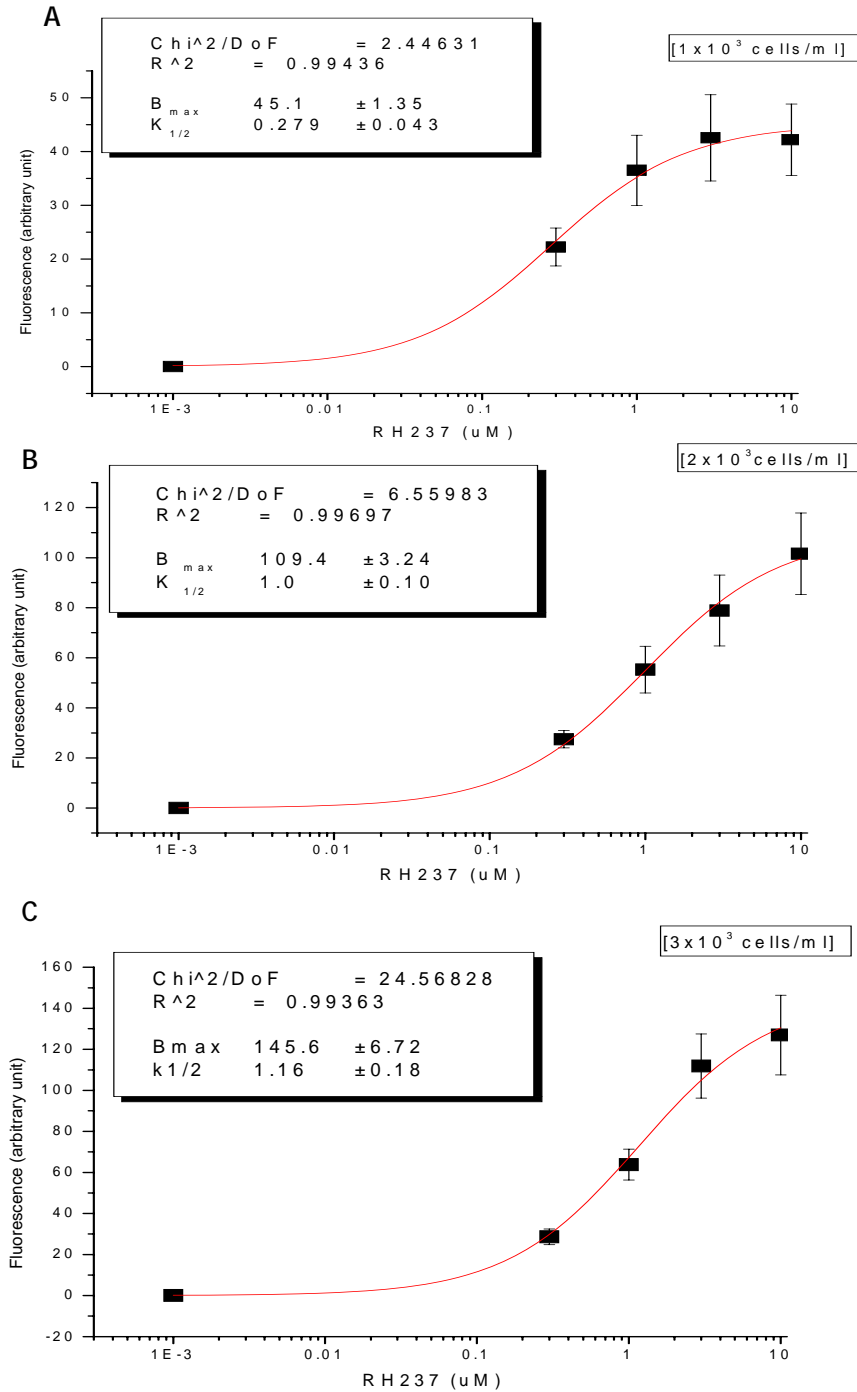


Figure 5.2 Relationship between fluorescence and RH237 concentration as measured on spectrophotometer

The relationship was fitted to the following equation based on Equation 5.2. Fluorescence = $B^{max} * K_{1/2} [RH237] / (1 + K_{1/2} * [RH237])$. Values are expressed as the mean ± SEM (n=6).

5.3.3 B_{max} and $K_{1/2}$ of saturating [RH237] binding to rabbit ventricular myocytes

Figure 5.3 below shows the relationship between numbers of cell per millilitre and B_{max} and $K_{1/2}$ values obtained from the sigmoidal fit. Both graphs show a linear relationship between cell concentration and both parameters.

5.3.3.1 B_{max} of the saturating [RH237] fluorescence

B_{max} is the fluorescence achieved at saturating [RH237]

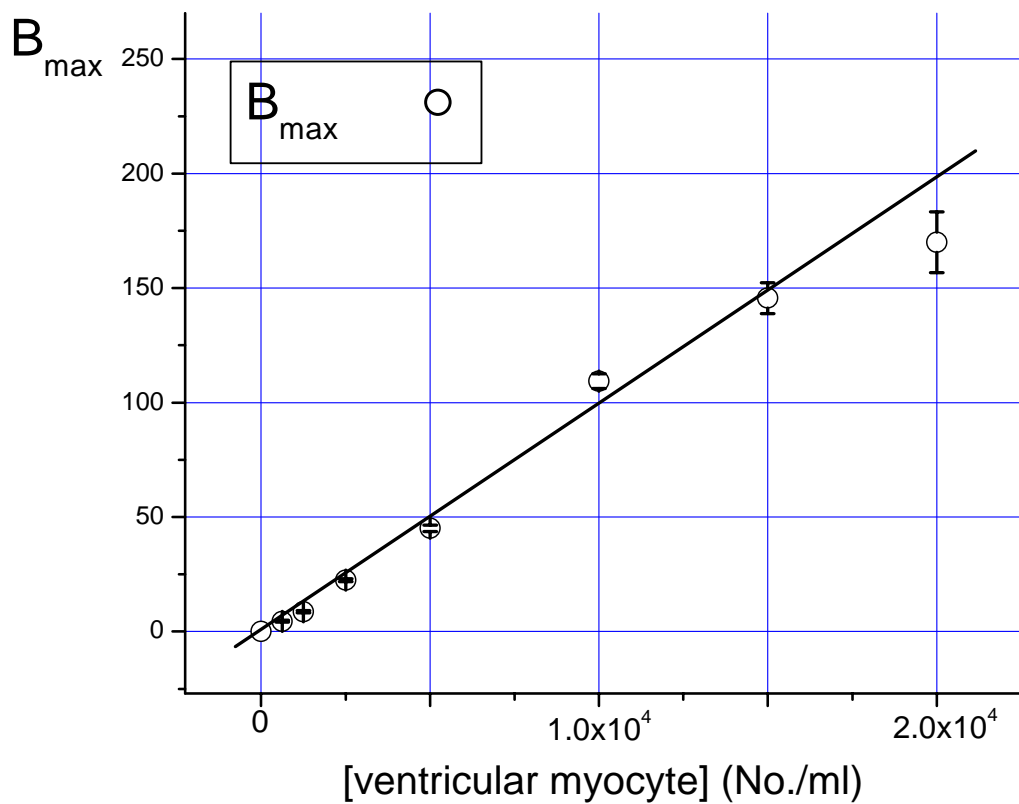


Figure 5.3 Correlation between the number of myocytes per millilitre and B_{max}

The cells isolated from rabbit ventricular myocytes and stained with RH237.

5.3.3.2 $K_{1/2}$ of the saturating [RH237] fluorescence

$K_{1/2}$ is the concentration of RH237 required to produce half maximal fluorescence

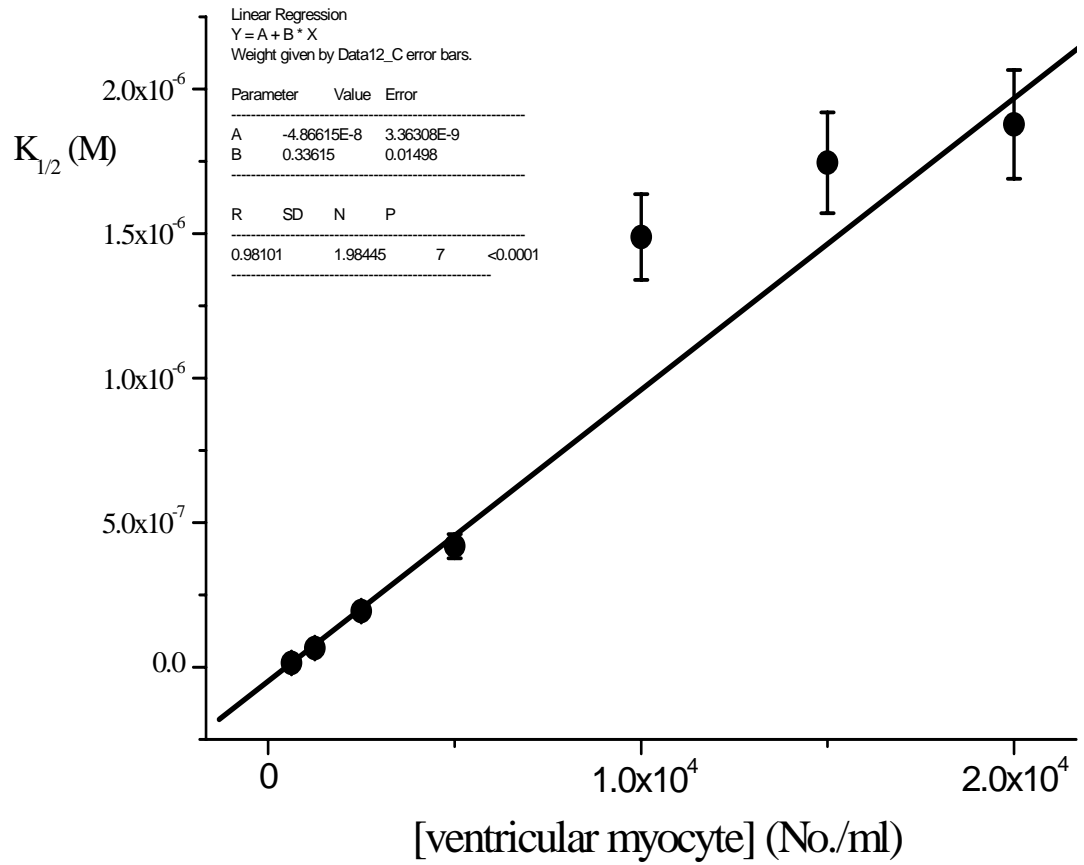


Figure 5.4 Correlation between the number of myocytes per millilitre and $K_{1/2}$

5.3.4 Correlation between amount of saturating [RH237] binding to rabbit heart tissue

Figure 5.5 shows the same graphs as in Fig 5.3 & 5.4 plotted as the relationship between the amount of cardiac tissue in gram wet weight, the maximum fluorescence at saturating [RH237] (B_{max}) and amount of RH237 required for 50% binding ($K_{1/2}$). Tissue weight was calculated by using the conversion factors;

$$1.0 \times 10^{-6} \text{ cell} = 1.5 \text{ mg protein and } 1.5 \text{ mg protein} = 0.015 \text{ g wet weight}$$

These values were based on previous measurements of total protein content of cells (Lorraine Bruce, PhD Thesis University of Glasgow 2001) and the conversion of total protein to tissue weight (Alexis Duncan, PhD Thesis University of Glasgow 2002).

These values can be used to estimate the extent of binding of RH237 to the whole heart when an aliquot of RH237 is injected as a bolus into the coronary circulation. Normally a bolus of 50 μl of 2.2mM RH237 is injected to load the heart. This represents $\sim 0.1 \mu\text{mole}$ of RH237 injected into approximately 5 gram of wet weight of heart, i.e. or 0.02 μmoles RH237 per gram tissue (wet weight). From the relationship shown in Figure 5.5, 0.33 μmoles RH237 per gram tissue (wet weight) provides 50% of maximal binding. This suggests that normal loading of the RH237 into rabbit hearts results in less than half maximal loading of the cardiac membranes with RH237.

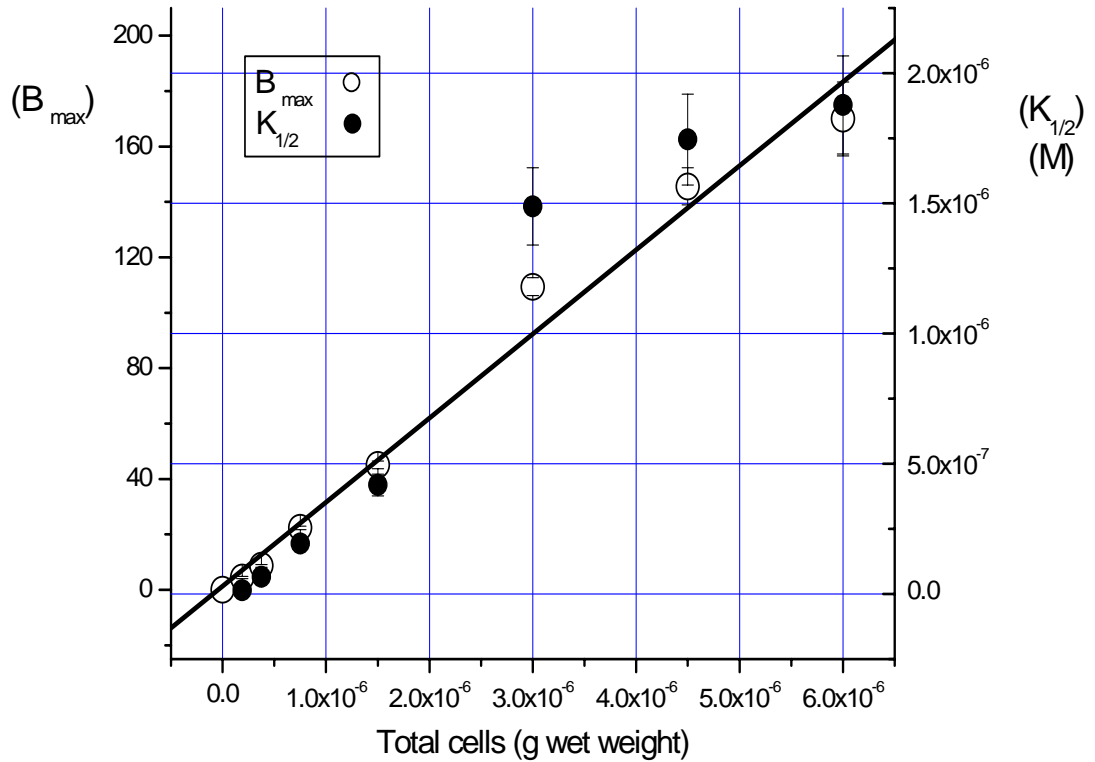


Figure 5.5 Relationship between total cells in gram wet weight, fluorescence at saturation and amount of RH237 required for 50% binding

5.4 Methods B

5.4.1 Measurement of the relative flow

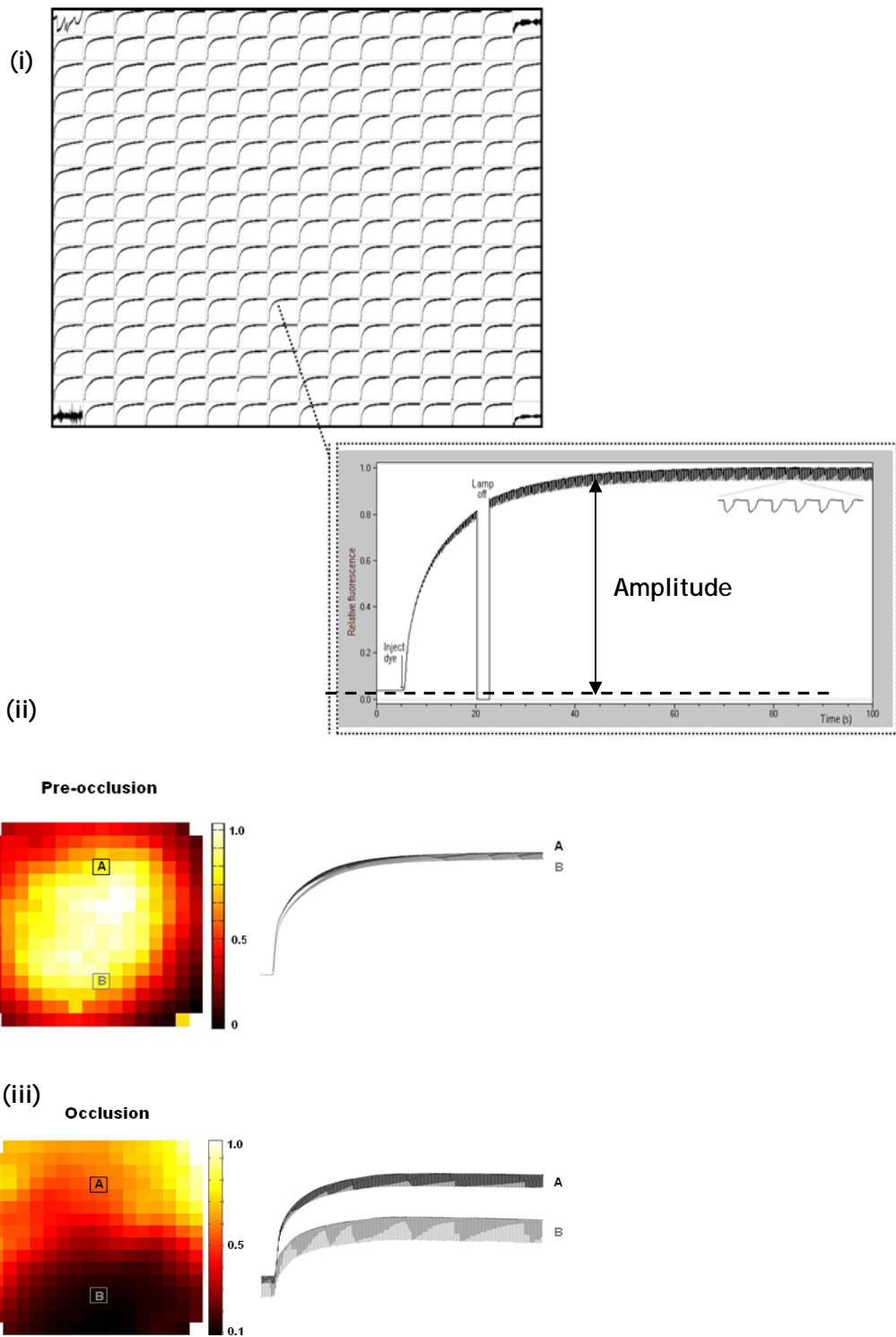
An attempt to assess regional myocardial flow was made by measuring the rate of rise of the regional fluorescence signal following the injection of a bolus of RH237 into the coronary circulation. The principle of this technique is that binding of RH237 to cardiac membrane is both very fast (<2s) and irreversible. Thus the local time-course of the rise in fluorescence on injection of RH237 reflected the extent of the local coronary circulation. We investigated whether the amplitude of the rise in fluorescence on injection of RH237 could be used to assess coronary flow.

The signals were recorded simultaneously from 256 photodiodes at the rate of 100 per second over 100 seconds. The OAP signals were transferred to MATLAB 7.0 and relative perfusion rate was calculated as the ratio between amplitude of

the increase in fluorescence on injection of RH237 under control conditions and the amplitude of the signal obtained on injection of the same amount of RH237 during occlusion or low-flow ischaemia.

Figure 5.6 (i) shows optical recordings from 252 photodiodes; each diode represents the RH237 signal from several hundred cells. Trace below is the time course signal from one diode which shows the time course of dye loading.

The relative flow was determined by examining the regional time-course of the rise in fluorescence on injection of a 50 μ L bolus of RH237 (1mM) into the coronary circulation. The relative perfusion rate was calculated as the ratio between pre-occlusion RH237 signal (ii) and the signal during the occlusion (iii). Therefore the range of signals in Figure 5.6 (ii) represents the distribution of amplitude signals (normalised) under control conditions. The high amplitude signals in the centre of the field are due to the higher levels of illumination (excitation) in this area. The signals in Figure 5.6 (iii) represent the signal amplitude relative to the previous control, therefore the range of signals reflect relative flow.



01/04/08

Figure 5.6 The optical signals from left ventricular epicardial of the rabbit heart

(i) the top panel shows a set of 256 fluorescence and RH237 signals that is recorded simultaneously and trace below represents signal from one pixel. The amplitude of the signal is shown on the expanded trace. (ii) and (iii) colour maps of the relative flow at pre-occlusion and during occlusion respectively. The amplitude of the rise in fluorescence on injection of RH237 in zone A and B at pre occlusion and during occlusion are shown in the right handside.

5.4.1.1 Protocol B

The experimental protocol is illustrated in Figure 5.7. The hearts were subjected to baseline recording of 10 minutes perfusing with $5\mu\text{M}$ of Blebbistatin in standard Tyrode's solution, followed by the first run from the flow rate of $30\text{ml}/\text{min}$ to $1\text{ml}/\text{min}$, then subjected to the second run from the flow rate of $2\text{ml}/\text{min}$ to $30\text{ml}/\text{min}$. Electrophysiological properties were recorded every minute of the entire experiment. The relative flow was determined by examining the time course of the rise in fluorescence on injection of a $10\mu\text{l}$ bolus of RH237 (1mM) into the coronary circulation. Bolus injection of RH237 was performed immediately after each low-flow ischaemia with ventricular pacing at 250ms cycle length.

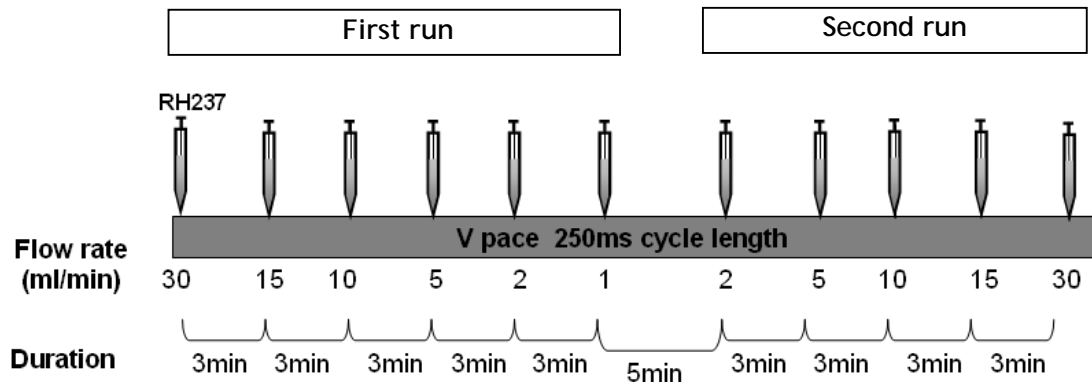


Figure 5.7 Experimental protocol

5.5 Results B

5.5.1 Relative perfusion rate during acute global low-flow ischaemia

Relative flow is evaluated as the ratio between RH237 signals from control ($30\text{ml}/\text{min}$) and the signal during low-flow (from $15\text{ml}/\text{min}$ to $1\text{ml}/\text{min}$). The "first run", RH237 signal was recorded from $30\text{ml}/\text{min}$ to $1\text{ml}/\text{min}$ and the "second run" was recorded from $2\text{ml}/\text{min}$ to $30\text{ml}/\text{min}$. The colour map was plotted as shown in panel (i). During low-flow ischaemia, the relative flow reduced corresponding with a variable decrease in APD_{50} in panel (ii). The

relation between flow rate and amplitude of RH237 fluorescence is shown in panel (iii).

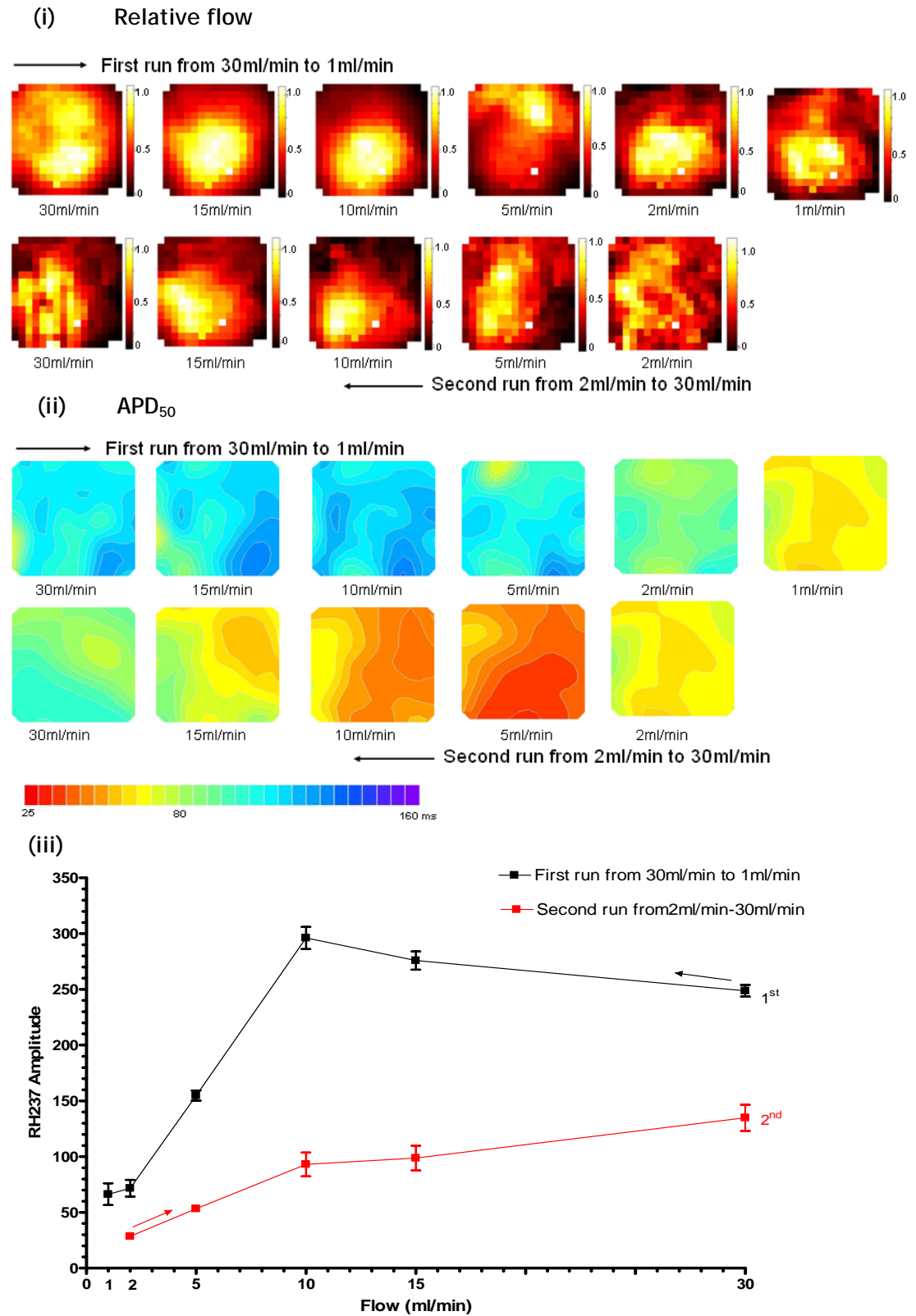


Figure 5.8 Relative flow and APD₅₀ during multiple flow rate.

5.5.2 Relative perfusion rate during acute regional myocardial ischaemia

During occlusion in Figure 5.9 (i)-(iii), the relative flow reduced in ischaemic area (a) corresponding with a variable decrease in APD_{50} (b). An exponential curve was fitted to the relation between flow and APD_{50} as shown in (c).

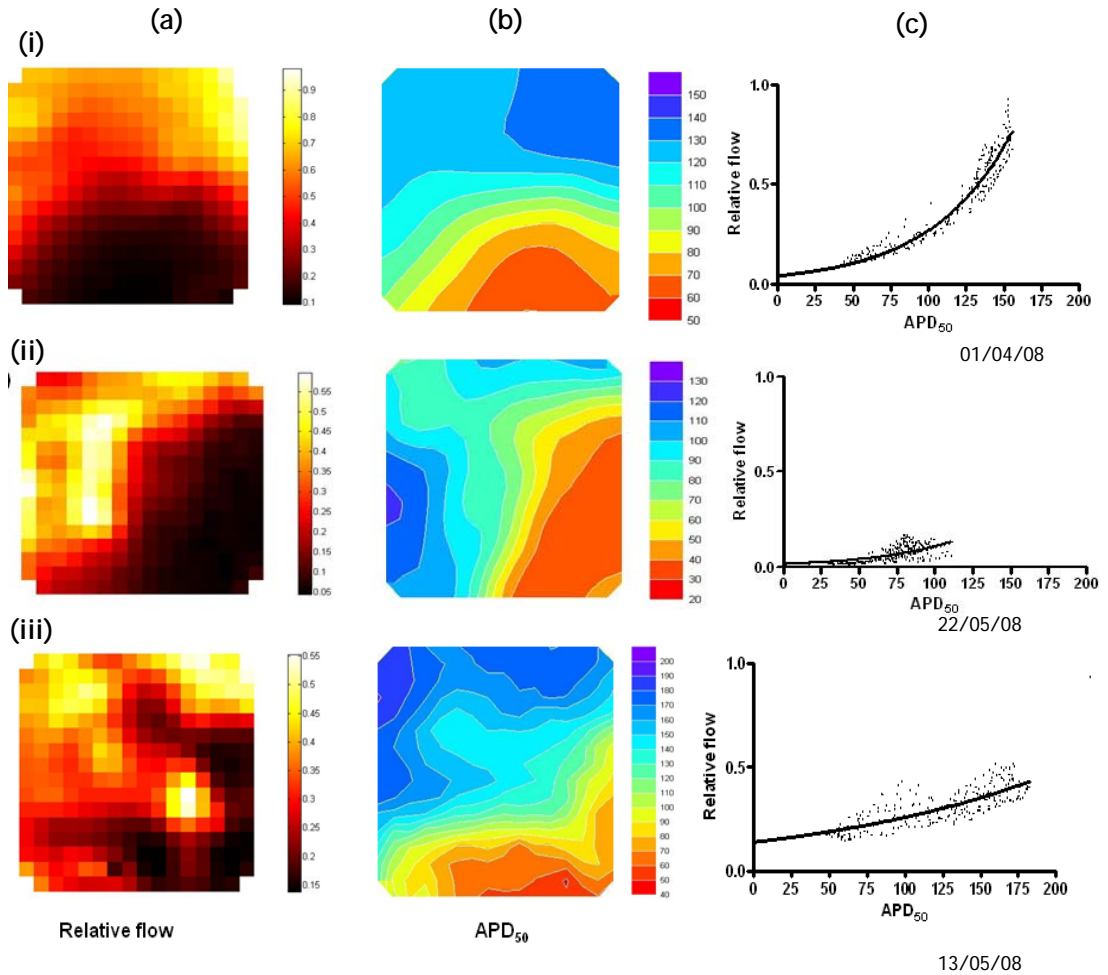


Figure 5.9 Relative flow vs. APD_{50}

Relative flow represents in panel (a) corresponding with contour map of APD_{50} in panel (b) and the correlation of relative flow and APD_{50} in panel(c).

5.6 Discussion and conclusion

The objective of these experiments was to assess the use of RH237 to measure the relative perfusion of the epicardial surface of the myocardium of rabbit hearts.

The kinetics of RH237 and relative affinity of RH237 binding to rabbit myocardium was assessed using suspensions of isolated rabbit ventricular myocytes stirred continuously in a cuvette in a fluorescence spectrophotometer. The RH237 dye is highly lipophilic and only forms a fluorescent product when bound to lipid membrane. The time course of binding to cell aggregates was faster than could be resolved using a simple cuvette system (<1-2s). This rapid association of the dye with tissue is an advantage when considering its use as a flow marker since the time course of the rise in fluorescence would reflect the rate of arrival of the dye at the tissue.

The sigmoidal relationship between the RH237 concentration and the fluorescence is as expected for the adsorption of the dye into the cardiac membrane reaching a maximal level when the membrane is saturated with the dye. The linear relationship between the maximum fluorescence (B_{max}) and the concentration of cells (or tissue) reflects the greater tissue area available at greater cell concentration (therefore requiring greater amounts of the dye). Finally, the linear relationship between the $K_{1/2}$ and the cell concentration indicates that the dye required for half maximal binding increases as the concentration of cells and membrane increases. This proportionality between half maximal binding and membrane area suggests that association of the dye to the membrane is a simple saturating adsorption process as described by the Langmuir isotherm. In terms of the use of the dye RH237 as a flow marker, this behaviour allows a direct comparison of membrane fluorescence with flow with the proviso that the amount of dye used remains well below the quantities required for maximal binding.

Converting the cell number to tissue weight, Figure 5.5 establishes the information that using 0.33 μ moles RH237 per gram tissue (wet weight) gives 50% of maximal binding. Thus the normal bolus of RH237 given to the heart will

result in < 50% loading of the heart and therefore remains well within the range that allows the fluorescence signal to be used to assess flow.

Relative myocardial blood flow measurement was performed in a Langendorff system conjunction with optical mapping techniques using RH237. The relative perfusion rate as shown in Figure 5.8 was calculated as the ratio between RH237 loading profile under control conditions (30ml/min) and the signal during the lower perfusion rates. The relationship described in Figure 5.8 (iii) indicates that amplitude signal does not give a unique relationship between flow and amplitude of the RH237 signal. There was clear hysteresis between the relationship observed decreasing flow (30 to 2ml/min) and on the increase (2ml to 30ml). In both cases an approximate proportionality was evident, but in both cases the relationship was non-linear. This suggested that this simple and convenient approach can be used to give an approximate indication of flow, but not an absolute measure.

This conclusion was re-inforced by the data shown in Figure 5.9, in three examples the relationship between APD and RH237 amplitude showed a non-linear correlation (fitted with an exponential curve). But, as shown in the 3 examples, the relationship was quite different. A further refinement of this technique is required to make the signal a better indication of the absolute flow. This is part of the future work of the laboratory, for the remainder of this thesis, this approach was used to provide an approximate assessment of coronary flow.

6 Arrhythmias, APD alternans and conduction in acute regional and global myocardial ischaemia

6.1 Introduction

Quantification of the extent of T-wave alternans in the ECG record of patients has been proposed as a non-invasive test to identify individuals who are susceptible to lethal ventricular arrhythmias (Pastore *et al.*, 1999). T-wave alternans was first reported in 1908 as a fluctuation in vector and amplitude of the T-wave which occurs on every alternate beat (review in (Takagi & Yoshikawa, 2003)). The cellular basis for alternating T-wave amplitude is thought to be alternate changes in the ventricular APD (Walker & Rosenbaum, 2003). Previous studies have attempted to understand the relationship among APD alternans, T-wave alternans, and ventricular arrhythmia during ischaemia (Takagi & Yoshikawa, 2003; Pastore & Rosenbaum, 2000; Laurita & Rosenbaum, 2008; Nearing *et al.*, 1991). There is a large body of circumstantial evidence suggesting the arrhythmic mechanism is associated with T-wave and APD alternans (Kurz *et al.*, 1993). The mechanism is based on the concept that heterogeneous prolongation of action potentials (increased dispersion of repolarization) can cause re-entrant arrhythmias via development of conduction block (Lopez *et al.*, 2007).

A study by Downar *et al.* using floating microelectrodes was the first to report that APD alternans associated with T-wave alternans appeared within 3-9 minutes of the onset of myocardial ischaemia caused by acute coronary occlusion. The recordings of transmembrane potential showed little change in AP amplitude but up to ~50% decrease of APD on each alternate beat (Downar *et al.*, 1977).

Further studies of APD and T-wave alternans used an open-chested anaesthetised dog preparation to map T-wave alternans over the surface of an ischaemic heart. This study showed that the magnitude of the T-wave alternans could be used to predict the appearance of arrhythmias (Carson *et al.*, 1986; Konta *et al.*, 1990). The mechanistic link between arrhythmias and T-wave alternans (and APD alternans) is unclear, although the incidence of arrhythmias has been linked to the increase dispersion of repolarization caused by the alternans phenomenon

(Takagi & Yoshikawa, 2003). One other study correlated the onset of ischaemia to the presence of arrhythmias and APD alternans using monophasic action potential (MAP) recordings (Abe *et al.*, 1989). The MAP technique provides a stable and accurate time course of transmembrane action potential in a region of the myocardium using a contact electrode (Franz, 1991). However, the number of simultaneous recordings that can be made is limited and therefore it cannot be easily used to provide spatial information (Qian *et al.*, 2003).

Computational models of myocardial electrophysiology such as mono-domain 2D sheet incorporating the Beeler-Reuter (BR) ion channel model have been developed to study the interrelationship between APD and Ca^{2+} transient alternans as a means of determining a cellular mechanism for the phenomenon. However, there are no predictive models that use the intracellular changes known to occur during ischaemia, and therefore the extent to which the published models can be used to explain T-wave alternans observed during acute ischaemia is unclear. (Qu *et al.*, 2000; Dhalla *et al.*, 2003).

In contrast, a recent theoretical study by Bernus *et al.* has proposed that ischaemia-related arrhythmias are triggered by Ca^{2+} mediated alternating conduction blocks in the ischaemic BZ, a scenario that may be able to produce alternating T-wave signals as well as sufficient conduction block to cause intramural re-entry (Bernus *et al.*, 2005). In support of this idea, a study by Abe *et al.* (Abe *et al.*, 1989) in the guinea pig ischaemic ventricular muscle has demonstrated high-grade-block rhythms that can predict re-entrant arrhythmias. Previous studies had suggested that 2:1 block can proceed to complete block within the core of the ischaemic zone, Lopez *et al.* (Lopez *et al.*, 2007) demonstrated that there might be one or more zones of complete block which contribute to increased heterogeneity of the myocardium and cause re-entrant arrhythmias in ischaemic ventricle. However, the mapping of the onset of re-entrant arrhythmias following higher order rhythms during regional ischaemia has not been performed experimentally, so it is not yet clear if this is an important initiating mechanism.

Optical mapping is a recently developed technique that can be applied to this problem. It allows measurement of depolarisation, repolarization, magnitude and phase of alternans. The link between alternans and arrhythmogenesis

mechanisms has been studied in a guinea pig model (Pastore *et al.*, 1999; Pastore & Rosenbaum, 2000). However, because of the requirement for eliminating (or reducing) movement artefact in optical mapping, the use of chemical uncoupling agents is problematic in that they may have side effects on the electrophysiology that will obscure electrophysiological response such as alternans (see Chapter 4).

6.2 Methods

6.2.1 Chronic Infarct induction

MI was induced in rabbit by permanent ligation of the left circumflex coronary artery. Adult male New Zealand white rabbits were given a general anaesthetic (Pentobarbitone 100 mg/kg) and after the left thoracotomy, the marginal branch of left circumflex coronary artery was ligated to produce an ischaemic area of 30-40% of left ventricle. Animals were sacrificed 8 weeks after the operation. This model has been used by the Glasgow group for a number of years and after 8 weeks reliably displays a distinct transmural infarct (Ng *et al.*, 1998; Burton *et al.*, 2000; Walker *et al.*, 2007). *In vivo* echocardiographic studies indicate that the average ejection fraction is reduced from ~70% to <50% by the procedure and the isolated Langendorff perfused hearts have a lower threshold for VF (determined by delivering a rapid constant current pulse train endocardially) than sham operated animals (Burton *et al.*, 2000).

6.2.2 Measurement of APD and repolarization alternans

Hearts were obtained as described in Methods (Chapter 2). The left coronary artery was ligated and the aorta was then quickly mounted and tied onto the cannula of Langendorff system. Tyrode's solution maintained at 37°C was perfused through the heart at 30ml/min, followed by perfusion with 5µM blebbistatin in Tyrode's solution to reduce the movement artefact.

The ECG was used to track beat-to-beat changes in repolarization heterogeneities. The area between two aligned alternate ECG traces was used as an index of alternans magnitude.

6.2.2.1 Experimental protocol

Experiments were divided into two groups: normal (stock or sham-operated) and infarcted hearts. Hearts from both groups were perfused with $5\mu\text{M}$ of blebbistatin in standard Tyrode's solution then subjected to the baseline recording of 5 minutes, followed by 15 minutes of regional ischaemia and 20 minutes reperfusion. Following this the hearts were subjected to 15 minutes global ischaemia (zero flow) and after 15mins of recovery a further 15 mins of low-flow (5ml/min) ischaemia and then 20 minutes reperfusion. ECG and other electrophysiological properties were recorded every minute of the entire experiment. Figure 6.1 shows the data from a typical experiment.

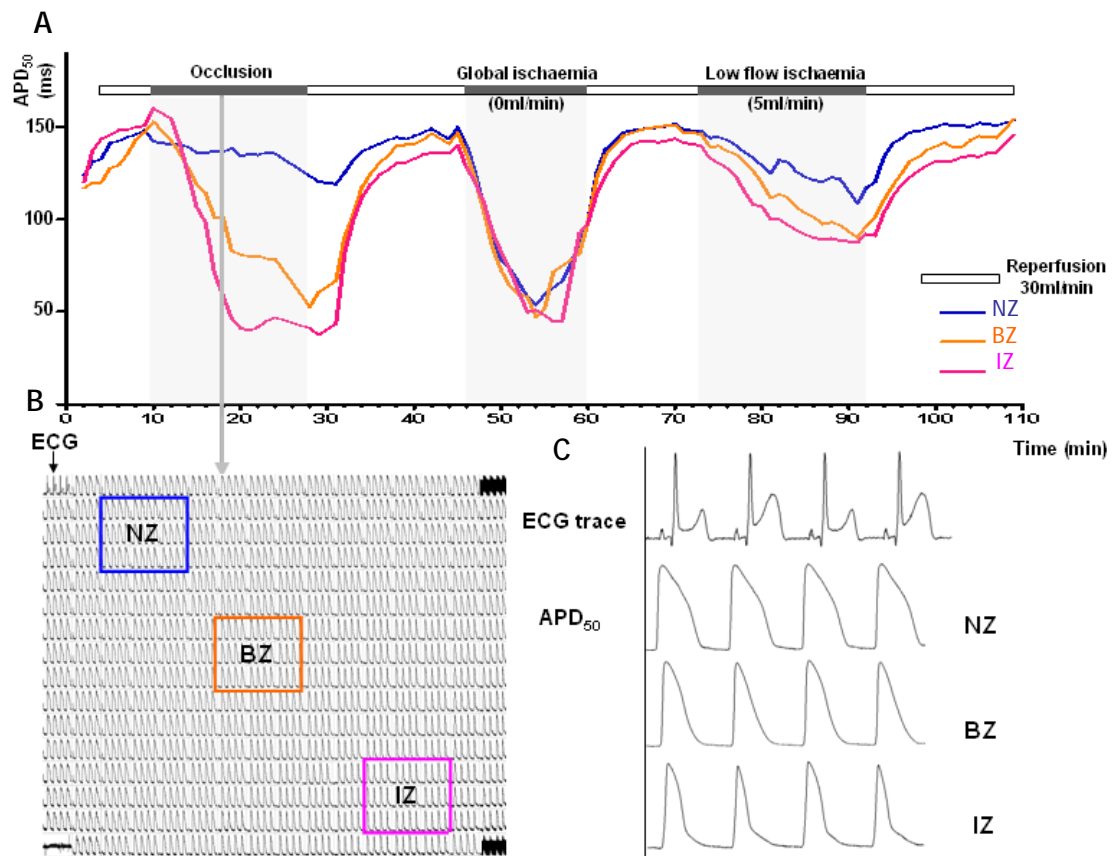


Figure 6.1 Experimental protocol

A: schematic of the protocol used in this set of experiments alongside measurements of APD from three regions shown in panel B. B: regions used to isolate the signals associated with normal zone (NZ), border zone (BZ) and infarct zone (IZ). C: typical ECG recordings alongside the corresponding optical signals.

APD was measured at 50% repolarization. APD alternans magnitude was estimated as the arithmetic difference between short and long adjacent APDs.

6.2.3 Measurement of CV

CV was measured during short (30s) periods of epicardial pacing, imposed prior to ischaemia, during ischaemia and during reperfusion. Local velocity vectors were calculated from the activation time delay between adjacent pixels speed and orientation of the local wavefront. Pacing at the left ventricle produced a roughly elliptical activation pattern, with a major and minor axis presumed to be parallel to the longitudinal and transverse axes of the fibres as shown in Figure 2.17 of Methods (Chapter 2). CV vectors were estimated by fitting a polynomial surface to the (x,y,t) coordinates of activity (Bayly *et al.*, 1998). The gradient of the surface at each pixel $(\delta x, \delta y)$ was converted to a local velocity magnitude and direction (angle).

OAPs were recorded within the mapping field (superimposed grid) as shown in Figure 6.2A (ii). OAPs exhibited a typical AP shape with fast depolarisation and slow repolarization. Examples of single-pixel recordings are shown. Figure 6.2B (i) shows the normal anisotropic AP conduction radially from the pacing site during control condition (pre-occlusion). Figure 6.2B (ii) shows the map of velocity vectors derived from these isochrones. Note that in the centre of the field, where the activation isochrones are evenly spaced, the CV vectors are similar in direction and magnitude.

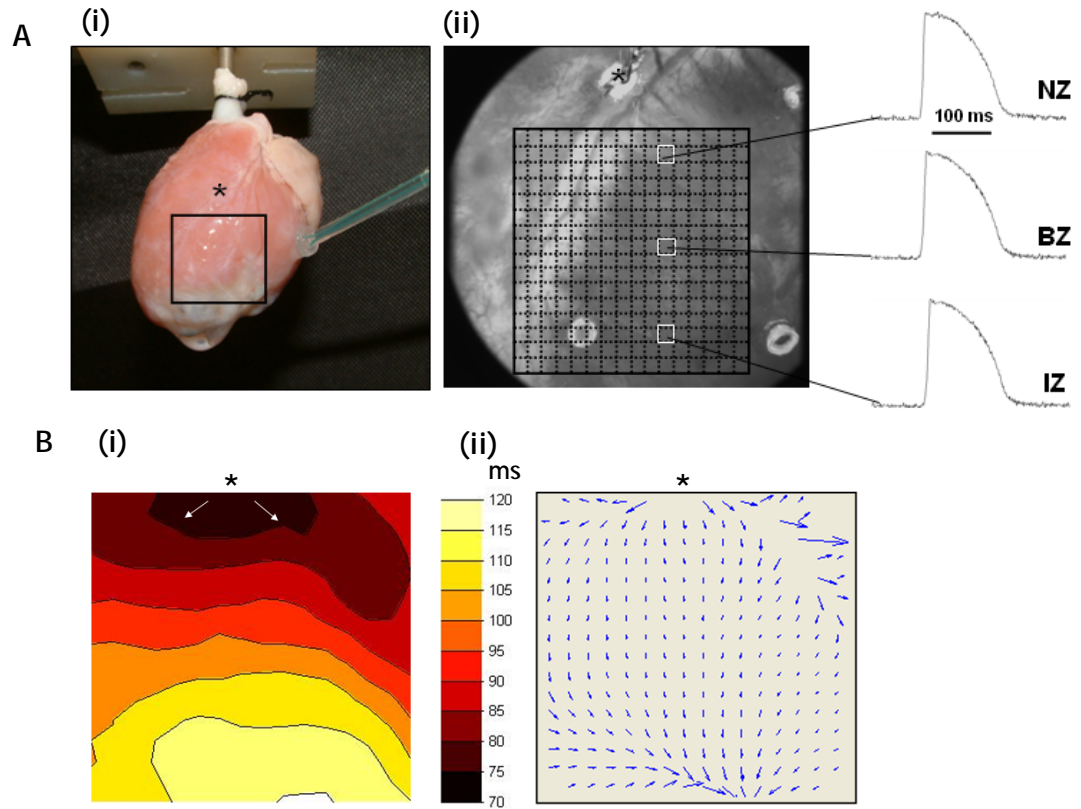


Figure 6.2 Example of CV analysis from optical mapping recordings

A: (i) Image of snared heart, the superimposed grid represents optical mapping field, (ii) CCD image of the heart. The 3 white squares show the position of 3 pixels and the corresponding OAPs are shown to the right. Their position represents the normal zone (NZ), border zone (BZ) and ischaemic zone (IZ) in the subsequent ligation procedure. Asterisk (*) represents the pacing site B: (i) Isochronal map of activation illustrated normal conduction from the pacing site (top centre). (ii) Map of CV vectors.

6.3 Results

6.3.1 Incidence of repolarization alternans during myocardial ischaemia and reperfusion

During acute regional ischaemia using blebbistatin as a motion artefact blocker, in 16 out of 30 hearts (~50%) alternans in both APD and T-wave shape was observed. In contrast, VF occurred during occlusion in only 8 out of 30 hearts (~27%) and VT occurred in 1 out of 30 (~3%). When BDM was used to reduce the movement, only 1 out of 8 hearts (~12.5%) displayed alternating of APD and T-wave during occlusion of the coronary artery.

Neither APD nor T-wave alternans were ever observed to arise during the reperfusion period when using either type of the motion artefact blockers. Comparable behaviour in hearts was seen during global ischaemia, but a higher incidence of arrhythmias and alternans was observed.

Normal hearts

		During ischaemia						Reperfusion						
		Total	Alternans	%	VF	%	VT	%	Alternans	%	VF	%	VT	%
	Control	7	2	28.6	2	28.6	0	0	0	0	0	0	0	0
Local	BLEB	30	16	53.3*	6	20+	0	0	0	0	0	0	0	0
	BDM	10	1	10	0	0	1	10	0	0	0	0	0	0
	Control	2	0	0	0	0	2	100	0	0	0	0	0	0
Global	BLEB	20	14	70**	13	65++	0	0	0	0	3	15	0	0
	BDM	7	1	14.3	1	14.3	0	0	0	0	0	0	0	0

Table 6.1 Incidence of alternans and arrhythmias in the normal hearts (stock)

Control indicates the data obtained from hearts that perfused with standard Tyrode's solution. Data compares between using blebbistatin (BLEB) and BDM as a motion artefact blocker. Data obtained from heart during regional ischaemia, global ischaemia and reperfusion. Control incidences of alternans, VF and VT were not significantly different from BLEB or BDM. Local ischaemic BLEB vs. BDM (alternans) $P=0.06$ (*); Local ischaemia BLEB vs. BDM (VF) $P=0.07$ (+). Global alternans BLEB vs. BDM (alternans) $P=0.02$ (**); Global ischaemia (VF) $P=0.03$ (++) . Fisher's exact test of relative risk (two sided).

When hearts with a chronic infarction scar were given a secondary acute regional ischaemic challenge (using blebbistatin as a motion artefact blocker), ~50% of hearts displayed both APD and T-wave alternans. VF occurred during acute ischaemia in only 2 out of 8 hearts (~25%) and VT occurred in 1 out of 8

hearts (~12.5%). These values were similar to those described for the non-infarcted hearts (Table 6.1).

Using BDM to reduce motion, no infarcted heart displayed alternating of APD and T-wave during acute ischaemia. APD and T-wave alternans were also absent from the reperfusion period regardless of motion artefact blocker used. However, the number of animals in this group was very low and statistical comparison was not meaningful.

In chronic infarction hearts, concurrent global ischaemia did not induce APD and T-wave alternans with either blebbistatin or BDM. Again, the low numbers in these experimental groups made statistical comparison of limited value.

		Infarcted hearts												
		During ischaemia						Reperfusion						
		Total	Alternans	%	VF	%	VT	%	Alternans	%	VF	%	VT	%
Local	BLEB	8	4	50	2	25	1	12.5	0	0	1	12.5	1	12.5
	BDM	2	0	0	0	0	0	0	0	0	0	0	0	0
Global	BLEB	3	0	0	0	0	0	0	0	0	0	0	0	0
	BDM	0	0	0	0	0	0	0	0	0	0	0	0	0

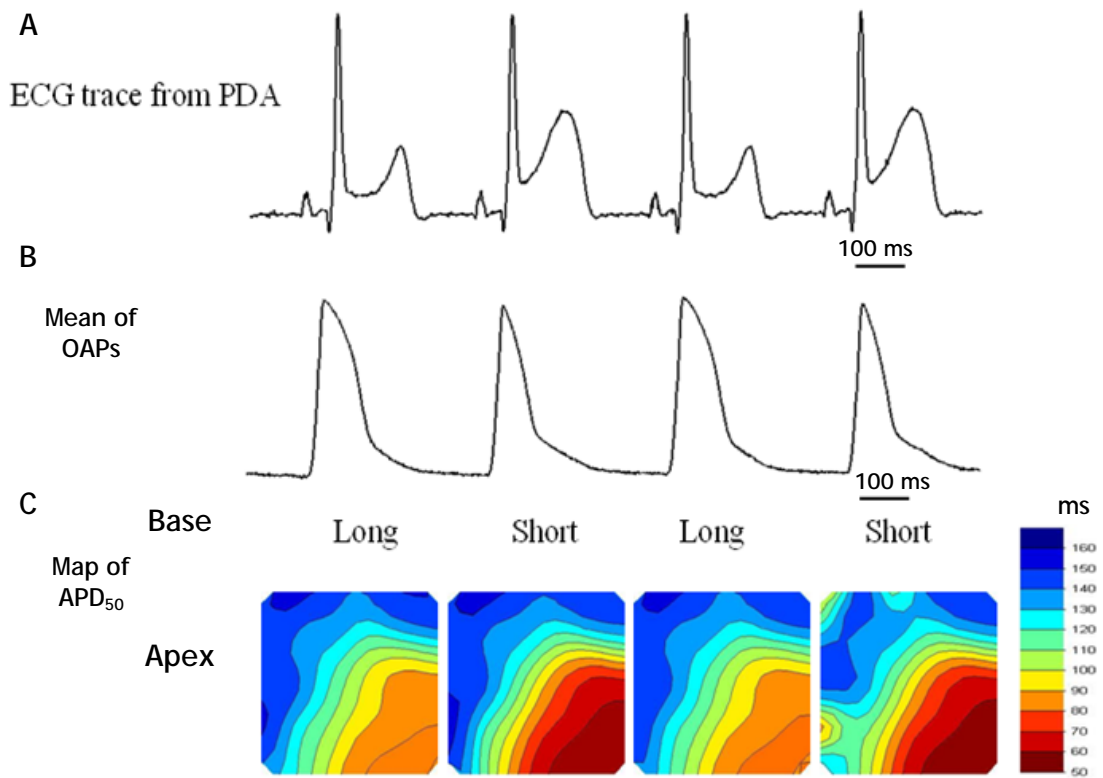
Table 6.2 Comparison of numbers of alternans and arrhythmias in the chronic infarcted hearts

Data compares between using blebbistatin (BLEB) and BDM as a motion artefact blocker. Data obtained from chronic infarcted heart during regional ischaemia, global ischaemia and reperfusion.

6.3.2 APD and repolarization alternans during regional myocardial ischaemia

Figure 6.3A shows the ECG trace of 4 sequential beats during acute regional ischaemia (8 minutes post occlusion). ECG displayed gross alternation of T-wave morphology between beats. The OAPs in Panel B represent the average of 3 by 3 pixels of recording from the same 4 sequential beats in the IZ. Contour maps of APDs shown in panel C are from the same period of recording. Variation of local repolarization alternans from base (NZ) to apex (IZ) is clearly visible from beat to beat.

Isochronal APD alternans maps were calculated as the difference between successive APD values as shown in Figure 6.3D. Maps obtained from three time points are shown: pre-ischaemia, after 8 minutes of ischaemia and after reperfusion for 15 minutes. During coronary artery occlusion, alternans magnitude increased locally, but a consistent gradient in alternans could not be detected in the reperfusion period.



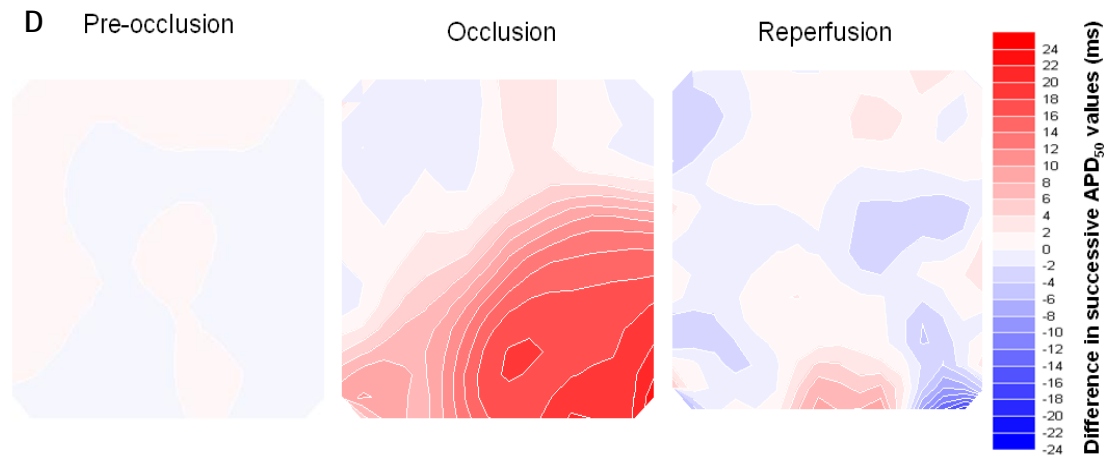


Figure 6.3 APD and T-wave alternans during acute myocardial ischaemia

A: ECG trace recorded from PDA corresponding with OAPs from selected 3 by 3 pixels in panel B. C: Contour maps of APD in successive beats showing alternating behaviour across the ventricular epicardial surface of rabbit heart after occlusion for 8 minutes, time shown in milliseconds. D: Contour maps of alternans magnitude.

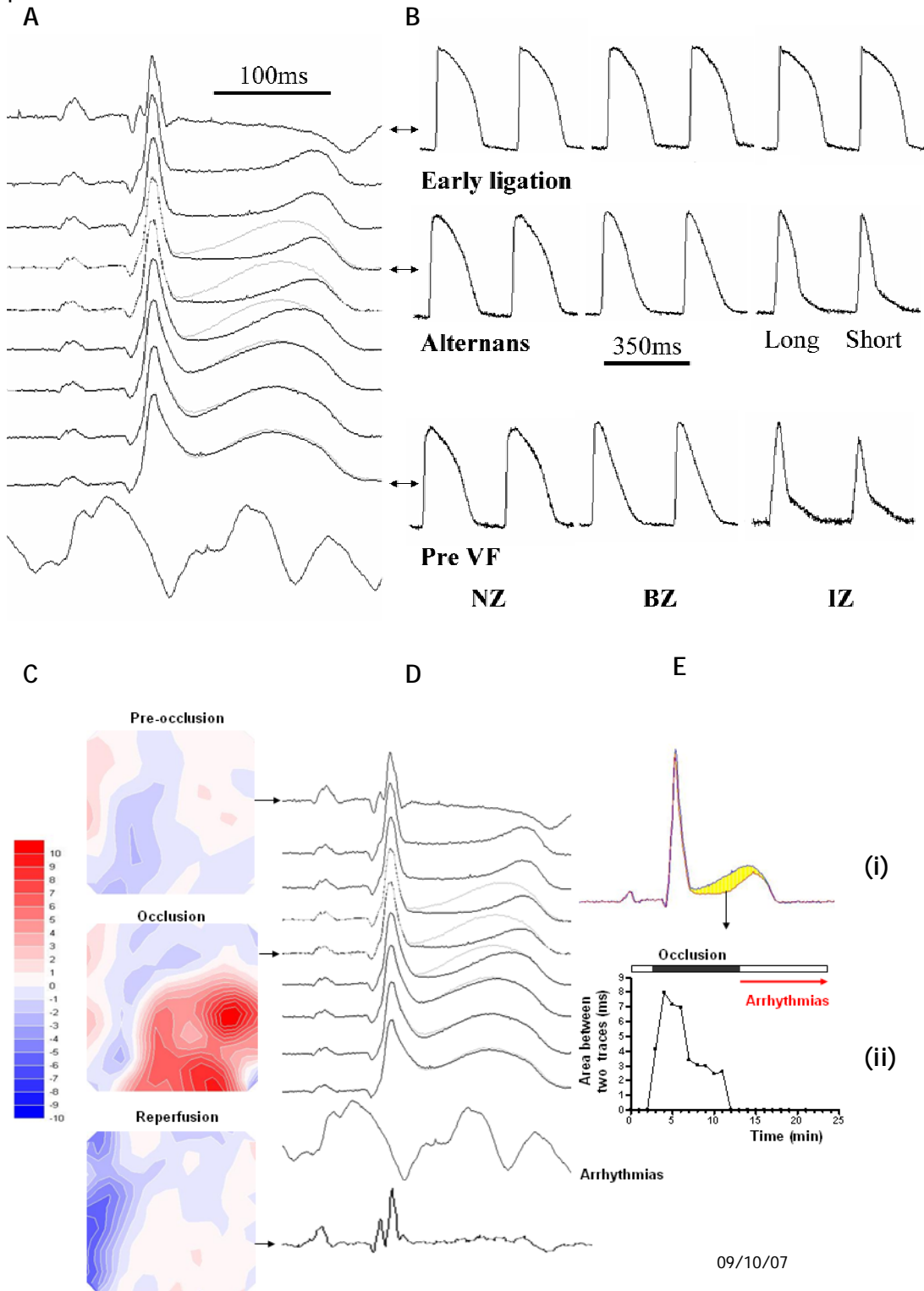
6.3.3 Alternans magnitude during acute regional myocardial ischaemia

The following two sections present data from hearts when arrhythmia was present and absent respectively, for comparison

6.3.3.1 Alternans magnitude during acute regional ischaemia in heart with arrhythmia

Figure 6.4 shows ECGs (A) and sample OAPs (B) at selected time points during a period of ligation. Action potential alternans became progressively more pronounced in the IZ until VF occurred at 12 mins post-occlusion. In contrast, ECG alternans reached a peak ~4 mins post-occlusion, and declined to undetectable levels by 12 mins. Alternans magnitude was essentially zero during reperfusion

period.



(Difference in successive APD50 values (ms))

Figure 6.4 APD and repolarization alternans in heart with arrhythmia

A: Progressive changes in ECG configuration with corresponding OAPs in panel B. ECG traces were recorded in the final 9 mins prior to VF at 14 mins. Optical recordings from sites in normal, 'border' and 'infarct' zones (NZ, BZ & IZ respectively) are shown next to corresponding ECGs. C: Map of alternans magnitude at pre-occlusion, 10 minute of occlusion and 15 minute of reperfusion.

D: Replicates A for reference. E: (i) schematic of alternans magnitude measurement represented by the yellow shaded area between 2 ECG traces, (ii) graph of area between 2 ECG traces over time from pre-occlusion to post-occlusion.

Maps of alternans (Panel C) indicate that maximal APD alternans occurred in the ischaemic zone. Plotting the magnitude of ECG alternans calculated as the area between aligned, consecutive ECGs confirms the transient nature of the phenomenon.

6.3.3.2 Alternans magnitude during acute regional ischaemia in heart *without arrhythmia*

Figure 6.5 A shows maps of alternans before, during and after coronary occlusion based on the regional OAPs (not shown). Alternans magnitude increased locally, the highest magnitude being observed in border and ischaemic zones after 12 minutes of coronary artery occlusion. The alternans magnitude then declined progressively during the maintained occlusion. Alternans was undetectable during the reperfusion period. Panel B represents the corresponding ECG traces before, during and after occlusion. Panel C (i) shows the alteration between 2 ECG traces. The magnitude of alteration of the area between two traces was plotted over the time as shown in Panel C (ii).

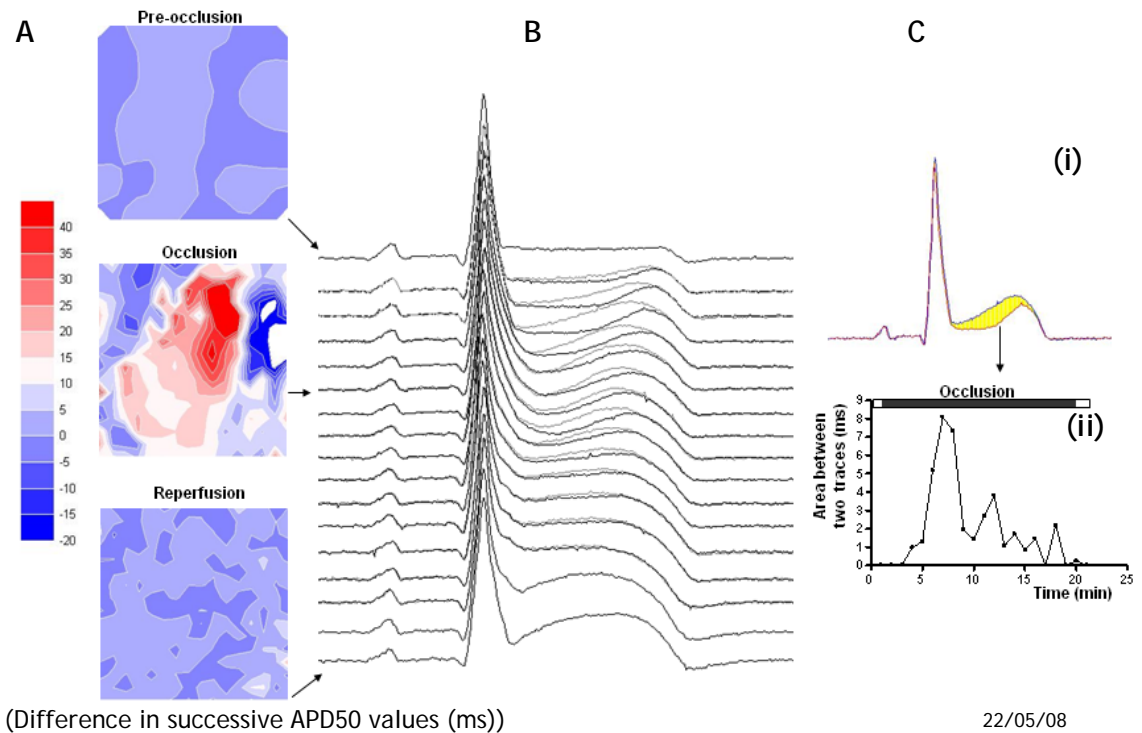


Figure 6.5 APD and repolarization alternans in heart without arrhythmia

A: Map of alternans magnitude, data obtained at pre-occlusion, 12 minute of occlusion and 15 minute of reperfusion. B: The top ECG traces was recorded 1 minute prior to occluding the coronary artery, the traces below represent 15 minute of occlusion. Successive ECG traces are shown in black and grey, showing 10-minute period of marked alternans and the last trace was recorded 15minute after reperfusion. C: (i) schematic of alternans magnitude measurement - the yellow shaded area between 2 ECG traces, (ii) graph of area between 2 ECG traces over time from pre-occlusion to post-occlusion.

Comparing the data in Figure 6.4 and 6.5, there was no obvious difference in the electrophysiological behaviour between a hearts that exhibited arrhythmias compared to one that did not. On average the maximum magnitude of alternans in hearts that developed arrhythmia was 4.5 ± 0.7 compared to 2.4 ± 0.6 in hearts with no arrhythmias (not significantly different).

6.3.4 APD and repolarization alternans during global low-flow and no-flow ischaemia

APD alternans was also evident in both low flow and no-flow global ischaemia. This occurred transiently and could not be easily correlated to changes in the ECG. As shown in Figure 6.6, ECG changes during global ischaemia are complex and cannot be interpreted as simple changes in T-wave or ST-segment changes.

For this reason, detailed analyses of APD alternans and ECG changes were not attempted.

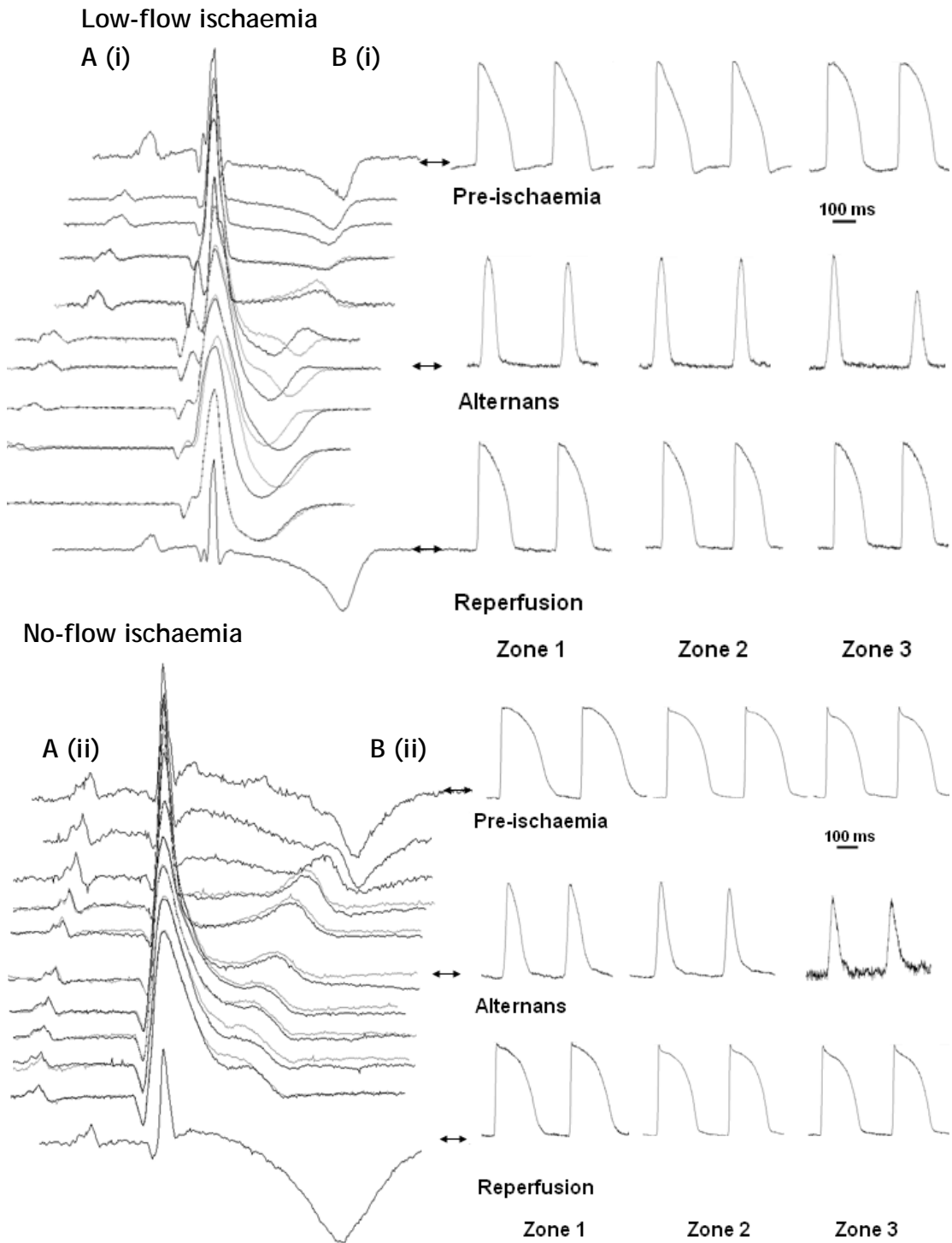
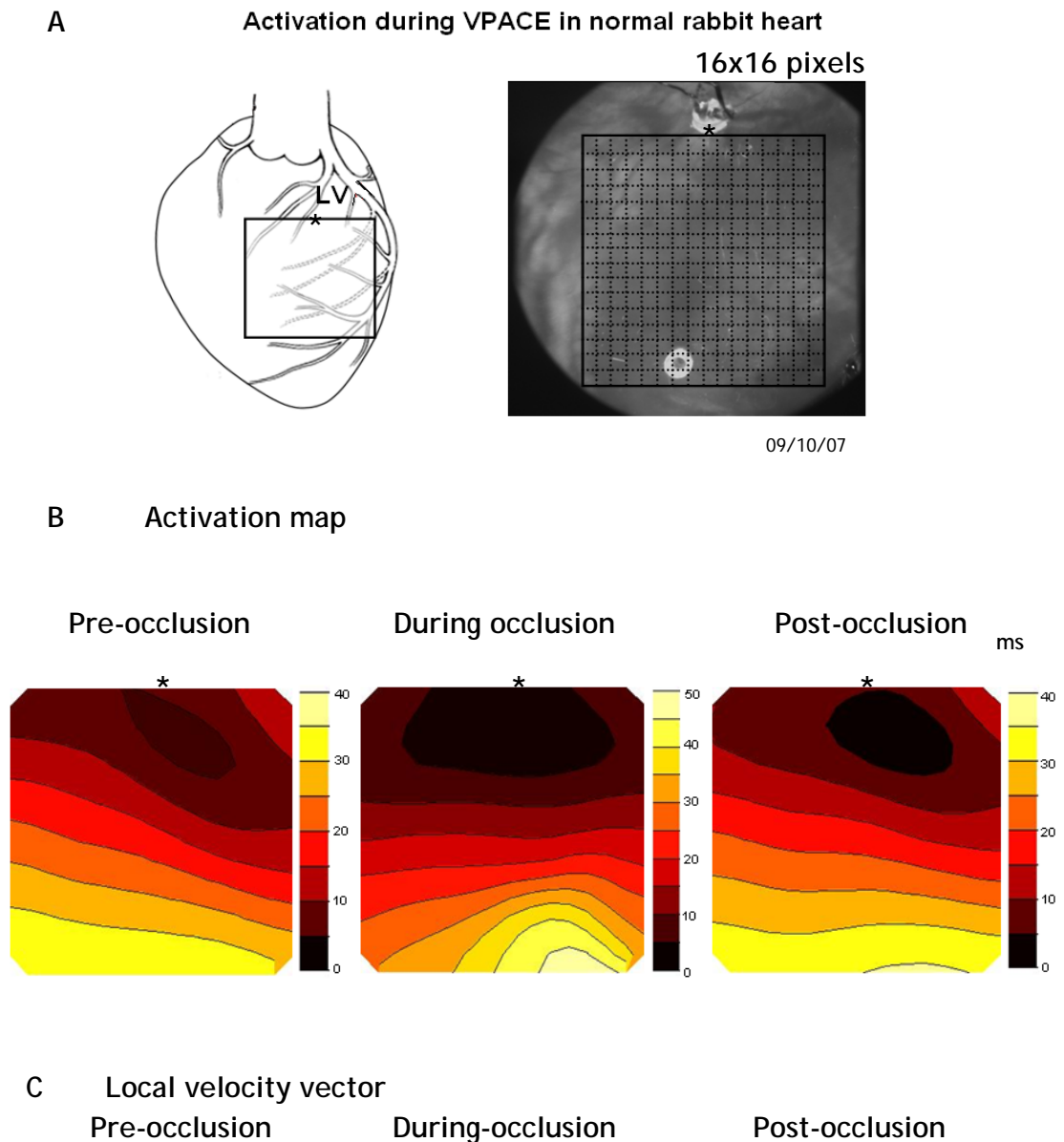


Figure 6.6 AP and repolarization alternans in low-flow and no-flow ischaemia

A (i&ii): Progressive changes in ECG configuration with corresponding OAPs. B: (i&ii) during low-flow and no-flow ischaemia respectively. ECG traces were recorded in the final 9 mins of global ischaemia. Optical recordings from sites in zone1,2 and 3 are shown next to corresponding ECGs.

6.3.5 Epicardial conduction during acute regional ischaemia

Figure 6.7A shows the mapping field and the pacing site (top centre). Panel B shows isochronal activation maps and Panel C the derived velocity vectors. During occlusion, the pattern of activation changed and conduction became slower, as seen by the crowding of the isochronal lines in the bottom right-hand corner of the field. This was confirmed in the velocity magnitude maps shown in panel D. Although the median velocity values were comparable across all three time points (pre-occlusion, during and post-occlusion were 42.3, 41.0 and 41.4 cm/sec, respectively), the minimum value was lower during occlusion compared to the pre- and post- time points.



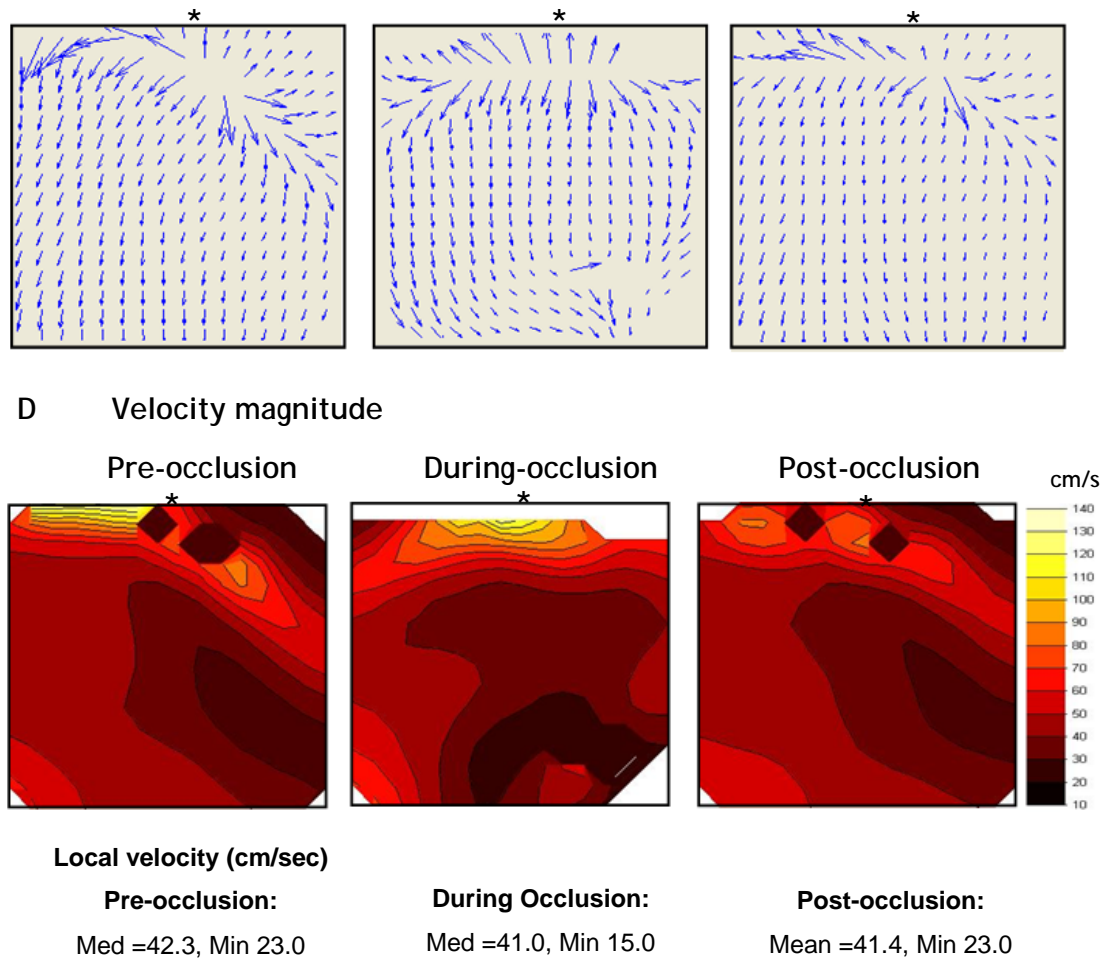


Figure 6.7 Epicardial activation during coronary artery ligation

A: Photograph of anterior surface of the LV imaged by CCD camera, mapping field is shown in the centre of figure. B: Isochronal maps of activation with 250 ms pacing cycle length at pre-occlusion, during occlusion and post-occlusion. The pacing site is shown by asterisk (*). C: CV vectors. D: Contour maps of local velocity. Median and minimum velocities are given below the figure; all have units cm/s.

6.3.6 Epicardial activation during low flow ischaemia

Figure 6.8A shows isochronal activation maps from 3 selected time points: prior to reduce the flow rate to 5ml/min, while the flow rate was reduced and after reperfusion (flow rate restored to 30ml/min). Global low-flow ischaemia had minimal effects on activation pattern, velocity direction and magnitude.

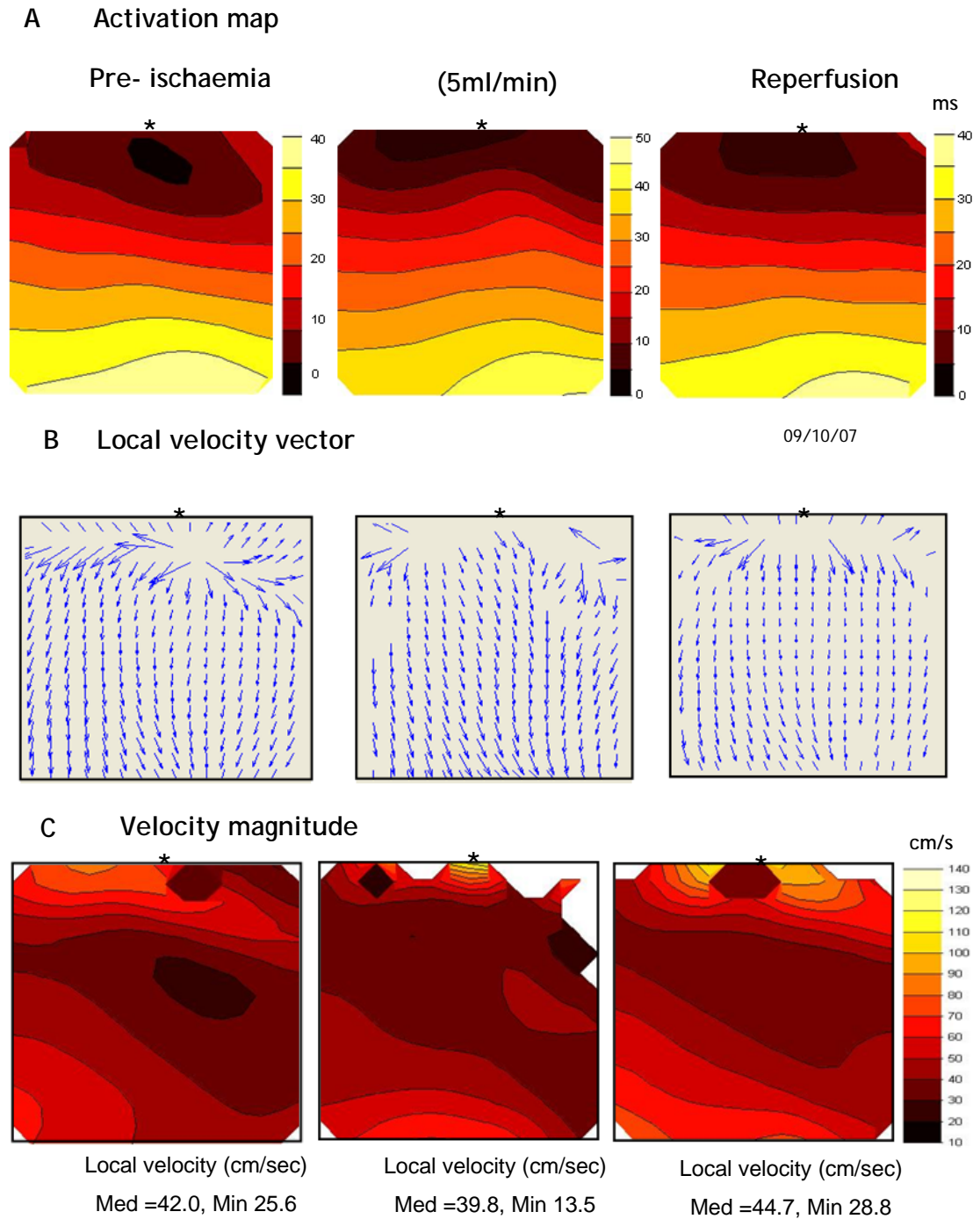
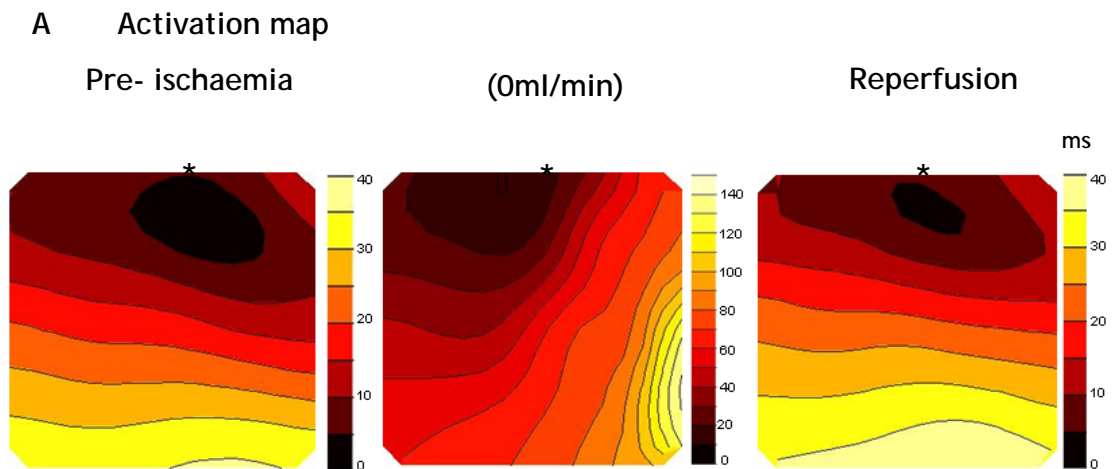


Figure 6.8 Epicardial activation during global low-flow ischaemia

A: Isochronal maps of activation with 250 ms pacing cycle length at pre-occlusion, during occlusion and post-occlusion. The pacing site is shown by asterisk (*). B: CV vectors. C: Contour maps of local velocity. Median and minimum velocities are given below the figure; all have units cm/s.

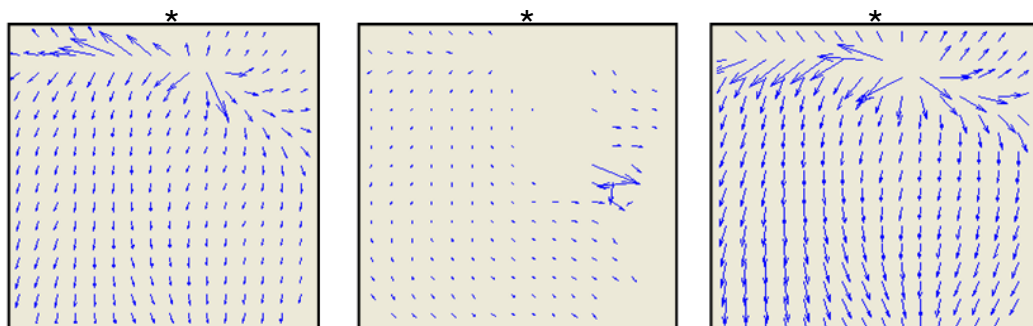
6.3.7 Epicardial activation during global ischaemia

During global no-flow ischaemia, there were marked changes in local conduction across the mapped area. This is most clearly seen in the isochronal maps which show both a change in direction of conduction away from the site of stimulation and a reduction in velocity, as indicated by the greater number of isochrone lines. These changes are reflected in the vector and velocity magnitude maps. However, in this example, velocity magnitudes were absent from parts of the field (white areas in 6.9C) due to a failure of the fitting procedure where anomalously low conduction velocities occurred.



09/10/07

B Local velocity vector



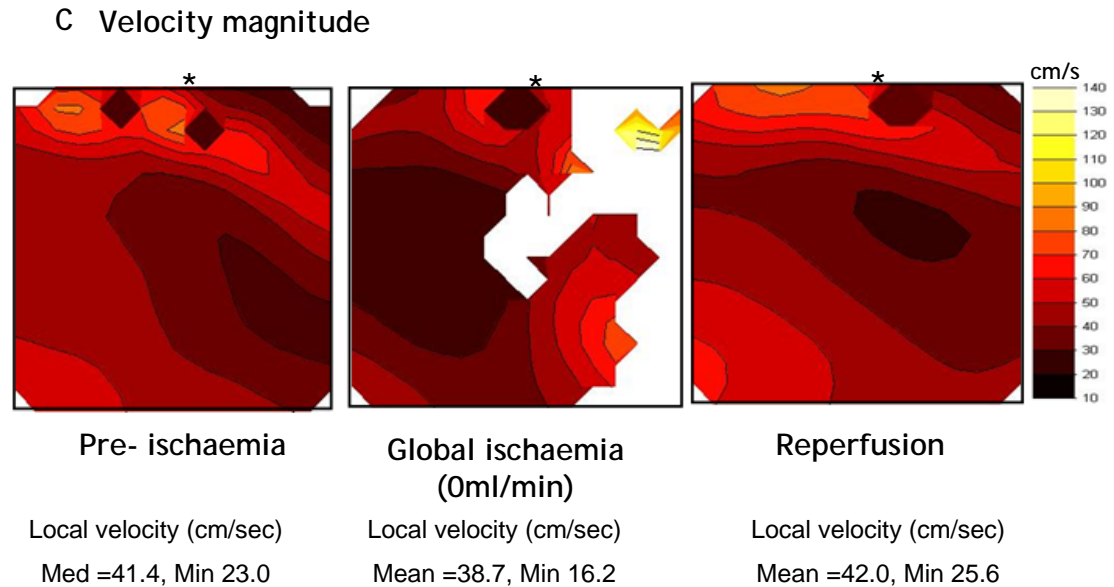


Figure 6.9 Epicardial activation during global no-flow ischaemia

A: Isochronal maps of activation with 250 ms pacing cycle length at pre-occlusion, during occlusion and post-occlusion. The pacing site is shown by asterisk (*). B: CV vectors. C: Contour maps of local velocity. Median and minimum velocities are given below the figure; all have units cm/s.

6.3.8 Summary of CV during regional ischaemia

CV was measured in the steady state from the normal, border and ischaemic zones during a period of coronary artery occlusion in 11 hearts. The results are summarized in Table 6.3, dividing the hearts into arrhythmic and non-arrhythmic groups. There were no significant changes in either mean velocity or lower 10th percentile (P10) in all three conditions (repeated-measures ANOVA). Although not significantly different, the lowest value of P10 for all conditions was observed in the ischaemic zone during occlusion in the arrhythmic group.

Non-Arrhythmia CV; N=5		Normal zone (cm.s ⁻¹)	Border zone (cm.s ⁻¹)	Ischaemic zone (cm.s ⁻¹)
Pre-Occlusion	Mean ± SEM	41.8 ± 5.1	58.3 ± 10.3	47.5 ± 2.8
	P10 ± SEM	35.1 ± 4.7	48.3 ± 6.8	43.5 ± 2.9
Occlusion	Mean ± SEM	44.2 ± 8.6	49.9 ± 9.4	45.9 ± 2.4
	P10 ± SEM	37.5 ± 6.3	43.8 ± 10.1	39.9 ± 1.2
Post-occlusion	Mean ± SEM	38.3 ± 4.5	39.1 ± 4.7	55.5 ± 4.8
	P10 ± SEM	33.1 ± 5.3	37.6 ± 5.7	46.0 ± 1.7

Arrhythmia CV; N=6				
Pre-Occlusion	Mean ± SEM	47.3 ± 5.4	60.7 ± 10.7	47.1 ± 5.1
	P10 ± SEM	36.5 ± 5.3	48.9 ± 7.3	39.4 ± 3.5
Occlusion	Mean ± SEM	60.6 ± 6.6	49 ± 9.4	38.3 ± 7.1
	P10 ± SEM	44.8 ± 7.0	39.8 ± 5.6	31.5 ± 6.0
Post-occlusion	Mean ± SEM	43.4 ± 5.6	49.6 ± 7.2	50.5 ± 5.3
	P10 ± SEM	34.4 ± 5.8	43.3 ± 5.5	43.0 ± 4.5

Table 6.3 Values are mean and standard error (SEM) of the CV in the rabbit heart during acute regional ischaemia.

N is the number of rabbit hearts. P10 represents the low 10th percentile of velocity values. Mean CV was calculated for the group of hearts that had arrhythmias during coronary artery occlusion and compared with mean CV values from the group of non-arrhythmic hearts.

The corresponding dataset for global low-flow ischaemia (Table 6.4) showed no significant changes in any of the parameters. In the case of global no-flow ischaemia, equivalent statistics could not be obtained due to the large number of clearly artefactual velocity estimates.

2ml/min CV; N=5		Basal zone (cm.s ⁻¹)	Middle zone (cm.s ⁻¹)	Apical zone (cm.s ⁻¹)
Pre-Ischaemia	Mean ± SEM	44.1 ± 5.4	39.0 ± 3.0	49.6 ± 8.8
	P10 ± SEM	35.4 ± 1.5	28.7 ± 0.9	40.8 ± 5.9
Low flow ischaemia	Mean ± SEM	29.6 ± 1.1	36.3 ± 10.4	50.9 ± 19.4
	P10 ± SEM	25.4 ± 1.7	29.0 ± 7.6	37.5 ± 12.3
Post-ischaemia	Mean ± SEM	46.9 ± 6.7	55.5 ± 12.9	53.5 ± 10.5
	P10 ± SEM	35.1 ± 2.7	39.7 ± 7.2	42.1 ± 6.0

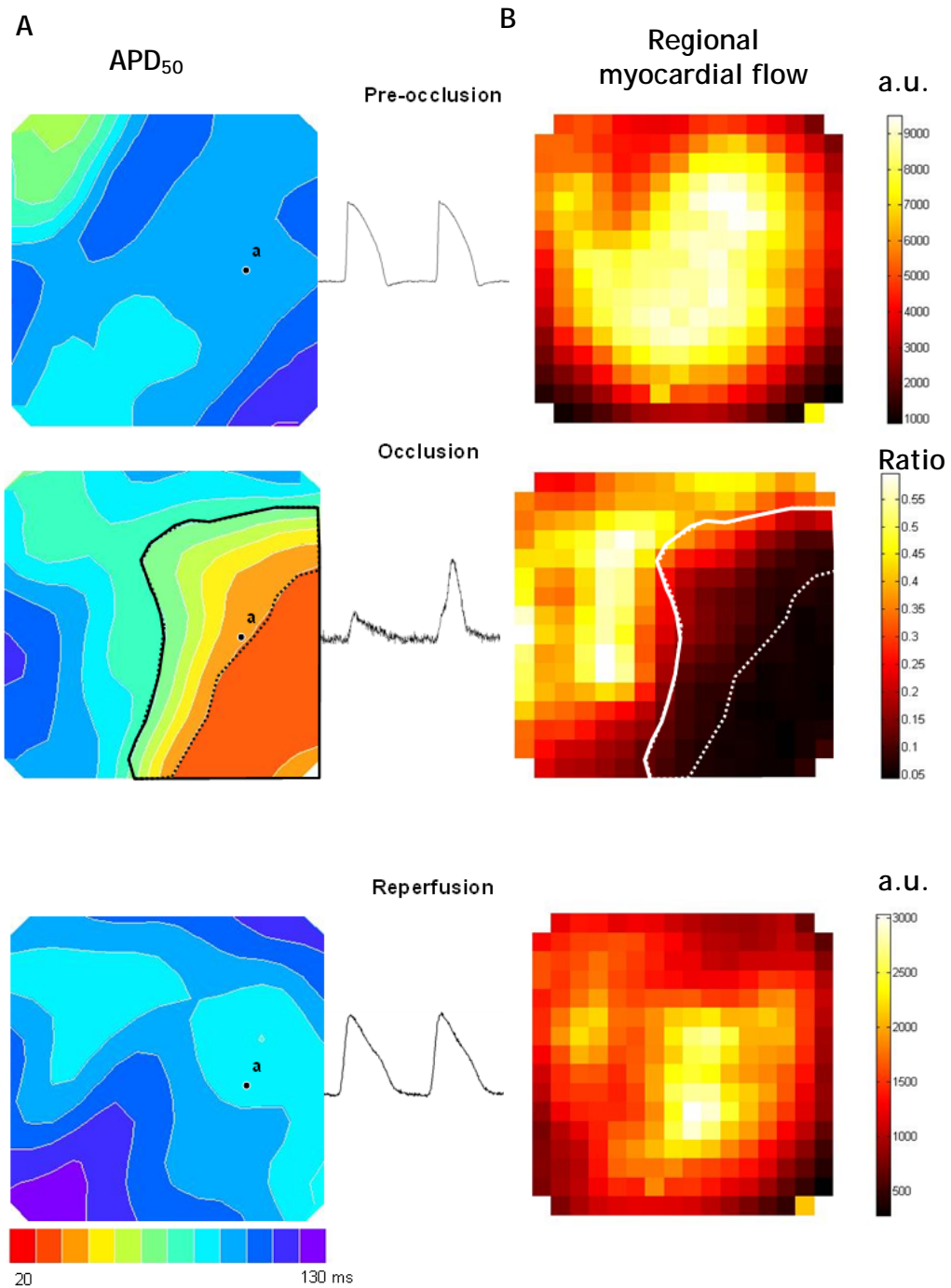
Table 6.4 Mean and standard error (SE) of the CV during global low flow ischaemia

N is the number of rabbit hearts. P10 represents the low 10th percentile of velocity values. Mean CV was calculated for the group of hearts that had arrhythmias during coronary artery occlusion and compared with mean CV values from the group of non-arrhythmic hearts.

6.3.9 Alternate beat analysis of local APDs at the sites of conduction block during local ischaemia

6.3.9.1 CV vectors in alternate beats in hearts *without arrhythmia*

Figure 6.10A shows the changes in APD₅₀ during the period of acute regional ischaemia. Panel B shows regional flow estimates at the same time points. During regional ischaemia an area of short APs were seen that corresponded closely with the region of reduced flow. A border zone of intermediate APD values was evident and corresponded to a region of intermediate flow. On the basis of APD, these regions were delineated into IZ and BZ. These arbitrary regions were subsequently used as markers to interpret conduction maps.

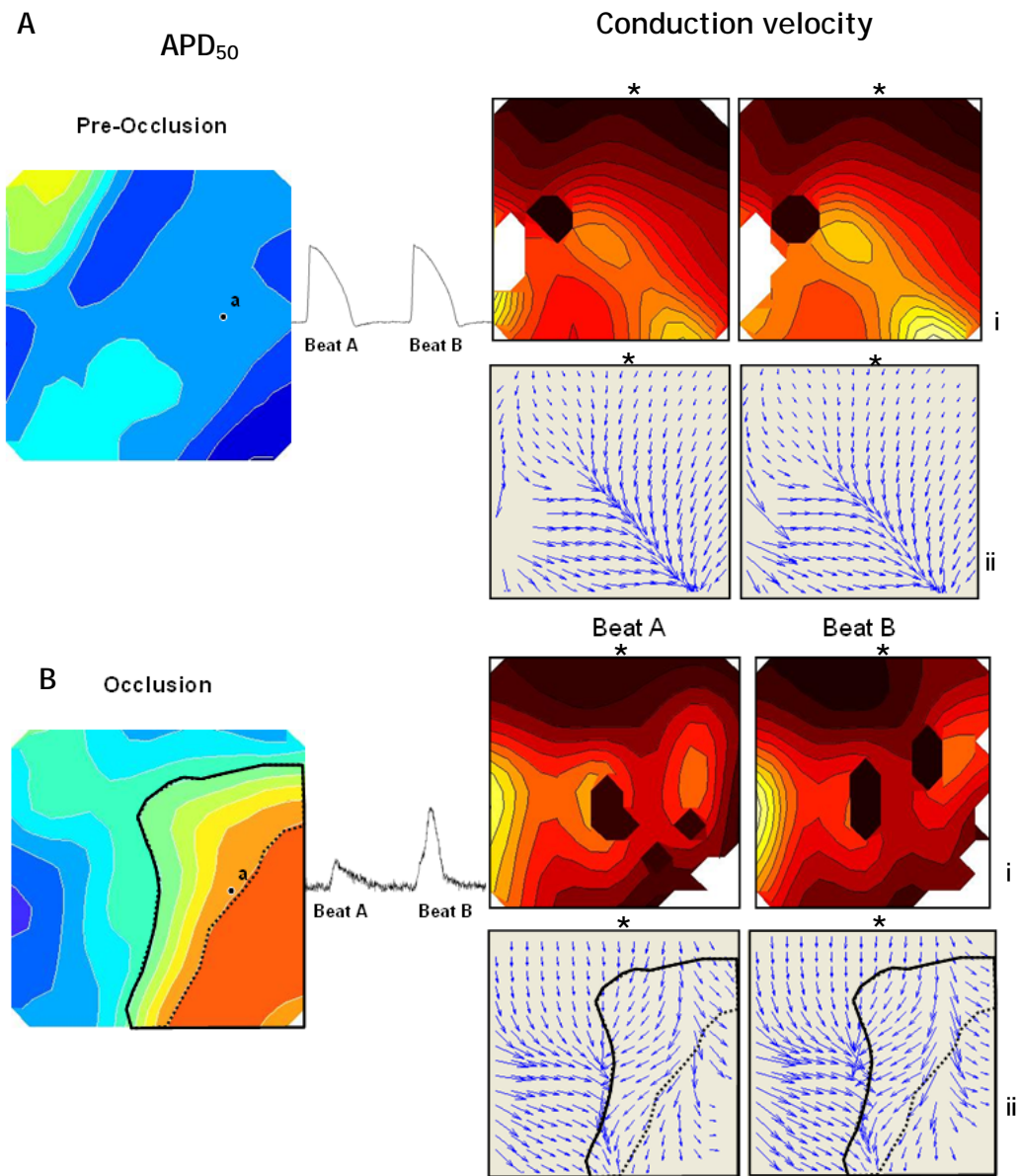


22/05/08

Figure 6.10 Comparison of APD₅₀ and regional myocardial flow

A: Contour maps of OAPs obtained before coronary artery was occluded, during occlusion and following release of occlusion (reperfusion). OAPs recorded from site “a” are shown alternating during ligation and not during reperfusion. B: Corresponding relative myocardial flow as a function of fluorescence arbitrary units is used, a.u. indicates arbitrary units. Dashed and solid lines indicate the ischaemic and border zones, respectively.

Figure 6.11 shows the CV vector analysis for the same experiment featured in Figure 6.10. Panel A illustrates APD_{50} for reference. Panel B shows the velocity magnitude (i) and velocity vector (ii) from 2 successive beats. When the coronary artery was occluded, the sample OAPs recorded from the area (marked as a) show marked changes in direction of conduction between alternating beats (Beat A and Beat B). Despite these marked changes there was still clear evidence of significant propagation from the pacing site into the ischaemic area when the coronary artery was occluded and on reperfusion.



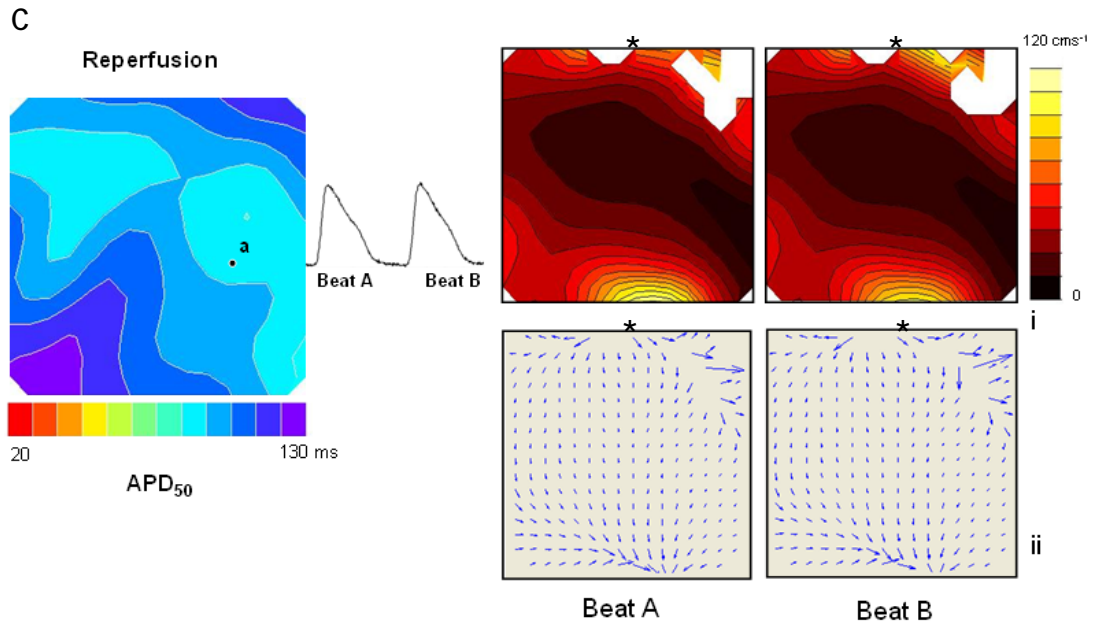


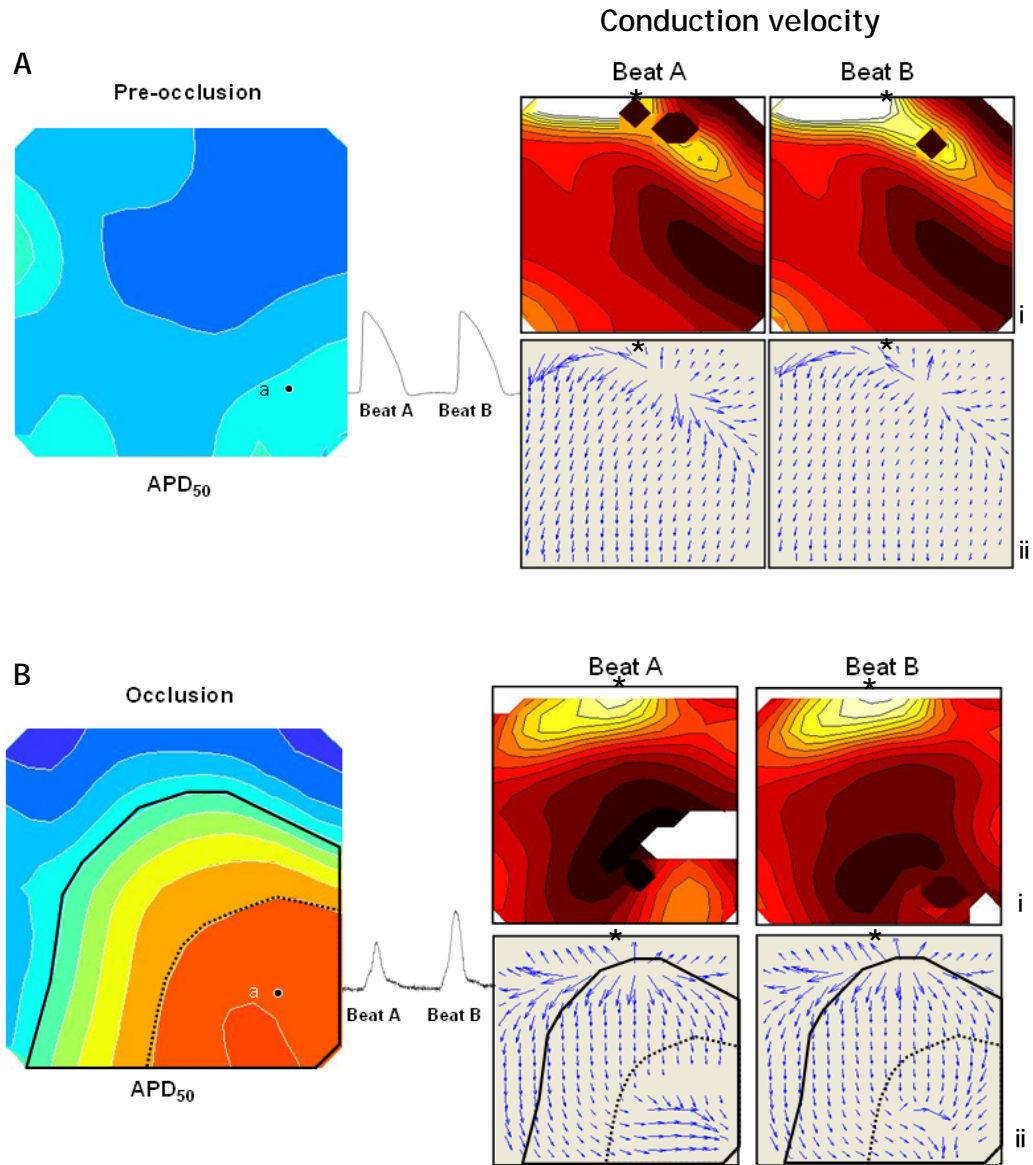
Figure 6.11 Alternating conduction velocities (non-arrhythmic heart)

Data obtained from the same heart as Figure 6.10. Left hand of figure shows APD maps; right hand shows CV magnitude (i) and vectors (ii) measured before occlusion, 17min after occlusion and 30 min after reperfusion. Dashed and solid lines indicate the ischaemic and border zones, respectively. Beat A and Beat B obtained from the 2 successive beats which showed short and long duration APs during ligation. Asterisk (*) represents the pacing site.

6.3.9.2 CV in heart with arrhythmia

The same approach was used to analyse equivalent data from a heart that developed arrhythmias in response to a local ischaemic challenge. As previously described, APD was used to delineate ischaemic and border zones (dashed and solid lines). Samples OAPs derived from a pixel within the ischaemic zone are shown between the two panels (marked "a" in Figure 6.12). Unlike the pre- and post- occlusion periods, the velocity magnitude and vector maps for beats A and B were different during occlusion in the regions corresponding to IZ and BZ. During beat A, a clear line of conduction block was evident and the OAP distal to the region of block was smaller and shorter in duration compared with beat B. All epicardial activation parameters returned to the pre-ischaemia pattern after reperfusion.

Across all the hearts studied, regions of conduction block were observed in 5/6 hearts that displayed arrhythmias versus 0/7 hearts that did not display arrhythmias during local ischaemia.



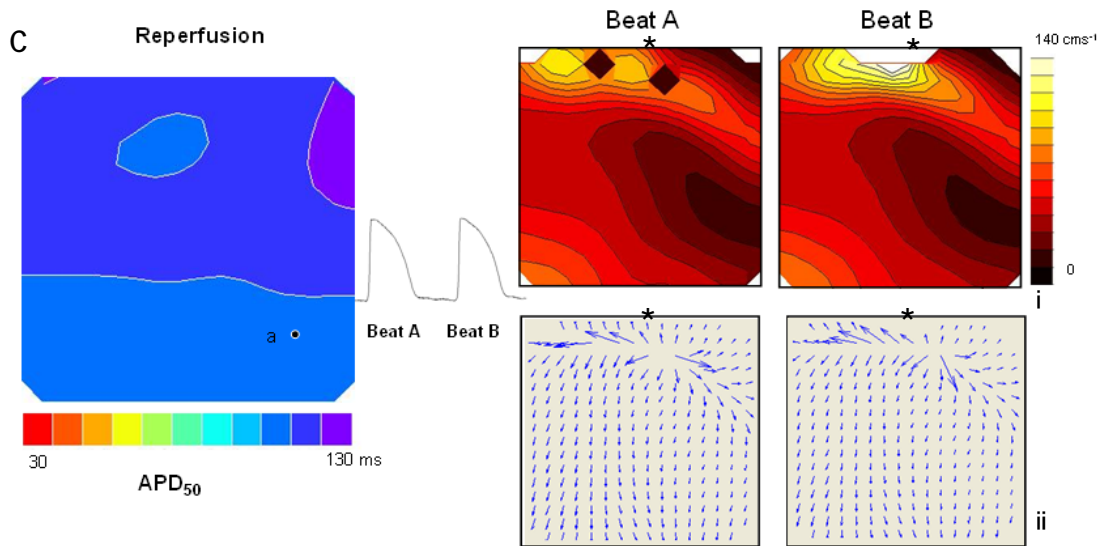


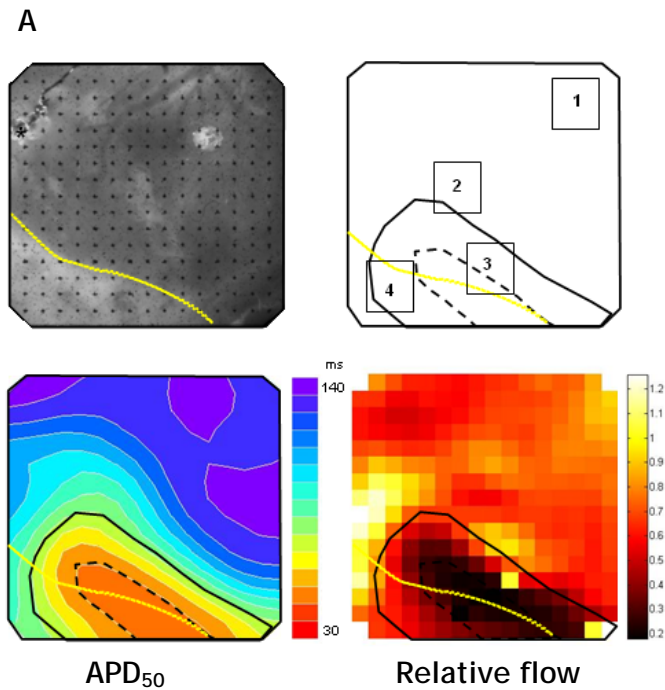
Figure 6.12 Alternating conduction velocities (leading to arrhythmia)

Left hand of figure shows APD maps; right hand shows CV magnitude (i) and vectors (ii) measured before occlusion, 11min after occlusion and 15 min after reperfusion. Dashed and solid lines indicate the ischaemic and border zones, respectively. Beat A and Beat B obtained from the 2 successive beats which showed short and long duration APs during ligation. Asterisk (*) represents the pacing site.

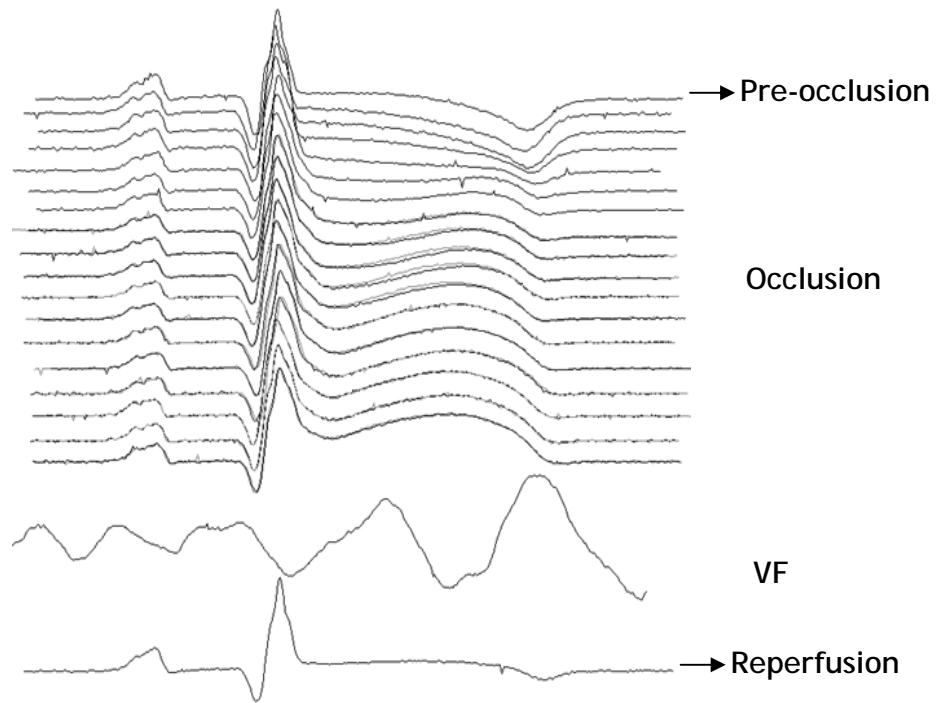
6.3.10 Ischaemia superimposed on LV with myocardial infarction

In a limited number of experiments, hearts with a myocardial infarction were subjected to a local ischaemic challenge. These experiments were technically difficult because the surface adhesions associated with the operative procedure tended to obscure the coronary vessels near the epicardial surface. Of the 8 attempted procedures, only 2 showed detectable changes on coronary artery occlusion. In the other 6 hearts, the inability to establish the position of an appropriate coronary artery to ligate may have resulted in limited ischaemia in the apical region containing the infarct. The experiment shown in Figure 6.13 shows the response to what was presumed to be a successful ligation. As shown in Panel A, ligation led to the development of a well-defined ischaemic area with close correspondence between APD₅₀ maps and relative perfusion index. The ECGs shown in Panel B displayed ST-segment elevation with a mild level of T-wave alternans prior to arrhythmia, similar in pattern to that observed in non-infarcted hearts (see e.g. Figure 6.4).

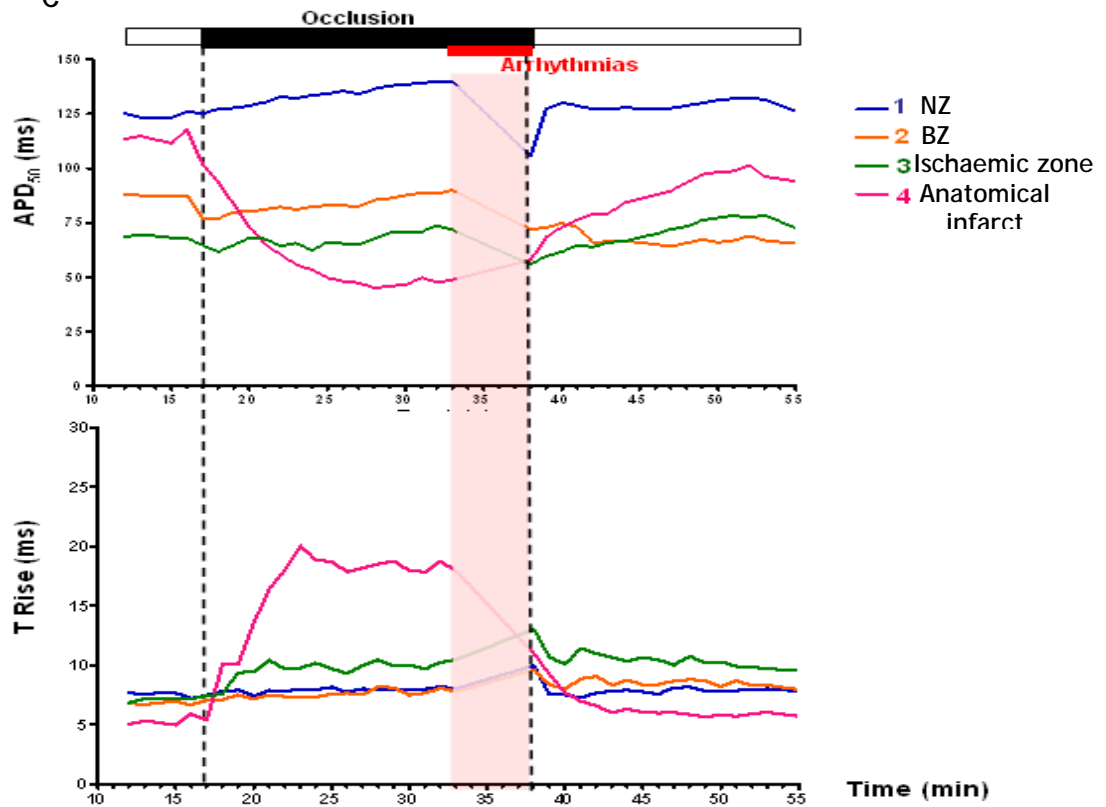
Interesting differences in AP duration and rise-time distribution were observed. Region 4 inside the anatomical infarct showed relatively normal electrophysiology both in control (pre-occlusion) conditions and in response to occlusion. In contrast, regions 2 and 3, situated at the border of the infarct and ischaemic zones respectively, had shorter than normal APs under control conditions. Moreover, these regions failed to show significant APD decrease during the ischaemic phase. On the other hand, rise times in these regions were relatively normal and region 3 showed a weak increase during ischaemia. There were not pronounced alternating changes in APD or conduction during ischaemia. Nor was there any evidence of conduction block despite the occurrence of arrhythmia.



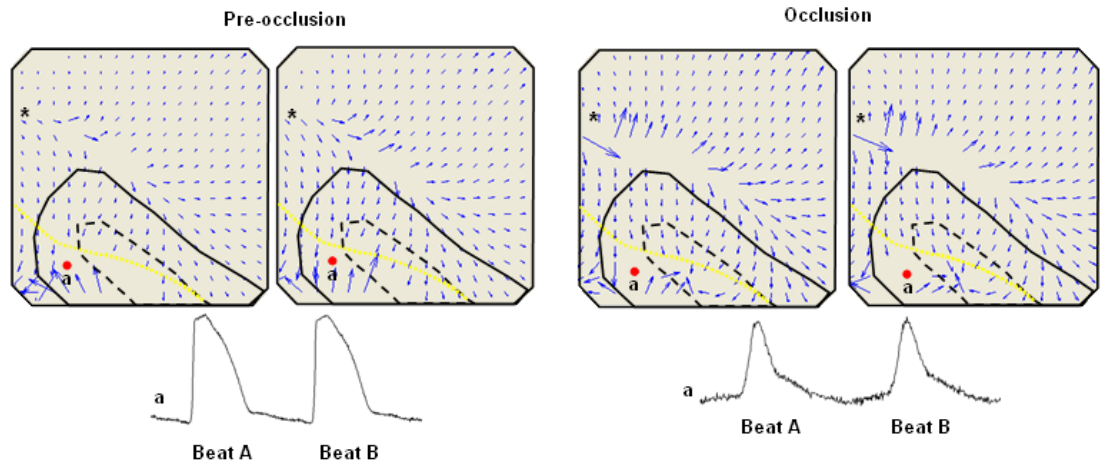
B ECG traces



C



D Velocity vector



E Velocity magnitude

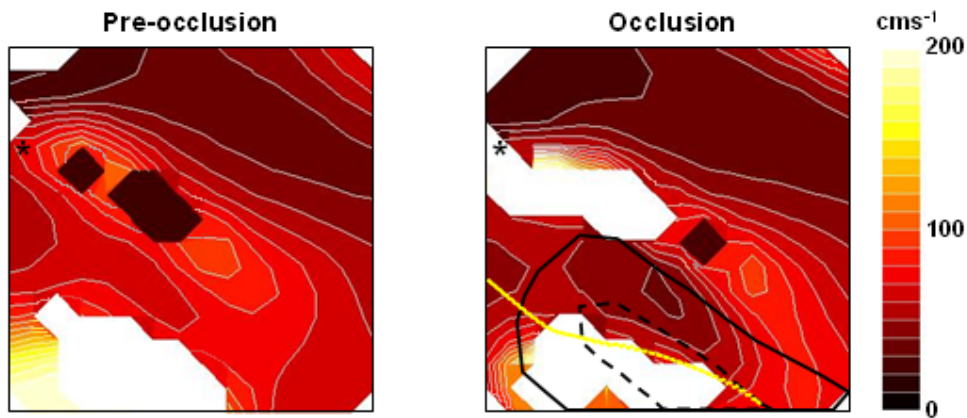


Figure 6.13 The effects of local ischaemia on hearts with an existing infarction scar

A: CCD image of the epicardial surface showing the infarct scar (bottom left) delineated by a yellow line. The adjacent panel is a reference diagram showing the relative positions of infarct scar, border and ischaemic zones and the 4 regions used in the subsequent OAP analysis. The lower panels show APD_{50} and relative perfusion maps of the myocardium during local ischaemia. Border and ischaemic zones are delineated on the basis of APD_{50} values as before. B: Corresponding ECG recordings prior to, during local ischaemia and on reperfusion. ECG records recorded at 1min intervals. C: Time course of APD and Rise time changes from OAPS recorded from the 4 regions shown in panel A. D and E: are velocity vector and magnitude maps of alternate beats with both infarct and ischaemic zones delineated.

6.4 Discussion

The experiments described in this chapter were designed to investigate the association of conduction block and APD alternans to arrhythmias during acute regional ischaemia produced using my novel calibrated snare arrangement (described in Chapter 2, section 2.2.2).

The main findings of this chapter are:

- The use of BDM is not a suitable uncoupler to use when investigating ischaemia-induced arrhythmias. Blebbistatin appears to preserve the arrhythmic status of the myocardium.
- Alternans of T-wave amplitude and APD occur during acute regional ischaemia. The T-wave alternans is a transient phenomenon, the APD alternans is sustained.
- Alternans of conduction block was commonly observed in hearts with arrhythmias and was rare in those that remained in sinus rhythm.
- Overall CV did not change in local, low-flow ischaemia.
- The presence of an existing infarct scar did not dramatically affect the changes in the electrophysiological changes in response to acute ischaemia.

6.4.1 The effects of mechanical uncouplers on ischaemia induced arrhythmias

Initially, this chapter described results comparing the influence of motion artefact blockers BDM and blebbistatin on predisposition to generate of APD alternans and arrhythmias during regional and global no-flow ischaemia in normal and chronic infarcted hearts. As shown in table 6.3 and 6.4, in the presence of BDM there was a lower incidence of APD alternans and arrhythmias than when blebbistatin was used in both normal and chronic infarction hearts. At the level of occurrence of alternans, the statistical significance of this finding

approached significance ($P = 0.06$), but for the occurrence of VF significance was achieved ($P < 0.05$). The incidence of alternans and arrhythmias in blebbistatin was not significantly different from that measured in the absence of mechanical uncouplers, although the common arrhythmia in the absence of uncouplers was VT (rather than VF). But the statistical power of this observation is weak due to the low number of animals in the respective groups. The lower number of arrhythmias and alternans observed in BDM confirms earlier studies (Qian *et al.*, 2003) and suggests that BDM is not a suitable uncoupler to examine arrhythmic behaviour. The similarity in the incidence of alternans and arrhythmias between the blebbistatin and control groups suggests that this uncoupling agent does not have major effects on the arrhythmic behaviour of isolated rabbit hearts.

In these experiments, APD alternans and arrhythmias appeared slightly more frequently during global ischaemia than regional ischaemia. Global ischaemia exhibited APD alternans in ~70% of hearts and arrhythmias in ~65% of hearts. On the other hand, regional ischaemia exhibited APD alternans in ~53% of hearts and arrhythmias in ~30% of hearts. The incidence of APD alternans in global vs. regional ischaemia was not statistically significant ($P=0.13$), but the incidence of VF between these two groups was significantly different. Interestingly, despite the low numbers of hearts in the control group, VT was common during global ischaemia under control conditions; but no VT was observed during local ischaemia. This contrasts with VF (and not VT) as the common arrhythmia in the presence of blebbistatin. The reason for these differences in the incidence of arrhythmias is uncertain, but some of the relevant factors will be discussed below and in the subsequent chapter (7).

6.4.2 Correlation between T-wave and APD alternans

T-wave and APD alternans was observed 3-15 minutes after onset of acute regional ischaemia. This was a similar time course to previous reports of APD alternans recorded using MAP electrodes (Qian *et al.*, 2003). However, the novel findings from the current study are: (i) in the continuous presence of regional ischaemia T-wave alternans reached maximal value after ~5mins of regional ischaemia but then declined to undetectable values before the arrhythmia commenced; (ii) OAPs in the IZ and BZ displayed alternating changes in AP

amplitude and duration during local ischaemia which developed with the same time course as T-wave alternans but remained despite a reduction in the corresponding alternation in the T-wave amplitude. Thus, unlike previous reports, it is unlikely that T-wave alternans is the mechanism underlying the generation of arrhythmias in acute regional ischaemia in this model. Previous work showed that T-wave alternans was associated with arrhythmogenesis but a causal link has been difficult to establish. This study confirms the association, but suggests that T-wave alternans does not need to present at the instance the arrhythmias to occur (Abe *et al.*, 1989; Downar *et al.*, 1977). Instead, the mechanism underlying arrhythmogenesis may involve conduction alternans and re-entry leading to the development of conduction block in the IZ.

The electrophysiological origin of the T-wave has been debated for some time, one argument suggests that the T-wave originates from transmural dispersion of APD (Antzelevitch *et al.*, 1998) while other arguments suggest that apex-base differences in repolarisation are dominant (Coronel *et al.*, 2002). Therefore discussion of the possible causes of alternating T-waves cannot be definitely attributed to changes in one axis of the heart. Alternating APD in a significant part of the LV may contribute to the alternating T-wave signal, but it is unclear why T-wave changes should disappear while APD alternans is retained as observed in this study. One possible explanation is that the apparent T-wave alternans observed in this study is due to alternating extents of ST-segment changes rather than changes in T-wave. Support for this comes from the evidence that alternans in AP characteristics may arise in part from alternating levels of conduction (slow or block) into the ischaemic region. The causal link between alternating ST-segment changes and either alternating APD or amplitude or conduction could not be easily made in this study because the imaging always involved only part of the ischaemic region. Therefore, the behaviour of the region imaged may not be representative of the entire local ischaemic event. However, the data presents strong evidence that alternating conduction properties including alternating block may be the basis of alternating T-wave during local ischaemia.

T-wave alternans was also observed during global ischaemia (Table 6.1). The corresponding optical signals were not analysed in the current study. This was omitted for several reasons: (i) the global nature of the ischaemia meant that

events (e.g. in the septum or RV) contribute to the ECG signal but were undetected by the optical signals, therefore extrapolation from optical to ECG may be problematic. (ii) Spatial heterogeneity of the optical signal during global ischaemia was at a much smaller scale than that seen during local ischaemia, thus local conduction was much harder to assess. Spatial and temporal changes will be discussed in more detail in Chapter 7.

6.4.3 Mechanisms for AP and conduction changes during ischaemia

A progressive decrease in APD₅₀ and increase in rise time occurred over 5-10 min of regional ischaemia and uniformly across the ventricle during global ischaemia and the map of local velocity vector also showed abrupt changes in CV in the IZ.

The basis of these electrophysiological changes has been extensively studied. As discussed in Chapter 1, prolongation of the T_{Rise} can be attributed to slowed CV or slowed rate of rise of the AP. The latter mechanism is thought to be dominant in this case since average CV is not significantly different. Depolarisation of the membrane potential by accumulation of extracellular potassium will inactivate the inward Na^+ current. This alone will slow the rate of depolarisation and explain increase rise time. Sufficient depolarisation may reduce available Na^+ current to the extent that an action potential fails to be elicited and this may explain the block of conduction observed.

As discussed in Chapter 1, the rate at which the Na^+ channel emerges from inactivation will depend on the membrane potential. The slower rate at depolarised potentials means that more time is required between APs to access a similar amount of the current. The time and voltage dependence of recovery from inactivation can explain the alternating block observed, simply in terms of the failure of an AP to generate a longer diastolic period and allow sufficient recovery of the Na^+ current from inactivation to permit an AP on the next beat. This analysis of alternate conduction has been modelled recently and alternans of AP conduction was evident (Arce *et al.*, 2000).

The shortening of APD evident in this study in both local and global ischaemia has been noted in a number of other studies (William & Desnond, 1983; Cabo *et*

al., 1997;Ehlert & Goldberger, 1997;Peuhkurinen, 2000). The cause of this is raised extracellular K^+ concentration as discussed in Chapter 1 causing: (i) inactivation of the inward currents (fast Na^+ channel and slow Ca^{2+} channel), and (ii) activation of the K^+ outward currents (I_{to} , I_{KATP}) (Kleber, 1984;Kleber & Wilde, 1986;Wit & Janse, 1993;Quinn *et al.*, 2003;Wilde *et al.*, 1988;Corretti *et al.*, 1991). Whether shortening of APD causes ischaemia-induced arrhythmias is not clear, some studies suggest that, the intrinsic differences in refractory period between normal and ischaemic areas contributed to the significant difference between activation and repolarization of APs (Efimov *et al.*, 1993). The heterogeneity of refractory periods caused by the varied extracellular potassium concentration may cause areas of conduction block and therefore arrhythmias as described by Moe (Moe *et al.*, 1964). These studies would suggest that changes in APD rather than rise time were the more critical of the two changes. This specific issue will be addressed by the analysis and discussion in Chapter 7.

6.4.4 Epicardial electrophysiology that precede arrhythmias

In this study, the epicardial activation characteristics of hearts where arrhythmias were precipitated by regional ischaemia were compared with hearts where arrhythmias did not occur. As shown in Table 6.3 conduction mean velocities across regions was not significantly different between arrhythmic and non-arrhythmic groups. The mean value of velocities in the lowest 10 percentile of the range showed a decrease during local ischaemia in the region where the ischaemic area developed, but the values were not statistically significantly different between the arrhythmic and non-arrhythmic groups. In both groups APD alternans magnitude increased locally with highest magnitude in the border and ischaemic zone accompanied by mark changes in activation pattern. However, APs were still capable of propagation into ischaemia area in hearts that remained electrically stable. In contrast, in hearts showing arrhythmias, the local conduction into the ischaemic area was very slow, effectively generating conduction block in the parts of the ischaemic border zone. Conduction block within the imaging field was more common in hearts that developed arrhythmias when compared with those when arrhythmias did not occur. This data suggests that the overall behaviour of the ventricle between non-arrhythmic and

arrhythmic hearts were not different and the critical areas of block that were associated with arrhythmias were in such limited areas that the mean CV (and the 10th percentile values) was not significantly different. As mentioned above, one of the limitations of the study is that the image field contained only part of the ischaemic zone, therefore events outside the field that may influence the outcome cannot be detected.

6.4.5 The effects of local ischaemia on hearts with an existing infarct

In a limited number of hearts, local ischaemia and global ischaemia was imposed in hearts with an existing infarct, by ligation of the same coronary artery proximal to the ligation that caused the infarct. This technically difficult procedure was attempted in order to mimic what is clinically a recognised feature of an acute ischaemic event in the presence of an infarct scar (Davies, 1981). In general, the majority of instances of sudden cardiac death occur in people with an existing infarct scar, therefore the presence of this scar may make arrhythmias more common during a local ischaemic event. Comparing the incidence of alternans and arrhythmias shown in Table 6.1 and 6.2 suggests that the presence of an infarct did not increase the incidence of either event significantly. In only 2 hearts (out of 8) was there regional ischaemia during the ligation, the reason for this lack of response is not known, but two possible reasons are: (i) the ligation procedure was less successful because the coronary vascular was more difficult to image due to adhesions associated with the earlier surgery (ii) revascularisation of the infarct means that the area containing the infarct was perfused by alternative coronary arteries. Despite this, the incidence of alternans and arrhythmias were similar suggesting that local ischaemia was being produced in a region outwith the imaging area.

In the example shown in Results, the ligation successfully created an ischaemic region that include the infarct scar. The electrophysiology of the scar 8 weeks after a ligation is similar to the normal myocardium due to the presence of strands of surviving myocardium within the scar (Walker *et al.*, 2007). In this

study a region within the infarct responded similarly to normal myocardium although there was clearly areas that did not. The generally similar behaviour may explain the similarly frequent occurrence of arrhythmias, but because of the low numbers of experiments where the ischaemic area could be imaged, the presence of alternans and conduction block could not be established. Further work is required to develop this technique to examine the effects of local ischaemia remote and local to the infarct scar.

7 Spatial and temporal heterogeneity of electrophysiological response to acute and global myocardial ischaemia

7.1 Introduction

Acute myocardial ischaemia is associated with the initiation of re-entrant ventricular arrhythmias, mainly VF. The arrhythmogenic mechanisms associated with acute ischaemia are still unclear and are difficult to study in human (Ehlert & Goldberger, 1997). Therefore, a wide variety of animal models have been used to study the arrhythmias in the acute phase of ischaemia.

In normal rabbit hearts subjected to regional ischaemia, onset of VF was most frequently observed 12-15 minutes after coronary artery occlusion (Bril *et al.*, 1991). This in contrast to dog and pig where there are two distinct phases (1A and B) of vulnerability (de Groot & Coronel, 2004).

The first phase of arrhythmias (phase 1A) occurred after occlusion of the coronary artery for 12-15 minutes. The second phase (1B arrhythmias) occurred from 15-45 minutes after occlusion (Ehlert & Goldberger, 1997). The mortality from sudden cardiac death in experimental animals was larger in phase 1B than 1A. However, is still unclear whether the mortality rate in human is larger in phase 1A or 1B (Coronel *et al.*, 2002).

A study of the prevalence of ventricular arrhythmias by Wit *et al* showed that, arrhythmias more frequently occurred in the experimental models than in clinical observation. Nevertheless, the form of arrhythmias in experimental models those seen clinically displayed similar patterns (Wit & Janse, 1992).

Previous studies have indicated that initiation of 1B arrhythmic behaviour may be associated with the activation of stretch-activated channels since the appearance of these arrhythmias was linked to increased LV wall stress (Coronel *et al.*, 2002). In the case of phase 1A arrhythmias, many studies have established that re-entry is responsible for sustained arrhythmias in this phase (Janse & Wit, 1989; Pogwizd & Corr, 1987; Janse *et al.*, 1980). On the other hand, the mechanisms responsible for the triggering of the delayed-arrhythmia remain unclear.

A study using an *in situ* heart model proposed that the site of origin of the delayed arrhythmia is in the surviving sub-endocardial Purkinje fibres of the infarcted myocardium and this surviving tissue played a role in arrhythmogenesis in this phase (Friedman *et al.*, 1973). Other investigations reported that re-entry is a mechanism responsible for the genesis of arrhythmias in both 2 phases. However, these studies did not make a distinction between arrhythmogenesis of the trigger and the mechanism for maintained arrhythmias (Kaplinsky *et al.*, 1979; de Groot *et al.*, 2001).

The purpose of this chapter is to examine in more detail the heterogeneity noted in the previous chapter to test the hypothesis that heterogeneity was an important determinant of arrhythmic behaviour.

7.2 Methods

Experiments were carried out on a total of 45 isolated rabbit hearts that were divided into two groups: normal (stock or sham) hearts and infarcted hearts produced by prior ligation of the left descending circumflex coronary artery 8 weeks prior to animal sacrifice (see 6.2.1 for details).

7.2.1 Acute regional myocardial ischaemia induction

Acute ischaemia was induced by occlusion of the Left posterior division of the coronary as described in the Method section (Chapter2, section 1.2.2).

7.2.2 Experimental protocol

The experimental protocol as illustrated in Figure 7.1. Hearts were subjected to the baseline recording of 10 minutes following perfusion with 5 μ M blebbistatin in standard Tyrode's solution, followed by the first run of 15 minutes regional ischaemia with 20 minutes of reperfusion. Finally, the heart was subjected to the second run of 15 minutes global low-flow ischaemia by reducing the flow rate to 5ml/min and then 20 minutes of reperfusion. Optical recordings were taken every minute of the entire experiment. Ventricular pacing followed by bolus injection of RH237 was performed prior to ischaemia, 12-15 minutes after ischaemia and 15-50 minute after reperfusion.

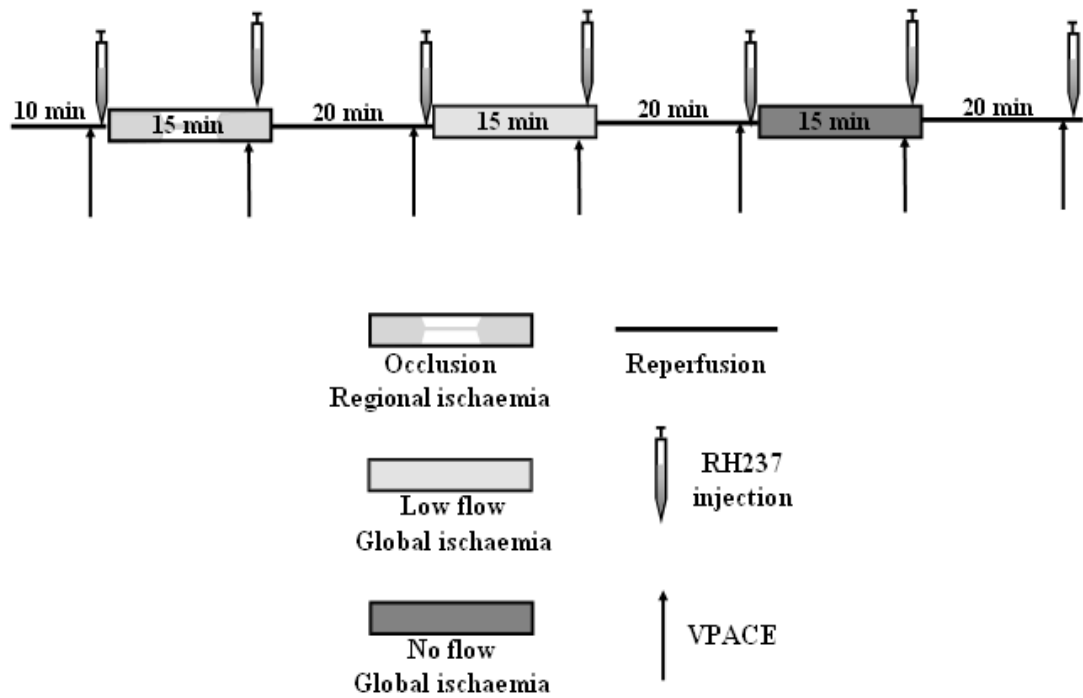


Figure 7.1 Experimental protocol

Schematic of the protocol used to compare the effects of local, low flow global and zero-flow global responses. RH237 dye injections were used to image epicardial flow. Ventricular pacing was used to estimate epicardial CV.

7.2.3 Data analysis

7.2.3.1 Frequency analysis

After VF had been induced and became established, the frequency components of the arrhythmia were analysed using Fast Fourier transforms (FFT) (Wang *et al.*, 1998; Brenner & Rader, 1976). Optical signals were analysed to create frequency power spectra for each pixel (software developed by Dr Francis Burton). Various parameters were derived from the individual power spectra, as shown in Figure 7.2:

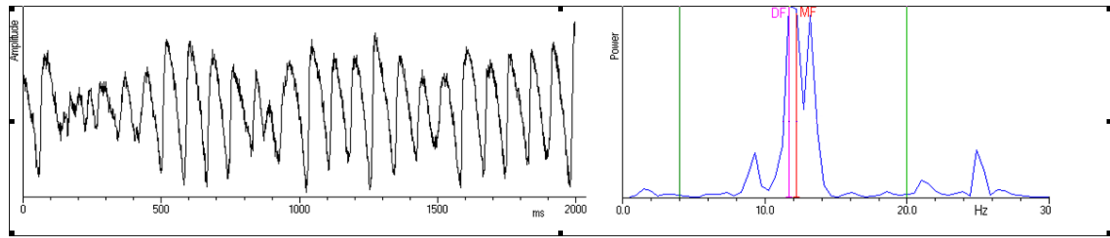


Figure 7.2 Power spectrum analysis

DF is peak or dominant frequency (DF) identified as the highest peak of the power spectrum within a specified frequency band (4-20 Hz).

MF is median frequency, which divides the total energy into two equal parts (above and below the median frequency).

DFD is a measure of concentration of energy in a single peak, varying between 0% (even spread of energy over the range of the spectrum) to 100% (all energy at single frequency). Thus, a large value of DFD indicates energy is concentrated in a narrow peak; a small value indicates the presence of a number of small peaks as in a more complex signal.

Parameter values were exported for statistical analysis and to generate colour coded maps of DF using software developed by Dr Francis Burton.

7.2.3.2 Sequence analysis

Quantification of time-dependant variability of the maps of coronary flow and optical voltage signals was performed using MATLAB. Parameter values (APD_{50} or T_{Rise}) were first normalized to the range 0-1. Three measures of variability over time were then calculated from these normalized values for each pixel in the field: a) standard deviation of values, b) range (max-min) of values, and c) mean of absolute difference between successive values. Finally, the mean value of a-c for all pixels was calculated.

7.2.4 Statistical analysis

Data were imported to InStat3 (GraphPad Software Inc., USA) to test the significance between two groups using paired t-tests, a p-value of less than 0.05 was considered significant. The rank correlation coefficient was used to describe the relationship between APD₅₀ and relative flow variability. Linear and non-linear regression testing were performed using GraphPad Prism4 (Software Inc., USA).

7.3 Results

7.3.1 Time of onset of ventricular arrhythmias during acute ischaemia and reperfusion

Within a few minutes after occlusion of the coronary artery, ECG traces showed elevation of the ST segment. This was accompanied by shortening of APD of OAPs in the ischaemic region. In this model of acute regional ischaemia, significant changes in ECG and APD were observed around 5-10 minutes after occlusion and arrhythmias occurred within 15-20 minutes. Figure 7.3 represents an example of ECG and OAP changes including arrhythmia (VT & VF) during the period of acute regional ischaemia.

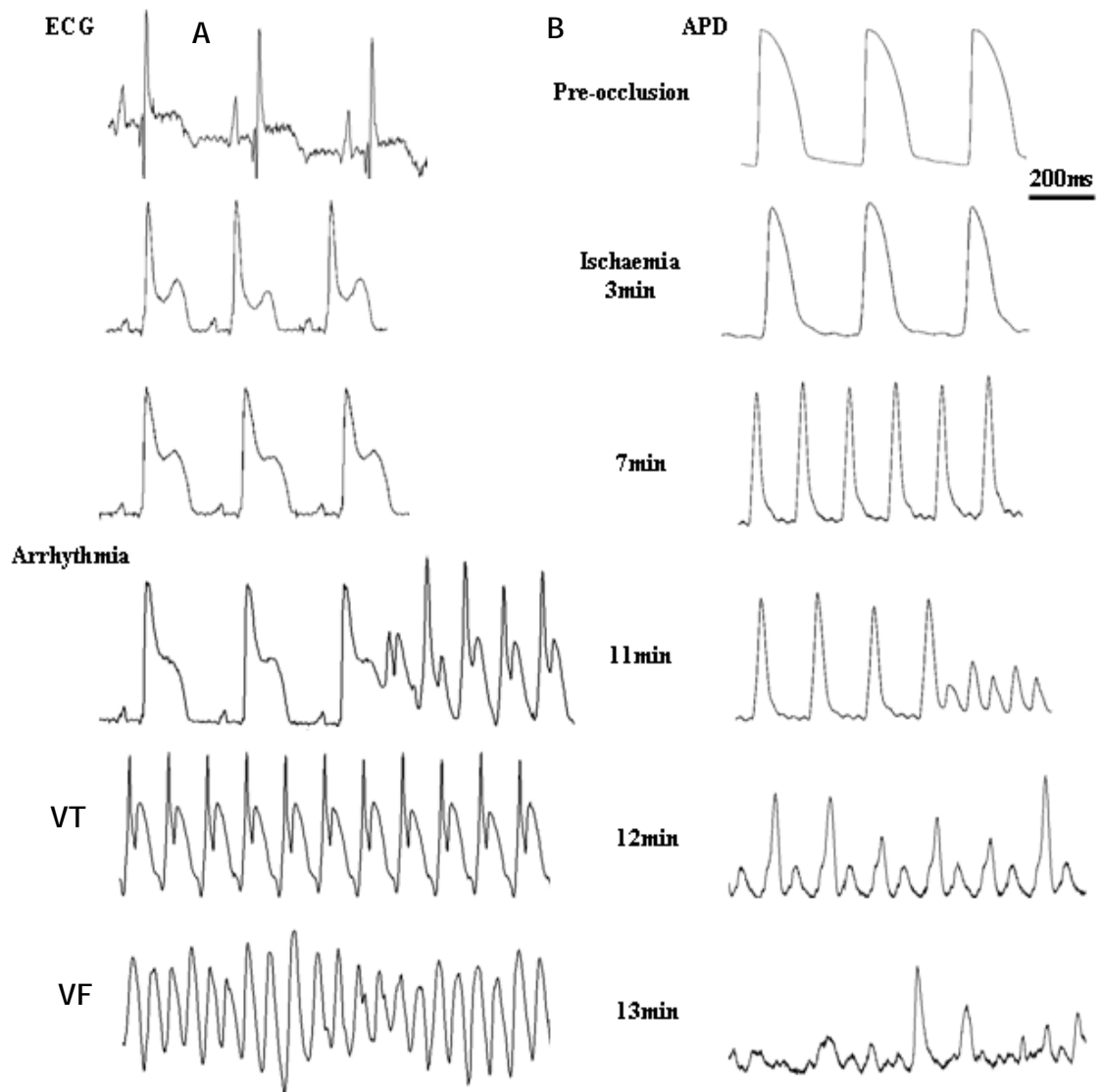


Figure 7.3 ECG traces and OAPs from the ischaemic region

A series of ECG traces (A) and OAPs in the ischaemic zone (B). Data were obtained from the normal heart at selected time points during 15 minutes of coronary artery occlusion.

In normal hearts with acute regional myocardial ischaemia, arrhythmias were seen in 8 out of 37 hearts (~22%) as shown in table 6.1. Mean time before onset of ischaemia and the first arrhythmias was 13.4 ± 1.5 minutes (n=8).

On the other hand, in chronic infarction hearts with an additional acute regional ischaemia, arrhythmias were found in 5 out of 8 hearts (~63%). Mean time before onset of arrhythmia in chronic infarction hearts was 14.2 ± 2.9 minutes (n=5) as illustrated below.

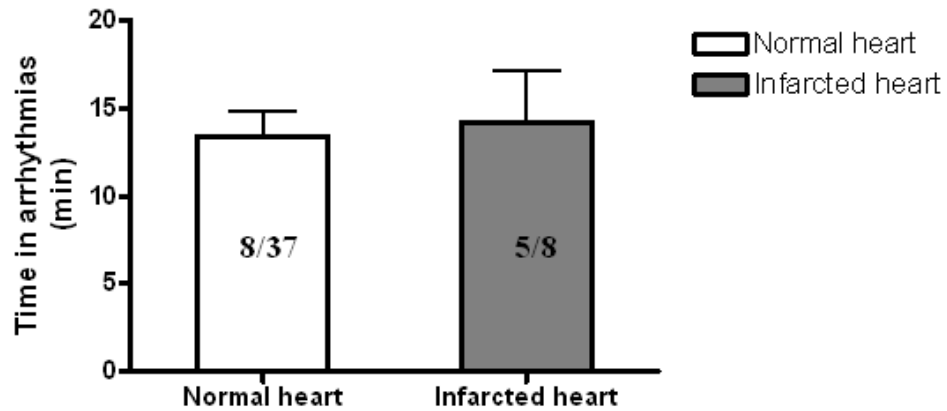


Figure 7.4 Time before onset of arrhythmias after start of acute regional ischaemia

Data represents mean \pm SEM, number in the column indicates the total number of hearts that arrhythmia was found when coronary artery occlusion.

7.3.2 Electrophysiology associated with re-entrant arrhythmias

7.3.2.1 Hearts *without arrhythmia* during acute regional ischaemia

The upper panel of Figure 7.5A shows the anterior surface of LV imaged by conventional CCD camera. Lower panel shows 252 locations of mapping area with 3 selected sites; NZ, BZ and IZ. Figure 7.5B (i) represent the changes in APD₅₀ during acute regional ischaemia. Panel 7.5B (ii) represents the rise time of the action potential from 10% to 90% depolarisation (T_{Rise}).

In contrast, there was no change in APD₅₀ in the NZ. A similar result was observed for the rise time. T_{Rise} is dramatically increased in the BZ and IZ but did not change in the NZ. However, unlike APD₅₀, the rise time did not reach a steady state by the end of occlusion.

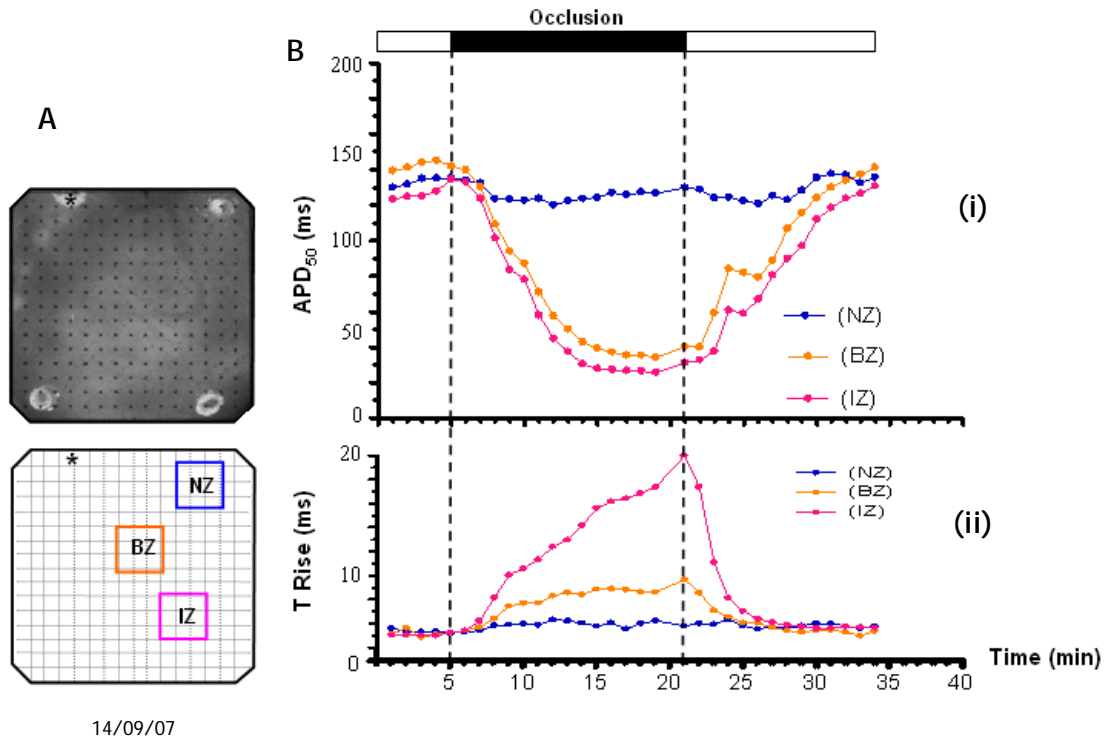


Figure 7.5 Time course of changes in APD₅₀ and T_{Rise} in heart without arrhythmia

A: CCD image of anterior surface of the LV. Panel below shows 252 pixels of mapping field with 3 selected zones; Normal zone (NZ), Border zone (BZ) and ischaemic zone (IZ). Asterisk (*) indicates the stimulation site that activated with 250 ms pacing cycle length. B: (i) and (ii) show time course of changes in APD₅₀ and T_{Rise} during acute regional ischaemia respectively.

7.3.2.2 Heart with arrhythmias during acute regional ischaemia

The upper panel of Figure 7.6A shows the anterior surface of the LV imaged by conventional CCD camera with 3 selected sites (NZ, BZ and IZ). Figure 7.6B shows the changes in APD₅₀ (i), and T_{Rise} (ii) during acute regional ischaemia. APD₅₀ is dramatically decreased and T_{Rise} increased in the IZ. In contrast, there was hardly any change in these parameters in the NZ. In this example, arrhythmias occurred when coronary artery was occluded for 12 minutes.

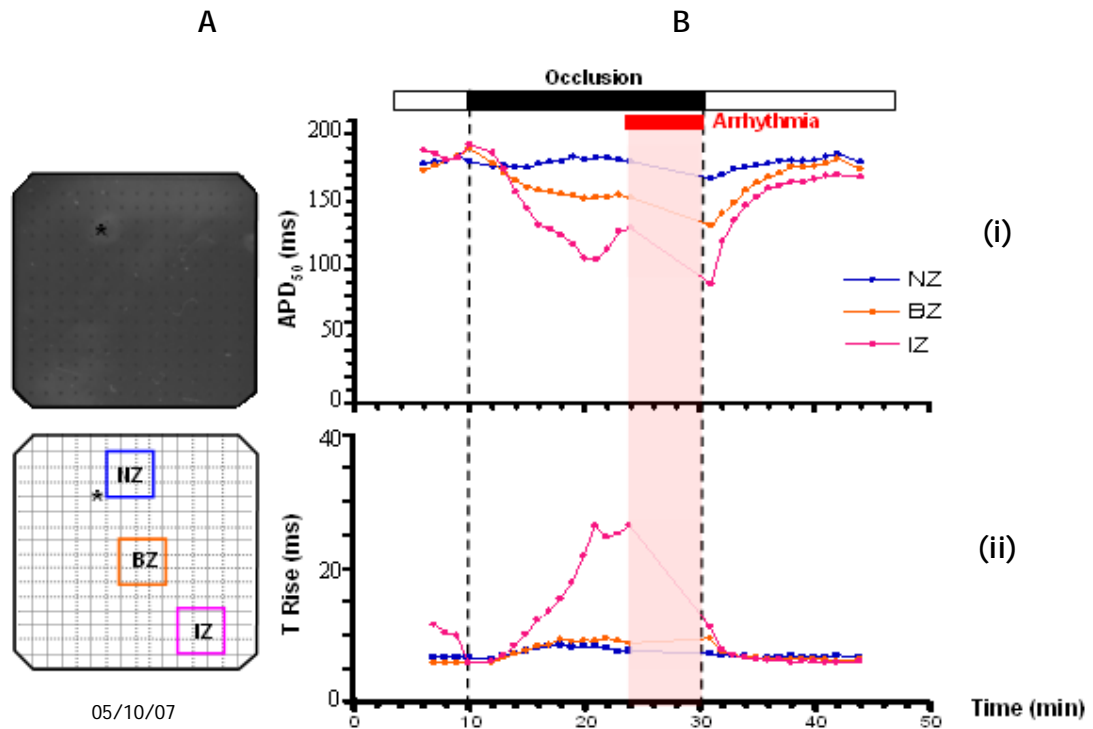


Figure 7.6 Time course of changes in APD₅₀ and T_{Rise} in heart with arrhythmia

A: Anterior surface of the LV imaged by CCD camera. Panel below shows 252 pixels of mapping field with 3 selected zones; Normal zone (NZ), Border zone (BZ) and ischaemic zone (IZ). Asterisk (*) indicates the stimulation site. B: (i) and (ii) show time course of changes in APD₅₀ and T_{Rise} during acute regional ischaemia respectively.

To quantify spatial variability, $P_{P95\%}$ was calculated as the difference between the 5th and the 95th percentile of the distribution of values of parameter P. Thus, $T_{Rise\ P95\%}$ represents the range of T_{Rise} values in the field. Significantly larger $T_{Rise\ P95\%}$ was observed in hearts with arrhythmias compared to those without. In 11 hearts when an arrhythmia occurred during acute myocardial ischaemia, $T_{Rise\ P95\%}$ was 90.0 ± 12.4 , N=11 compared to 24.1 ± 5.7 ($P < 0.001$) in 8 hearts without appearance of arrhythmia as shown below. Because T_{Rise} did not increase above normal in the NZ, it seems likely that occurrence of re-entrant arrhythmia in this model is associated with slower AP upstrokes.

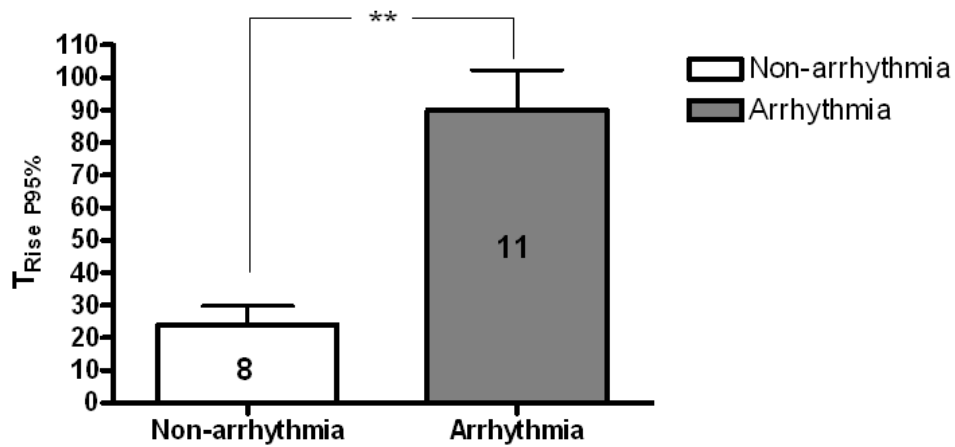


Figure 7.7 $T_{Rise P95\%}$ in hearts with and without arrhythmia

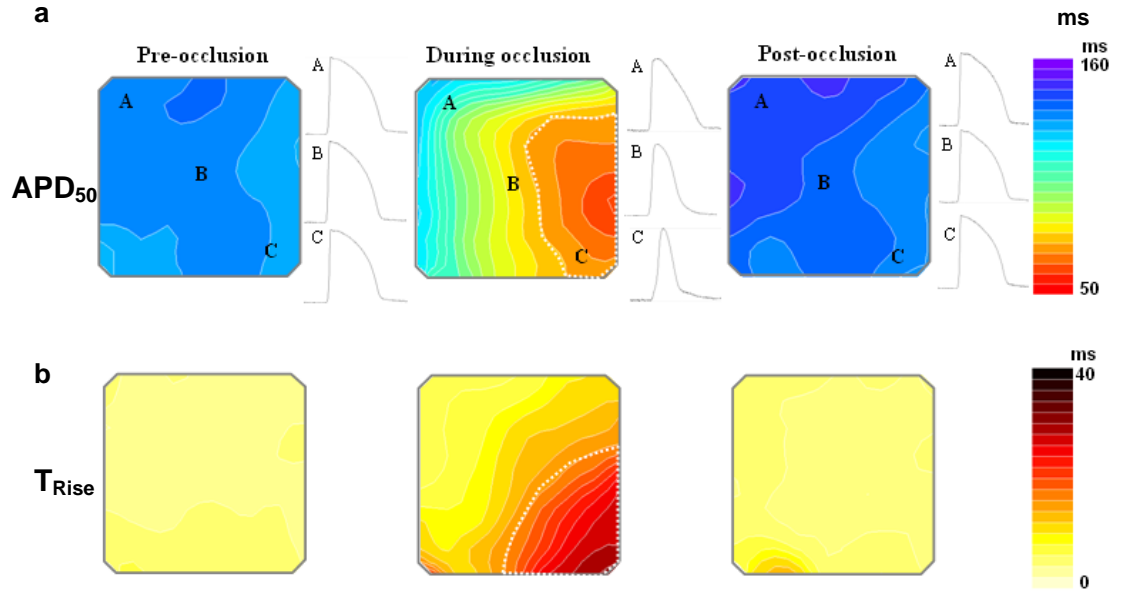
Data represents mean \pm SEM, number in the column indicates the total number of hearts in each group. (** $P < 0.001$)

7.3.2.3 Gradients of APD_{50} and T_{Rise} in acute myocardial ischaemia

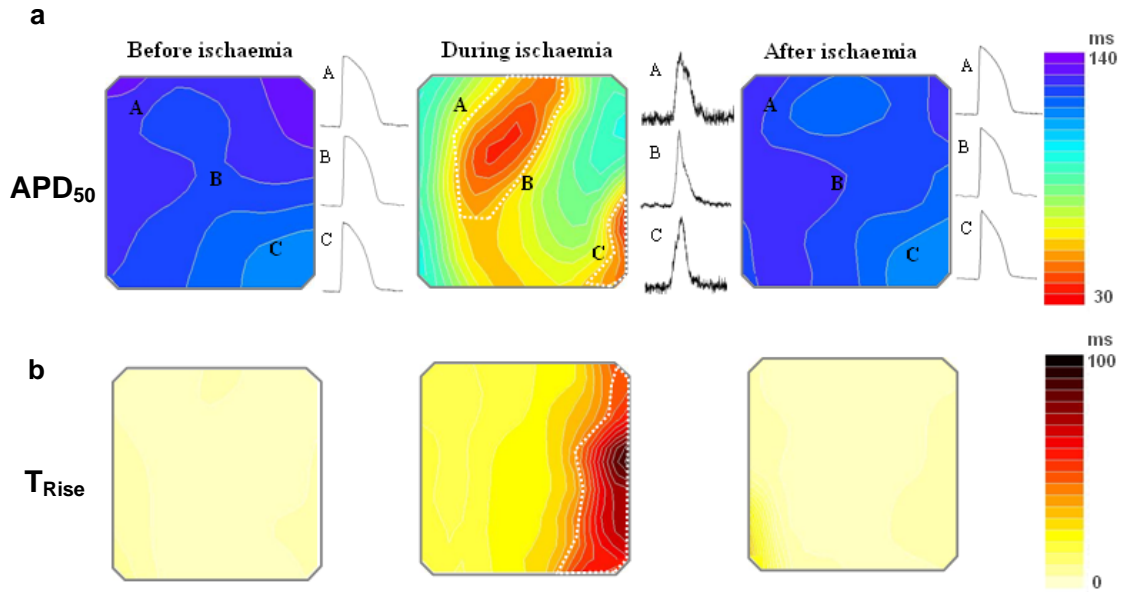
Acute regional myocardial ischaemia produced spatial gradients of APD_{50} across the imaged field, from nearly normal (pre-ischaemic) values (120 ± 1.1 ms) to considerably shorter values (37.6 ± 1.0 ms) in the corner of the field. The region where APD_{50} was reduced to 50% of the pre-ischaemic values is indicated by white-dotted lines as shown in Figure 7.8 (i) a and (ii) a. The equivalent plot for T_{Rise} is shown in Figure 7.8 (i) b. There was an approximate (but, interestingly, not exact) correspondence between the regions experiencing short APD and those showing increased rise time as illustrate in Figure 7.8 (iii).

In contrast, the pattern observed during acute global no-flow ischaemia (0ml/min) was much more variable and heterogeneous with regions of shorter and lower amplitude APs occurring anywhere in the imaged area (see Figure 7.8 (ii)). Furthermore the unlike the situation observed during regional myocardial ischaemia, the region of most profound decrease in APD did not correspond well to the same region showing increased T_{Rise} as shown in Figure 7.8(ii) and illustrated in Figure 7.8 (iii).

(i) Local ischaemia



(ii) Global-no flow ischaemia (0ml/min)



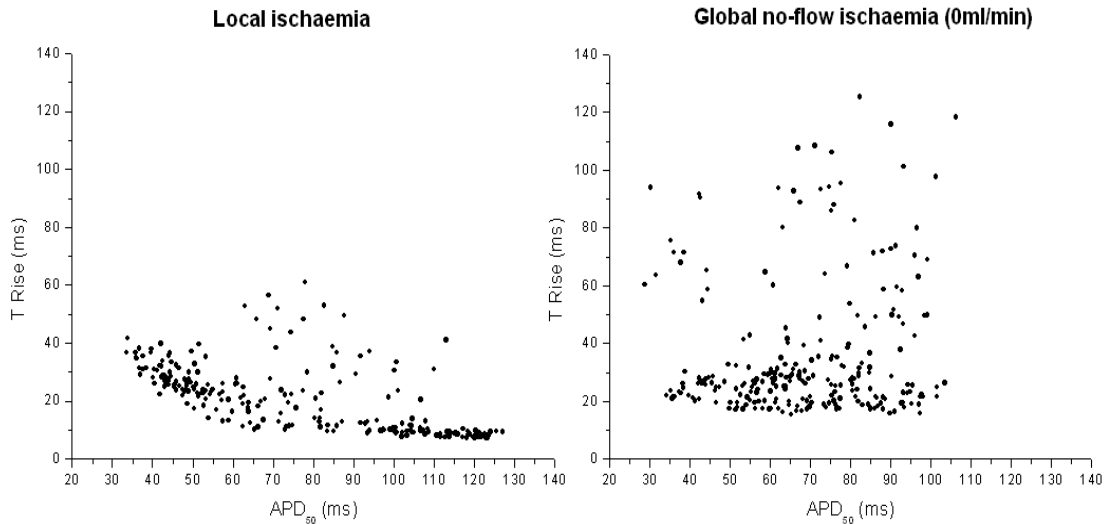
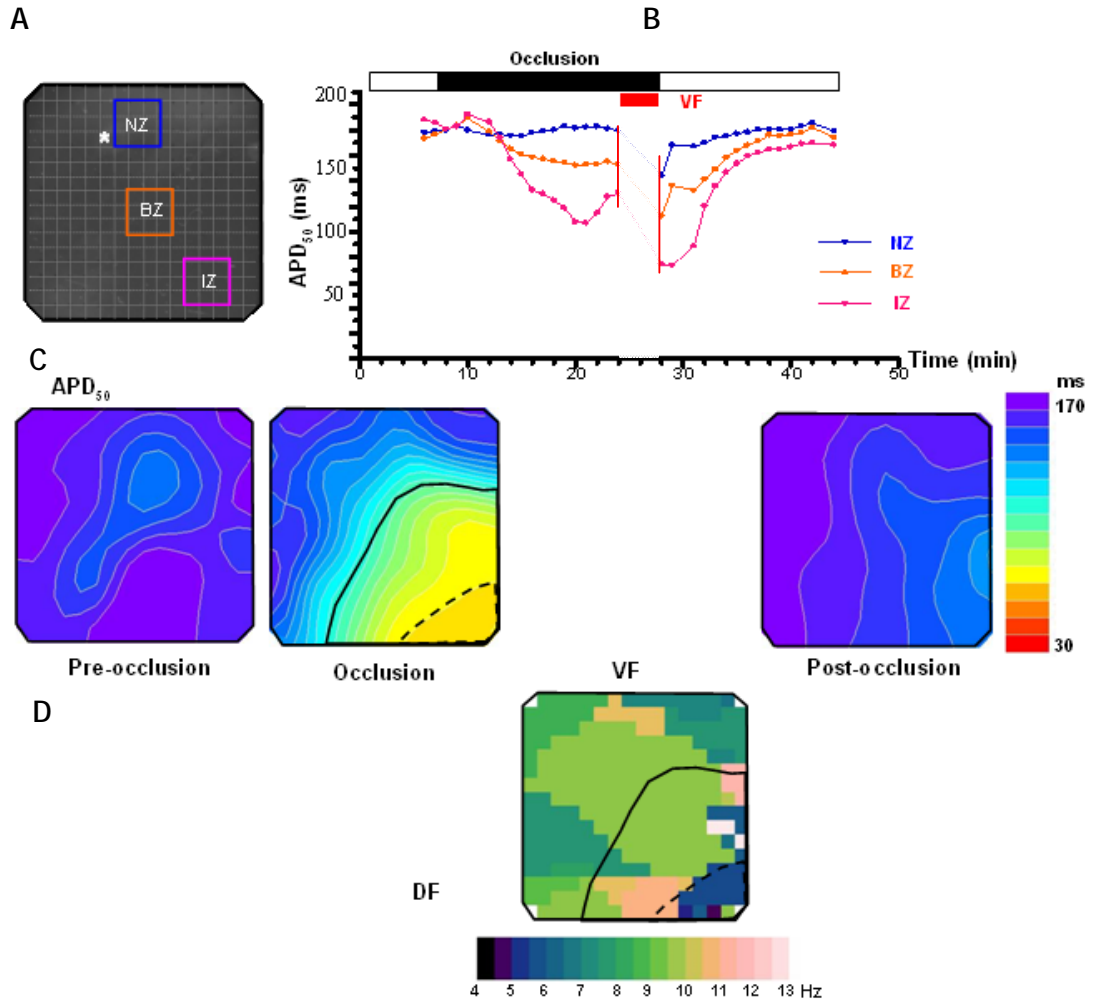
(iii) Correlation of APD₅₀ and T_{Rise}

Figure 7.8 Rise time vs. APD₅₀ during acute regional and global no-flow ischaemia

Scatter plots of APD₅₀ vs. T_{Rise} in different stages: before, during and after acute myocardial ischaemia. (i) acute regional ischaemia . (ii) acute global no-flow ischaemia. Optical action potentials show from three selected sites, A: Normal zone, B: Border zone and C: Ischaemic zone. (iii) Correlation between APD₅₀ and T_{Rise} in local and global no-flow ischaemia.

7.3.2.4 Frequency analysis of VF in acute regional ischaemia

Acute regional ischaemia dramatically affected the dispersion of DF of the VF signal. Most of the mapped area exhibited DF values of 7-11 Hz. In this case, DF values were significantly lower in the IZ.



05/10/07

Figure 7.9 Non-uniform changes in electrophysiology during acute regional ischaemia

A: shows 16x16 pixels from the entire array.

B: Time course of changes in APD_{50} during 45 minutes of acute regional ischaemia and reperfusion corresponds with the record from 3 selected regions; NZ, BZ and IZ in A. C: Contour maps of APD_{50} that recorded during ischaemia and reperfusion and when the VF was appeared, black dashed and solid line indicate the ischaemia and border zones, respectively. D: Corresponding colour code map of DF.

In all cases of VF during acute regional ischaemia (N=5), there appeared to be a sharp changes in DF at the border and ischaemic regions, although the mean value of DF in the IZ was not significantly less than in the NZ. The statistical analysis of mean DF, MF and DFD in NZ, BZ and IZ during regional ischaemic VF are shown in Figure 7.10 A, B and C.

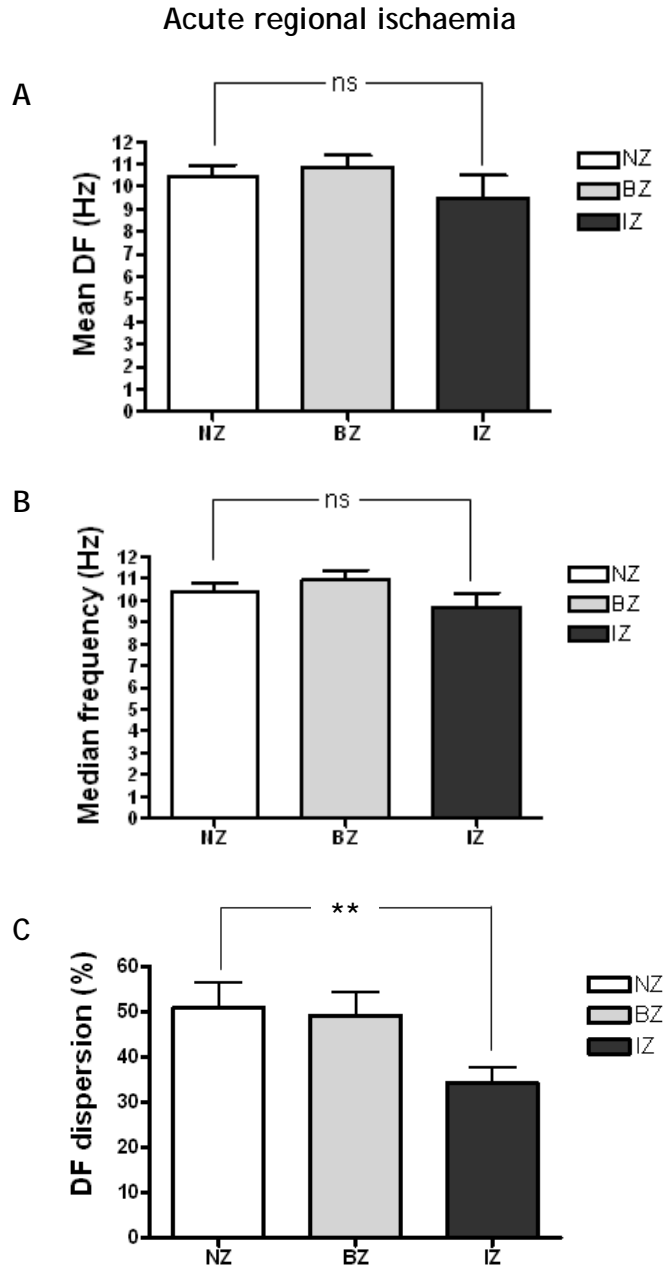


Figure 7.10 Mean values of VF parameters after regional ischaemia

(** P<0.01)

7.3.2.5 Frequency analysis of VF in acute global no-flow ischaemia

Data from Figure 7.11 was obtained from the same heart as Figure 7.9. Acute global no-flow ischaemia (0 ml/min) dramatically affected the distribution of dominant frequency. In this experiment, the map of DF in Figure 7.11 D showed no correspondence with the ischaemic zone; the area where APD_{50} was most reduced was not the same area where the lowest frequencies (either dominant or median) of VF were seen.

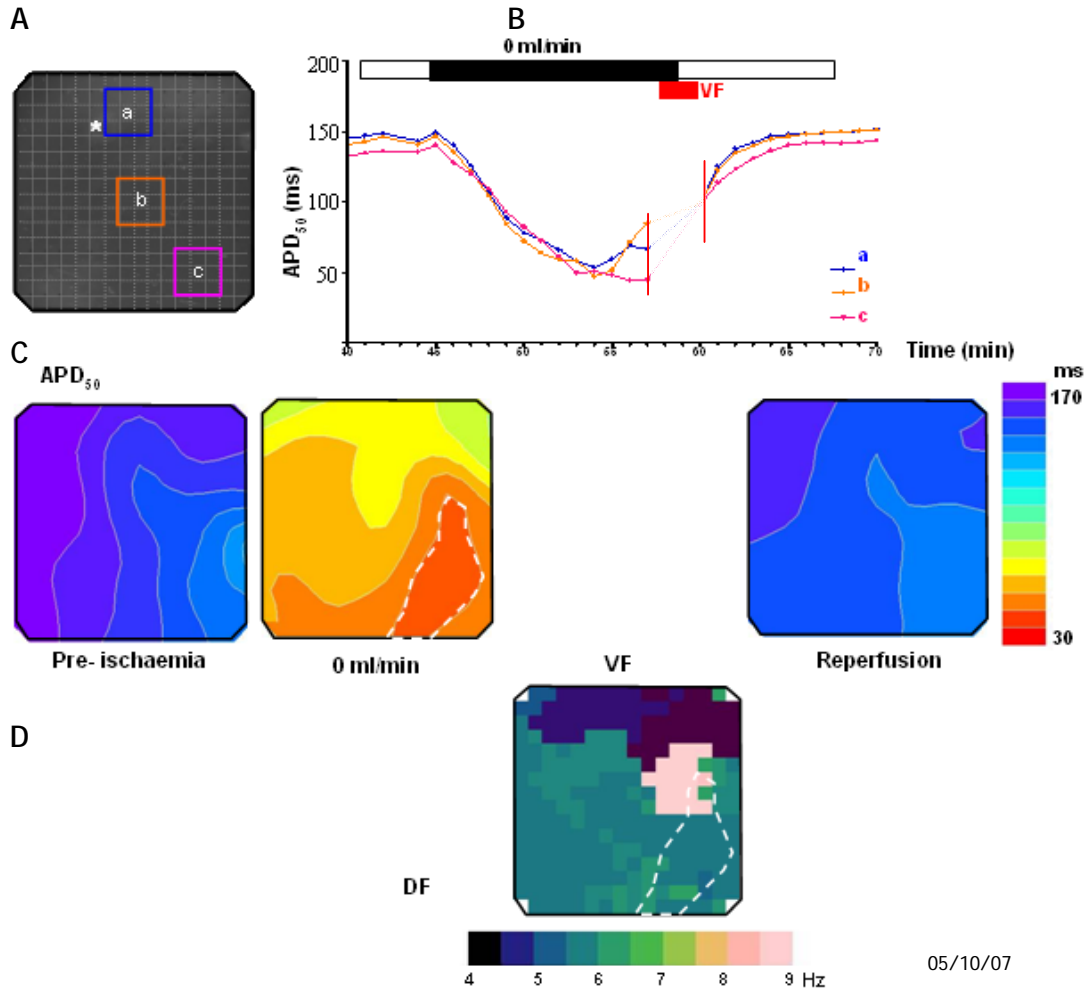


Figure 7.11 Non-uniform changes during acute global no-flow ischaemia

B: Time course of changes in APD_{50} during 30 minutes of acute global no flow ischaemia and reperfusion corresponds with the record from 3 selected regions; a,b and c in panel A. C: Contour maps of APD_{50} that recorded during no-flow ischaemia and reperfusion and when the VF occurred. White dot line indicates the area where the shortest in APD_{50} was found. D: Corresponding colour code map of DF.

In all cases of VF during acute global ischaemia (N=5), there were a large range of DF values across the image. There were no statistically significant differences among the 3 areas (Fig 7.12)

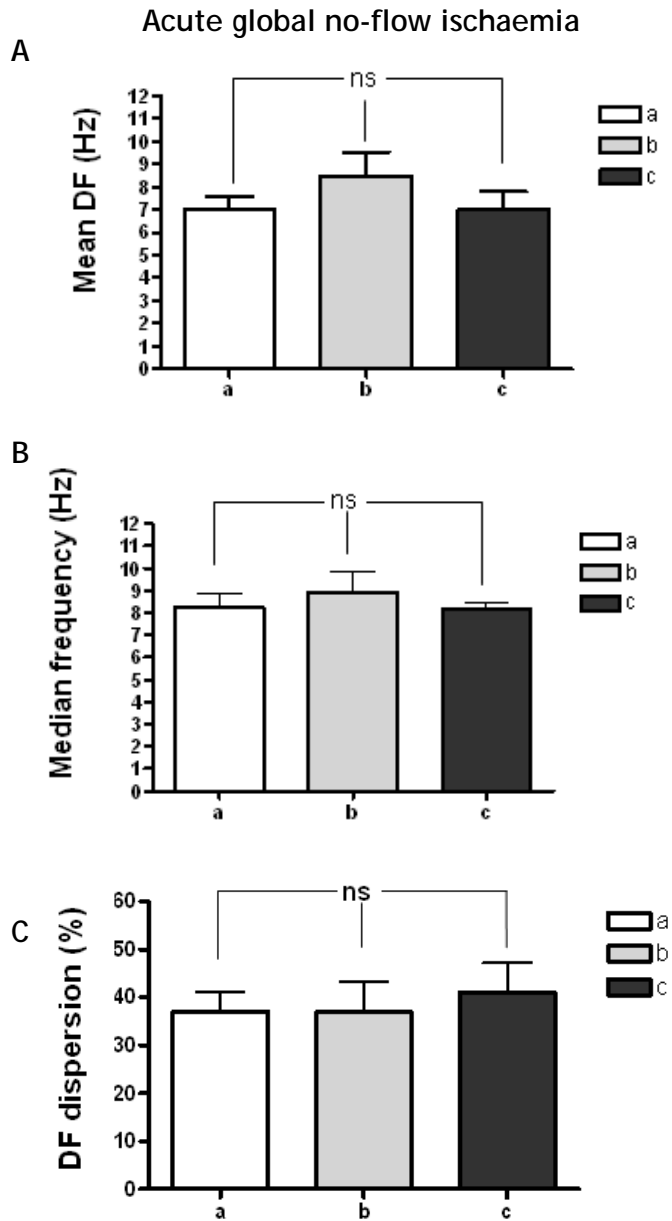
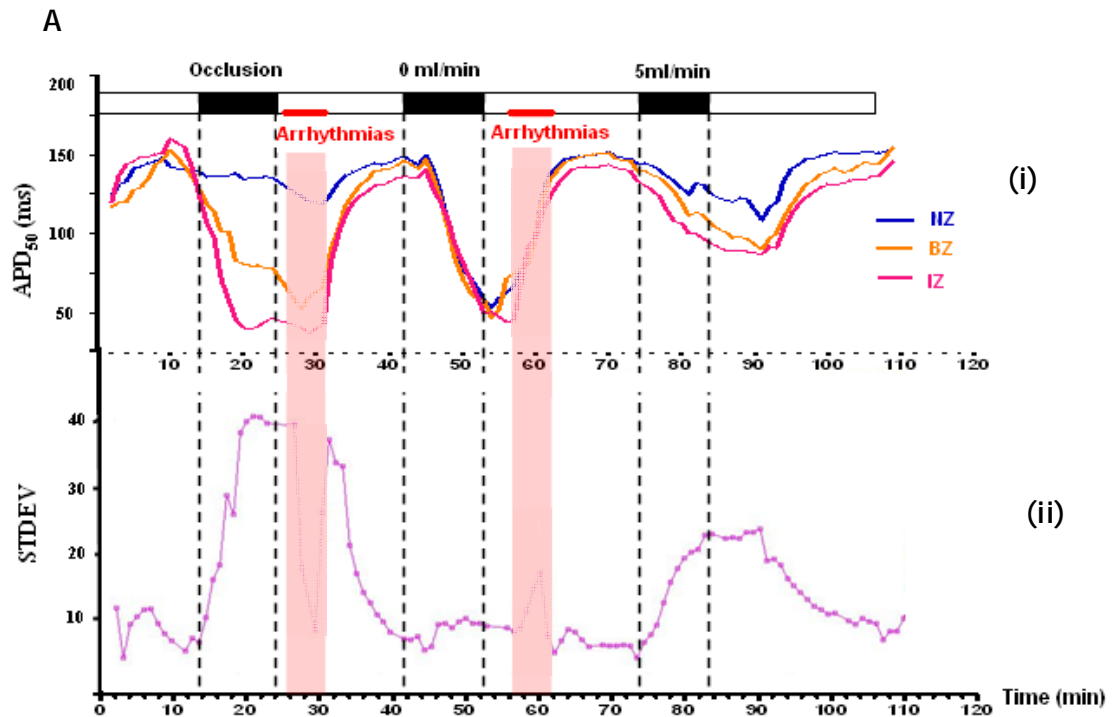


Figure 7.12 Mean values of VF parameters after global no-flow ischaemia

7.3.3 Non uniform changes in APD_{50} and T_{Rise} during acute myocardial ischaemia

7.3.3.1 Spatial variability of electrophysiology in acute regional and global ischaemia

Figure 7.13 shows that, during regional ischaemia, there was a marked decrease in APD_{50} and an increase in T_{Rise} in the BZ and IZ but no change in the NZ. In contrast, global ischaemia caused a decrease in APD_{50} and increase in T_{Rise} in all 3 zones that was more rapid in the case of no-flow (0 ml/min) compared to low-flow (5 ml/min) ischaemia. To quantify the spatial variation in each parameter over the field, the standard deviation of values at all sites was calculated and plotted below the means of the three sites. By the end of the test period, APD_{50} had reached a steady state value, but T_{Rise} continued to increase during global low-flow ischaemia on mean value.



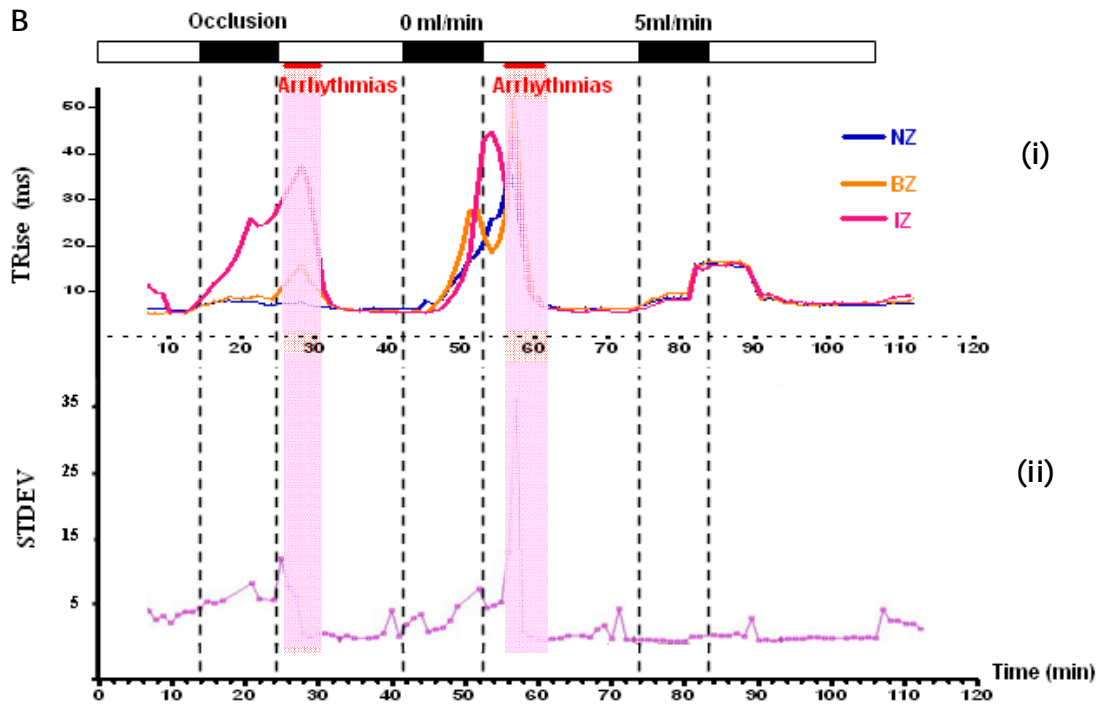


Figure 7.13 Time course of changes in parameter variability during acute regional ischaemia, global no-flow and low flow ischaemia

(i) represents the changes from 3 selected zones, Normal zone (NZ), Border zone (BZ) and ischaemic zone (IZ) and (ii) shows the standard deviation. Time course of parameters APD_{50} (A) and T_{Rise} (B) and plotted with their variability, (STDEV=standard deviation of all biads).

7.3.3.2 Temporal variability of electrophysiology in acute regional and global ischaemia

Figure 7.14 shows typical examples of the temporal evolution of APD_{50} (i) and T_{Rise} (ii) distribution during acute regional and global ischaemia. Colour maps of normalized parameters measured every minute between 5 and 12 minutes after coronary artery occlusion were plotted. Acute regional ischaemia demonstrated a much more stable pattern of variation, clearly determined by the gradient, when compared with both global no-flow and low-flow ischaemia conditions.

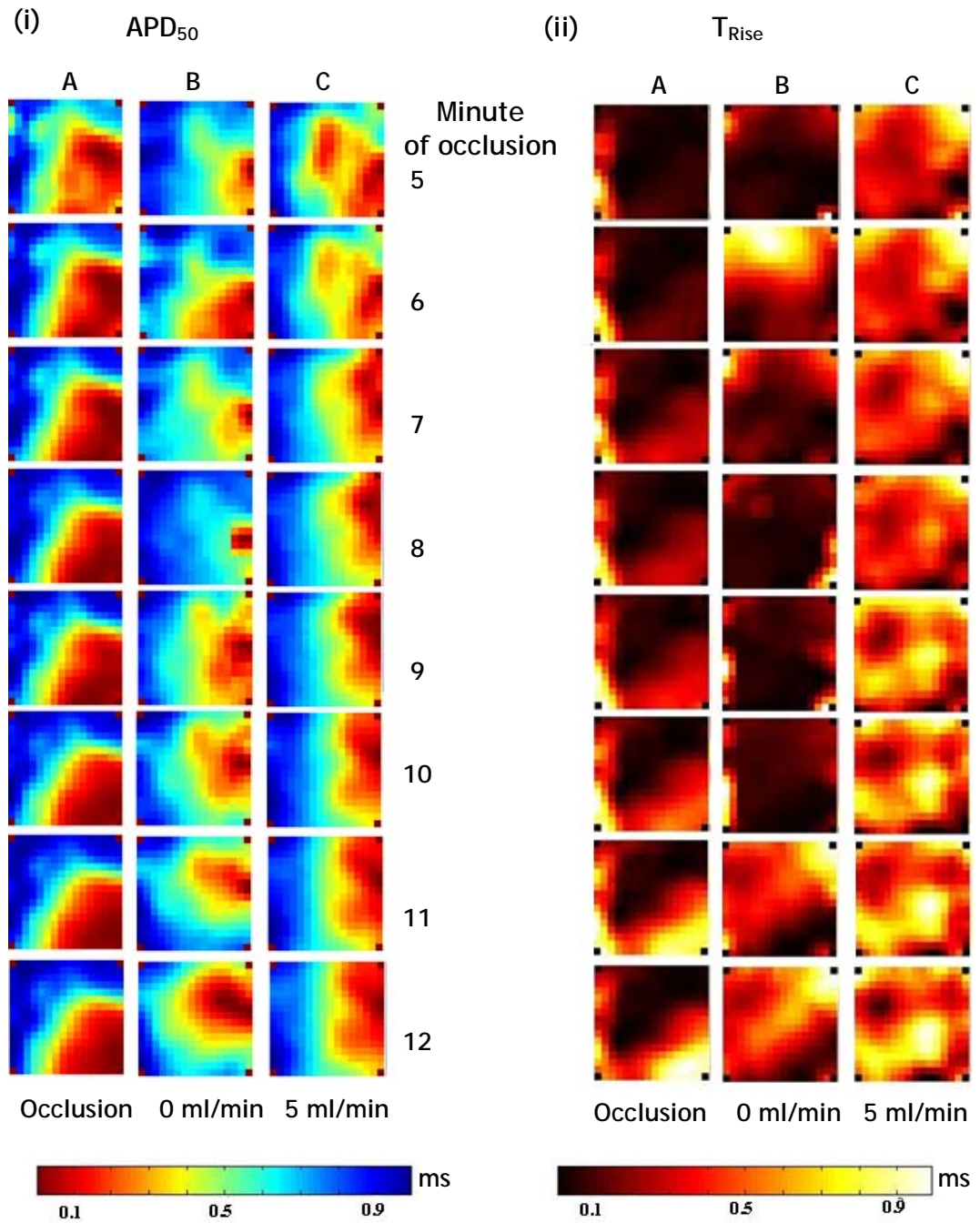


Figure 7.14 Colour maps of variability of APD₅₀ (i) and T_{Rise} distribution (ii)

A indicates constancy of regional ischaemia gradient (occlusion). B shows lability of global ischaemia gradient (0 ml/min) and C shows intermediate variability of low-flow ischaemia (5 ml/min).

Figure 7.15 illustrates the constancy vs. lability of APD_{50} and T_{Rise} of local vs global ischaemia respectively, shown by graphing changes in mean value of each parameter in 9 (4x4 pixel) sub-regions. As expected, acute local ischaemia again showed a greater stability of APD_{50} and T_{Rise} gradients compared to global low-flow and global no-flow ischaemia.

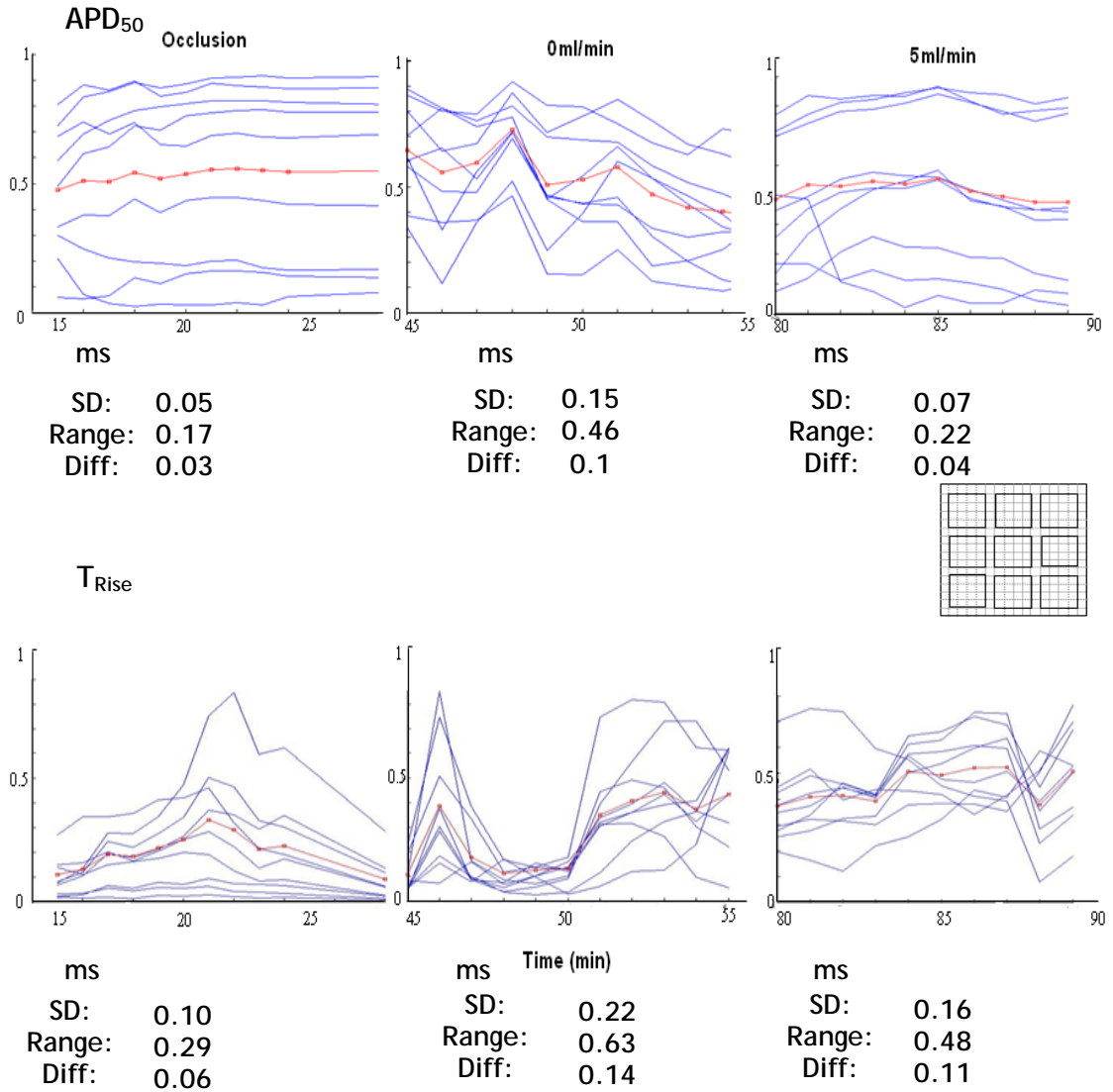


Figure 7.15 Normalized variability of APD_{50} and T_{Rise} gradient during acute regional and global ischaemia

Mean values of standard deviation (SD), range of values (Range) and mean absolute difference (Diff) for both parameters, recorded during regional, global no-flow and global low-flow ischaemia, are shown below each graph.

Global no-flow ischaemia (0ml/min) dramatically affected all three measures of variability for both parameters (Figure 7.16). These data suggest a fundamental difference in behaviour between no- (or low-) flow ischaemia and regional.

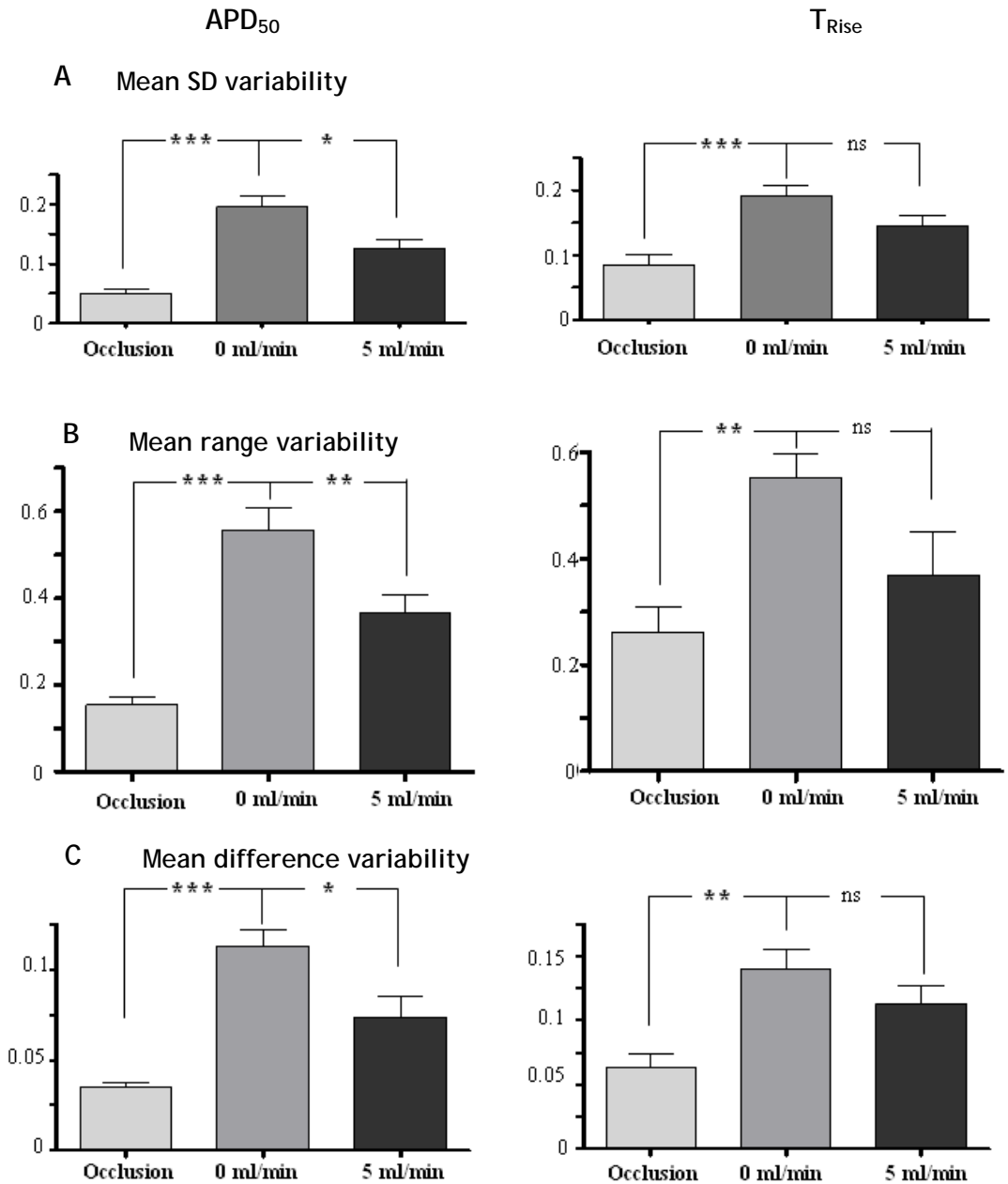


Figure 7.16 SD variability, range variability and difference variability of APD₅₀ and T_{Rise}

A: means of SD variability; B: means of range variability; C: mean of difference. Data obtained during acute regional, global no-flow (0ml/min) and global low-flow (5 ml/min) ischaemia from 6 experiments. Asterisks (*) denote a statistically significant different between groups (* P<0.05; ** P<0.01; *** P<0.001).

7.3.4 VF following local ischaemia in infarcted hearts

Figure 7.17 shows data from the same heart as Figure 6.16 in which local ischaemia was imposed on a local infarct producing an IZ overlapping the existing infarct scar region (indicated with the yellow dotted line). The ischaemic and BZ were established on the basis of APD_{50} (Panel B) and correlated with the local perfusion map (Panel A). Colour code map of DF during ischaemic VF in Panel C shows relatively homogeneous distribution of DF in the normal zone, with values 9-10 Hz. Higher frequencies were seen in the IZ and BZ, with a locus of very high frequencies bordering the infarct proper.

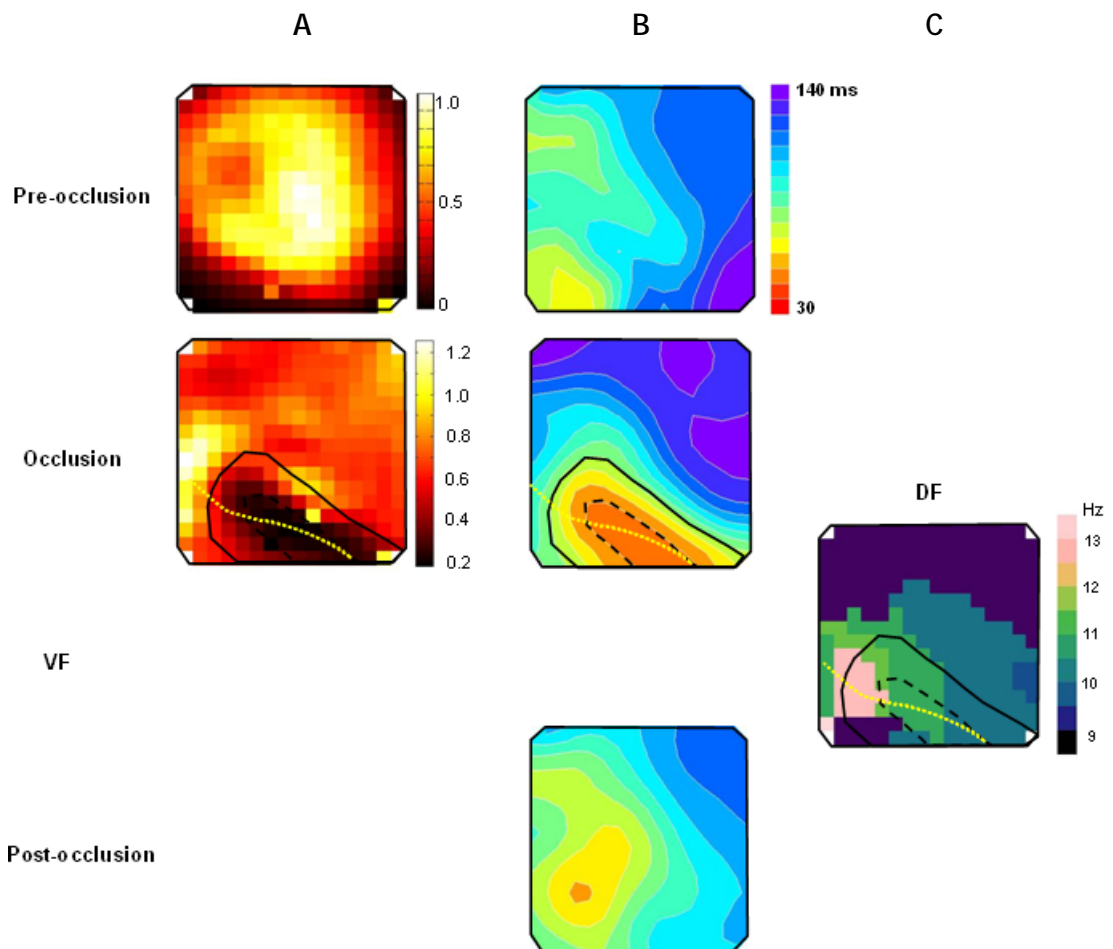


Figure 7.17 Electrophysiological changes in ischaemic region of chronic infarcted heart

A: Relative flow with infarct border (see Figure 6.16A) indicated with yellow dotted line. B: APD_{50} , C: Dominant frequency map of VF.

However, in the analysis of 5 hearts where VF followed local ischaemia, there was no statistical difference in any of the VF parameters between regions. Mean data is shown in Figure 7.18 alongside the data for normal hearts (Figure 7.10) for comparison as this is corresponding normal heart follow local ischaemia. VF parameters in infarcted hearts were not significantly different from those in normal hearts (ANOVA).

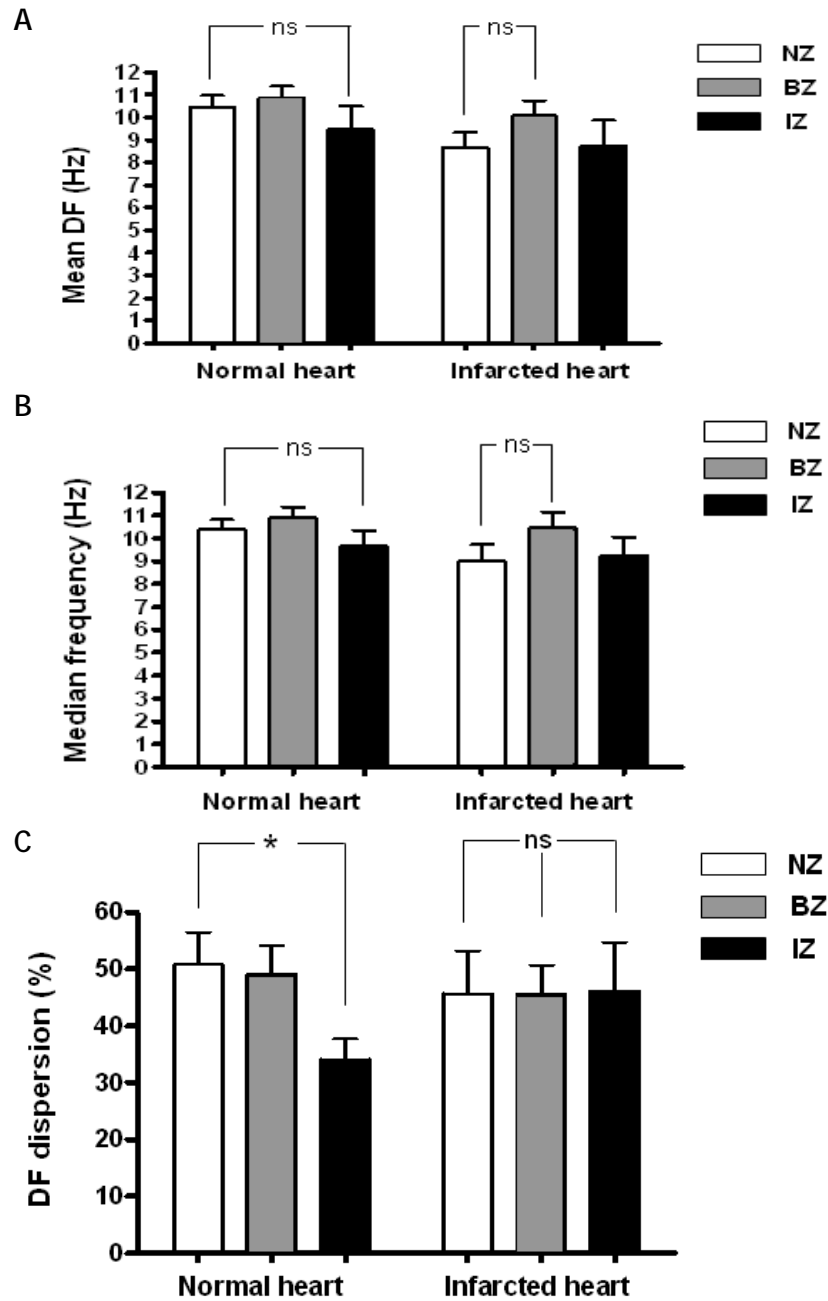


Figure 7.18 Comparison of VF frequency parameters in normal vs infarcted hearts

Data represents mean \pm SEM. Asterisks (*) indicates a statistically significant different between groups when * refer to $P < 0.01$ and ns indicates no statistically significant difference.

7.4 Discussion and conclusion

The main findings of this chapter are:

- (i) Onset time of arrhythmias was remarkably consistent, occurring 13-14 minutes after coronary artery occlusion regardless of the presence of an infarct.
- (ii) The likelihood of arrhythmia occurring was related to the extent of T_{Rise} elevation, as quantified by $T_{\text{Rise P95\%}}$.
- (iii) The greatest temporal variability in APD_{50} and T_{Rise} was seen in global no-flow ischaemia compared with local and low-flow ischaemic challenges.
- (iv) Local VF frequencies (dominant and median) were unaffected by the presence of local ischaemia and/or a chronic infarct scar. Only the dispersion of VF frequencies was reduced in the ischaemic region.

7.4.1 Onset of VF

Life-threatening arrhythmias, especially VF, are considered as a primary cause of sudden cardiac death. In humans, VF occurs within minutes or hours after the beginning of chest pain. However, it is not uncommon for the ischaemic event to be silent (i.e. not accompanied by symptoms) therefore data concerning the timing of events prior to the onset of VF is difficult to determine unambiguously in human.

In animal models, it has been clearly demonstrated that ventricular arrhythmias can occur in two distinct phases. An early phase (phase 1) is evident where VF appears within the first 30 minutes of ischaemia. This early phase VF is correlated with a period of reversible injury, when reperfusion can restore almost complete tissue function. A later phase of VF has been observed at 90 minutes or more after the beginning of ischaemia, this corresponds to a phase of

irreversible injury and the beginning of the processes involved in creating an infarct scar (Clements-Jewery *et al.*, 2005).

This data from our model support the results from one previous study on anaesthetized rabbit (Bril *et al.*, 1991) reporting that arrhythmias occurred within 12-15 minutes after coronary occlusion, their onset being restricted to a relatively narrow time window. In our model, as in that of Bril *et al.*, the majority of normal hearts did not in fact succumb to arrhythmia (and only a small majority of infarcted hearts did so). Comparison with other findings in the literature is complicated by the diversity of responses reported, not only between species, but amongst different rabbit models. Curtis (Curtis, 1998), who reviewed a wide range of models, concluded that it was not possible to make out any consistent pattern. In one study using Langendorff-perfused hearts (Rees & Curtis, 1993), VF did not occur at all during acute regional ischaemia even after $[Ca^{2+}]$ of the perfusing solution was raised to 2.8 mM to increase arrhythmia susceptibility (Rees & Curtis, 1992) (compared with 1.9 mM in our experiments). Several sources of variation were suggested to account for the markedly different results obtained in different studies, including perfusate $[K^+]$, the size of the IZ, and heart rate. A lower sinus rate is associated with lower incidence of ischaemia-induced VF. Sinus rate is generally higher in blood-perfused hearts *in vivo* than in Langendorff preparations, and the situation in global ischaemia is complicated by the fact that sinus rate is further decreased due to SA and AV node ischaemia.

A limited incidence of VF during Phase 1 implies that many hearts would survive into a later phase if ischaemia was maintained. The experiments described so far have involved limited periods of ischaemia. An attempt to address the issue of arrhythmogenesis in more long-term ischaemia is the subject of the next chapter.

7.4.2 Temporal variability of electrophysiological parameters

The analysis of temporal variability shown in Figures 7.14 & 7.15 indicates that global ischaemia (no-flow and low-flow) showed significantly higher temporal variability than that seen during local ischaemia. Assuming the local AP characteristics reflect the local state of the tissue, this suggests that the

metabolic state must fluctuate with time under global ischaemic conditions, but remain relatively static when the ischaemia is produced by regional reduction in perfusion. The reason for this difference is not clear. Previous work has shown that ischaemic challenges can result in oscillations in mitochondrial function and consequent APD changes in isolated single cells (O'Rourke *et al.*, 1999). If this behaviour occurred in large groups of cells in the myocardium this behaviour might result in the type of changes seen here.

An alternative explanation is the alteration in the local perfusion of the myocardium due to local dilatation and constriction of pre-capillary vessels. Temporal variation in metabolic state and coronary flow has been observed in studies of NADH fluorescence (Steenbergen *et al.*, 1977) and capillary flow (Brasch *et al.*, 1999) in ischaemic rat hearts. Why these oscillatory mechanisms operate under conditions of global ischaemic rather than local ischaemia is still unknown. These questions will be explored further in Chapter 10 (Appendix).

7.4.3 Frequency analysis of VF

Conflicting views exist on the role of the ischaemic zone once VF is initiated. On one hand, Janse *et al.* have argued, from results of experiments on isolated pig and dog hearts, that the IZ plays a crucial role in the maintenance of VF by causing wave fragmentation (Janse *et al.*, 1980). On the other hand, it has been argued by (Rankovic *et al.*, 1999) on the basis that activation rate and wave organization in the peri-ischaemic region (following VF induction in dog hearts) was not affected by ischaemia; in other words, the IZ has a passive "bystander" role. It was hoped that my experiments would throw light on the matter. A second rationale for looking at VF is that certain characteristics of VF activity are known to depend on local electrophysiological properties of the myocardium. In particular, VF cycle length, the time-domain equivalent to dominant frequency, has been shown to correlate with refractoriness (de Groot *et al.*, 2001) and metabolic state of the heart (Caldwell *et al.*, 2007). Therefore, optical recordings were made during VF whenever it occurred and were analysed as described above.

A limitation of these experiments is that there were no VF recordings taken in non-ischaemic conditions for comparison, because VF was invariably rapidly

converted back to sinus rhythm in order to continue the protocol. Nevertheless, it is still possible to characterize variation of dominant frequency in relation to the previously demarcated IZ.

The main finding was that, although dominant frequency of VF showed distinct 'domains' (defined as areas of equal DF), their boundaries were not consistently correlated with the IZ. Furthermore, dominant frequencies both higher and lower than those in the NZ were detected inside or close to the IZ. Infarcted hearts showed a similarly varied pattern. This is in marked contrast to a previous study on isolated, blood-Tyrode's perfused pig hearts (Zaitsev *et al.*, 2003). They showed a stable and uniform domain of reduced dominant frequency coincident with their ischaemic zone (determined at the end of the experiment with dye injection and tetrazolium staining) leading to a bimodal distribution of DF. The varied nature of the response seen in this study was borne out in the summary statistics which showed small but non-significant reductions in dominant (and median) frequencies in the IZ compared to NZ. However, a significant increase in DFD was seen in the IZ of normal hearts. In relation to this observation, it is interesting to note that in Figure 2C&D of Zaitsev *et al.* the power spectrum of signals from the IZ is much narrower than the others (NZ, and NZ/IZ pre-ischaemia) implying a similar increase in dispersion.

8 Optical mapping of prolonged ischaemia

8.1 Introduction

As discussed in earlier chapters, in many animal models of acute regional ischaemia, there are two distinct periods where the incidence of VF is very high (Curtis, 1998). Phase 1 occurs after ~15min while phase 2 occurs after ~45mins post- occlusion. Previous chapters of this thesis have featured the arrhythmias that arise in phase 1, but it is uncertain whether rabbit hearts display a distinct second phase since the local ischaemic intervention was only for 15 mins. In this chapter, the local ischaemic was imposed for ~60min in an effort to determine whether under these conditions a second phase of arrhythmias occurs.

The mechanisms underlying this second phase of arrhythmias are uncertain, but one possibility is changes to the electrical properties of the myocardium that result from longer-term exposure to ischaemic conditions. Many studies have suggested that cell-to-cell electrical uncoupling of ventricular myocytes plays an important role in arrhythmogenesis during ischaemia. Reduced myocardial cardiac gap junction conductance has been thought to precipitate ischaemia-induced arrhythmias (Boengler *et al.*, 2005; Cascio *et al.*, 2005; Kleber, 2003). Closure of gap junction channels and increased intercellular resistance during prolonged ischaemia leads to slow and heterogeneous conduction of the electrical impulse (de Groot & Coronel, 2004; Severs *et al.*, 2004; Baba *et al.*, 2005; Kleber *et al.*, 1986; Lindsey *et al.*, 2006).

Intracellular and extracellular acidosis that develops during ischaemia has been known to reduce gap junction conductance. Furthermore, prolonged periods of intracellular acidification causes rearrangement of gap junctions from intercalated disc to lateral walls over a period of 1-3 hours (Gutstein *et al.*, 2001; Wasson *et al.*, 2004). Many studies suggested that the changes in intercellular communication of these gap junction complexes may be a key substrate for arrhythmias during myocardial ischaemia (Duffy *et al.*, 2004; Duffy *et al.*, 2002; Owens *et al.*, 1996; Green & Severs, 1993). Two possible consequences of these longer-term changes are: (i) altered intercellular conductance during long-term ischaemia may be the basis of the second phase of

arrhythmic behaviour. (ii) On reperfusion after long-term ischaemia, the redistribution of gap junctions will be retained and this will affect the electrophysiology of the reperfused myocardium. My aim in this section of the work was to determine whether prolonged local myocardial ischaemia causes electrophysiological changes during and after the ischaemic challenge.

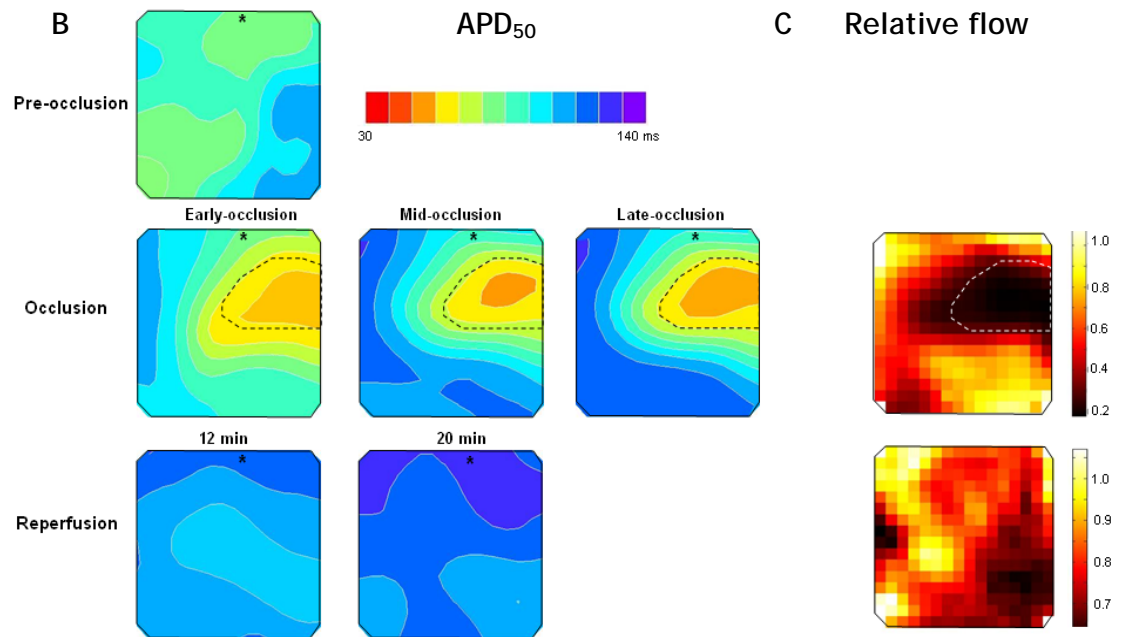
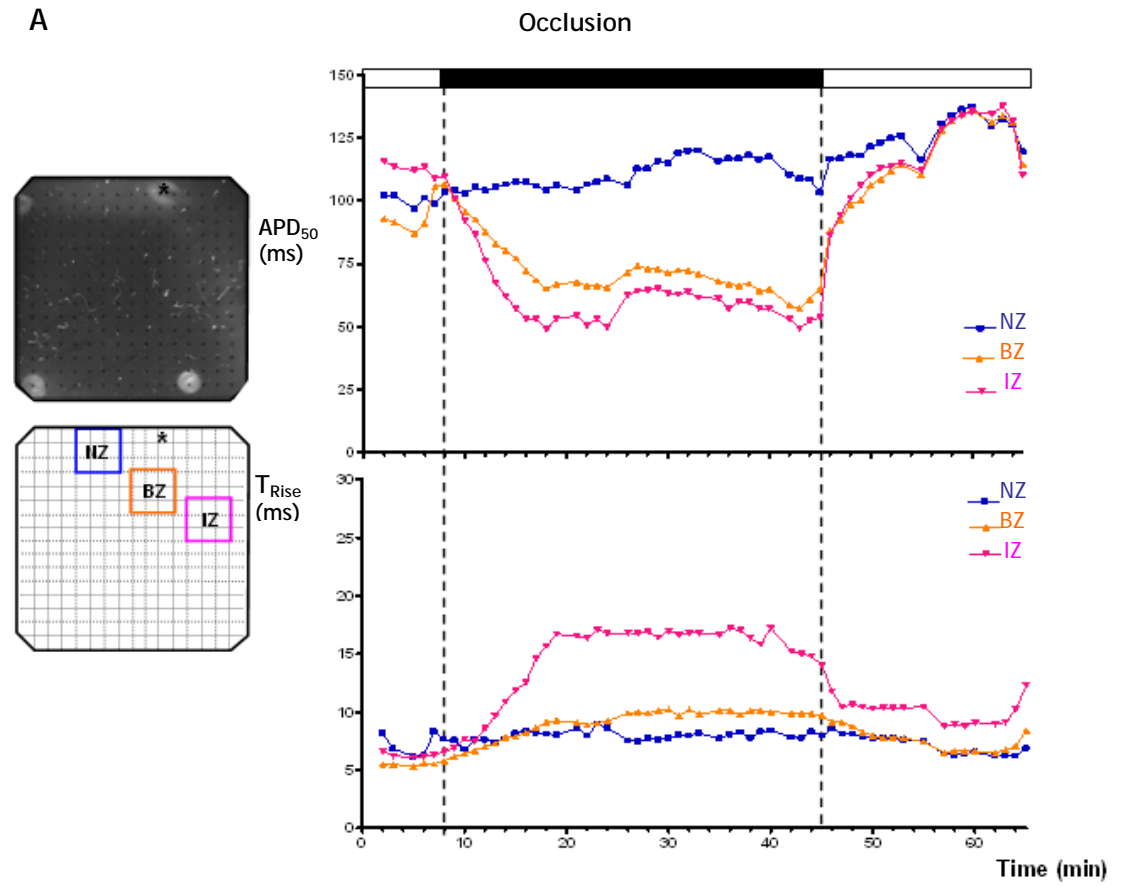
8.2 Methods

Hearts isolated from adult male New Zealand white rabbits weighing between 3 and 3.5 kg were Langendorff perfused as described in Chapter 2. The left posterior division of the coronary artery was isolated and a snare installed as described in Chapter 2. The heart was then loaded with the voltage sensitive dye RH237 and the electrophysiology of the epicardial surface distal to the snare recorded. The snare was tightened so as to occlude the coronary artery for 50-60 minutes followed by reperfusion. The relative flows and changes in electrophysiology during prolonged ischaemia and reperfusion were determined using the OPTIQ analysis programme. Epicardial CV was measured in response to epicardial pacing. The epicardial pacing protocol was applied prior to ischaemia, during the coronary artery occlusion (measured at 20, 30 and 40 minutes) and on reperfusion. Activation and 2D velocity vector maps were created as described in section 6.2.2.

8.3 Results

8.3.1 *Prolonged ischaemia*

Signals from the entire array (Figure 8.1A) were used to examine the time and pattern of epicardial activation during occlusion (40 minutes). Panel B shows the contour map of APD₅₀ during prolonged ischaemia from early-occlusion (12 min), mid-occlusion (30 min) and late-occlusion (~40 min). Prolonged regional myocardial ischaemia demonstrated a gradient of APD₅₀ from nearly normal values to much shorter at the centre. The region where APD₅₀ was shortest is indicated by black-dotted lines corresponding with the region of low relative flow rate (white dotted line in panel C).



D Local velocity vector

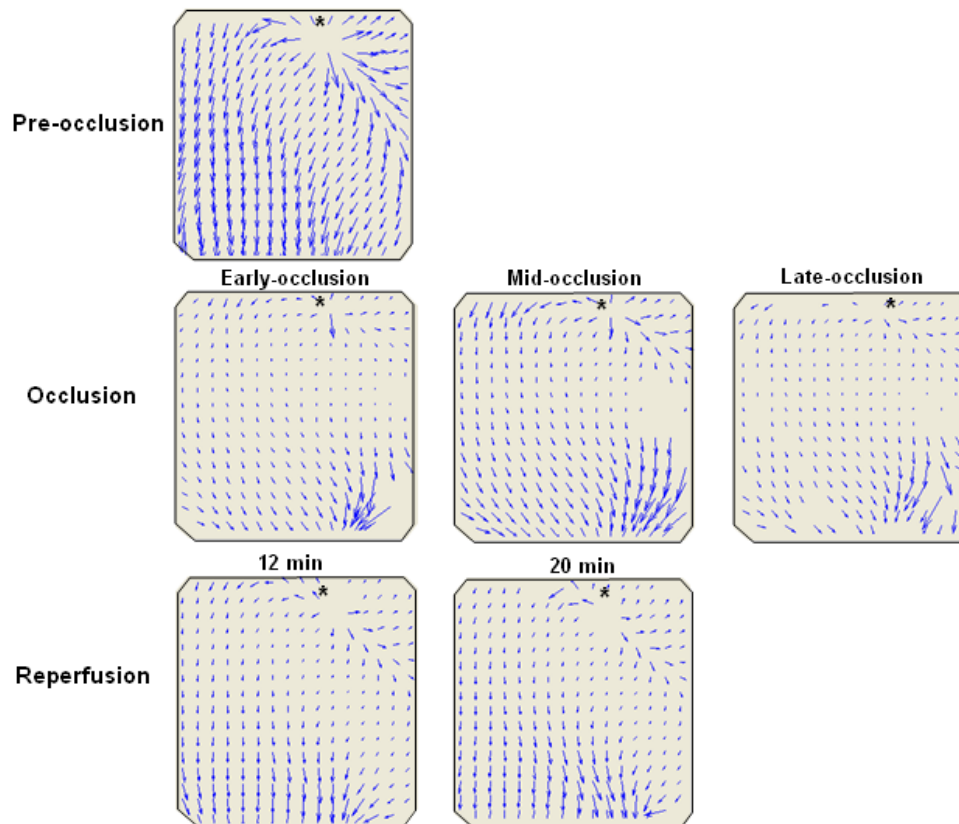


Figure 8.1 Optical mapping of prolonged ischaemia

A: Time course of changes in APD_{50} and T_{Rise} during 1 hour of ischaemia and reperfusion. Signals were derived from 3 selected regions; non-ischaemic zone (NZ), border zone (BZ) and ischaemic zone (IZ). Black-dashed lines indicate the ischaemic zones that corresponds well the relative flow (Panel C). Asterisk (*) represents the pacing site. APD_{50} (panel B) were measured before occlusion, 12, 30 and 40 min after occlusion and after reperfusion for 12 and 20 min. D: local velocity vectors.

Figure 8.2 shows isochronal activation maps of prolonged ischaemia. The epicardial activation was recorded at pre-occlusion, occlusion for 12 minutes (early), 30 minutes (mid) and 40 minutes (late) and reperfusion at 12 minutes and 20 minutes.

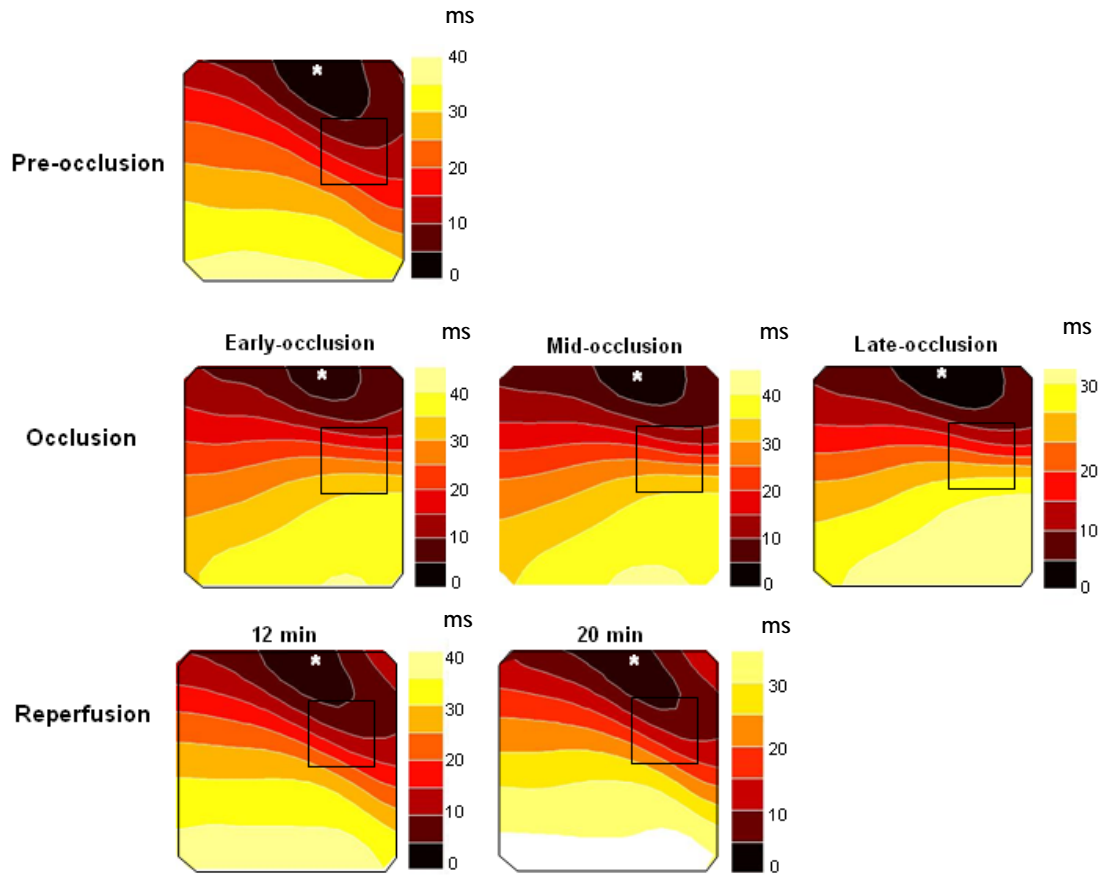


Figure 8.2 Isochronal maps of activation during prolonged ischaemia

Data obtained from the same experiment as Figure 8.1. Activation maps before, during and after prolonged occlusion. CV was measured before occlusion, 12, 30 and 40 min after occlusion and after reperfusion for 12 and 20 min. Asterisk (*) represents the pacing site.

Table 8.1 compares APD_{50} and T_{Rise} during long (~60mins) and short (15 min) local myocardial ischaemia. Data represent the average value of 3 hearts in each group. APD_{50} and T_{Rise} from the entire array (252 sites) and ischaemic region (3x3 sites) of prolonged ischaemia hearts show no statistically significant difference from short ischaemia hearts on early occlusion (12 minutes) and on reperfusion.

	APD ₅₀ (ms)				TRise (ms)			
	252 sites		3x3 sites		252 sites		3x3 sites	
	Prolonged ischaemia	Short ischaemia	Prolonged ischaemia	Short ischaemia	Prolonged ischaemia	Short ischaemia	Prolonged ischaemia	Short ischaemia
Early-occlusion	118.4±7.8	90.1±14.2	61.8±7.9	55.4±9.4	9.6±0.3	12.1±0.9	15.7±1.4	17.5±2.9
Mid-occlusion	129.8±7.9	-	73.1±8.2	-	9.9±0.4	-	16.9±0.8	-
Late occlusion	122.6±6.8	-	72.7±7.9	-	9.5±0.1	-	15.5±1.7	-
15 min Reperfusion	137.8±9.8	130.7±19.6	135.1±7.1	148.9±6.9	7.3±0.5	8.4±0.5	7.8±0.9	6.7±0.3
20 min Reperfusion	143.8±7.4	-	142.0±6.1	-	7.2±0.4	-	7.6±0.9	-

Table 8.1 Comparison of APD₅₀ and TRise between prolonged and short ischaemia

Data represents mean±SEM, ns indicates no statistically significant difference between groups (P>0.05).

	Median (ms)		P05 (ms)	
	Prolonged ischaemia	Short ischaemia	Prolonged ischaemia	Short ischaemia
Pre-occlusion	49.7±1.8	47.4±4.9	28.5±5.1	31.4±4.4
Early-occlusion	46.7±1.2	44.0±5.2	23.6±3.6	28.3±3.8
Mid-occlusion	50.6±1.8	-	23.5±2.4	-
Late-occlusion	46.8±2.4	-	22.6±1.7	-
Reperfusion	46.3±3.7	46.2±4.0	22.5±2.6	28.1±1.9

Table 8.2 Comparison of velocity magnitudes

Median (50th percentile) and lower 5th percentile velocity values for all pixels between prolonged ischaemia and short duration of ischaemia (15 minutes). Data from 3 hearts in each group.

Table 8.2 shows comparison of average value of CV in during long (~60mins) and short (15 min) local ischaemia. No significant differences were observed across all values. Therefore there was no detectable additional effect of prolonged ischaemia on myocardial electrophysiology.

8.4 Discussion

Prolonged myocardial ischaemia establishes gradients of APD and slower AP upstrokes similar to short periods of ischaemia and the effects can be reversed. The increase in OAP rise time reached a maximal value after 18-20mins, while APD values reached minimum values after 13-15mins. This is consistent with the time course observed during short ischaemic periods where OAP rise time had seldom reached a steady value by the end of the 15min occlusion period. In none of the 3 hearts did arrhythmias occur after ~15 mins; nor did any occur during

the subsequent 24 mins. There were no further changes in APD or rise time or CV between minute 15 and minute 40 of occlusion. This suggests that there is no significant phase 2 in rabbit hearts, but further work is required to establish this more confidently. Longer periods of ischaemia could be employed. Furthermore, hearts that do develop arrhythmias after 15 mins could be electrically defibrillated and local ischaemia maintained for longer to determine whether arrhythmias are more likely in this group of hearts.

It also has been reported that myocardial tissue dysfunction especially reperfusion arrhythmias can be caused by reperfusion after prolonged ischaemia (Sasaki *et al.*, 2007; Brill *et al.*, 1991; Conci *et al.*, 2006; Gettes *et al.*, 1991). In our study, reperfusion arrhythmias did not appear after 40 minutes of coronary artery occlusion and full reversal of electrophysiology was apparently obtained after the prolonged period of ischaemia. This suggests that there were no significant changes in the distribution of gap junctions over this time period, since both median (50th percentile) CV and the P05 (low 5th percentile) values were not significantly different.

9 Discussion

The main aim of this thesis was to identify the electrophysiological processes that occur during acute regional ischaemia and chronic infarction and link these changes to the occurrence of arrhythmias. These investigations were performed on the isolated perfused rabbit heart using a combination of a novel snare technique and optical mapping. The main findings of this thesis were:

1. Acute coronary artery occlusion for 15 minutes produced dramatic gradients of APD across the epicardial surface that correlate with the gradients of local ischaemia. These effects can be completely reversed when the coronary artery occlusion was released.
2. Re-entrant arrhythmias occurred in a sub-group of experiments, this behaviour was associated primarily with slower AP upstrokes in the presence of a steep APD gradient.
3. T-wave alternans behaviour was associated with the onset of acute regional ischemia but was not maintained during ischaemia. Alternans was not present when regional block precipitated re-entrant activity and subsequent ventricular tachycardia. These data suggest that T-wave alternans can be used as a marker for arrhythmias but unlikely to be a mechanism underlying the generation of arrhythmias in acute regional ischaemia in rabbit heart models.

9.1 Technical aspects in acute regional ischaemia model using optical mapping

Optical mapping composes of three main components. (i) A heart stained with a fluorescent voltage sensitive dye (RH237). (ii) An illumination system and optics and a camera to excite and collect the emitted fluorescence signal light (iii) the system to display and store signals from the photo detection (Efimov *et al.*, 2004; Salama & Choi, 2001).

The use of a vascular snare to cause acute regional myocardial ischaemia and reperfusion in rabbit hearts is based on a similar approach in an open chest model (Conci *et al.*, 2006; Vanoli *et al.*, 2004; Muders & Elsner, 2000; Hongo *et al.*, 1997). Most studies to date have used *ex vivo* models, specifically Langendorff-perfused hearts, to study ischaemia induced arrhythmias because this model: (i) avoids the complication that the cardiac output determines the extent of coronary flow, a situation that would exist *in vivo* and in the working heart preparation (ii) avoids complications associated with *in vivo* studies such as the associated anaesthetic and surgery (Rodriguez *et al.*, 2006).

In this study, acute local ischaemia was produced by a refinement of a snare technique used previously in this laboratory. As described on chapter 4, two motion artefact blockers were compared in this study. I found that BDM (15 mM) and blebbistatin (5 μ M) are effective agents for suppressing the movement artefact in whole rabbit hearts but BDM at this concentration was found to dramatically affect the electrical properties of the heart and its ability to recover from an ischaemic period. In contrast, blebbistatin appeared to have minimal long-term detrimental effects on the isolated rabbit heart.

In this study, we mapped the anterior epicardial surface of the heart. With the present optical setup, electrophysiology of acute ischaemia and reperfusion can be recorded only within the mapping area, which is limited to a $\sim 1.3 \times 1.3$ cm square on the anterior epicardial surface. If the coronary artery system has a trifurcated pattern or the vessels available for snaring are obscured by surface adhesions, obtaining a large area (greater than $\sim 25\%$ of pixels) of reduced perfusion is difficult. This situation could be improved with the development of panoramic mapping necessitating redesign of the heart chamber.

9.2 Electrical activity in the ischaemic area

The work in this thesis has shown that local ischaemia causes arrhythmias in $\sim 50\%$ of hearts within 15 minutes of occlusion. These characteristics were no different in hearts with an existing infarct scar. In the initial few minutes following occlusion, ST segment elevation accompanied local decrease in AP durations and increase in AP rise times. Dividing the data on the basis of

whether an arrhythmia occurred, there was no difference in APD but greater rise times were seen in the ischaemic zone. Another difference between the two sub-groups was the common occurrence of intermittent conduction block between the interfaces of the ischaemic and normal zones in heart which developed arrhythmias. However, the event marking re-entry, i.e. conduction around the line of block and retrograde passage through this line into excitable tissue, was never observed. The episodic nature of recording meant that such 'randomly' timed events could not easily be captured. In three cases, the start of VF, as indicated by the ECG trace, was captured but the route of the initial re-entry circuit could not be discerned on the epicardial surface (where it would appear as a classic figure-of-eight pattern). Therefore it is likely that re-entry occurred inside the wall of the ventricle. Further work is required to establish the pathway of the initiating event.

A prolonged period of ischaemia did not reveal a second period (Phase 2) of arrhythmias as has been observed in other animal models. However, the results suggested that long-term ischaemia may have detrimental effects on the electrophysiology of the heart post-reperfusion. These effects may be related to gap-junction remodelling and it remains to be seen whether this is the case.

Spatio-temporal variability in electrophysiological parameters occurred during local, low flow and no-flow global ischaemia, the latter two interventions displayed higher temporal variability than that observed during local ischaemia. The reason for the variations in electrophysiology with time is not known, but the possibility of temporal variations in regional perfusion was considered.

9.3 Future work

Future work should include:

- Detailed examination of the metabolic control of coronary perfusion and its effects on the electrophysiology of the heart. For instance, is the shape and size of the ischaemic zone influenced by metabolic control of the coronary flow?

- Improved design of the optical imaging system to permit: (i) imaging without the use of mechanical uncouplers; (ii) imaging the complete ventricular surface; (iii) allow simultaneous measurements of electrical activity and tissue perfusion and/or metabolic activity; (iv) incorporation of electrophysiological data into a computational model of the heart to allow rigorous testing of the conditions necessary to cause arrhythmias. (Sung *et al.*, 2000).
- Improved techniques for coronary artery occlusion to: (i) image the coronary artery vasculature *in vitro*; (ii) minimise surrounding tissue damage on arterial occlusion; (iii) occlude more than one coronary artery. Improve techniques to allow coronary artery occlusion of hearts with an existing infarct scar.

9.4 Clinical relevance

My study shows that the rabbit model of acute regional ischaemia and reperfusion reproduces many electrophysiological characteristics associated with myocardial ischaemia in human such as slow conduction, conduction block and re-entrant excitation (Fozzard & Makielski, 1985; Janse & Kleber, 1981; Mandapati *et al.*, 1998; Pinto & Boyden, 1999; Pogwizd & Corr, 1987). These techniques may provide the new insight into the study of other electrical heterogeneities associated with sudden cardiac death.

9.5 Conclusion

This thesis describes the development of a method to produce acute regional ischaemia in isolated perfused rabbit hearts and the application of this approach to the study of electrophysiological changes associated with acute myocardial ischaemia. The results of this study provide insight into the cellular mechanisms for the initiation and maintenance of arrhythmias that follow coronary artery occlusion and therefore aid the design of future therapies to prevent sudden arrhythmic death.

10 Appendix

Preliminary data on electrophysiological effects of coronary vasodilation in acute ischaemic myocardium

10.1 Introduction

The temporal variability of AP electrophysiology observed in low flow and global ischaemia noted in Chapter 7 could be based in variations in the local control of flow through the coronary circulation. As with most capillary beds, local metabolites control flow by acting on the pre-capillary arteriole to cause vasodilatation. A build up of metabolites such as H^+ and adenosine cause vasodilatation. Once increased perfusion has removed the metabolites, a constant vasoconstrictor tone ensures that reduced flow is restored. This autoregulatory control over coronary vasomotor tone has been examined in many studies e.g. (Dole, 1987; Chilian & Layne, 1990) and can be described in terms of a balance between vasoconstrictor and vasodilator influences as illustrated in Figure 10.1.

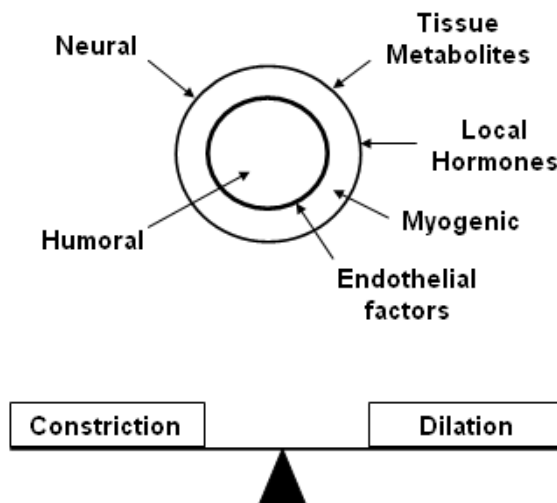


Figure 10.1 The balance of vascular tone

Picture illustrated the vessel tone that is determined by the balance between vasoconstrictor and vasodilator influences. (Klabunde, 2004)

Although the vasodilatory role of local metabolites is well known, the mechanisms underlying the chronic vasoconstrictor tone are less certain. Myogenic tone, i.e. variable vasoconstrictor activity that ensures constant flow through an arteriole in the face of varying pressure is one factor. Chronic endothelin release is another candidate (Kusmic *et al.*, 2006; Gorman & Sparks, 1982). However, the specific role of endogenous agents in maintaining the flow during acute ischaemia remains poorly understood.

Indirect evidence exists to suggest that coronary flow and subsequent local cardiac metabolism is not constant during global ischaemia. Over periods of seconds/minutes, the myocardium can show a considerable variation in local metabolic state (Steenbergen *et al.*, 1977). Close correlation between coronary artery perfusion and metabolic state has been observed in rat heart (Brasch *et al.*, 1999). In this chapter, I use our novel method of flow measurement to examine whether flow and electrophysiological parameters vary during global ischaemia. I also show data from some preliminary experiments designed to investigate whether temporal and spatial aspects of perfusion and electrophysiology can be altered by vasoactive compounds.

10.2 Methods

The Langendorff model of isolated perfused rabbit heart was used in conjunction with optical mapping as described in Chapter 2. Sodium nitroprusside (SNP) at 1 mM was used as a peripheral vasodilator that affects both arteries and veins (Verner, 1974).

The protocol is shown in Figure 10.2.

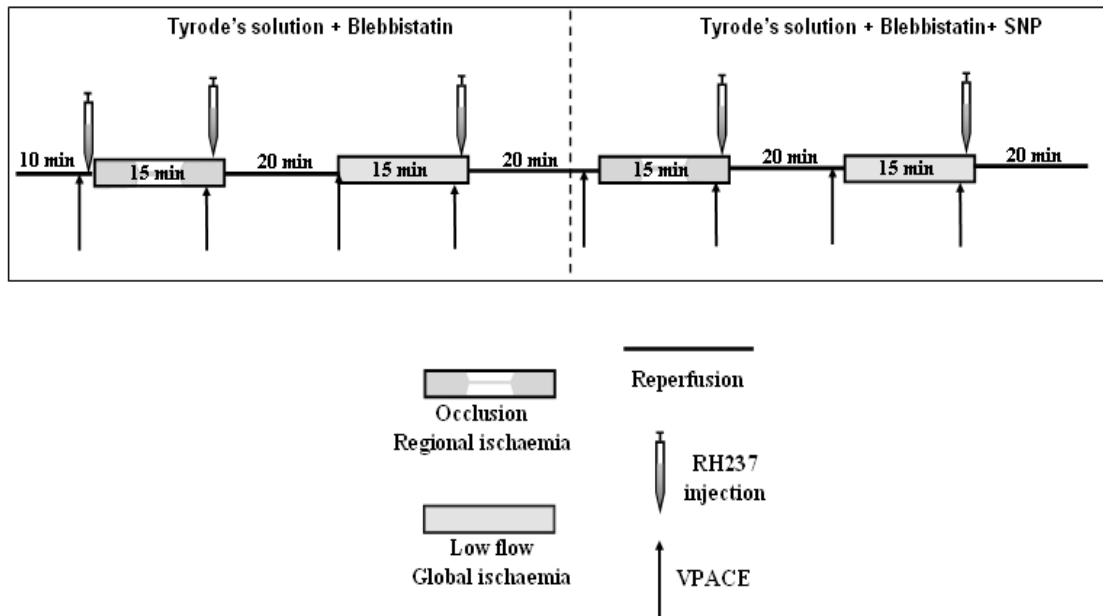
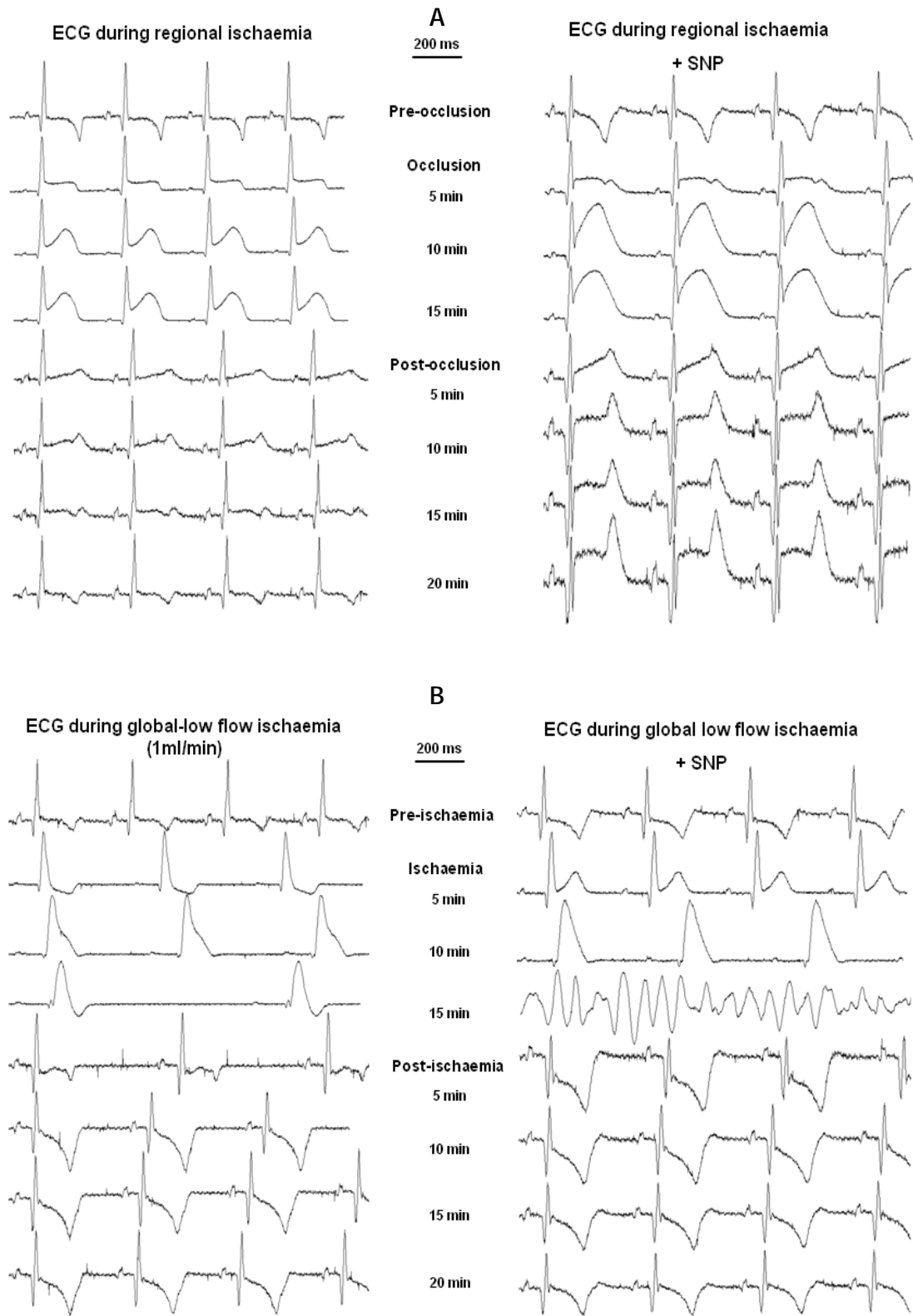


Figure 10.2 Experimental protocol

The hearts were subjected to the baseline recording by 10 minutes perfusion with 5 μ M of Blebbistatin in standard Tyrodes solution, followed by the first run of 15 minutes regional ischaemia with 20 minutes of reperfusion. Flow rate was then reduced to 1ml/min in a second run of 15 minutes low flow-global ischaemia followed by 20 minutes of reperfusion. These runs were repeated with 1 mM of SNP. Electrophysiological properties were recorded every minute of the entire experiment. The ventricular pacing followed by bolus injection of RH237 was performed prior to ischaemia, 12-15 minutes after ischaemia and 15-20 minute after reperfusion.

10.3 Results

Within a few minutes after occlusion of the coronary artery, ECG traces showed the elevation of the ST segment and an associated decrease in APD recorded optically. In this model of acute regional ischaemia, significant changes in ECG and APD were observed around 5 minutes after occlusion. Figure 10.3 shows examples of ECG changes during periods of acute regional ischaemia in the presence and absence of SNP.



18/06/09

Figure 10.3 ECG traces from PDA during acute ischaemia

A: ECG traces during regional ischaemia and B: global low flow ischaemia. Data obtained from the normal heart perfused with standard Tyrodes solution (ST) and ST+SNP during 15 minutes of coronary artery occlusion and 20 minutes of reperfusion.

Acute regional myocardial ischaemia demonstrated a gradient of APD_{50} from nearly normal values to much shorter at the corner. On the other hand, acute global low-flow ischaemia (1ml/min) produced various regions of short and low amplitude of APD. However, when the heart was perfused with solution containing SNP, the shape of the OAPs changed in both regional and low-flow ischaemic myocardium.

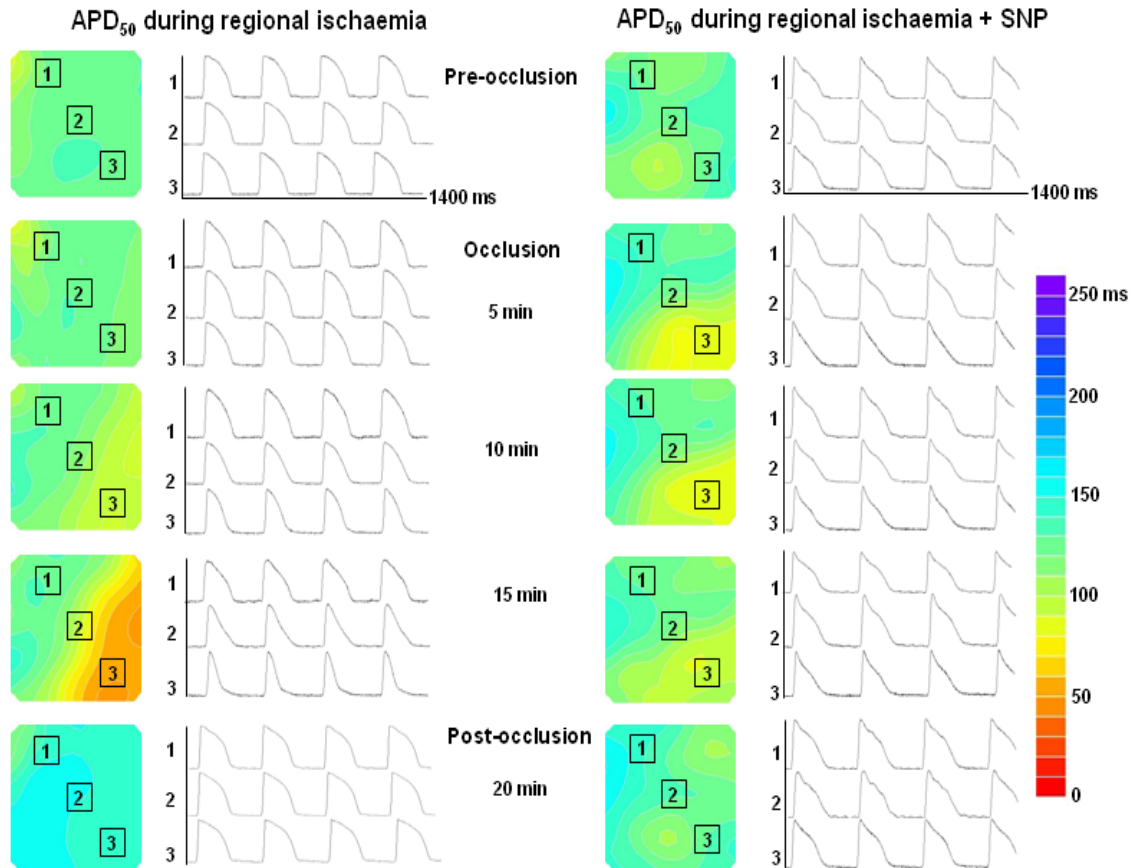


Figure 10.4 Optical imaging of APD_{50} during acute regional and global low-flow ischaemia

Maps of APD_{50} at different stages of local ischaemia: before; during and after occlusion. Example of optical action potentials show from three selected sites, 1: Normal zone, 2: Border zone and 3: Ischaemic zone.

Figure 10.5 illustrates relative flow and APD₅₀ before and after the coronary perfusion was reduced in standard Tyrode's solution (i) and the solution containing SNP (ii).

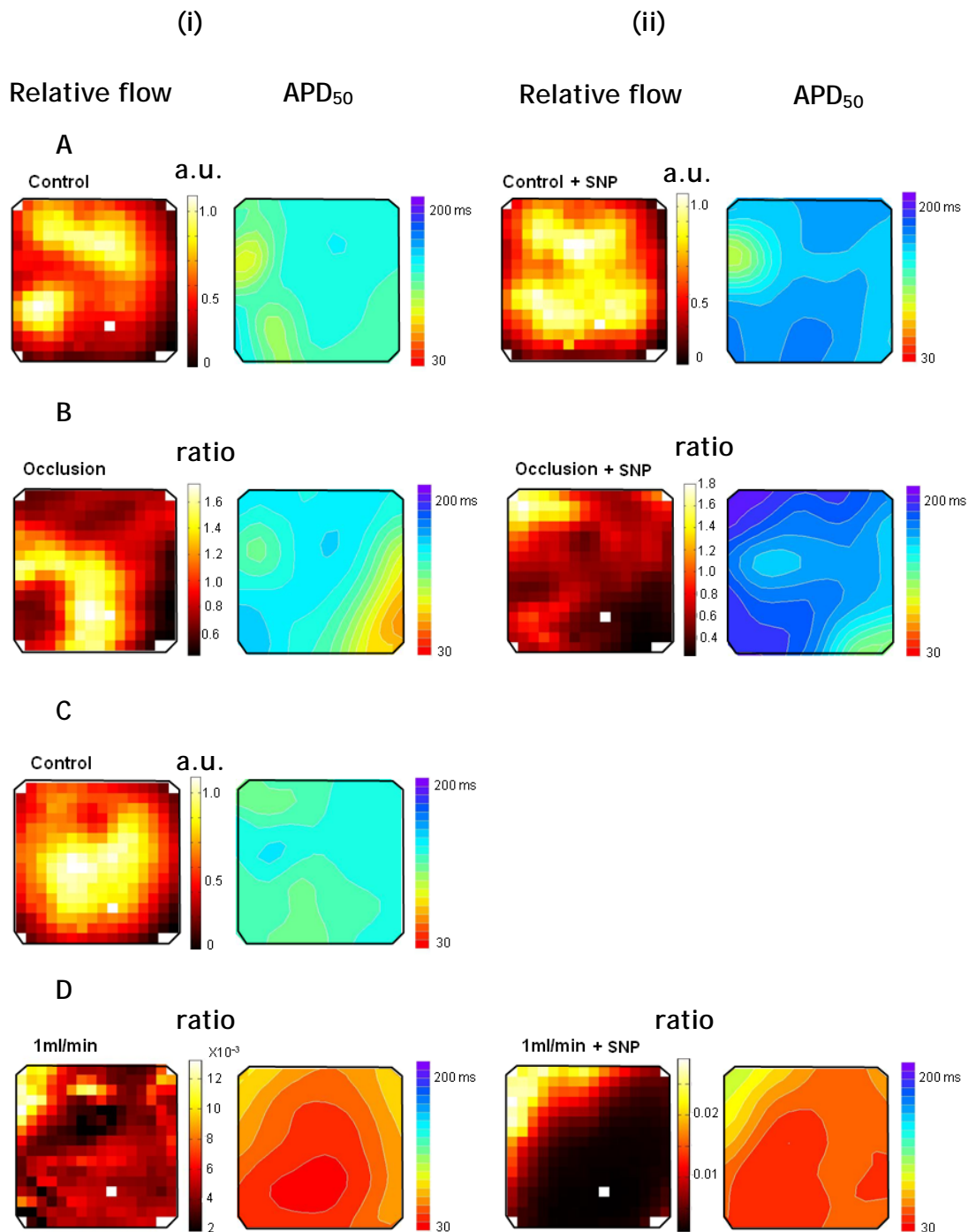


Figure 10.5 Optical mapping of flow and APD during local and low flow ischaemia

A: Relative flow and APD₅₀ of the heart at pre-occlusion, (i) perfused with standard Tyrodes solution (ST); (ii) perfused with ST + SNP. B: Relative flow and APD₅₀ during occlusion. C & D: Relative flow and APD₅₀ during low flow ischaemia (1ml/min).

The diagram below (Figure 10.6) shows a way of displaying APD data as a cumulative histogram of APD_{50} plotted as a percentage of sites. Under control conditions, the APDs conform to a narrow band of values at ~120ms. During local ischaemia, a population of sites show a very short APD. Interestingly, in the presence of SNP, the control distribution was similar to normal but the number of sites showing reduced APD was considerably less.

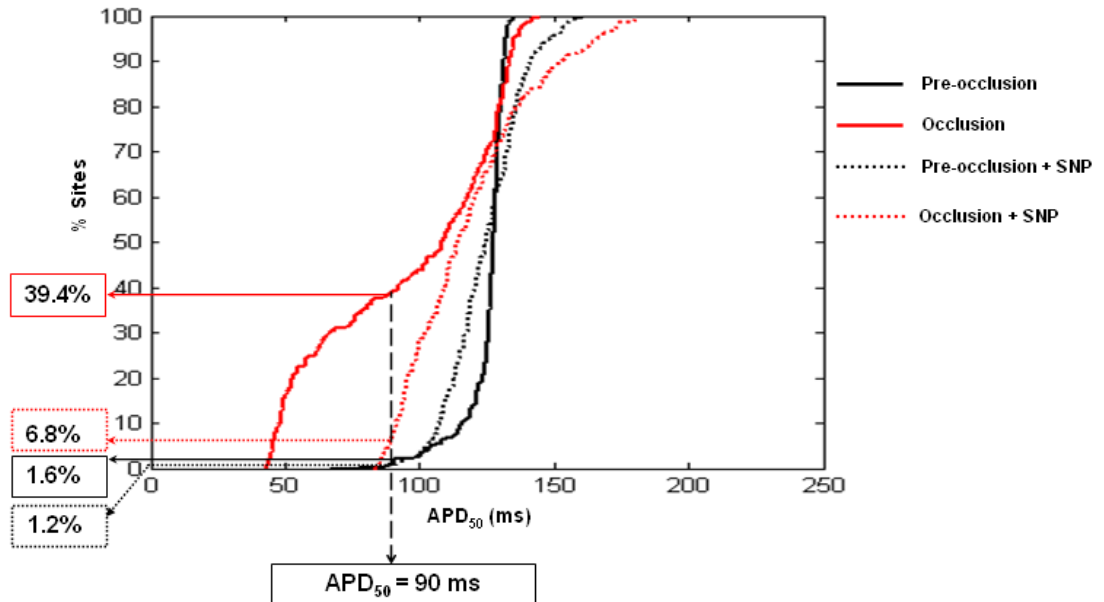


Figure 10.6 Correlation between APD_{50} and percentage of the number of sites

Figure 10.7 shows the spatio-temporal behaviour of APD_{50} and T_{Rise} during acute regional ischaemia in a heart that was perfused first with normal solution and then with solution contained SNP.

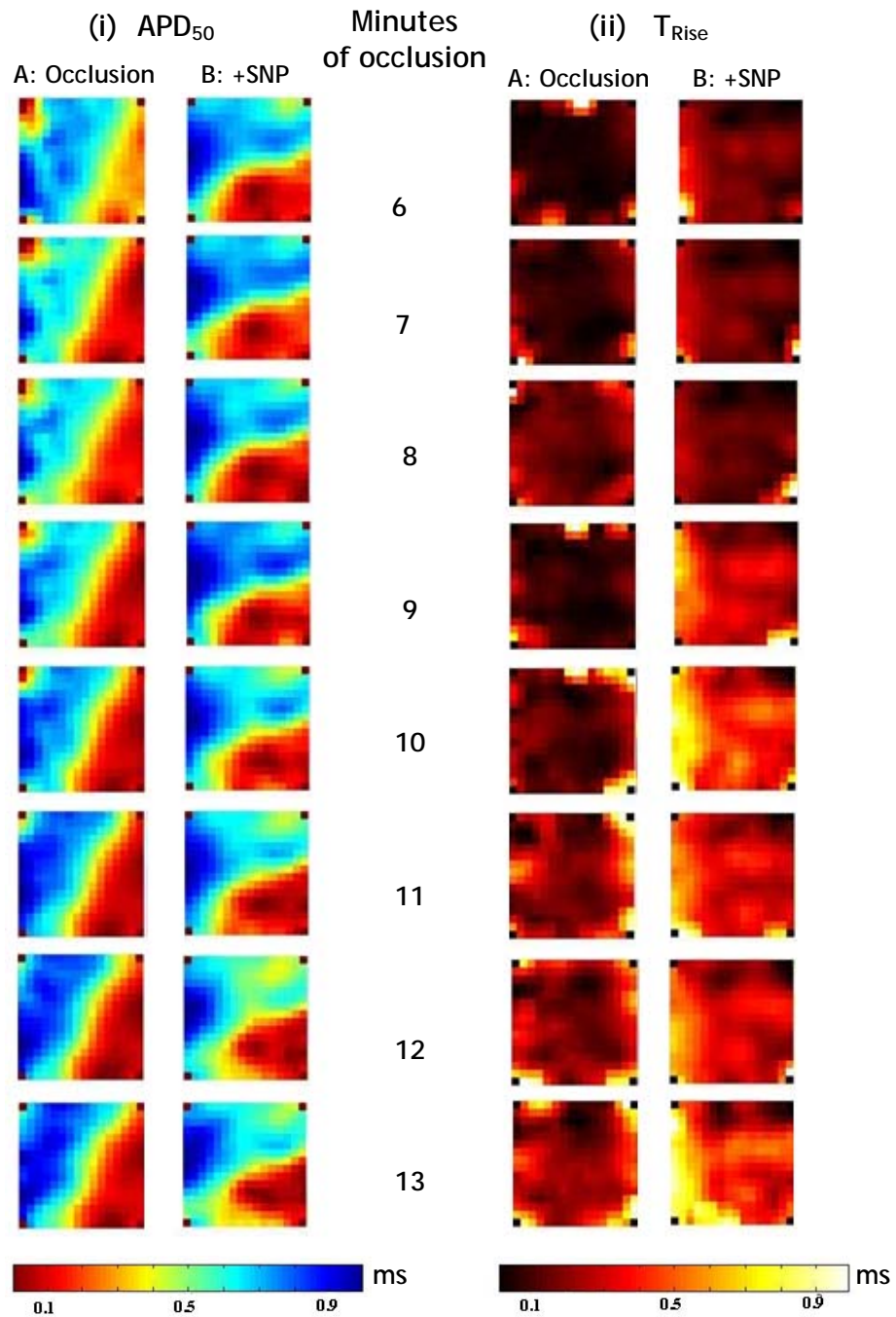


Figure 10.7 Colour map of variability of APD_{50} gradient (i) and T_{Rise} gradient (ii)

A: Maps of APD_{50} and T_{Rise} on sequential minutes during local ischaemia with and without the inclusion of SNP in the perfusate to maximise endothelium dependant vasodilation.

10.4 Discussion and conclusion

Our data suggest that the perfusion with SNP, an agent designed to stimulate endothelium-dependant vasodilation, was able to affect the shape of the local

ischaemic zone and the resultant electrophysiology. SNP also affected the pattern of coronary flow observed during low flow ischaemia. Further studies are required, but these initial studies suggest that the shape of the infarct was affected by factors that control coronary flow. Further work is required to understand what are the key vascular factors in determining the shape and the extent of the local ischaemia. Further work would include the use of endothelin antagonists (to block tonic vasoconstrictor tone), adenosine antagonists to block adenosine antagonists and prostacyclin inhibitors in an effort to examine what influences vascular smooth muscle under conditions of local ischaemia and global ischaemia. The work raises the interesting possibility that the gradient of electrophysiological changes observed in going from normal to ischaemic myocardium may be critical in generating conduction block and arrhythmias. Factors that influence vascular response to hypoxia may change this gradient and therefore may be pro- or anti-arrhythmic.

References

Abe, S., Nagamoto, Y., Fukuchi, Y., Hayakawa, T., & Kuroiwa, A. (1989). Relationship of alternans monophasic action potential and conduction delay inside the ischemic border zone to serious ventricular arrhythmia during acute myocardial ischemia in dogs. *Am. Heart J.* **117**, 1223-1233.

Akar, F. G., Roth, B. J., & Rosenbaum, D. S. (2001). Optical measurement of cell-to-cell coupling in intact heart using subthreshold electrical stimulation. *Am. J. Physiol. Heart Circ. Physiol.* **281**, H533-H542.

Alex, J., Cale, A. R. J., Griffin, S. C., Cowen, M. E., & Guvendik, L. (2005). Connexins: The basis of functional coupling of myocytes. *J. Clin. Basic Cardiol.* **8**, 19-22.

Alexander, L. K., Keene, B. W., Small, J. D., Yount, B. Jr., & Baric, R. S. (1993). Electrocardiographic changes following rabbit coronavirus-induced myocarditis and dilated cardiomyopathy. *Adv. Exp. Med. Biol.* **342**, 365-370.

Allen, D. G. & Orchard C.H. (1983). Intracellular calcium concentration during hypoxia and metabolic inhibition in mammalian ventricular muscle. *J. Physiol. (London)* **339**, 107-122.

Allessie, M. A., Schalij, M. J., & Kirchhof, C. J. H. J. (1990). Electrophysiology of spiral waves in two directions; The role of anisotropy. *Ann NY Acad Sci* **591**, 247-256.

Allingham, J. S., Smith, R., & Rayment, I. (2005). The structural basis of blebbistatin inhibition and specificity for myosin II. *Nat. Struct. Mol. Biol.* **12**, 378-379.

American heart association statistics committee and stroke statistics subcommittee (2007). Heart disease and stroke statistics, 2007 update: A report from American heart association statistics committee and stroke statistics subcommittee. *Circulation* **115**, e67-e171.

Antzelevitch, C., Sicouri, S., Yan, G. X., & Shimizu, W. (1998). Cellular basis for QT dispersion. *J. Electrocardiol.* **30**, 168-175.

Arce, H., Xu, A. X., Gonzalez, H., & Guevara, M. R. (2000). Alternans and higher-order rhythms in an ionic model of a sheet of ischemic ventricular muscle. *Chaos* **10**, 411-426.

Artigas, P., Al'Aref, S. J., & Andersen, O. S. (2006). 2,3-Butanedione Monoxime affects cystic fibrosis transmembrane conductance regular channel function through phosphorylation dependent and phosphorylation independent mechanisms: The role of bilayer material properties. *Mol Pharmacol* **70**, 2015-2026.

Asimakis, G. K. & Lick, S. (2002). Postischemic recovery of contractile function is impaired in SOD2^{+/-} but not SOD1^{+/-} mouse heart. *Circulation* **105**, 981-986.

Avitall, B., Naimi, S., & Levine, H. J. (1988). Prolongation of the conduction time of early premature beat: a marker of ventricular action potential duration. *Am. Heart J.* **116**, 1247-1252.

Baba, S., Dun, W., Cabo, C., & Boyden, P. A. (2005). Remodeling in cells from different regions of the reentrant circuit during ventricular tachycardia. *Circulation* **112**, 2386-2396.

Baer, F. M., Theissen, P., Voth, E., Schneider, C. A., Schicha, H., & Sechtem, U. (1994). Morphologic Correlate of Pathological Q-Waves As Assessed by Gradient-Echo Magnetic-Resonance-Imaging. *American Journal of Cardiology* **74**, 430-434.

Baker, L. C., London, B., Choi, B. R., Koren, G., & Salama, G. (2000). Enhanced dispersion of repolarization and refractoriness in transgenic mouse hearts promotes reentrant ventricular tachycardia. *Circ Res* **86**, 396-407.

Barker, P. S., Mcleod, A. G., & Alexander, J. (1930). The excitatory process observed in the exposed human heart. *Am Heart J* **5**, 720-742.

Bayly, P. V., KenKnight, B. H., Rogers, J. M., Hillsley, R. E., Ideker, R. E., & Smith, W. E. (1998). Estimation of conduction velocity vector fields from epicardial mapping data. *IEEE Trans Biomed Eng* **45**, 563-571.

Berkich, D. A., Salama, G., & LaNoue, K. F. (2003). Mitochondrial membrane potentials in ischemic hearts. *Arch. Biochem. Biophys.* **420**, 279-286.

Bernus, O., Zemlin, C. W., Zaritsky, L. M., Mironov, S. F., & Pertsov, A. M. (2005). Alternating conduction in the ischaemic border zone as a precursor of reentrant arrhythmias: A simulation study. *Europace* **7**, S93-S104.

Bers, D. M. (2001). *Excitation-contraction coupling and cardiac force*, 2 ed. Kluwer Academic Press, Dordrecht/Boston/London.

Bers, D. M. (2002). Cardiac excitation-contraction coupling. *Nature* **415**, 198-205.

Blanchard, E. M., Smith, G. L., Allen, D. G., & Alpert, N. R. (1990). The effect of 2,3-butane-dione monoxime on initial heat, tension and aequorin light output of ferret papillary muscles. *Pflugers Arch* **416**, 219-221.

Boban, M., Stowe, D. F., Kampine, J. P., Goldberg, A. H., & Bosnjak, Z. J. (1993). Effects of 2,3-butanedione monoxime in isolated hearts: Protection during reperfusion after global ischemia. *J Thorac Cardiovasc Surg* **105**, 532-540.

Boengler, K., Dodoni, G., Rodriguez-Sinovas, A., Cabestrero, A., Ruiz-Meana, M., Gres, P., Konietzka, I., Lopez-Iglesias, C., Garcia-Dorado, D., Di, L. F., Heusch, G., & Schulz, R. (2005). Connexin 43 in cardiomyocyte mitochondria and its increase by ischemic preconditioning. *Cardiovasc.Res.* **67**, 234-244.

Bold, F., Sachs, F., & Franz, M. R. (2001). Tarantula peptide inhibits atrial fibrillation. *Nature* **409**, 35-36.

Bolick, D. R., Hackel, D. B., Reimer K.A., & Ideker, R. E. (1986). quantitative analysis of myocardial infarct structure in patients with ventricular tachycardia. *Circulation* **74**, 1266-1279.

Braasch, W. & Bing, R. J. (1968). Early changes in Energy Metabolism in Myocardium Following Acute Artery Occlusion in Anesthetized Dogs. *Circ.Res.* **23**, 429-438.

Branyas, N. A., Cain, M. E., Cox, J. L., & Cassidy, D. M. (1990). Transmural ventricular activation during consecutive cycles of sustained ventricular tachycardia associated with coronary artery disease. *Am.J.Cardiol.* **65**, 861-867.

Brasch, F., Neckel, M., Volkmann, R., Schmidt, G., Hellige, G., & Vetterlein, F. (1999). Mapping of capillary flow, cellular redox state, and resting membrane potential in hypoperfused rat myocardium. *Am.J Physiol Heart Circ Physiol* **277**, H2050-H2064.

Brenner, N. & Rader, C. (1976). A new principle for Fast Fourier transformation. *IEEE* **264-266**.

Bril, A., Forest, M. C., & Gout, B. (1991). Ischemia and reperfusion-induced arrhythmias in rabbits with chronic heart failure. *Am J Physiol* **261**, H301-H307.

Burashnikov, A. & Antzelevitch, C. (1998). Acceleration-induced action potential prolongation and early afterdepolarizations. *J Cardiovascular Electrophysiol* **9**, 934-948.

Burton, F. L. & Cobbe, S. M. (2001). Dispersion of ventricular repolarization and refractory period. *Cardiovascular Research* **50**, 10-23.

Burton, F. L., McPhaden, A. R., & Cobbe, S. M. (2000). Ventricular fibrillation threshold and local dispersion of refractoriness in isolated rabbit hearts with left ventricular dysfunction. *Basic Research in Cardiology* **95**, 359-367.

Cabo, C., Deruyter, B., Coromilas, J., & Wit, A. L. (1997). Mechanisms for absence of inverse relationship between coupling intervals of premature impulses initiating reentrant ventricular tachycardia and intervals between premature and first tachycardia impulses. *Circulation* **96**, 3136-3147.

Cabo, C. & Wit, A. L. (1997). Cellular electrophysiologic mechanisms of cardiac arrhythmias. *Cardiol.Clin.* **15**, 517-538.

Caldwell, J., Burton, F. L., Smith, G. L., & Cobbe, S. M. (2007). Heterogeneity of ventricular fibrillation dominant frequency during global ischemia in isolated rabbit hearts. *Journal of Cardiovascular Electrophysiology* **18**, 854-861.

Carson, D. L., Cardinal, R., Savard, P., & Vermeulen, M. (1986). Characterization of unipolar waveform alteration in acutely ischaemic porcine myocardium. *Cardiovasc.Res.* **20**, 521-527.

Cascio, W. E., Johnson, T. A., & Gettes, L. S. (1995). Electrophysiologic changes in ischemic ventricular myocardium: I. Influence of ionic, metabolic, and energetic changes. *J.Cardiovasc.Electrophysiol.* **6**, 1039-1062.

Cascio, W. E., Yang, H., Muller-Borer, B. J., & Johnson, T. A. (2005). Ischemia-induced arrhythmia: the role of connexins, gap junctions, and attendant changes in impulse propagation. *J.Electrocardiol.* **38**, 55-59.

Cha, Y. M., Birgersdottergreen, U., Wolf, P. L., Peters, B. B., & Chen, P. S. (1994). The Mechanism of Termination of Reentrant Activity in Ventricular-Fibrillation. *Circulation Research* **74**, 495-506.

Chen, Z., Higashiyama, A., Yaku, H., Bell, S., & Fabian, J. (1997). Altered expression of troponin T isoforms in mild left ventricular hypertrophy in the rabbit. *J Mol Cell Cardiol* **29**, 2345-2354.

Cheng, Y., Li, L., Nikolski, V., Wallick, D. W., & Efimov, I. R. (2004). Shock-induced arrhythmogenesis is enhanced by 2,3-butanedione monoxime compared with cytochalasin D. *Am.J.Physiol Heart Circ.Physiol* **286**, H310-H318.

Chilian, W. M. & Layne, S. M. (1990). Coronary microvascular responses to reductions in perfusion pressure; Evidence for persistent arteriolar vasomotor tone during coronary hypoperfusion. *Circulation Research* **66**, 1227-1238.

- Chou, C. C. & Chen, P. S. (2007). Remodelling of action potential and intracellular calcium cycling dynamics during subacute myocardial infarction promotes ventricular arrhythmias in Langendorff-perfused rabbit hearts. *J. Physiol* **580**, 895-906.
- Chung, N. A. Y., Lydakis, C., Belgore, F., Blann, A. D., & Lip, G. Y. H. (2002). Angiogenesis in myocardial infarction - An acute or chronic process? *European Heart Journal* **23**, 1604-1608.
- Clark, C., Foreman, M. I., Kane, K. A., Macdonale, F. M., & Parratt, J. R. (1980). Coronary artery ligation in anesthetised rats as a method for the production of experimental dysrhythmias and for the determination of infarct size. *J Pharmacol Methods* **3**, 357-368.
- Clements-Jewery, H., Hearse, D. J., & Curtis, M. J. (2005). Phase 2 ventricular arrhythmias in acute myocardial infarction: a neglected target for therapeutic antiarrhythmic drug development and for safety pharmacology evaluation. *British Journal of Pharmacology* **145**, 551-564.
- Conci, E., Pachinger, O., & Metzlet, B. (2006). Mouse models for myocardial ischaemia/reperfusion. *Journal Cardiology* **13**, 239-244.
- Cook, G. J. R., Houston, S., Barrington, S. F., & Fogelman, I. (1998). Technetium-99m-labeled HL91 to identify tumor hypoxia: Correlation with fluorine-18-FDG. *Journal of Nuclear Medicine* **39**, 99-103.
- Coronel, R., Wilms-Schopman, F. J., & de Groot, J. R. (2002). Origin of ischemia-induced phase 1b ventricular arrhythmias in pig hearts. *J. Am. Coll. Cardiol.* **39**, 166-176.
- Corretti, M. C., Koretsune, Y., Kusuoka, H., Chacko, V. P., Zweier, J. L., & Marban, E. (1991). Glycolytic Inhibition and Calcium Overload as Consequences of Exogenously Generated Free Radicals in Rabbit Hearts. *J Clin Invest.* **88**, 1014-1025.
- Cox, J. L., Daniel, T. M., & Boineau, J. P. (1973). The electrophysiologic time-course of acute myocardial ischemia and the effects of early coronary artery reperfusion. *Circulation* **48**, 971-983.
- Currie, S. & Smith, G. L. (1999). Enhanced phosphorylation of phospholamban and downregulation of sarco endoplasmic reticulum Ca²⁺ ATPase type 2 (SERCA 2) in cardiac sarcoplasmic reticulum from rabbits with heart failure. *Cardiovasc. Res.* **41**, 135-146.

Curtis, M. J. (1998). Characterisation, utilisation and clinical relevance of isolated perfused heart models of ischaemia-induced ventricular fibrillation. *Cardiovascular Research* 39, 194-215.

Davies, M. J. (1981). Pathological View of Sudden Cardiac Death. *British Heart Journal* 45, 88-96.

Day, S. B. & Johnson, J. A. (1958). The distribution of the coronary arteries of the rabbit. *Anat.Rec.* 132, 633-643.

de Groot, J. R. & Coronel, R. (2004). Acute ischemia-induced gap junctional uncoupling and arrhythmogenesis. *Cardiovasc.Res.* 62, 323-334.

de Groot, J. R., Wilms-Schopman, F. J., Opthof, T., Remme, C. A., & Coronel, R. (2001). Late ventricular arrhythmias during acute regional ischemia in the isolated blood perfused pig heart. Role of electrical cellular coupling. *Cardiovasc.Res.* 50, 362-372.

de Tombe, P. P., Burkhoff, D., & Hunter, W. C. (1992). Comparison between the effects of 2-3 butanedione monoxime (BDM) and calcium chloride on myocardial oxygen consumption. *J Mol Cell Cardiol* 24, 783-797.

de Tombe, P. P., Wannenburg, T., Fan, D., & Little, W. C. (1996). Right ventricular contractile protein function in rats with left ventricular myocardial infarction. *Am J Physiol* 271, H73-H79.

Dhalla, N. S., Rupp, H., Angel, A., & Pierce, G. N. (2003). Pathogenesis of ischaemia heart disease. Springer.

Ding, L., Splinter, R., & Knisley, S. B. (2001). Quantifying spatial localization of optical mapping using Monte Carlo simulations. *IEEE Trans Biomed Eng* 48, 1098-1107.

Dole, W. P. (1987). Autoregulation of the coronary circulation. *Prog Cardiovasc Dis* 29, 293-323.

Downar, E., Janse, M. J., & Durrer, D. (1977). The effect of acute coronary artery occlusion on subepicardial transmembrane potentials in the intact porcine heart. *Circulation* 56, 217.

Dubey, A. & Solomon, R. (1989). Magnesium, myocardial ischaemia and arrhythmia. The role of magnesium in myocardial infarction. *Drugs* 37, 1-7.

Duffy, H. S., Ashton, A. W., O'Donnell, T. P., Coombs, W., Taffet, S. M., Taffet, S. M., Delmar, M., Elmar, M., & Spray, D. C. (2004). Regulation of Connexin43 Protein complexes by intracellular acidification. *Circ Res* **94**, 215-222.

Duffy, H. S., Sorgan, P. L., Girvin, M. E., O'Donnell, T. P., Coombs, W., Taffet, S. M., Delmar, M., & Spray, D. C. (2002). pH-dependent intramolecular Binding and structure involving Cx43 cytoplasmic domains. *The journal of Biological Chemistry* **277**, 36706-36714.

Durrer, D., Van Dam, R. T., & Frend, G. E. (1970). Total excitation of the isolated human heart. *Circulation* **41**, 899-912.

Efimov, I. R., Huang, D. T., Rendt, J. M., & Salama, G. (1993). Mapping of refractory periods with voltage-sensitive dyes. *IEEE Trans Biomed Eng* **93**, 703-704.

Efimov, I. R., Huang, D. T., Rendt, J. M., & Salama, G. (1994). Optical mapping of repolarization and refractoriness from intact hearts. *Circulation* **90**, 1469-1480.

Efimov, I. R., Nikolski, V. P., & Salama, G. (2004). Optical imaging of the heart. *Circ.Res.* **95**, 21-33.

Ehlert, F. A. & Goldberger, J. J. (1997). Cellular and pathophysiological mechanisms of ventricular arrhythmias in acute ischemia and infarction. *Pace-Pacing and Clinical Electrophysiology* **20**, 966-975.

El-Sherif, N., Smith, R. A., & Evans, K. (1981). Canine ventricular arrhythmias in the late myocardial infarction period: Epicardial mapping of reentrant circuits. *Circ Res* **49**, 255-265.

Elena, L. C., Jorge, A., del Valle, N., & del Valle, H. F. (2008). Ischaemic shortening of action potential duration as a result of KATP channel opening attenuates myocardial stunning by reducing calcium influx. *Molecular and Cellular Biochemistry* **236**, 53-61.

Elliott, A. C., Smith, G. L., & Allen, D. G. (1989). Simultaneous measurements of action potential duration and intracellular ATP in isolated ferret heart exposed to cyanide. *Circulation Research* **64**, 583-591.

Engblom, H., Hedstrom, E., Heiberg, E., Wagner, G. S., Pahlm, O., & Arheden, H. (2005). Size and transmural extent of first-time reperfused myocardial infarction assessed by cardiac magnetic resonance can be estimated by 12-lead electrocardiogram. *American Heart Journal* **150**.

Engels, W., Reuters, P. H. C. M., Daemen, M. J. A. P., Smits, J. F. M., & Vandervusse, G. J. (1995). Transmural changes in mast-cell density in rat-heart after infarct induction in-vivo. *Journal of Pathology* 177, 423-429.

Farman, G. P., Tachampa, K., Mateja, R., Cazorla, O., & de Tombe, P. P. (2007). Blebbistatin: use as inhibitor of muscle contraction. *Pflugers Arch-Eur J Physiol* 424, 375-383.

Fedorov, V. V., Lozinsky, I. T., Sosunov, E. A., & Efimov, I. R. (2007). Application of blebbistatin as an excitation-contraction uncoupler for electrophysiologic study of rat and rabbit hearts. *Heart Rhythm*. 4, 619-626.

Fenoglio J.J.Jr, Karagueuzian, H. S., Friedman, P. L., Albala, A., & Wit, A. L. (1979). Time course of infarct growth toward the endocardium after coronary occlusion. *Am J Physiol* 236, H356-H370.

Ferrero, J. M., Torres, V., Montilla, F., & olomar E (2000). Stimulation of reentry during acute myocardial ischaemia: Role of ATP-sensitive potassium current and acidosis. *Computers in Cardiology* 27, 239-242.

Fozzard, H. A. (1980). Electrophysiology of the heart: the effects of ischemia. *Hosp.Pract.* 15, 61-71.

Fozzard, H. A. (1985). Electromechanical dissociation and its possible role in sudden cardiac death. *J.Am.Coll.Cardiol.* 5, 31B-34B.

Fozzard, H. A. & DasGupta, D. S. (1976). ST-segment potentials and mapping. Theory and experiments. *Circulation* 54, 533-537.

Fozzard, H. A. & Makielski, J. C. (1985). The Electrophysiology of Acute Myocardial Ischemia. *Annual Review of Medicine* 36, 275-284.

Franz, M. R. (1991). Method and theory of monophasic action potential recording. *Progress in cardiovascular disease* 33, 347-368.

Friedman, P. L., Fenoglio J.J.Jr, & Wit, A. L. (1975). Timecourse for reversal of electrophysiological and ultrastructural abnormalities in subendocardial Purkinje fibers surviving extensive myocardial infarction in dogs. *Circ Res* 36, 127-144.

Friedman, P. L., Stewart, J. R., & Wit, A. L. (1973). Spontaneous and induced cardiac arrhythmias in subendocardial purkinje fibers surviving extensive myocardial infarction in dogs. *Circ Res* 33, 612-626.

- Gariyban, L. & Lily, L. S. (2007). The electrocardiogram. In *Pathophysiology of heart disease*, ed. Lilly, L. S., pp. 80-117. Lippincott Williams & Wilkins, a Wolters Kluwer business, Baltimore.
- Gelzer, A. R. M., Koller, M. L., Otani, N. F., & Gilmour, R. F. (2008). Dynamic mechanism for initiation of ventricular fibrillation *in vivo*. *Circulation* **118**, 1123-1129.
- Gettes, L. S., Cascio, W. E., Johnson, T., & Fleet, W. F. (1991). Local myocardial biochemical and ionic alterations during myocardial ischaemia and reperfusion. *Drugs* **42 Suppl 1**, 7-13.
- Giordano, F. J. (1999). Angiogenesis: mechanisms, modulation, and targeted imaging. *J.Nucl.Cardiol.* **6**, 664-671.
- Giordano, F. J. (2008). Oxygen, oxidative stress, hypoxia, and heart failure. *The Journal of Clinical Investigation* **115**, 500-508.
- Gorman, M. W. & Sparks, H. V. (1982). Progressive coronary vasoconstriction during relative ischemia in canine myocardium. *Circulation Research* **51**, 411-420.
- Gottlieb, G., Kubo, S. H., & Alonso, D. R. (1981). Ultrastructure characterization of the border zone surrounding early experimental myocardial infarcts in dogs. *Am.J.Physiol* **103**, 292-303.
- Gough, W. B., Mehra, R., Restivo, M., & Zeiler, R. H. (1985). Reentrant ventricular arrhythmias in the late myocardial infarction period in the dog, 13: correlation of activation and refractory maps. *Circ.Res.* **57**, 432-442.
- Gray, R. A., Jalife, J., Panfilov, A. V., Baxter, W. T., Cabo, C., Davidenko, J. M., & Pertsov, A. M. (1995). Mechanisms of cardiac fibrillation. *Science* **270**, 1222-1223.
- Green, C. R. & Severs, N. J. (1993). Distribution and role of gap junctions in normal myocardium and human ischaemic heart disease. *Histochemistry* **99**, 105-120.
- Griendling, K. K., Sorescu, D., & Ushio, F. M. (2008). NAD(P)H oxidase: role in cardiovascular biology and disease. *Circ.Res.* **86**, 494-501.
- Gross, E. R. & Gross, G. J. (2006). Ligand triggers of classical preconditioning and postconditioning. *Cardiovascular Research* **70**, 212-221.

Gunduz, D., Kasseckert, S. A., Hartel, F. V., Aslam, M., Abdallah, Y., Schafer, M., Piper, H. M., Noll, T., & Schafer, C. (2006). Accumulation of extracellular ATP protects against acute reperfusion injury in rat heart endothelial cells. *Cardiovasc.Res.* **71**, 764-773.

Gutstein, D. E., Morley, G. E., Tamaddon, H., Aidya, D., Chneider, M. D., Chien, H. J., Tuhmann, H., & Ishman, G. I. (2001). Conduction slowing and sudden arrhythmic death in mice with cardiac-restricted inactivation of connexin43. *Circ Res* **88**, 333-339.

Hake, U., Schmid, F. X., Iversen, S., Dahm, M., Mayer, E., Hafner, G., & Oelert, H. (1993). Troponin-T - A Reliable Marker of Perioperative Myocardial-Infarction. *European Journal of Cardio-Thoracic Surgery* **7**, 628-633.

Han, R., Li, Y., Zhang, J., Zhang, L., Xie, F., Cheng, J., & Zhao, Z. (2008). Langmuir isotherm and pseudo second order kinetic model for the biosorption of methylene blue onto rice husk. *IEEE Trans Biomed Eng* 3545-3548.

Harris, A. S. (1950). Delayed development of ventricular ectopic rhythms following experimental coronary occlusion. *Circulation* **1**, 1318.

Harris, A. S. & Rojas, A. G. (1943). The initiation of ventricular fibrillation due to coronary occlusion. *Exp Med Surg* **1**, 105.

Hasenfuss, G. (1998). Animal models of human cardiovascular disease, heart failure and hypertrophy. *Cardiovasc.Res.* **39**, 60-76.

Hasenfuss, G., Mulieri, L. A., & Blanchard, E. M. (1991). Energetics of isometric force development in control and volume-overload human myocardium. Comparison with animal species. *Circ Res* **68**, 836-846.

Hausenloy, D. J. & Yellon, D. M. (2006). Survival kinases in ischemic preconditioning and postconditioning. *Cardiovasc.Res.* **70**, 240-253.

Henderson, A. R., Gerhardt, W., & Apple, F. S. (1998). The use of biochemical markers in ischaemic heart disease: summary of the roundtable and extrapolations. *Clinica Chimica Acta* **272**, 93-100.

Heusch, G., Guth, B. D., & Ross, J. Jr. (1987). Recruitment of coronary vasodilator reserve by nifedipine attenuates exercise induced myocardial ischemia in dog. *Circulation* **75**, 482-490.

Heusch, G. & Schulz, R. (1996). Myocardial hibernation: adaptation to ischaemia. *Eur.Heart J.* **17**, 824-828.

Higuchi, T., Wester, H. J., & Schwaiger, M. (2007). Imaging of angiogenesis in cardiology. *European Journal of Nuclear Medicine and Molecular Imaging* 34, S9-S19.

Hix, C. D. (1993). Magnesium in congestive heart failure, acute myocardial infarction and dysrhythmias. *J Cardiovasc Nurs* 8, 19-31.

Homans, D. C., Pavek, T., Laxson, D. D., & Bache, R. J. (1994). Recovery of transmural and subepicardial wall thickening after subendocardial infarction. *Journal of the American College of Cardiology* 24, 1109-1116.

Hongo, M., Ryoike, T., & Ross, J. Jr. (1997). Animal models of heart failure: recent developments and perspectives. *Trend Cardiovasc Med* 7, 161-167.

Indik, J. H., Donnerstein, R. L., Kern, K. B., Goldman, S., Gaballa, M. A., & Berg, R. A. (2006). Ventricular fibrillation waveform characteristics are different in ischemic heart failure compared with structurally normal hearts. *Resuscitation* 69, 471-477.

Janse, M. J., Cinca, J., Morena, H., Fiolet, J. W., Kleber, A. G., de Vries, G. P., Becker, A. E., & Durrer, D. (1979). The "border zone" in myocardial ischemia. An electrophysiological, metabolic, and histochemical correlation in the pig heart. *Circ.Res.* 44, 576-588.

Janse, M. J., Coronel, R., Wilms-Schopman, J. G., & de Groot, J. R. (2003). Mechanical effects on arrhythmogenesis: from pipette to patient. *Progress in Biophysics & Molecular Biology* 82, 187-195.

Janse, M. J. & Kleber, A. G. (1981). Electrophysiological changes and ventricular arrhythmias in the early phase of regional myocardial ischemia. *Circ.Res.* 49, 1069-1081.

Janse, M. J., Kleber, A. G., Downar, E., & Durrer, D. (1977). [Electrophysiological changes during acute myocardial ischemia and possible mechanisms for ventricular arrhythmias (author's transl)]. *Ann.Cardiol.Angiol.(Paris)* 26 Suppl, 551-554.

Janse, M. J., van Capelle, F. J., & Morsink, H. (1980). Flow of "injury" current and patterns of excitation during early ventricular arrhythmias in acute regional myocardial ischemia in isolated porcine and canine hearts. Evidence for two different mechanisms. *Circ Res* 47, 151-165.

Janse, M. J. & Wilms-Schopman, F. (1982). Effect of Changes in Perfusion-Pressure on the Position of the Electrophysiologic Border Zone in Acute Regional

Ischemia in Isolated Perfused Dog and Pig Hearts. *American Journal of Cardiology* 50, 74-82.

Janse, M. J. & Wit, A. L. (1989). Electrophysiological mechanism of ventricular arrhythmias resulting from myocardial ischemia and infarction. *Physiol Rev* 69, 1049-1169.

Jastrzebski, M., Kukla, P., & Bacier, B. (2008). [J-wave associated idiopathic ventricular fibrillation--a new arrhythmogenic syndrome?]. *Kardiol.Pol.* 66, 447-449.

Johns, T. N. P. & Olson, B. J. (1954). Experimental myocardial infarction.I. A method of coronary occlusion in small animals. *Ann Surg* 140, 675-682.

Kamiya, H., Watanabe, G., Saito, A., Oi, T., Omita, S., Htake, H., & Anamori, T. (2002). Real-time and continuous monitoring of myocardial blood flow using a thermal diffusion method. *European Journal of Cardio-Thoracic Surgery* 21, 748-752.

Kaplinsky, E., Ogawa, S., Balke, C. W., & Dreifus, L. S. (1979). 2 Periods of Early Ventricular Arrhythmia in the Canine Acute Myocardial-Infarction Model. *Circulation* 60, 397-403.

Kaufmann, P. A. & Camici, P. G. (2005). Myocardial blood flow measurement by PET: Thechnical aspects and clinical applications. *The journal of nuclear medicine* 46, 75-88.

Klabunde, R. E. (2004). Vascular function. In *Cardiovascular physiology concepts* pp. 91-116. Lippincott Willium and Wilkins.

Kleber, A. G. (1984). Extracellular potassium accumulation in acute myocardial ischemia. *J.Mol.Cell Cardiol.* 16, 389-394.

Kleber, A. G. (2000). ST-segment elevation in the electrocardiogram: a sign of myocardial ischemia. *Cardiovasc.Res.* 45, 111-118.

Kleber, A. G. (2003). Cell-to-cell coupling between host and donor cells in the in situ myocardium. *Circ.Res.* 92, 1176-1178.

Kleber, A. G. & Fast, V. (1997). Molecular and cellular aspects of re-entrant arrhythmias. *Basic Res.Cardiol.* 92 Suppl 1, 111-119.

Kleber, A. G. & Janse, M. J. (1982). Conduction- velocity in acutely ischemic myocardium. *Circulation* 66, 157.

Kleber, A. G., Janse, M. J., Wilms-Schopman, F. J., Wilde, A. A., & Coronel, R. (1986). Changes in conduction velocity during acute ischemia in ventricular myocardium of the isolated porcine heart. *Circulation* **73**, 189-198.

Kleber, A. G. & Wilde, A. A. (1986). Regulation of intracellular sodium ions in acute reversible myocardial ischemia--a perspective. *J.Mol.Cell Cardiol.* **18 Suppl 4**, 27-30.

Knisley, S. B. & Neuman, M. R. (2003). Simultaneous electrical and optical mapping in rabbit hearts. *Ann Biomed Eng* **31**, 32-41.

Kolega, J. (2004). Phototoxicity and photoinactivation of blebbistatin in UV and visible light. *Biochem Biophys Res Commun* **320**, 1020-1025.

Kolipaka, A., Chatzimavroudis, G. P., White, R. D., O'Donnell, T. P., & Setser, R. M. (2005). Segmentation of non-viable myocardium in delayed enhancement magnetic resonance images. *International Journal of Cardiovascular Imaging* **21**, 303-311.

Konta, T., Ikeda, K., Yamaki, M., Nakamura, K., Honma, K., Kubota, I., & Yasui, S. (1990). Significance of discordant ST alternans in ventricular fibrillation. *Circulation* **78**, 1047-1059.

Krucker, T., Siggins, G. R., & Halpain, S. (2000). Dynamic actin filaments are required for stable long term potentiation (LTP) in area CA1 of the hippocampus. *Proc Natl Acad Sci USA* **97**, 6856-6861.

Kurz, R. W., Mohabir, R., Ren, L., & Ranz, M. R. (1993). Ischaemia induced alternans of action potential duration in the intact-heart:dependence on coronary flow, preload and cycle length. *European Heart Journal* **14**, 1410-1420.

Kusmic, C., Abbate, A. L., Coceani, F., Ambuceti, G., Azzerini, G., & Arsicchi, R. (2006). Paradoxical coronary microcirculatory constriction during ischemia: a synergic function for nitric oxide and endothelin. *Am.J Physiol Heart Circ Physiol* **291**, H1814-H1821.

Lalu, M. M., Pasini, E., Schulze, C. J., Ferrari-Vivaldi, M., Ferrari-Vivaldi, G., Bachetti, T., & Schulz, R. (2005). Ischaemia-reperfusion injury activates matrix metalloproteinases in the human heart. *Eur.Heart J.* **26**, 27-35.

Lancaster, E. R. (1882). On the valves of the heart of "Ornithorhynchus paradoxus" compared to those man. *Proc Zool Soc Lond* **52**, 42-64.

Langmuir, I. (1916). The constitution and fundamental properties of solids and liquids. *J.Am.Chem.Soc.* **38**, 2221-2295.

- Laurita, K. R. & Rosenbaum, D. S. (2008). Cellular mechanisms of arrhythmogenic cardiac alternans. *Progress in Biophysics & Molecular Biology* **97**, 332-347.
- Lee, B. H., Kim, W. H., Choi, M. J., Rho, J. R., & Kim, W. G. (2002). Chronic heart failure model in rabbits based on the concept of the Bifurcation/trifurcation coronary artery branching pattern. *Artificial organs* **26**, 360-365.
- Lee, M. H., Lin, S. F., Ohara, T., Omichi, C., Okuyama, Y., Chudin, E., Garfinkel, A., Weiss, J. N., Karagueuzian, H. S., & Chen, P. S. (2001). Effects of diacetyl monoxime and cytochalasin D on ventricular fibrillation in swine right ventricles. *Am.J Physiol Heart Circ Physiol* **280**, H2628-H2696.
- Lerner, D. L., Beardslee, M. A., & Saffitz, J. E. (2001). The role of altered intercellular coupling in arrhythmias induced by acute myocardial ischaemia. *Cardiovascular Research* **50**, 263-269.
- Lewick, J. E. (2003). The cardiac excitation and contraction myocyte. In *Cardiovascular physiology* pp. 24-43. Oxford University Press, Euston London.
- Lewis, T. (1909). Experimental production of paroxysmal early tachycardia and the effects of ligation of the coronary arteries. *Heart* **1**, 98.
- Li, D. S., Li, C. Y., Yong, A. C., & Kilpatrick, D. (1998). Source of electrocardiographic ST changes in subendocardial ischemia. *Circulation Research* **82**, 957-970.
- Li, L., Jin, Q., Huang, J., Cheng, K. A., & Ideker, R. E. (2008). Intramural foci during long duration fibrillation in the pig ventricle. *Circulation Research* **102**, 1256-1264.
- Lichten, P. R. & Engel, H. J. (1979). Assessment of regional myocardial blood flow using the inert gas washout technique. *Cardiovasc Radiol* **2**, 203-216.
- Lindsey, M. L., Escobar, G. P., Mukherjee, R., Goshorn, D. K., Sheats, N. J., Bruce, J. A., Mains, I. M., Hendrick, J. K., Hewett, K. W., Gourdie, R. G., Matrisian, L. M., & Spinale, F. G. (2006). Matrix metalloproteinase-7 affects connexin-43 levels, electrical conduction, and survival after myocardial infarction. *Circulation* **113**, 2919-2928.
- Liu, Y., Cabo, C., Salomonsz, R., Delmar, M., Devidenko, J., & Jalife, J. (1993). Effects of diacetyl monoxime on the electrical properties of sheep and guinea pig ventricular muscle. *Cardiovasc.Res.* **27**, 1991-1997.

Liu, Y. H., Yang, X. P., & Nass, O. (1997). Chronic heart failure induced by coronary artery ligation in Lewis inbred rats. *Am J Physiol* **272**, H722-H727.

Lopez, A., Arce, H., & Guevara, M. R. (2007). Rhythms of high-grade block in an ionic model of a strand of regionally ischemic ventricular muscle. *Journal of Theoretical Biology* **249**, 29-45.

Luke, R. A. & Saffitz, J. E. (1991). Remodeling of ventricular conduction pathways in healed canine infarct border zones. *J Clin Invest.* **87**, 1594-1602.

Mandapati, R., Asada, Y., Baxter, W. T., Gray, R., Davidenko, J., & Jalife, J. (1998). Quantification of effects of global ischemia on dynamics of ventricular fibrillation in isolated rabbit heart. *Circulation* **98**, 1688-1696.

Martin, T. N., Groenning, B. A., Murray, H. M., Steedman, T., Foster, J. E., Elliot, A. T., Dargie, H. J., Selvester, R. H., Pahlm, O., & Wagner, G. S. (2007). ST-Segment deviation analysis of the admission 12-lead electrocardiogram as an aid to early diagnosis of acute myocardial infarction with a cardiac magnetic resonance imaging gold standard. *Journal of the American College of Cardiology* **50**, 1021-1028.

Meola, F. (1879). La commozione toracica. *G.Int.Sci.Med.* **1**, 923-937.

Michiels, C. (2004). Physiological and pathological responses to hypoxia. *Am.J.Pathol.* **164**, 1875-1882.

Michiels, C., Arnould, T., & Remacle, J. (2000). Endothelial cell responses to hypoxia: initiation of a cascade of cellular interactions. *Biochim.Biophys.Acta* **1497**, 1-10.

Miller, S., Helber, U., Brechtel, K., Nagele, T., Hahn, U., Kramer, U., Hoffmeister, H. M., & Claussen, C. D. (2003). MR imaging at rest early after myocardial infarction: detection of preserved function in regions with evidence for ischemic injury and non-transmural myocardial infarction. *European Radiology* **13**, 498-506.

Mills, W. R., Mal, N., Forudi, F., Popovic, Z. B., Penn, M. S., & Laurita, K. R. (2006). Optical mapping of late myocardial infarction in rats. *Am.J.Physiol Heart Circ.Physiol* **290**, H1298-H1306.

Mines, G. R. (1913). On dynamic equilibrium in the heart. *J Physiol* **46**, 349-382.

Miura, T., Downey, J. M., Ooiwa, H., Ogawa, S., Adachi, S., Noto, T., Shizukuda, Y., & Iimura, O. (1989). Progression of myocardial infarction in a collateral flow deficient species. *Jpn Heart J* **30**, 695-708.

Mizumaki, K., Fujki, A., & Tani, M. (1993). Effects of acute ischemia on anisotropic conduction in canine ventricular muscle. *Pace-Pacing and Clinical Electrophysiology* 16, 1656-1663.

Moe, G. K., Rheinboldt, W. C., & Abildskov, J. A. (1964). A computer model of atrial fibrillation. *Am.Heart J.* 67, 200.

Muders, F. & Elsner, D. (2000). Animal models of chronic heart failure. *Pharmacological Research* 41, 605-612.

Murray, C. E., Jennings, R. B., & Reimer K.A. (1986). Preconditioning with ischaemia: a delay of lethal cell injury in ischemic myocardium. *Circulation* 74, 1124-1136.

National center for health statistics (1992). Detailed diagnosis and procedures, National Hospital Discharge Survey, 1990. *Vital and health statistics* 113, 92-1774.

Nearing, B., Huang, A. H., & Verrier, R. L. (1991). Dynamic tracking of cardiac vulnerability by complex demodulation of the T-wave. *Science* 252, 437-440.

Neumann, F. J., Kosa, I., Dickfeld, T., Blasini, R., Gawaz, M., Hausleiter, J., Schwaiger, M., & Schomig, A. (1997). Recovery of myocardial perfusion in acute myocardial infarction after successful balloon angioplasty and stent placement in the infarct-related coronary artery. *J.Am.Coll.Cardiol.* 30, 1270-1276.

Ng, G. A., Cobbe, S. M., & Smith, G. L. (1998). Non-uniform prolongation of intracellular Ca^{2+} transients recorded from the epicardial surface of isolated hearts from rabbits with heart failure. *Cardiovasc.Res.* 37, 489-502.

Nuss, H. B., Kass, D. A., Tomaselli, G. F., & Marban, E. (1999). Cellular basis of ventricular arrhythmias and abnormal automaticity in heart failure. *Am.J Physiol Heart Circ Physiol* 46, H80-H91.

Nygren, A., Baczko, I., & Giles, W. R. (2006). Measurements of electrophysiological effects of components of acute ischemia in Langendorff-perfused rat hearts using voltage-sensitive dye mapping. *J.Cardiovasc.Electrophysiol.* 17 Suppl 1, S113-S123.

O'Rourke, B., Kass, D. A., Tomaselli, G. F., Kaab, S., Tunin, R., & Marban, E. (1999). Mechanisms of altered excitation-contraction coupling in canine tachycardia-induced heart failure. *Circulation Research* 84, 562-570.

Owens, L. M., Fralix, T. A., Murphy, E., Cascio, W. E., & Gettes, L. S. (1996). Correlation of ischemia-induced extracellular and intracellular ion changes to

cell to cell electrical uncoupling in isolated blood perfused rabbit hearts. *Circulation* **94**, 10-13.

Page, A. M. (2004). Probing with light: how the confocal laser scanning microscope is transforming our view of the brain. *Neuropathology and Applied Neurobiology* 1-5.

Pastore, J. M., Girouard, S. D., Laurita, K. R., Akar, F. G., & Rosenbaum, D. S. (1999). Mechanism linking T-wave alternans to the genesis of cardiac fibrillation. *Circulation* **99**, 1385-1394.

Pastore, J. M. & Rosenbaum, D. S. (2000). Role of structural barriers in the mechanism of alternans-induced reentry. *Circ Res* **87**, 1157-1163.

Pennock, G. D., Yun, D. D., Agarwal, P. G., Spooner, P. H., & Goldman, S. (1997). Echocardiographic changes after myocardial infarction in a model of left ventricular diastolic dysfunction. *Am J Physiol* **273**, H2018-H2029.

Peuhkurinen, K. J. (2000). Ischaemic heart disease at the cellular level. *IJBEM* **2**, 1-8.

Pfeffer, M. A., Pfeffer, J. M., & Fishbein, M. C. (1979). Myocardial infarct size and ventricular function in rats. *Circ Res* **44**, 503-512.

Pinto, J. M. B. & Boyden, P. A. (1999). Electrical remodeling in ischemia and infarction. *Cardiovascular Research* **42**, 284-297.

Podesser, B., Wollenek, G., Seiteiberber, R., & Tschabitscher, M. (1997). Epicardial branches of the Coronary Arteries and their distribution in the rabbit heart: the rabbit heart as a model of regional ischemia. *The Anatomical record* **247**, 521-527.

Pogwizd, S. M. & Corr, B. B. (1987). Reentrant and non-reentrant mechanisms contribute to arrhythmogenesis during early myocardial ischemia: Results using three-dimensional mapping. *Circ Res* **61**, 352-371.

Pogwizd, S. M., Qi, M., Yuan, W. L., & Samarel, A. M. (1999). Upregulation of Na⁺/Ca²⁺ exchanger expression and function in an arrhythmogenic rabbit model of heart failure. *Circ Res* **85**, 1009-1019.

Qian, Y. W., Sung, R. J., Lin, S. F., Province, R., & Clusin, W. T. (2003). Spatial heterogeneity of action potential alternans during global ischemia in the rabbit heart. *Am. J Physiol Heart Circ Physiol* **285**, H2733.

Qu, Z., Garfinkel, A., Chen, P. S., & Weiss, J. N. (2000). Mechanisms of discordant alternans and induction of re-entry in simulated cardiac tissue. *Circulation* **102**, 1644-1670.

Quinn, F. R., Currie, S., Duncan, A. M., Miller, S., Sayeed, R., Cobbe, S. M., & Smith, G. L. (2003). Myocardial infarction causes increased expression but decreased activity of the myocardial Na⁺-Ca²⁺ exchanger in the rabbit. *J. Physiol* **553**, 229-242.

Rankovic, V., Patel, N., Jain, S., Robinson, N., Goldberger, J., Horvath, G., & Kadish, A. (1999). Characteristics of ischemic and peri-ischemic regions during ventricular fibrillation in the canine heart. *J Cardiovasc Electrophysiol* **10**, 1090-1100.

Rees, S. A. & Curtis, M. J. (1992). UK-66914 inhibits ventricular fibrillation as a consequence of I_{k block}. *J Mol Cell Cardiol* **24**, S56.

Rees, S. A. & Curtis, M. J. (1993). Specific IK1 blockade: a new antiarrhythmic mechanism? Effect of RP58866 on ventricular arrhythmias in rat, rabbit, and primate. *Circulation* **87**, 1979-1989.

Riccio, M. L., Koller, M. L., & Gilmour, R. F. (1999). Electrical restitution and spatiotemporal organization during ventricular fibrillation. *Circ Res* **84**, 955-963.

Rodriguez, B., Ferrero, J. M., & Trenor, B. (2002). Mechanistic investigation of extracellular K⁺ accumulation during acute myocardial ischemia: a simulation study. *American Journal of Physiology-Heart and Circulatory Physiology* **283**, H490-H500.

Rodriguez, B., Trayanova, N., & Noble, D. (2006). Modeling cardiac ischemia. *Ann.N.Y.Acad.Sci.* **1080**, 395-414.

Romero, L., Trenor, B., Ferrero, M., Errero, J. M., & Alonso, M. (2007). The Safety factor approach in the analysis of reentrant patterns of activation in the ischemic virtual heart. *Computers in Cardiology* **34**, 317-320.

Rosen MR, Gelband, H., Merker, C., & Hoffman, B. F. (1973). Mechanisms of digitalis toxicity: Effects of ouabain on phase four of canine Purkinje fiber transmembrane potentials. *Circ* **47**, 681-689.

Rosenbaum, D. S. & Jalife, J. (2001). Basic principles. In *Optical Mapping of Cardiac Excitation and Arrhythmias* pp. 2-93. Futura Publishing Company, Armonk, New York.

Ryan, T. J., Anderson, J. L., Antman, E. M., Braniff, B. A., Brooks, N. H., Califf, R. M., Hillis, L. D., Hiratzka, L. F., Rapaport, E., Riegel, B. J., Russell, R. O., Smith, E. E., III, & Weaver, W. D. (1996). ACC/AHA guidelines for the management of patients with acute myocardial infarction: executive summary. A report of the American College of Cardiology/American Heart Association Task Force on Practice Guidelines (Committee on Management of Acute Myocardial Infarction). *Circulation* **94**, 2341-2350.

Sakamoto, T., Limouze J, Combs, C. A., Straight, A. F., & Sellers, J. R. (2005). Blebbistatin, a myosin II inhibitor, is photoinactivated by blue light. *Biochemistry* **44**, 584-588.

Salama, G. & Choi, B. R. (2001). Optical mapping of impulse propagation in the atrioventricular node. In *Optical mapping of cardiac excitation and arrhythmias*, eds. Rosenbaum, D. S. & Jalife, J., pp. 177-196. Futura, New York.

Samie, F. H., Mandapati, R., Gray, R. A., Watanabe, Y., Zuur, C., Beaumont, J., & Jalife, J. (2000). A mechanism of transition from ventricular fibrillation to tachycardia : effect of calcium channel blockade on the dynamics of rotating waves. *Circ.Res.* **86**, 684-691.

Sasaki, H., Shimizu, M., Ogawa, K., Okazaki, F., Taniguchi, M., Taniguchi, I., & Mochizuki, S. (2007). Brief ischemia-reperfusion performed after prolonged ischemia (ischemic postconditioning) can terminate reperfusion arrhythmias with no reduction of cardiac function in rats. *Int Heart J* **48**, 205-213.

Sawyer, D. B. (2002). Role of oxidative stress in myocardial hypertrophy and failure. *J.Mol.Cell Cardiol.* **34**, 379-388.

Scamp, F. & Vassort, G. (1994). Effect of extracellular ATP on the Na⁺ current in rat ventricular myocytes. *Circ.Res.* **74**, 710-717.

Schulz, R. (2000). Ischemic preconditioning. *Basic Res.Cardiol.* **95**, 271.

Schwartz, P. J., Billman, G. E., & Stone, H. L. (1984). Autonomic mechanisms in ventricular fibrillation induced by myocardial ischaemia during exercise in dogs with healed myocardial infarction: An experimental preperation for sudden cardiac death. *Circulation* **69**, 790-800.

Seshiah, P. N. (2002). Angiotensin II stimulation of NAD(P)H oxidase activity:upstream mediators. *Circ.Res.* **91**, 406-413.

Severs, N. J., Copper, S. R., Dupont, E., Yeh, H. I., Ko, Y. S., & Matsushita, T. (2004). Gap junction alterations in human cardiac disease. *Cardiovasc.Res.* **62**, 368-377.

Sievers, B., John, B., Brandts, B., Franken, U., van Bracht, M., & Trappe, H. J. (2004). How reliable is electrocardiography in differentiating transmural from non-transmural myocardial infarction? - A study with contrast magnetic resonance imaging as gold standard. *International Journal of Cardiology* **97**, 417-423.

Sinha, M. K., Gaze, D. C., Collinson, P. O., & Kaski, J. C. (2002a). Increased levels of Ischemia Modified Albumin (IMA) following direct current cardioversion. *Circulation* **106**, 668.

Sinha, M. K., Gaze, D. C., Collinson, P. O., & Kaski, J. C. (2002b). The role of ischemia modified albumin (IMA) a new biochemical marker of myocardial ischaemia in the early diagnosis of acute coronary syndromes. *Circulation* **106**, 455.

Sinha, M. K., Gaze, D. C., Tippins, J. R., Collinson, P. O., & Kaski, J. C. (2003). Ischemia modified albumin is a sensitive marker of myocardial ischemia after percutaneous coronary intervention. *Circulation* **107**, 2403-2405.

Sinusas, A. J. (2004). Imaging of angiogenesis. *J.Nucl.Cardiol.* **11**, 617-633.

Sladek, T., Filkuka, J., Dolezel, S., Vasku, J., Hartmannova, B., & Travnicko, J. (1984). The border zone of the early myocardial infarction in dogs; its characteristic and viability. *Basic Res.Cardiol.* **79**, 344-349.

Smeets, J. L. R. M., Allessie, M. A., Lammers, W. J. E. P., Bonke, F. I. M., & Hollen, J. (1986). The wavelength of cardiac impulse and reentrant arrhythmias in isolated rabbit atrium; The role of heart rate, autonomic transmitters, temperature, and Potassium. *Circ Res* **58**, 96-108.

Spach, M. S., Dolber, P. C., & Heidlage, J. F. (1988). Influence of the passive anisotropic properties on directional differences in propagation following modification of sodium conductance in human atrial muscle. A model of reentry based anisotropic discontinuous propagation. *Circ.Res.* **62**, 811-832.

Staat, P., Rioufol, G., & Piot, C. (2005). Postconditioning the human heart. *Circulation* **112**, 2143-2148.

Stapleton, M. T., Fuchsbauer, C. M., & Allshire, A. P. (1998). BDM drives protein dephosphorylation and inhibits adenine nucleotide exchange in cardiomyocytes. *Am.J.Physiol* **275**, H1260-H1266.

Steenbergen, C., Deleeuw, G., Barlow, C., Chance, B., & Williamson, J. R. (1977). Heterogeneity of the hypoxic state in perfused rat heart. *Circulation Research* **41**, 606-615.

Straight, A. F., Cheung, A., Limouze J, Chen, I., Westwood, N. J., Sellers, J. R., & Mitchison, T. J. (2003). Dissecting temporal and spatial control of cytokinesis with a myosin II inhibitor. *Science* **299**, 1743-1747.

Sung, D., Omens, J. H., & McCulloch, A. D. (2000). Model-based analysis of optically mapped epicardial activation patterns and conduction velocity. *Annals of Biomedical Engineering* **28**, 1085-1092.

Takagi, M. & Yoshikawa, J. (2003). T wave alternans and ventricular tachyarrhythmia risk stratification: A review. *Indian Pacing Electrophysiol.J.* **3**, 67.

Takahashi, T. & Lopshire, J. C. (2004). Optical mapping of the functional reentrant circuit of ventricular tachycardia in acute myocardial infarction. *Heart Rhythm.* **1**, 451-459.

Thygesen, K. & Alpert, J. S. (2007). Universal Definition of myocardial infarction. *Circulation* **116**, 2634-2653.

Ursell, P. C., Gardner, P. I., Albala, A., Fenoglio J.J.Jr, & Wit, A. L. (1985). Structural and electrophysiological changes in the epicardial border zone of canine myocardial infarcts during infarct healing. *Circ Res* **56**, 436-451.

Vanoli, E., Bacchini, S., Panigada, S., Pentimalli, F., & Adamson, P. B. (2004). Experimental models of heart failure. *European Heart Journal Supplements* **6**, F7-F15.

Verner, I. R. (1974). Sodium nitroprusside: theory and practice. *Postgrad Med J* **50**, 576-581.

Vetterlein, F., Miihlfeld, C., Cetegan, C., & Hellige, G. (2006). Redistribution of connexin43 regional acute ischemic myocardium: influence of ischemic preconditioning. *Am.J Physiol Heart Circ Physiol* **291**, 813-819.

Vinten-Johansen, J., Yellon, D. M., & Opie, L. H. (2005). Postconditioning: a simple, clinically applicable procedure to improve revascularization in acute myocardial infarction. *Circulation* **112**, 2085-2088.

Walker, M. L. & Rosenbaum, D. S. (2003). Repolarization alternans: implications of the mechanism and prevention of sudden cardiac death. *Cardiovasc.Res.* **57**, 599-614.

Walker, N. L., Burton, F. L., Kettlewell, S., Smith, G. L., & Cobbe, S. M. (2007). Mapping of epicardial activation in a rabbit model of chronic myocardial infarction. *J Cardiovasc Electrophysiol* **18**, 862-868.

Wang, L., Li, C. Y., Yong, A. C., & Kilpatrick, D. (1998). Fast Fourier transform analysis of ventricular fibrillation intervals to predict ventricular refractoriness and its spatial dispersion. *Pacing Clin. Electrophysiol.* **21**, 2588-2595.

Wasson, S., Reddy, H. K., & Dohrmann, M. L. (2004). Current Perspectives of Electrical remodeling and its therapeutic implications. *J Cardiovasc Pharmacol Therapeut* **9**, 129-144.

White, F. C., Carroll, S. M., Magnet, A., & Bloor, C. M. (1992). Coronary collateral development in Swine after coronary artery occlusion. *Circ Res* **71**, 1490-1500.

Widimsky, P., Gregor, P., Cervenka, V., & Visek, V. (1984). Two-Dimensional Echocardiography in Acute Transmural and Non-Transmural Myocardial-Infarction. *Cor et Vasa* **26**, 12-&.

Wilde, A. A. M., Peters, R. J. G., & Janse, M. J. (1988). Catecholamine Release and Potassium Accumulation in the Isolated Globally Ischemic Rabbit Heart. *Journal of Molecular and Cellular Cardiology* **20**, 887-896.

Wilensky, R. L., Trantum-Jensen, J., Coronel, R., Wilde, A. A., Fiolet, J. W., & Janse, M. J. (1986). The subendocardial border zone during acute ischemia of the rabbit heart: an electrophysiologic, metabolic, and morphologic correlative study. *Circulation* **74**, 1137-1146.

William, J. P. & Desnond, J. S. (1983). Arrhythmias and cellular electrophysiological changes during myocardial ischaemia and reperfusion. *Cardiovascular Research* **17**, 363-372.

Wit, A. L. & Janse, M. J. (1992). Experimental models of ventricular tachycardia and fibrillation caused by ischemia and infarction. *Circulation* **85**, 132-142.

Wit, A. L. & Janse, M. J. (1993). *The ventricular arrhythmias of ischemia and infarction: Electrophysiological mechanisms*, pp. 1-648. Futara Publishing Company, Mount Kisco, New York.

Xia, Y., Roman, L. J., & Zweier, J. L. (1998a). Inducible nitric oxide synthase generates superoxide from the reductase domain. *J. Biol. Chem.* **273**, 22635-22639.

Xia, Y., Tsai, A. L., Berkich, D. A., & Zweier, J. L. (1998b). Superoxide generation from endothelial nitric oxide synthase. A calcium/calmodulin dependent and tetrahydrobiopterin regulatory process. *J. Biol. Chem.* **273**, 25804-25808.

- Yan, G. X. & Kleber, A. G. (1992). Changes in extracellular and intracellular pH in ischemic rabbit papillary muscle. *Circ.Res.* **71**, 460-470.
- Yan, G. X., Kleber, A. G., & Cascio, W. E. (1989). [Electrical cell-to-cell coupling in the myocardium]. *Sheng Li Ke.Xue.Jin.Zhan.* **20**, 294-300.
- Yang, X. P., Sabbah, H. N., Liu, Y. H., Sharow, V. G., Mascha, E. J., Alwan, I., & Carretero, O. A. (1993). Ventriculographic evaluation in three rat models of cardiac dysfunction. *Am J Physiol* **265**, H1946-H1952.
- Ye, J., Yang, L., Sethi, R., Copps, J., Ramjiawan, B., Summers, R., & Deslauriers, R. (1997). A new technique of coronary artery ligation: Experimental myocardial infarction in rats in vivo with reduced mortality. *Mol Cell Biochem* **176**, 227-233.
- Yellon, D. M., Alkhulaifi, A. M., Browne, E. E., & Pugsley, W. B. (1992). Ischaemic preconditioning limits infarct size in the rat heart. *Cardiovasc.Res.* **26**, 983-987.
- Yellon, D. M. & Baxter, G. F. (2000). Protecting the ischaemic and reperfused myocardium in acute myocardial infarction: distant dream or near reality? *Heart online* **83**, 381-387.
- Yellon, D. M. & Opie, L. H. (2006). Postconditioning for protection of the infarcting heart. *Lancet* **367**, 456-458.
- Yoshida, T., Maulik, N., & Engelman, R. M. (2000). Targeted disruption of the mouse Sod1 gene makes the hearts vulnerable to ischemic reperfusion injury. *Circ.Res.* **86**, 264-269.
- Ytrehus, K., Liu, Y., Tsuchida, A., Miura, T., Liu, G. S., Yang, X. M., Herbert, D., Cohen, M. V., & Downey, J. M. (1994). Rat and rabbit heart infarction: effects of anesthesia, perfusate, risk zone, and method of infarct sizing. *Am J Physiol* **267**, H2383-H2390.
- Zaitsev, A. V., Guha, P. K., Sarmast, F., Kolli, A., Berenfeld, O., Pertsov, A. M., de Groot, J. R., Coronel, R., & Jalife, J. (2003). Wavebreak formation during ventricular fibrillation in the isolated, regionally ischemic pig heart. *Circ.Res.* **92**, 546-553.
- Zhao, Z. Q., Corvera, J. S., & Halkos, M. E. (2003). Inhibition of myocardial injury by ischemic postconditioning during reperfusion; comparison with ischemic preconditioning. *Am.J Physiol Heart Circ Physiol* **285**, H579-H588.

Zhao, Z. Q. & Vinten-Johansen, J. (2006). Postconditioning: Reduction of reperfusion-induced injury. *Cardiovasc.Res.* **70**, 200-211.